Environmental controls on the distribution of bacterial tetraether membrane lipids: Constraints on the MBT-CBT paleothermometer

Francien Peterse

Environmental controls on the distribution of bacterial tetraether membrane lipids: Constraints on the MBT-CBT paleothermometer

Omgevingsinvloeden op de verdeling van
bacteriele tetraether membraanlipiden en
toepassing van de MBT-CBT paleothermometer

(met een samenvatting in het Nederlands)

Proefschrift

ter verkrijging van de graad van doctor aan de Universiteit Utrecht
op gezag van de rector magnificus, prof.dr. G.J. van der Zwaan,
ingevolge het besluit van het college voor promoties
in het openbaar te verdedigen op
donderdag 15 september 2011 des middags te 4.15 uur

door

Francien Peterse

geboren op 6 juni 1980 te Amsterdam

Promotoren: Prof. dr. ir. J.S. Sinninghe Damsté

Prof. dr. ir. S. Schouten

ha die pa, voor jou

Table of contents

Summary

Branched glycerol dialkyl glycerol tetraethers (GDGTs) are membrane lipids of soil bacteria that occur ubiquitously in soils, peats, and marine sediments. The structures of the branched GDGTs vary in the number of methyl groups (4 to 6) attached to the alkyl chains and can contain up to two cyclopentane moieties. An empirical study showed that their distribution in over 130 globally distributed soils is mainly controlled by mean annual air temperature (MAT) and soil pH, and can be expressed using the Methylation of Branched Tetraethers (MBT) index and the Cyclisation of Branched Tetraethers (CBT) index. The CBT index relates with soil pH, whereas the MBT index is related to both MAT and, to a lesser extent, soil pH. The combination of the MBT and CBT indices can then be used as a proxy for paleotemperature and past soil pH; the so-called MBT-CBT proxy. Branched GDGTs are transported with soil organic matter by rivers and deposited in marine coastal regions, where down-core analysis of branched GDGTs may yield an integrated MAT record for the river basin. However, before this proxy can be confidently applied, the exact influence of environmental controls on the distribution of branched GDGTs needs to be further investigated and possible constraints on its applicability need to be examined.

The influence of MAT and soil pH on the distribution of branched GDGTs, and thus the MBT-CBT proxy, was assessed in different natural settings. The direct effect of temperature changes was determined by analyzing branched GDGTs in soil transects away from two hot springs. The distribution of branched GDGTs in these geothermally heated soils changed substantially; MBT index values decrease with increasing distance from the hot spring and decreasing soil temperature. Although the slope of this relation is similar to that based on the global soil calibration set, the intercept is different. This difference can be explained by the use of in situ soil temperature in the relation for the geothermally heated soils rather than MAT, which was used in the initial study.

The influence of soil pH on the degree of cyclisation and the abundance of branched GDGTs was tested in soils from long term pH manipulated field plots with a pH range of 4.5-7.5. The distribution of core lipid (CL) and intact polar lipid (i.e. with headgroup still attached; IPL)-derived branched GDGTs was analyzed for each plot. The CBT index values of both CLs and IPL-derived branched GDGTs were significantly related with the actual soil pH, confirming the direct influence of soil pH on the distribution of branched GDGTs. Also, CBT-based pH estimates were similar to actual soil pH. Furthermore, soil pH affected the abundance of branched GDGTs, which showed a decrease with increasing pH. The abundance of *Acidobacteria*, suggested as a potential source of branched GDGTs, is also known to increase with decreasing pH, providing further support for this suggestion.

Analysis of branched GDGTs in soils along an altitude transect on Mount Gongga in China showed that among the many varying environmental factors, MAT and soil pH explain most of the variation in the distribution of branched GDGTs. Despite the relatively large scatter, the temperature lapse rate of MBT-CBT-based MAT estimates resembles the lapse rate caused by adiabatic cooling of air with increasing altitude. Based on this (indirect) relation between branched GDGTs and altitude, the MBT-CBT proxy was suggested as a proxy for paleoelevation, in addition to soil *n*-alkane δD values. To assess their suitability as proxies for paleoelevation, the relation of altitude of both branched GDGTs and the δD of *n*-alkanes in soils along the slopes of Mt. Gongga and Mt. Kilimanjaro (Tanzania) was studied. The data show that both proxies can be subject to relatively large uncertainties, but that a combination of both proxies likely results in a more reliable paleoelevation reconstruction.

Although the MBT-CBT proxy was found to correlate best with annual MAT, several studies suggest a potential seasonal bias in MBT-CBT-derived air temperature estimates, for example caused by a season of optimum growth of the bacteria that produce branched GDGTs. Therefore, the distributions and abundance of CL and IPL-derived branched GDGTs in mid-latitude soils from eight different locations were monitored over an annual cycle. MBT-CBT-reconstructed temperatures remained constant throughout the year and also branched GDGT abundances (both CL and IPL-derived) showed no bias towards a specific season. These results indicate that seasonality does not influence MBT-CBT-derived temperature estimates, and that the turnover time of the branched GDGT pool in soils is in the order of one year or more.

Branched GDGTs in Svalbard soils and nearby fjord sediment were analyzed to verify if the MBT-CBT proxy is applicable in high latitude environments, characterized by a low MAT, and to what extent branched GDGT distributions in marine sediments reflect those on land. Although branched GDGT concentrations in the soils were relatively low due to the cold climate and little soil development, MBT-CBT based MAT estimates were similar to the measured MAT (ca. -4°C and -6°C, respectively). The distribution of branched GDGTs in the fjord sediments was strikingly different from that in the soils, and was dominated by branched GDGTs with one cyclopentane moiety. This resulted in unrealistic MAT estimates, and suggests that at least part of the branched GDGTs in coastal marine environments receiving little soil organic matter may be predominantly produced in situ. The MBT-CBT proxy should therefore only be used for marine coastal sediments at sites receiving a substantial input of soil organic matter relative to the amount of marine organic matter, i.e. close to a river mouth.

More information on the possible origin of the branched GDGTs was gained by the analysis of IPL-branched GDGTs. Branched GDGTs with a glucose, glycuronic acid, hexose-glycuronic acid, phospho-hexose, or hexose-phosphoglycerol head group were identified in a Swedish peat, based on mass spectrometry. Changes in distribution of these IPL-branched GDGTs with depth in the Swedish peat bog were monitored using a newly developed Selected Reaction Monitoring (SRM) method. The response, as a measure for concentration, of all monitored IPLs increased below the water table, suggesting that they are primarily produced in this part of the peat. This is supported by the increase of absolute concentrations of CL and IPL-derived branched GDGTs below the water table. The trends of the individual IPLs with depth are different, but phospholipids show a larger increase in response with depth compared to glycolipids. The relatively large abundance of the less stable phospholipids implies that branched GDGTs are presumably produced by anaerobic bacteria in the anoxic part of the peat. Comparison of the IPL trends with 16S rRNA data hints toward *Acidobacteria* as possible producers of the branched GDGTs. Further application of the SRM method on two different soil types showed that most IPL-branched GDGTs were also present in these soils, albeit in different distributions.

The soil set on which the MBT-CBT proxy was initially calibrated, was extended to 278 globally distributed surface soils to recalibrate the proxy. As only 26% of these surface soils contained all nine different branched GDGTs, soils containing the seven most common branched GDGTs were selected for calibration purposes. Regression analysis resulted in new transfer functions for pH and MAT, based on the CBT index and adjusted MBT index (MBT'): pH= $7.90 - 1.97 \times$ CBT (r^2=0.70, RMSE=0.8) and MAT $= 0.81 - 5.67 \times$ CBT $+ 31.0 \times$ MBT' (r^2=0.59, RMSE=5.0 °C, n=176). The correlation coefficient of the new function is substantially lower than that of the original equation. Other statistically derived functions only marginally improved the correlation coefficient, while these functions could not be explained straightforwardly by physiological mechanisms. Local factors or seasonality cannot fully explain the re-

maining scatter in the calibration, but reconstructed MATs for soils from arid regions tend to substantially underestimate the actual MAT, which indicates that absolute branched GDGT-derived MAT records should be interpreted with caution. Application of the new transfer functions on previously published MBT-CBT derived paleotemperature records shows that trends remain similar, but that absolute temperature estimates and the amplitude of temperature changes are lower for most records, although in agreement with independent proxy data.

Application of the MBT-CBT proxy on a loess-paleosol sequence in China resulted in a paleotemperature record covering the last 34 kyr. The record shows that air temperatures varied in phase with northern hemisphere summer insolation, and that the onset of deglacial atmospheric warming started around 19 kyr BP, parallel in timing with other continental records. Comparison of the branched GDGT-based MAT record with oxygen isotope records of stalagmites from Chinese caves, representing East Asian summer monsoon precipitation, shows that the intensification of the summer monsoon lagged that of deglacial atmospheric warming. The results indicate that the onset of deglacial atmospheric warming and the intensification of the summer monsoon may have been controlled by different factors.

In conclusion, the data presented in this thesis show that temperature and soil pH are indeed the main controls the distribution of branched GDGTs in soils, and that the MBT and CBT indices are suitable as paleothermometer and proxy for past soil pH in terrestrial settings as well as coastal marine sites receiving a substantial input of soil organic matter. However, care must be taken in interpreting absolute MAT values generated with this proxy.

Samenvatting

Vertakte glycerol dialkyl glycerol tetraethers (GDGTs) zijn membraanlipiden van bacteriën die voorkomen in bodems, veen, en mariene sedimenten. De moleculaire structuur van de vertakte GDGTs varieert in de hoeveelheid methylgroepen (4 tot 6) en cyclopentaangroepen (tot 2) die de vertakte GDGT bevat. Uit een empirisch onderzoek van meer dan 130 bodems is gebleken dat de samenstelling van vertakte GDGTs in bodems vooral afhankelijk is van de jaargemiddelde luchttemperatuur (MAT) en van de pH van de bodem. Deze relaties kunnen worden uitgedrukt in de 'Methylation of Branched Tetraethers' (MBT) index en de 'Cyclisation of Branched Tetraethers' (CBT) index. De CBT index is gerelateerd aan bodem pH, terwijl de MBT index een verband vertoont met zowel MAT als, hoewel in mindere mate, bodem pH. De combinatie van de twee indices kan gebruikt worden als proxy for paleotemperatuur en –pH: de zogenaamde MBT-CBT proxy. Vertakte GDGTs worden, met ander bodemmateriaal, door erosie via rivieren naar zee getransporteerd, waar ze worden afgezet in het kustgebied. Bestudering van veranderingen in de samenstelling van vertakte GDGTs in een afzetting van kustsedimenten kan leiden tot een reconstructie van temperatuurveranderingen in het stroomgebied van de rivier in het verleden. Voordat de MBT-CBT proxy algemeen kan worden toegepast, zal eerst het precieze effect van de omgevingsfactoren op de samenstelling van de vertakte GDGTs en de mogelijke grenzen aan de toepasbaarheid van de proxy verder onderzocht moeten worden.

De invloed van MAT en bodem pH op de samenstelling van vertakte GDGTs, en dus op de MBT-CBT proxy, is op verschillende manieren onderzocht. Het directe effect van temperatuurveranderingen is vastgesteld door het analyseren van vertakte GDGTs in bodems bemonsterd langs een rechte lijn steeds verder van twee warmwaterbronnen af. De samenstelling van vertakte GDGTs in deze geothermische verwarmde bodems veranderde duidelijk; de MBT index nam af met toenemende afstand van de bron, en dus met afnemende bodemtemperatuur. De helling van de relatie die dit verband beschrijft, is vergelijkbaar met die gebaseerd op de mondiale bodemkalibratieset, het snijpunt met de y-as is echter anders. Dit verschil wordt wellicht verklaard door het gebruik van in situ bodemtemperatuur voor de relatie in deze studie, terwijl MAT is gebruikt in de mondiale kalibratie van de MBT-CBT proxy.

De invloed van de pH van de bodem op de mate van cyclisatie en de concentratie van vertakte GDGTs is vervolgens getest in bodems afkomstig van een veldexperiment, waarin de pH van elk proefveld al gedurende decennia kunstmatig constant wordt gehouden. De pH van de verschillende proefvelden varieerde tussen de 4.5 en 7.5. Bepaling van de samenstelling van zowel de core tetraethers (CLs) alsmede de intacte polaire tetraethers (IPLs), waar nog een polaire groep aan de kop van de tetraether vast zit, in deze bodemmonsters laat zien dat de CBT index waarden significant gerelateerd zijn met de gemeten bodem pH. Dit wijst erop dat bodem pH direct van invloed is op de samenstelling van vertakte GDGTs. Daarnaast zijn de met de CBT index berekende pH waarden nagenoeg gelijk aan de gemeten bodem pH. Bodem pH bleek ook de concentratie van vertakte GDGTs in de bodem te beïnvloeden, aangezien de hoeveelheid vertakte GDGTs afnam met toenemende pH. Van *Acidobacteriën*, gesuggereerd als mogelijke producenten van vertakte GDGTs, is bekend dat zij ook in hogere aantallen voorkomen bij afnemende pH, hetgeen deze suggestie ondersteunt.

De samenstelling van vertakte GDGTs in bodems op de helling van de Gongga berg in China laat zien dat zelfs wanneer er meerdere veranderende omgevingsfactoren een rol spelen, het grootste deel van de variatie in de samenstelling van vertakte GDGTs toch kan worden verklaard door MAT en bodem pH. On-

danks de aanzienlijke spreiding in de data, is de op MBT-CBT gebaseerde verticale temperatuurgradiënt nagenoeg gelijk aan de adiabatische afkoeling van de atmosfeer met toename in hoogte. Deze (indirecte) relatie van vertakte GDGTs met hoogte suggereert dat de MBT-CBT proxy in bodems mogelijk ook gebruikt kan worden als proxy voor paleohoogte, als aanvulling op δD waarden van plantwassen. Om de geschiktheid van deze methode te testen, werden zowel vertakte GDGTs als de δD van plantwassen gemeten in bodems van de hellingen van de Gongga berg en de Kilimanjaro (Tanzania). De resultaten laten zien dat beide proxies weliswaar hun onzekerheden hebben, maar dat de combinatie van de proxies kan leiden tot betrouwbaardere reconstructies van de paleohoogte.

Over het algemeen wordt de beste correlatie gevonden tussen de MBT-CBT proxy en de jaarlijkse MAT, al wordt in meerdere studies gesuggereerd dat de met de proxy berekende temperaturen een afwijking richting een bepaald seizoen laten zien, mogelijk veroorzaakt door een periode van optimale groeiomstandigheden voor de bacteriën die vertakte GDGTs produceren. Om deze reden zijn de samenstelling en de concentratie van zowel CL als IPL-afkomstige vertakte GDGTs in bodems op acht verschillende locaties over de loop van een jaar gemeten. De met de MBT-CBT proxy berekende temperaturen zijn op alle locaties het hele jaar door constant, en ook de concentraties van de vertakte GDGTs (zowel CL als IPL-afkomstig) variëren niet met de seizoenen. Uit deze resultaten blijkt dat seizoenen MBT-CBT-gebaseerde temperaturen niet beïnvloeden, en dat de omzettingstijd van vertakte GDGTs in bodems in elk geval langer is dan een jaar.

De samenstelling van vertakte GDGTs in bodems en fjord sediment op en rond Svalbard is bestudeerd om na te gaan of de MBT-CBT proxy ook toepasbaar is in Arctische gebieden, gekenmerkt door een lage MAT, en om te bepalen of de samenstelling van vertakte GDGTs in mariene sedimenten wel overeenkomt met die in de bodem op het nabije continent. Hoewel de concentratie van vertakte GDGTs in de bodems door het koude klimaat en de geringe mate van bodemvorming relatief laag is, komt de met de MBT-CBT berekende MAT goed overeen met de gemeten MAT (respectievelijk rond de -4°C en -6°C). De samenstelling van vertakte GDGTs in het sediment in het fjord is daarentegen heel anders dan die in de bodems, en wordt gedomineerd door vertakte GDGTs met een cyclopentaangroep. Deze afwijkende samenstelling heeft onrealistische MAT waarden tot gevolg en suggereert dat tenminste een deel van de vertakte GDGTs in kustgebieden, die weinig organisch bodemmateriaal van het land ontvangen, in situ geproduceerd moet zijn. Het wordt daarom aanbevolen om de MBT-CBT proxy alleen toe te passen in mariene sedimenten waar er voldoende aanvoer is van organische stof uit bodems ten opzichte van de hoeveelheid aanwezig marien organisch materiaal, zoals bijvoorbeeld bij riviermondingen het geval is.

Meer informatie over de mogelijke herkomst van vertakte GDGTs kan voortkomen uit de analyse van IPL-vertakte GDGTs. Met gebruik van massaspectrometrie zijn IPL-vertakte GDGTs met verschillende suiker- en fosfaatgroepen, of combinaties daarvan, geïdentificeerd in een Zweeds veen. Met de ontwikkeling van een Selected Reaction Monitoring (SRM) methode zijn vervolgens veranderingen in de samenstelling van deze hoofdgroepen met diepte in het Zweedse veen bepaald. De IPLs zijn in een hogere concentratie aanwezig in het veen onder de waterspiegel, hetgeen suggereert dat ze voornamelijk in dit deel van het veen worden geproduceerd. Dit werd bevestigd door de absolute gesommeerde hoeveelheden CL en IPL-afkomstige vertakte GDGTs, die ook in concentratie toenemen onder de waterspiegel. De verschillende IPL-vertakte GDGTs volgen elk een andere trend met diepte, maar in het algemeen neemt de concentratie van fosfolipiden meer toe met diepte dan die van glycolipiden. De hogere concentratie van de relatief minder stabiele fosfolipiden impliceert dat vertakte GDGTs naar alle waarschijnlijkheid worden

geproduceerd door anaërobe bacteriën in het anoxische gedeelte van het veen. Vergelijking van de trends van de IPLs met 16S rRNA data doet vermoeden dat vertakte GDGTs worden geproduceerd door *Acido-bacteriën*. De toepassing van de SRM methode op twee verschillende bodems liet zien dat de meeste van de in het veen geïdentificeerde IPLs ook hier aanwezig zijn, hoewel in een andere samenstelling.

Voor een MBT-CBT rekalibratie studie zijn alle tot nu toe op vertakte GDGTs geanalyseerde bodems toegevoegd aan de initiële mondiale bodemset die de basis vormde voor de ontwikkeling van de MBT-CBT proxy. Slechts 26% van de 278 bodems bevatte alle negen individuele vertakte GDGTs. Om deze reden werden alle bodems die de zeven meest voorkomende vertakte GDGTs bevatten geselecteerd voor de nieuwe kalibratie. Regressieanalyse leverde een nieuwe functie op om pH en MAT te berekenen met behulp van de CBT index en een aangepaste MBT index (MBT'): pH $= 7.90 - 1.97 \times$CBT (r^2=0.70, RSME=0.8) en MAT $= 0.81 - 5.67 \times$CBT $+ 31.0 \times$MBT' (r^2=0.59, RSME=5.0 °C, n=176). De determinatiecoëfficiënt van de nieuwe MAT-functie is lager dan die van de originele functie. Andere, op statistische methoden gebaseerde functies, verbeterden de determinatiecoëfficiënt maar in geringe mate, terwijl de mathematische opbouw van deze functies niet direct kan worden verklaard met de veronderstelde achterliggende fysiologische mechanismen. Lokale omgevingsfactoren of de invloed van seizoenen kunnen de overgebleven variatie in de kalibratie niet verklaren, maar berekende MATs voor bodems uit droge gebieden zijn vaak relatief te laag ten opzichte van gemeten MAT. Dit wijst er op dat voorzichtigheid geboden is bij de interpretatie van de absolute, op vertakte GDGTs gebaseerde temperaturen voor zulke gebieden. De toepassing van de nieuwe MAT-functie op reeds gepubliceerde MBT-CBT paleotemperatuurreconstructies laat zien dat de trends niet veranderen, maar dat de absolute temperaturen en de amplitude van de temperatuurveranderingen over het algemeen iets lager worden, maar nog wel in overeenstemming zijn met onafhankelijke proxy data.

De toepassing van de MBT-CBT proxy op een loess-paleosol sequentie in China resulteerde in een reconstructie van de paleotemperatuur van de laatste 34 duizend jaar. De reconstructie laat zien dat veranderingen in luchttemperatuur in fase liepen met de zomerinsolatie op het noordelijk halfrond en toont aan dat de opwarming van de atmosfeer na de laatste deglaciatie rond 19 duizend jaar geleden begon, hetgeen overeenkomt met de uitkomst van andere studies die de continentale luchttemperatuur reconstrueren. Een vergelijking van de temperatuurreconstructie, gebaseerd op vertakte GDGTs, met neerslagreconstructies voor oost Azië, gebaseerd op zuurstofisotopen in stalagmieten, liet zien dat de zomermoeson pas sterker werd nadat de atmosfeer opwarmde. Dit wijst erop dat beide processen waarschijnlijk gedreven zijn door verschillende factoren.

Concluderend kan gesteld worden dat de data die in dit proefschrift worden gepresenteerd laten zien dat temperatuur en bodem pH inderdaad de belangrijkste factoren zijn die de samenstelling van vertakte GDGTs in bodems bepalen, en dat de MBT en CBT indices geschikt zijn als paleothermometer en proxy voor bodem pH in bodems en in mariene sedimenten in kustgebieden die voldoende bodem organisch materiaal ontvangen. Toch is voorzichtigheid geboden bij de interpretatie van de absolute MAT waarden die met behulp van deze proxy worden gegenereerd.

Chapter 1

General outline and introduction

1.1 Climate variability

The earth's history is characterized by episodes of large climatic changes, which often coincide with changes in the mixture of atmospheric greenhouse gases. Especially variations in the concentration of CO_2 have appeared to be a strong driver for climate change. Since the industrial revolution, human activity has increased the level of CO_2 in the atmosphere, which is predicted to cause significant warming of the earth's surface (IPCC, 2007). For the prediction of the exact consequences of continuing rise of the CO_2 level for our future climate, global climate models are used. These models are generally validated by simulating present-day climate and past climatic changes and comparing the results with climate records. For example, an episode of extreme warmth and high CO_2 concentrations in the past, like the Early Eocene (56-48 Ma), provides a future analog for periods of global warming and increased CO_2 concentrations. Hence, the better we understand the mechanisms that explain climate changes of the past, the more accurate the modeled predictions for the future will be. However, the instrumental records that serve as comparison for the output data of these models only go back a limited amount of time. The global temperature record, for example, only covers just over the past 100 years (Peterson and Vose, 1997).

Extension of instrumental temperature records can be achieved by the application of so-called climate proxies, which are preserved, measureable characteristics of the past that can be (quantitatively) linked to an environmental parameter. Application of these proxies on a sedimentary record provides valuable information on past climatic variations, e.g. temperature, crucial for the testing of climate models. Records of both sea surface temperatures (SST) as well as (continental) air temperatures are essential data sources for the models, as ocean-atmosphere interactions are, together with greenhouse gasses, responsible for the global redistribution of heat, and thereby form an important control on the earth's climate (Wang et al., 2004).

1.2 Reconstruction of past temperatures

There are various methods to reconstruct past sea surface or air temperatures. SSTs, for example, are recorded in the oxygen isotopic composition of calcite or opal containing shells that are preserved in marine sediments. The ratio of ^{18}O and the lighter ^{16}O that is incorporated in the shells depends, amongst others, on the temperature of the sea water, so that SSTs can be derived by analyzing this ratio in a shell (Urey, 1947; Epstein et al., 1953). The elemental composition of the shells also provides information on past SSTs. Calcareous shells substitute Ca by Mg depending on the water temperature. Hence, SSTs can be estimated based on the Mg/Ca ratio of the shell (Nurnberg et al., 1996; Elderfield and Ganssen, 2000). A temperature signal can furthermore be obtained from fossil organic molecules present in sediments. For example, the ratio in which haptophyte algae produce $C_{37:2}$ and $C_{37:3}$ long-chain unsaturated ketones depends on temperature (Brassell et al. 1986). This relation is quantified in the U^{k}_{37} index (Unsaturation ratio of long chain (C_{37}) Ketones (alkenones)), which enables the reconstruction of past SSTs by analyzing the ratio in which these alkenones are present in a sedimentary record (*Fig. 1.1*; Brassel et al., 1986; Müller et al., 1998). SSTs are also recorded by the distribution of isoprenoid tetraether membrane lipids of marine Thaumarchaeota. These archaea synthesize their membranes with a varying number of cyclopentane moieties, depending on the temperature of their environment (Schouten et al., 2002; Wuchter et al., 2004). The number of cyclopentane moieties that is incorporated in the membrane shows a positive linear relation with temperature. The TEX_{86} (TetraEther indeX of tetraethers consisting of 86 carbon atoms) was developed to translate changes in the relative abundance of the membrane lipids into SST (*Fig. 1.2*; Schouten et al., 2002).
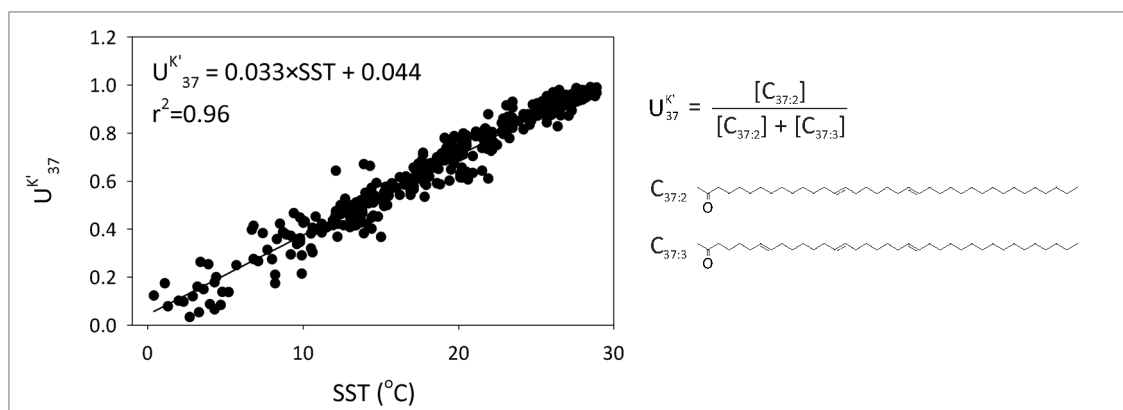
Fig. 1.1. Definition and molecular structures of the alkenones used for the $U^{K'}_{37}$ ratio and the relationship between $U^{K'}_{37}$ and annual mean SST for surface sediments from the global ocean between 60°S and 60°N (*Müller and Fischer, 2004*).

In contrast to SST, the reconstruction of long term terrestrial temperatures is less straightforward, because fewer suitable proxies exist and sedimentary archives on land generally reach less far back in time compared to those in the marine realm. Nevertheless, there are several proxies that are regularly applied to obtain continental temperature records. A widely used tool to reconstruct continental temperatures is, for example, the inventory of pollen assemblages (e.g., Colinvaux et al., 1996). Pollen are relatively well preserved in lake sediments and peat bogs, and quantitative temperature estimates can be derived from comparison of sedimentary pollen assemblages with the modern analog. However, the accuracy of this method is lower for glacial continental temperature reconstructions, as there are no modern analogues to calibrate glacial assemblages (Hatté et al., 2009). This method furthermore assumes that plant-climate interactions have remained constant throughout time, whereas physiological studies have shown that these interactions are sensitive to changes in e.g. CO_2 concentration (Street-Perrott et al., 1997). A second plant based proxy uses the proportion of untoothed leaves from woody dicot species in a floral sample to reconstruct paleotemperatures. Baily and Sinnot (1915) were the first to report the positive relation between annual mean air temperature (MAT) and the proportion of untoothed leaves. This relation was changed into a quantitative method based on linear regressions of extant untoothed species and MAT, consequently enabling the reconstruction of paleotemperature by analyzing the margins of fossil leaves (a.o., Wolfe, 1971; Greenwood et al., 2004). Possible sources of uncertainty that are linked with this method are that the linear regression models do not take adaptation to changes in the environment into account (Jordan, 1997; Little et al., 2010). Also the effects of preferential preservation of (un)toothed leaves and the extinction of species are not considered (Jordan, 1997).

By making use of the temperature sensitivity of the oxygen isotopic composition of precipitation, paleotemperature records have been derived from isotope measurements of water trapped in ice masses. The best known examples of such records are those from Greenland and Antarctica, of which for the latter location the longest record has been retrieved, extending 800,000 years (GRIP, 1993; Jouzel et al., 1987; Lüthi et al., 2008). Obviously, ice core records are limited to ice covered sites, although these are most often locations for which other proxy data are not available. Similarly, oxygen isotopes trapped in cave stalagmites can be used to reconstruct past temperatures. Also the isotopic value of the carbon and trace metals in the stalagmites, as well as the thickness of the annual growth bands contain paleoclimate data (e.g. Burns et al., 1998; Li et al., 2005; Shakun et al., 2007). However, the isotopic values of the elements preserved

in ice cores and speleothem archives are, besides temperature, also influenced by factors like the origin of precipitation, seasonality, and precipitation amount, which may add to the uncertainty of the temperature signal (Jouzel et al., 1997). A last example of a method that used oxygen isotopic values to infer paleotemperatures is based on animal bone and tooth enamel. Bones and teeth contain biogenic apatite, of which the oxygen isotopic value is related to temperature, as this value is mainly determined by the oxygen isotopic composition of the animal's drinking water. The drinking water, in its turn, is related to the isotopic composition of meteoric water, containing a temperature signal (e.g. Longinelli, 1984). Thus, past temperature records can be generated, albeit in low resolution, based on oxygen isotopic measurements on fossil bones and teeth (e.g. Fricke et al., 1998; Kohn and Law, 2006)
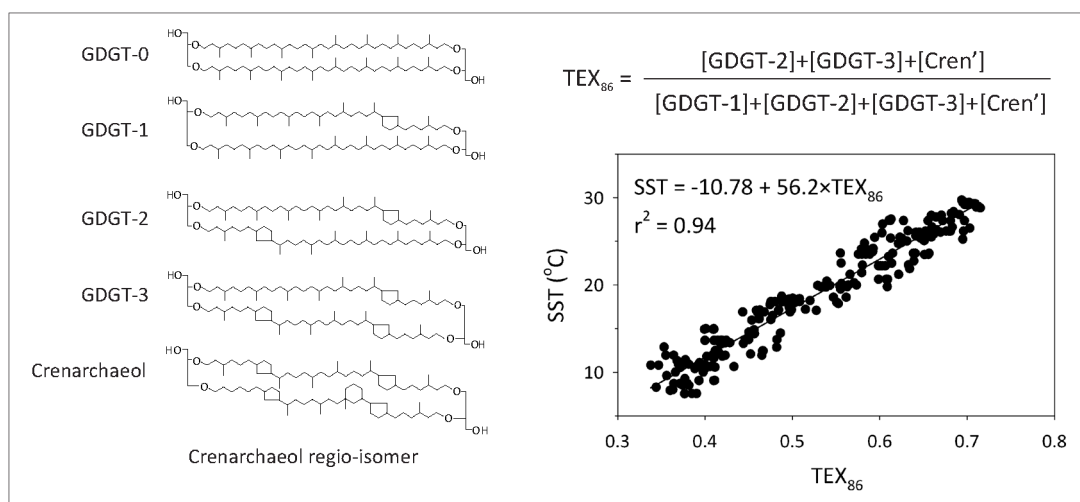

$$TEX_{86} = \frac{[GDGT\text{-}2]+[GDGT\text{-}3]+[Cren']}{[GDGT\text{-}1]+[GDGT\text{-}2]+[GDGT\text{-}3]+[Cren']}$$

$$SST = -10.78 + 56.2 \times TEX_{86}$$
$$r^2 = 0.94$$

Fig. 1.2. Definition and molecuar structures of the isoprenoid GDGTs for the calculation of the TEX_{86} and the reation of annual mean SST at 0 m water depth with TEX_{86} values (*Kim et al., 2008*).

Another method that yields low resolution, although generally considered accurate, temperature records, is based on noble gas dissolved in groundwater. The solubility of atmospheric noble gases in water is temperature dependant, so that paleotemperatures can be inferred from their concentration in ancient groundwater basins (Mazor, 1972; Andrews and Lee, 1979).

Lakes provide generally suitable settings to obtain continuous, high resolution paleotemperature records. The climatic information can be retrieved from the fossils of aquatic organisms that are preserved in the sediments of lakes. Assemblages of e.g. chironomid larvae or diatoms show a strong relationship with summer temperatures, so that a summer temperature record can be inferred from down-core variations in their distribution in lake sediments (e.g., Lotter et al., 1997; Kurek et al., 2009; Pienitz et al., 1995), although it has been shown that the temperature signal of chironomids can at times be overruled by changes in pH, water chemistry, and lake productivity (Velle et al., 2005). After the detection of Thaumarchaeotal isoprenoid tetraether membrane lipids in lakes, and the confirmation of their temperature dependence in these settings (Powers et al., 2004), also applications of the TEX_{86} on lake sediments have resulted in quantitative past continental temperature reconstructions (Powers et al., 2005; Tierney et al., 2008). However, the applicability of this proxy on lake sediments has been shown to be limited to large lake systems only (Blaga et al., 2009; Powers et al., 2010), and present studies indicate that TEX_{86} inferred temperatures reflect that of sub-surface water masses rather than representing lake surface temperatures (Blaga et al., 2011).

In summary, many of the available continental temperature proxies are besides temperature also sensitive to changes in other environmental parameters, making it difficult to extract a pure temperature signal. Hence, there is a need for new continental temperature proxies which would, among other things, be globally applicable, provide quantitative temperature estimates, have temperature as main environmental control, and are not or limited influenced by changes in e.g. precipitation or CO_2 concentration.

1.3 The MBT-CBT continental paleothermometer

Recently, a new proxy was proposed based on the distribution of branched glycerol dialkyl glycerol tetraether (GDGT; *Fig. 1.3*) membrane lipids (Weijers et al., 2007c). These branched GDGTs were first discovered in a Holocene Dutch peat bog, after which their molecular structure was identified with nuclear magnetic resonance spectroscopy (Sinninghe Damsté et al., 2000). Unlike the GDGTs of archaea, the carbon skeleton of the branched GDGTs is not isoprenoidal, but consists of branched carbon skeletons. The branched GDGTs possess 4 to 6 methyl groups attached to their tetraether backbone, and can contain up to two cyclopentane moieties that are formed by internal cyclization (Weijers et al., 2006a). Due to their mixed archaeal (membrane spanning tetraethers, ether lipids) and bacterial (branched alkyl chains) characteristics, their exact origin was only determined after the examination of the stereo-configuration of the glycerol moieties, which was found to be typical for bacteria (Weijers et al., 2006a). The bacteria that synthesize branched GDGTs are currently unknown, although it has been suggested that species within the phylum of *Acidobacteria* may be their source (Weijers et al., 2009).
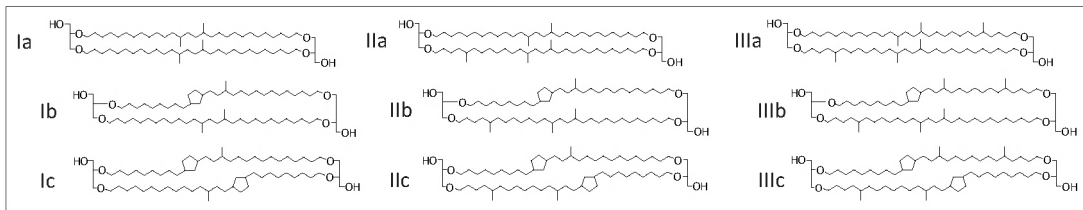
Fig. 1.3. Molecular structures of branched GDGTs.

The idea to use these branched GDGTs as proxy for continental air temperatures resulted from an empirical study on their relative abundance in globally distributed soils. This study showed that the different local MATs explain a large part of the global variation in relative branched GDGT distributions, i.e. the number of methyl branches increases with decreasing temperatures (*Fig. 1.4*; Weijers et al., 2007c), whereas soil pH was shown to influence the degree of cyclisation of the branched GDGTs, as concentrations of branched GDGTs with cyclopentane moieties increased with soil pH. The definition of two indices, the Methylation of Branched Tetraethers (MBT) and the Cyclisation of Branched Tetraethers (CBT), enables quantification of the relation between branched GDGT distributions, MAT and soil pH. The indices were defined as follows:

$$MBT = [Ia+Ib+Ic]/[Ia+Ib+Ic+IIa+IIb+IIc+IIIa+IIIb+IIIc] \tag{1.1}$$
$$CBT = -LOG\ ([Ib+IIb]/[Ia+IIa]) \tag{1.2}$$

The Roman numerals in the equations refer to the abundance of the molecules in *Fig. 1.3*.

The MBT index describes the relation with MAT, and the CBT index with soil pH (*Fig. 1.5a, b*):

$$MBT = 0.28 + 0.025 \times MAT \qquad (r^2=0.62) \qquad (1.3)$$
$$CBT = 3.33 + 0.38 \times pH \qquad (r^2=0.70) \qquad (1.4)$$

The MBT index also relates, although to a lesser extent, with soil pH. Consequently, substitution of pH by the CBT index then results in a function to estimate MAT, solely based on the distribution of branched GDGTs (*Fig. 1.5c*):

$$MBT = 0.122 + 0.187 \times CBT + 0.020 \times MAT \qquad (r^2=0.77) \qquad (1.5)$$

Branched GDGTs have also been found in lakes and coastal marine sediments, where they are likely deposited with soil organic matter after erosion and subsequent transportation by rivers (Hopmans et al., 2004; Kim et al., 2006). Hence, down-core analysis of branched GDGT distributions in river-dominated coastal sediments may yield an integrated temperature record for a river catchment area. For example, the deglacial atmospheric warming in tropical central Africa was reconstructed using the MBT-CBT proxy (i.e. Eq. 1.5) in a sediment core retrieved from the Congo River fan (Weijers et al., 2007a). The timing and extent of the warming is in good agreement with previous estimates for this area based on e.g., pollen or stalagmites. The MBT-CBT proxy has also been applied on longer geological timescales; the brief episode of extreme warmth during the Paleocene-Eocene thermal maximum (PETM; ~55 Ma) was reconstructed by analyzing the branched GDGT distributions in a marine sediment core from the Arctic Ocean (Weijers et al., 2007b).

Thus, the MBT-CBT proxy seems to be a promising tool to obtain paleoclimatic information that can contribute to a better understanding of the timing and the driving forces of climatic changes in the past. However, as with most new proxies, further studies are needed to constrain the validity and applicability of the MBT-CBT proxy.
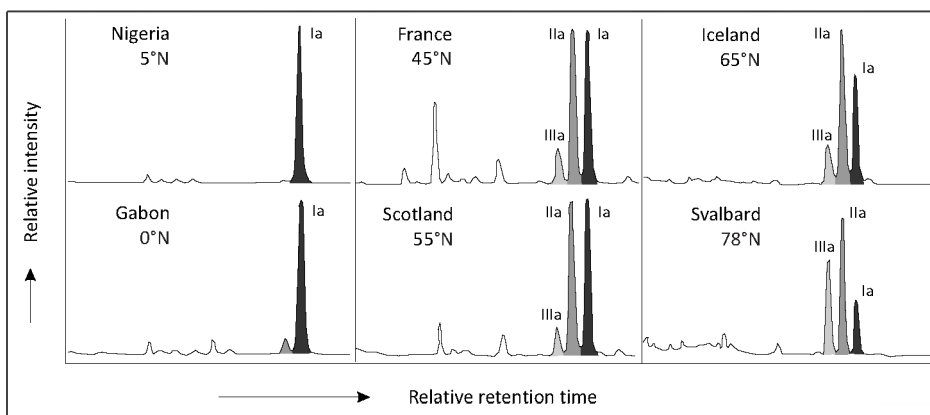

Fig. 1.4. HPLC-MS base peak chromatograms of soils from tropical, temperate, and cold areas illustrating typical branched GDGT distributions. The degree of methylation of the branched GDGTs increases with decreasing temperatures (*Weijers et al, 2007c*). Roman numerals refer to the structures in *Fig. 1.3*.
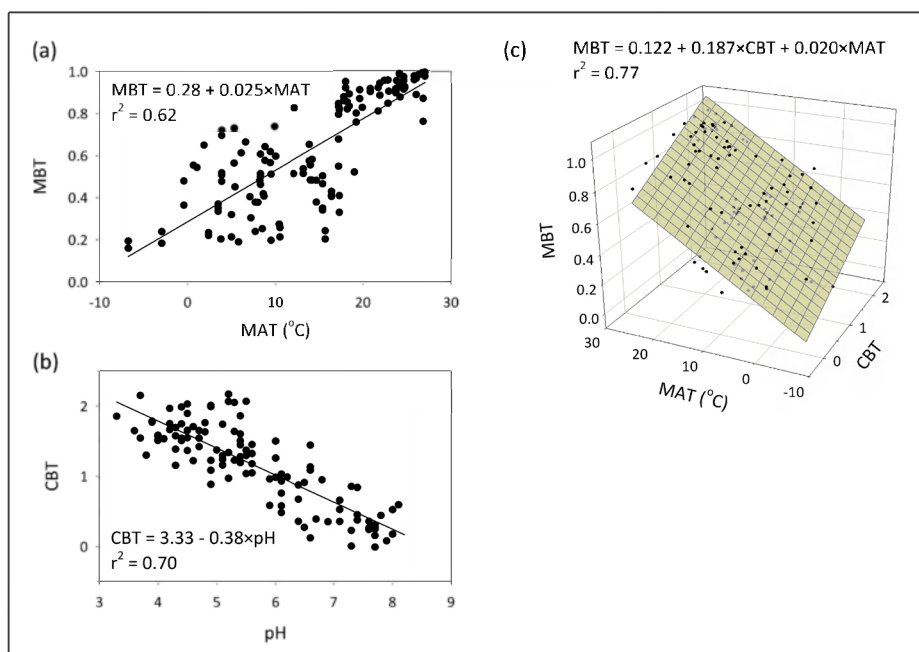
Fig. 1.5. Regression plots of a) the MBT index and MAT, b) the CBT index and pH for the soils of the global calibration set, and c) the 3D calibration plot of the MBT and CBT indices with MAT (*Weijers et al., 2007c*).

1.4 Scope and framework of this thesis

Initial studies have shown empirical relations of the MBT and CBT indices with environmental parameters, but the direct influence of changes in temperature and soil pH on the distribution of branched GDGTs has not been tested. Also, the possible impact of environmental factors other than temperature and pH has not yet been thoroughly evaluated, although it was suggested that precipitation may influence the distribution of branched GDGTs in soils (Weijers et al., 2007c). Furthermore, it is not clear in what type of environments the MBT-CBT proxy is applicable. Thus, the aim of this thesis was to constrain the impact of environmental factors and the applicability of the proxy in a variety of settings. In the first part, branched GDGTs are analyzed in natural or (semi-)controlled settings with only one varying environmental parameter, so that the impact of that specific parameter on the distribution of branched GDGTs can be determined. In the second part, the proxy is further constrained and tested in a variety of settings in order to test the applicability of the proxy.

The influence of the main environmental parameters thought to control the branched GDGT distribution in soils, i.e. temperature and pH, is tested in the first part of this thesis. **Chapter 2** describes the direct influence of changes in soil temperature on branched GDGT distributions. To this end, branched GDGTs were analyzed in geothermally heated soils. Their distributions along a temperature transect changed according to what was expected based on the general branched GDGT distributions in warm and cold soils, i.e. an increase in the number of methyl branched with decreasing temperature (*cf. Fig. 1.4*). A strong correlation was observed between the MBT index and in situ soil temperature, confirming that this is an important factor controlling this proxy.

The direct influence of soil pH on the abundance and distribution of branched GDGTs is reported in **Chapter 3**. Analysis of core lipids (CLs) and derivatives of their intact and presumably living precursors,

i.e. intact polar lipid (IPL)-derived branched GDGTs in a long term pH manipulated field experiment confirmed that soil pH is an important control on the degree of cyclisation of branched GDGTs, as a strong correlation between CBT and soil pH was found and CBT-based pH estimates resembled the measured pH of the soil. The concentration of total branched GDGTs decreased with increasing soil pH, suggesting *Acidobacteria*, showing a similar trend, as a possible biological source for these compounds.

In **Chapter 4** it is shown that temperature and pH are the main controls on branched GDGT distributions in an area with many varying environmental factors, i.e. along an altitude transect on Mount Gongga in China. The decrease in MBT-CBT-derived temperatures with altitude resembles the measured temperature lapse rate, despite a relatively large degree of scatter. Additionally, branched GDGT distributions were tested as a proxy for paleoelevation, complementary to plant wax δD analyzed in the same soils along two different mountain slopes. The results show that both proxies can be subject to relatively large uncertainties, but that a combination of plant wax δD and the MBT-CBT proxy may result in more reliable paleoelevation reconstructions.

The second part of this thesis decribes the constraints on the application of the MBT-CBT proxy as paleothermometer. In **Chapter 5** it was tested if a seasonal bias in reconstructed temperatures can occur due to a season of optimal growth for the branched GDGT-producing organisms. Mid-latitude soils from eight different locations were therefore sampled in time series over one year and analyzed on both CL and IPL-derived branched GDGTs. Both MBT-CBT-reconstructed temperatures as well as branched GDGT concentrations showed no bias towards a specific season. These results indicate that seasonality does not influence MBT-CBT-derived temperature estimates, and that the turnover time of branched GDGTs in soils is thus in the order of one year or more.

To determine if branched GDGTs can be applied in Arctic marine sediments, the MBT-CBT proxy was applied on modern Svalbard soils and coastal sediments (**Chapter 6**). Despite the short growing season and the slow rate of soil formation, MBT-CBT-based temperatures are similar to measured MAT for soils. However, the limited input of soil organic matter (OM) and in situ production of branched GDGTs in the fjord sediment resulted in unrealistic MBT-CBT temperature estimates. It was therefore suggested that the MBT-CBT proxy should only be used at sites with substantial input of soil OM relative to the amount of marine OM, i.e. close to river mouths.

In order to shed light on the origin of the branched GDGTs, intact branched GDGTs in a Swedish peat were analyzed (**Chapter 7**). The changes in head group composition throughout the peat profile were monitored with a newly developed Selected Reaction Monitoring (SRM) assay. The results suggest that branched GDGTs are mainly produced in the anoxic part of the peat, and hint again towards *Acidobacteria* as potential producer of branched GDGTs. Further application of the SRM method indicated that imilar IPL branched GDGTs are present in soils, albeit in different distributions.

In **Chapter 8**, the MBT index was redefined for the seven most common branched GDGTs and, together with the CBT index, recalibrated based on an extended global surface soil calibration set. Comparison of the new empirical calibration with statistically derived indices to describe the relation of branched GDGTs with MAT and soil pH showed that a pure statistical approach leads to a marginal improvement only of the calibration accuracy. Furthermore, the statistically derived indices no longer reflect the physiological mechanisms supposedly underlying the functioning of the MBT-CBT proxy, and thus a slightly adjusted MBT index, MBT', based on seven branched GDGTs is proposed. Comparison of the new MBT'-CBT calibration with previously published paleotemperature records based on the original

MBT-CBT calibration showed that the trends and timing of events remains unchanged, but that absolute MAT estimates are generally lower.

Chapter 9 describes the first application of the MBT-CBT paleothermometer in a loess profile. This yielded a continuous air temperature record for East Asia that covers the past 34,000 years, based on branched GDGTs in a loess-paleosol sequence from the Mangshan plateau in China. Comparison of this record with other loesspaleosol proxy records and stalagmite $\delta^{18}O$ records indicates that the onset of deglacial atmospheric warming and the intensification of the East Asian Summer Monsoon (EASM) precipitation was decoupled, and that strengthening of EASM precipitation unambiguously lagged deglacial warming and Northern Hemisphere insolation. This shows that the MBT-CBT proxy is applicable in loess settings.

In summary, the results described in this thesis show that temperature and pH have indeed a strong control on the distribution of branched GDGTs in soils, and that other parameters do not greatly affect this. This supports the general suitability of the MBT and CBT indices as paleothermometer and proxy for past soil pH. The results furthermore indicate that the turnover time of branched GDGTs in soils is relatively long, and that, as a consequence, absolute temperatures generated by the proxy are not biased towards a specific season. However, its global applicability on marine sediments is constrained to those recovered from areas that receive a substantial input of terrestrial OM relative to the amount of marine OM to prevent a disturbed signal due to the possible contribution of in situ produced branched GDGTs. Furthermore, the absolute temperature estimates as well as temperature records for areas that receive very low amounts of precipitation should be interpreted with care. Nevertheless, the MBT/CBT proxy can be applied in a variety of sites and time periods and can yield valuable unique paleoclimatic information.

Chapter 2

Distribution of branched tetraether lipid in geo-thermally heated soils: Implications for the MBT-CBT temperature proxy

Francien Peterse, Stefan Schouten, Jaap van der Meer, Marcel T.J. van der Meer, Jaap S. Sinninghe Damsté, 2009. *Organic Geochemistry* 40, 201-205.

Abstract

Branched glycerol dialkyl glycerol tetraether (GDGT) membrane lipids occur in soils and peat bogs and are assumed to be produced by anaerobic bacteria. Two indices based on the distribution of these lipids in soils, the Cyclisation of Branched Tetraethers (CBT) index and the Methylation of Branched Tetraethers (MBT) index have been shown to linearly relate to pH, and to annual mean air temperature (MAT) and pH, respectively. To directly evaluate the impact of changes in soil temperature on the MBT-CBT proxy, we determined these indices in soils sampled from a transect away from two hot springs in California, which provided a set of soils similar in composition but with different temperatures (12-41 °C). The CBT values of these geothermally heated soils show a good relation with pH ($r^2=0.76$), similar to that of a global MBT-CBT calibration set. Also, the relationship between MBT, soil pH and temperature for the geothermally heated soils is similar to that of a global soil calibration set, although the intercept for the geothermally heated soils is significantly lower, likely because our data set is based on in situ soil temperatures rather than MAT. The results confirm the dependence of the MBT index on soil temperature and pH and support the applicability of the MBT-CBT indices as a proxy for continental palaeotemperatures and past soil pH.

2.1 Introduction

Branched glycerol dialkyl glycerol tetraether lipids (GDGTs; I–III, *Fig. 2.1*) were discovered in peat deposits and identified using nuclear magnetic resonance (NMR) spectroscopy by Sinninghe Damsté et al.(2000). Subsequently, they were found in coastal marine and lake sediments, likely derived from river-transported terrestrial soil organic matter (OM; Schouten et al., 2000; Hopmans et al., 2004; Weijers et al., 2006b; Kim et al., 2006). Unlike the GDGTs of archaea, the carbon skeleton of branched tetraether lipids is not iso-prenoid but comprises branched chains. The branched GDGTs vary in the total number of methyl groups (4–6) attached to their two membrane-spanning alkyl chains. Furthermore, they can contain up to two cyclopentane moieties (*Fig. 2.1*) which are formed by internal cyclization (Weijers et al., 2006a).

As the branched GDGTs show a mixture of archaeal (membrane-spanning tetraethers, ether lipids) and bacterial characteristics (branched alkyl chains), assignment of their origin was ambiguous. However, based on the fact that branched dialkyl glycerol diethers have been found in thermophilic bacteria (Langworthy et al., 1983; Huber et al., 1992; Sinninghe Damsté et al., 2007) and that non-isoprenoid lipids have not been reported in archaea, Sinninghe Damsté et al. (2000) suggested bacteria to be the most likely producers of branched GDGTs. Weijers et al. (2006a) determined the stereo-configuration of the glycerol moieties of branched GDGTs and found them to be identical to those in bacterially synthesized glycerol moieties and opposite to those in archaeal synthesized glycerol moieties, confirming a bacterial origin for the branched GDGTs. Furthermore, they found that branched GDGTs are most abundant in the anoxic zone of peat bogs, suggesting that anaerobic bacteria are the source. However, the exact phylogenetic group of bacteria responsible for their production is unknown.
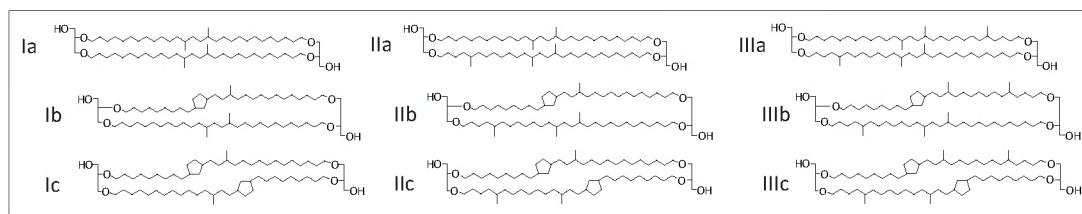
Fig. 2.1. Molecular structures of branched GDGTs.

In an empirical study, Weijers et al. (2007c) analyzed about 130 soils from 90 different locations worldwide to determine the main environmental controls on the relative distribution of branched GDGTs. They found that the number of methyl groups relates to the annual mean air temperature (MAT) and soil pH, and that the number of cyclopentane moieties linearly relates to soil pH alone. In order to quantify the change in relative distributions, two indices were developed: the Methylation of Branched Tetraethers (MBT) index, and the Cyclisation of Branched Tetraethers (CBT) index. These are defined as:

$$MBT = [Ia+Ib+Ic]/[Ia+Ib+Ic+IIa+IIb+IIc+IIIa+IIIb+IIIc] \qquad (2.1)$$
$$CBT = -LOG\ ([Ib+IIb]/[Ia+IIa]) \qquad (2.2)$$

The numbers refer to the structures in *Fig. 2.1*. The indices are strongly related to pH and MAT (*Table 2.1*) and were successfully applied as proxies to reconstruct past soil pH and MAT in several areas of different geological age. Analysis of the GDGT distribution in the river-transported soil OM in a sediment core recovered close to the river mouth of the Congo Basin resulted in a temperature record for tropical

Africa representing the last 25,000 yr (Weijers et al., 2007a). The MBT-CBT proxy was also used to reconstruct continental air temperatures for the Arctic continent during the Palaeocene–Eocene thermal maximum (PETM; Weijers et al., 2007b) and showed a warming in MAT of ca. 8 °C. Finally, Schouten et al. (2008a) reconstructed the MAT for the Greenland landmass during the late Eocene and the early Oligocene. The MBT-CBT-derived temperatures were in agreement with other MAT reconstructions based on pollen assemblages and showed a long term cooling at the Eocene–Oligocene boundary.

Despite these promising results these proxies have only been empirically established and some uncertainty exists over their calibration and the impact of other environmental factors. For example, the MAT for each sample in the soil data set of Weijers et al. (2007c) was estimated from the closest possible weather station, and was not measured at the sampling sites themselves. Furthermore, the proxy is based on a large variety of different soils from all over the world, so multiple environmental factors could have potentially influenced the indices. The distribution of branched GDGTs in soils from Mt. Kilimanjaro in Tanzania, for example, changed with altitude and therefore with temperature. However, MBT-CBT-derived MAT values slightly overestimated the *in situ* measured annual MAT (Sinninghe Damsté et al., 2008), suggesting the possible influence of other environmental factors.

In this study, we have evaluated the direct impact of temperature on the MBT-CBT proxy by analyzing the branched GDGT distribution in geothermally heated soils around hot springs where soil temperature decreases with increasing distance from the spring. The ongoing geothermal heating results in a relatively constant soil temperature gradient over the annual cycle, while other soil properties and environmental parameters at each sampling site are similar.

2.2. Material and methods

2.2.1. Soil location and sampling

The samples were collected around two hot springs. Leonard's hot spring (41°36.086 N, 120°05.135 W) and "Ray's" hot spring (41°31.855 N, 120°04.966 W) are located in Surprise Valley in northwestern California, USA (*Table 2.2*). From the edge of Leonard's spring, soil samples were taken in a transect perpendicular to the spring at 10, 30, 60 and 150 cm distance. Similarly, soil samples were taken at 10, 20, 40, 80 and 250 cm distance from "Ray's" spring. Soil temperature was measured in the field at 10 cm depth with an Ama-Digit ad 20th digital thermometer. The samples, comprising the upper 10 cm, were collected with a small scoop and stored in geochemical bags. They were transported to the laboratory in an insolated cooling box at -80 °C and kept at -20 °C until analysis. Soil pH was determined with freeze dried samples in distilled water (10:25 w/v), after vigorous shaking of the mixture for 1 min and allowing the particles to settle for 30 min.

Table 2.1. Linear relationships of MBT and CBT indices with soil pH and temperature for global calibration set of Weijers et al. (*2007c*) and Californian hot springs.

| Relationship | Weijers et al. (*2007c*) | | Californian hot springs | |
	Equation	r^2	Equation	r^2
CBT vs. pH	CBT = 3.33 - 0.38×pH	0.70	CBT = 5.06 - 0.6×pH	0.76
MBT vs. T	MBT = 0.28 + 0.025×MAT	0.62	MBT = 0.052 + 0.019×Soil_T	0.65
CBT vs. T	-	-	CBT = 0.45 - 0.0007×Soil_T	0.001
MBT vs. pH	MBT = 1.35 - 0.13×pH	0.37	MBT = 1.65 - 0.14×pH	0.30

Table 2.2. Location, soil temperature, pH and branched GDGT concentrations of Californian hot springs.

| Location | Distance from spring (cm) | Soil temp. at 10 cm depth (°C) | soil pH | Branched GDGTs (ng/g dry wt soil)[a] | | | | | | | | | Total branched GDGT (μg/g dry wt soil) |
				Ia	Ib	Ic	IIa	IIb	IIc	IIIa	IIIb	IIIc	
	10	35.5	8.6	377	510	156	583	452	68	166	33	7	2.4
Leonard's hot spring	30	28.0	8.4	67	97	78	44	95	24	8	4	2	0.39
	60	19.6	8.6	18	48	26	36	73	18	7	6	2	0.23
	150	14.1	8.6	19	32	14	56	64	13	38	8	3	0.25
	10	41.6	7.0	123	43	37	18	5	2	2	0.3	1	0.23
	20	33.0	6.1	568	57	19	102	7	2	8	2	0.4	0.76
Ray's hot spring	40	25.2	6.9	79	6	1	48	3	n.d.[b]	10	1	1	0.15
	80	19.5	7.0	112	7	1	63	3	0.3	13	1	1	0.20
	250	12.4	7.7	1	0.2	0.5	3	0.5	n.d.	3	0.1	0.2	0.009

[a] Roman numbers refer to structures in *Fig. 2.1.*
[b] Below detection limit.

2.2.2. GDGT analysis

Samples were freeze dried and powdered with a mortar and pestle. Repeated extraction (3×) using a mixture of dichloromethane (DCM):MeOH 9:1 (v/v) with an accelerated solvent extractor (ASE 200, Dionex) at 7.6×10^6 Pa and 100 °C was performed for 5 min. The combined extracts were dried using a rotary evaporator under near vacuum. Remaining water was removed by dissolving the sample in DCM and passing it over a Na_2SO_4 column. The samples were dried under a N_2 flow and weighed, after which 0.15–1.0 μg of an internal C_{46} GDGT standard was added (cf. Huguet et al., 2006). The extracts were separated into apolar and polar fractions using an activated Al_2O_3 column and elution with hexane: DCM 9:1 (v/v) and DCM:MeOH 1:1 (v/v), respectively. After evaporation of the solvent under N_2, the polar fraction (containing the GDGTs) was ultrasonically dissolved in a hexane:propanol (99:1, v/v) mixture at a concentration of about 3 mg/ml and filtered over a 0.45 μm (Ø 4 mm) prior to analysis using high performance liquid chromatography/atmospheric pressure chemical ionization–mass spectrometry (HPLC/APCI–MS).

2.2.3. HPLC/APCI–MS

An Agilent 1100 series LC/MSD equipped with automatic injector and Chemstation software according to Hopmans et al. (2000), with minor modifications according to Schouten et al. (2007a), was used. Separation was achieved with an Alltech Prevail Cyano column (150×2.1 mm; 3 μm) with hexane: propanol (99:1, v/v), flow rate 0.2 ml/min, as eluent. Each sample was eluted isocratically for the first 5 min, then with a linear gradient to 1.6% propanol in 45 min. The injection volume was 10 μl. Single ion monitoring (SIM) of the M^+ ions of the internal C_{46} GDGT standard, crenarchaeol and the branched GDGTs (Weijers et al., 2007) were used for detection and quantification. Absolute quantification of the GDGTs was achieved by comparison of peak areas with that of the internal standard, and correcting for the different response factors (Huguet et al., 2006).

2.3. Results and discussion

2.3.1. Branched GDGT distribution in soil transects

Two transects were sampled from Leonard's hot spring and "Ray's" hot spring. These springs are fed by geothermally heated water and, consequently, warm the surrounding soil. As the geothermal influence decreases with distance from each spring, the soil temperature decreases with increasing distance from both springs (*Table 2.2*). Leonard's spring had a water temperature of 58 °C and soil temperature varied from 35.5 °C at 10 cm distance from the spring to 14.1 °C at 150 cm. The water temperature of "Ray's" spring was 89 °C and soil temperature varied from 41.6 °C to 12.4 °C at 10 and 250 cm distance, respectively. The soil pH around Leonard's spring was relatively constant, between 8.4 and 8.6, while that around "Ray's" spring varied from 7.0 at 10 cm from the spring to 6.1 at 20 cm, and increased to 7.7 at 250 cm (*Table 2.2*).

In all the soil samples branched GDGTs were detected. The concentrations ranged from 0.23 to 2.4 μg/g dry weight soil in the transect from Leonard's spring, and from 0.009 to 0.76 μg/g dry weight soil in the "Ray's" spring transect (*Fig. 2.2*). The highest concentrations were found close to the hot springs, at 10 cm for Leonard's, and at 20 cm distance for "Ray's". In the field we observed that, at these specific sites, the clayey soil had a greyish blue colour and a sulfurous smell, indicating anaerobic conditions. The high abundance of branched GDGTs at the sampling positions therefore seems in agreement with the idea that anaerobic soil bacteria are producers of these membrane lipids (Weijers et al., 2006a).

The distribution of the branched GDGTs changes with increasing distance from both springs (e.g. *Fig. 2.3*). At Leonard's, GDGT-I is relatively abundant compared to GDGT-II close to the spring, but GDGT-II becomes dominant in samples taken further away from the spring. The relative amount of GDGT-III increases from 30 cm to 150 cm from the spring, but remains the least abundant of all the GDGTs. At "Ray's", GDGT I is most abundant, except at 250 cm distance from the spring, where GDGT-II and GDGT-III are more abundant and occur in about equal amounts. This change in distribution pattern for both hot springs is in agreement with distributions observed globally, where branched GDGT distributions in soils from warm areas are dominated by GDGT-I, whereas the GDGT distribution in soils from temperate areas is dominated by GDGT-II (Weijers et al., 2007c).
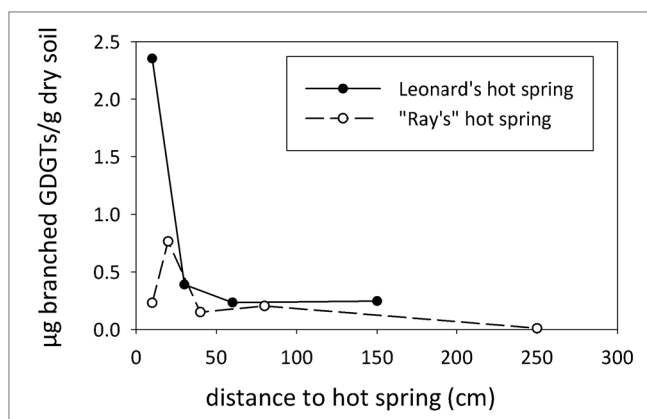
Fig. 2.2. Summed branched GDGT concentrations in soil transects from Leonard's hot spring and "Ray's" hot spring.

2.3.2. CBT and MBT indices

The changes in branched GDGT distribution around the springs were reflected in the MBT index (Eq. 2.1), i.e. for Leonard's spring MBT values changed from 0.44 close to the spring to 0.26 at the farthest sampling site. For "Ray's" spring the MBT index changed from 0.88 close to the spring edge to 0.21 at the site furthest from the spring. We compared the CBT and MBT indices Eqs. 1.1 and 1.2, with in situ pH and soil temperature. A linear relationship was found between CBT index and soil pH ($r^2=0.76$; *Fig. 2.4a; Table 2.1*). The fraction of the variance that was explained by this relationship is slightly greater than that reported by Weijers et al. (2007c), who found an explained variance of $r^2=0.70$ (*Table 2.1*). *In situ* soil temperature did not contribute significantly in explaining the variability in CBT (*Fig. 2.4b; Table 2.1*). To examine whether the CBT and pH for the hot spring data show the same type of relationship as the global soil calibration set of Weijers et al. (2007c), the homogeneity of slopes was tested and an analysis of covariance (ANCOVA) performed. We did not find a significant difference between both datasets, neither for the slope (homogeneity of slopes test, df=1, 119, $F=3.2$, $P=0.08$) nor the intercept (ANCOVA, df=1, 120, $F=0.26$, $P=0.61$).

In contrast to the CBT, the MBT index related to *in situ* soil temperature and, although to a much lesser degree, to soil pH (*Fig. 2.4c and d; Table 2.1*). This result is similar to that of Weijers et al. (2007c), who also showed linear relationships of MBT with MAT ($r^2=0.62$) and to a lesser degree soil pH ($r^2=0.37$; *Table 2.1*). The MBT–pH–temperature relationship of the hot spring dataset was statistically compared with the MBT–pH–MAT relationship of the global soil calibration set of Weijers et al. (2007c). The slopes of both relationships did not differ significantly (homogeneity of slopes test; slope versus pH: df=1,137, $F=0.56$, $P=0.46$; slope vs. temperature: df=1,137, $F=2.16$, $P=0.14$), but the intercept did (ANCOVA, df=1,139, $F=9.68$, $P=0.002$). The intercept for the hot spring dataset was lower than that of the global calibration set, which might be explained by the fact that we used in situ soil temperature for our data set, while MAT was used for the global soil calibration set. Alternatively, the difference might suggest the need for local calibrations rather than one global calibration, as also suggested by Sinninghe Damsté et al. (2008).
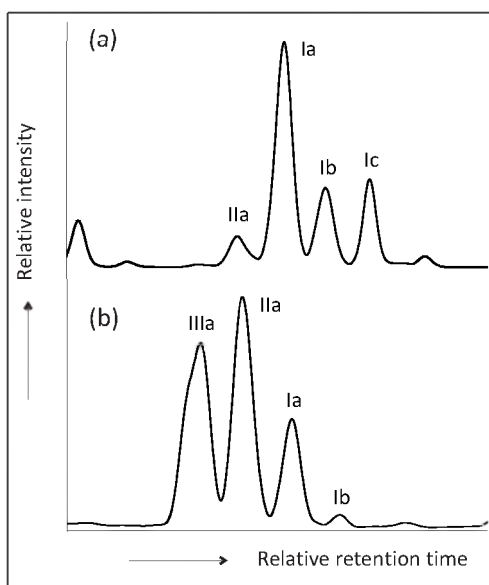
Fig. 2.3. HPLC/MS base peak chromatograms of soils in the vicinity of "Ray's" hot spring, showing differences in branched GDGT distributions in geothermally heated soils at a) 10 cm (41.6 °C) and b) 250 cm (12.4 °C) from the edge of the hot spring. Roman numerals refer to structures in *Fig. 2.1*.

2.3.3. Implications

Our results confirm the observations of Weijers et al. (2007c) that the CBT index of branched GDGTs is mainly determined by soil pH and that the MBT index is predominantly determined by both temperature and soil pH. In contrast to the approach taken by Weijers et al. (2007c), we analyzed a set of quite similar soils where in situ temperature and, to a lesser extent, soil pH were the main varying environmental parameters. Even though we found quite strong relationships, some scatter remains. Part of the scatter may be explained by the heterogeneity of soils in general. Despite the fact that we sampled similar soil types, there always remain some soil parameters and environmental factors that may vary to some degree (e.g. soil OM content, oxygen availability, texture, moistness, etc.) and which could play a role in the distribution of the branched GDGTs. Furthermore, it is unknown how fast the branched GDGT-producing organism(s) biosynthesize(s) the membrane lipids and adapt(s) them to changes in temperature or pH. Our results reflect the average branched GDGT abundance in the upper 10 cm at each site. Any variation in branched GDGT abundance or distribution pattern due to soil parameter changes within these 10 cm would therefore not be apparent and the exact soil depth at which the organisms thrive remains unclear. Finally, part of the GDGTs in the studied soils might be derived from fossil material as our extraction procedure likely yields core GDGTs from both living and fossil material. Constraining the exact depth of GDGT production and analyzing GDGTs derived only from living cell material, i.e. with a polar head group still attached, may therefore potentially further improve the relationship between MBT-CBT and soil temperature and pH.
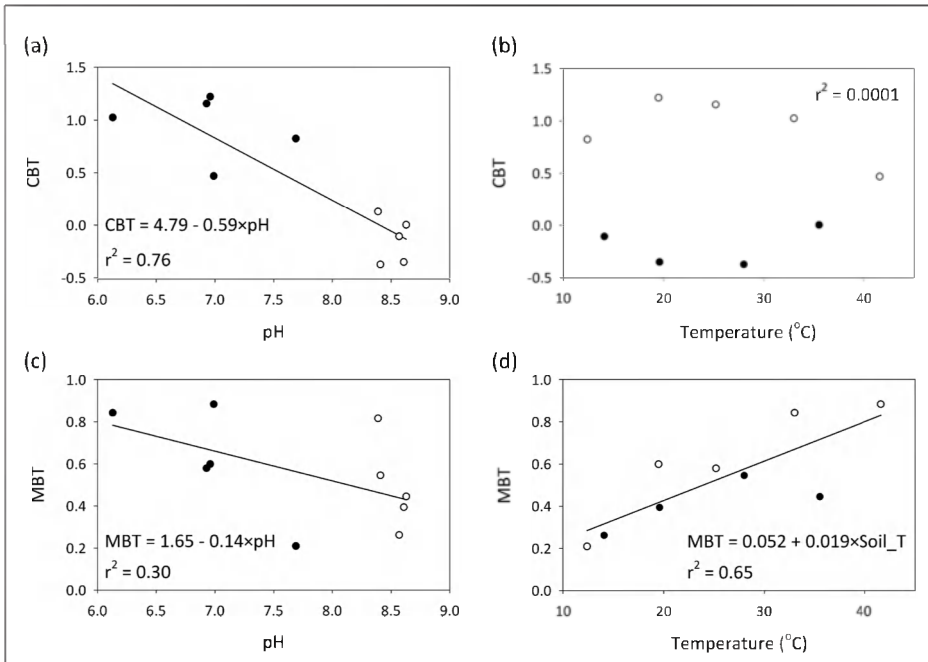
Fig. 2.4. Cross plots of cyclisation ratio of branched tetraethers (CBT) and methylation index of branched tetraethers (MBT) in soils vs. environmental parameters: a) CBT vs. soil pH, b) CBT vs. soil temperature, c) MBT vs. soil pH, and d) MBT vs. soil temperature.

2.4. Conclusions

Our study confirms the idea that the MBT index is mainly controlled by soil temperature and pH, and that the CBT index relates linearly with soil pH. The relationships found are similar to those of the global data set of Weijers et al. (2007c), although there is a statistically significant difference in the intercept of the relationship of MBT with temperature. This is possibly because we used *in situ* soil temperature rather than MAT. Our results generally support the use of the MBT-CBT indices as a tool for the reconstruction of continental palaeotemperatures and the determination of past soil pH.

Chapter 3

Influence of soil pH on the abundance and distribution of core and intact polar lipid-derived branched GDGTs in soil

Abstract

Branched glycerol dialkyl glycerol tetraether (GDGT) lipids occur in soils worldwide and are presumed to be produced by soil bacteria. They form the base of the MBT-CBT proxy (methylation of branched tetraethers/cyclisation of branched tetraethers) for palaeoclimate reconstruction. The degree of cyclisation and methylation, expressed in the CBT and MBT indices, has been shown to relate to soil pH, and to both temperature and soil pH, respectively. To evaluate the direct impact of soil pH on the abundance and distribution of branched GDGTs, either present as core lipids or derived from intact polar lipids (IPLs), long term (>45 years) soil pH manipulation plots, with a pH range of 4.5–7.5, were analyzed. The CBT index values of both core and IPL-derived branched GDGTs was significantly ($r^2=0.93$, $P=0.0004$ and $r^2=0.93$, $P=0.0005$, respectively) linearly related to actual soil pH, confirming the direct influence of pH on the distribution of branched GDGT. In contrast, the MBT index was only influenced to a minor extent by the changes in soil pH. Branched GDGT abundances decreased with increasing soil pH, supporting the idea that *Acidobacteria* may be a possible source of these orphan membrane lipids.

3.1 Introduction

Branched glycerol dialkyl glycerol tetraether (GDGT; *Fig. 3.1*) lipids are ubiquitous in soils and peats (Sinninghe Damsté et al., 2000; Weijers et al., 2006b), as well as in lake (e.g. Powers et al., 2004; Blaga et al., 2009) and coastal sediments (e.g. Schouten et al., 2000; Hopmans et al., 2004), where they originate mainly from river-transported soil organic matter and/or soil erosion. Branched GDGTs were first discovered and identified by Sinninghe Damsté et al. (2000) and are, based on the stereo chemistry of their glycerol moieties, thought to be of bacterial origin (Weijers et al., 2006a). The exact type of bacteria that synthesizes them is not known, though it has been suggested that species within the phylum *Acidobacteria* may be the source (Weijers et al., 2009).

The structures of branched GDGTs vary in the amount of methyl branches (4–6) attached to the alkyl chains, and can contain up to two cyclopentane moieties (Sinninghe Damsté et al., 2000; Weijers et al., 2006a). An empirical study based on a set of globally distributed soils has shown that the distribution of branched GDGTs in a soil is related to the annual mean air temperature (MAT) and the pH of that soil (Weijers et al., 2007c). The number of cyclopentane moieties in branched GDGTs relates to soil pH, whereas the number of methyl branches is related both MAT and soil pH. These relationships are expressed in the Cyclisation of Branched Tetraethers (CBT) index and the Methylation of Branched Tetraethers (MBT) index. The combination of these two indices allows it to be used as a proxy for palaeotemperature and past soil pH (e.g. Weijers et al., 2007a,b; Schouten et al., 2008a; Rueda et al., 2009).

Several studies have evaluated the applicability of the indices as a palaeoclimate proxy by comparing measured and estimated temperature and soil pH (e.g. Sinninghe Damsté et al., 2008; Rueda et al., 2009; Peterse et al., 2009a,b,c; Tierney and Russell, 2009; Tyler et al., 2010). Although these studies generally support the empirical relationship of soil pH with the degree of cyclisation of branched GDGTs, the direct impact of soil pH on the MBT and CBT indices has not been tested. In this study, we analyzed the abundance and distribution of branched GDGT in soils from longterm soil pH manipulation plots, where the soils have been kept at constant pH in the range 4.5–7.5 for almost 50 years. Climatic parameters and other soil properties that may influence the branched GDGTs were generally constant along the pH transect (Kemp et al., 1992), leaving soil pH as the only varying control on the abundance and distribution branched GDGTs in the plots. We analyzed branched GDGTs present as core lipid (CL-derived GDGTs), presumed to be of fossil origin, as well as those derived from intact polar lipids (IPL-derived GDGTs), presumed to be from recently active organisms, following the approach of Pitcher et al. (2009).

3.2. Material and methods

3.2.1. Field site and sample collection

Soil samples were obtained from pH-manipulated plots at the Scottish Agricultural College, Craibstone, Scotland (57°11'N, 2°12'W) in September 2007. The soil pH of the plots has been maintained since 1961 with a range of 4.5–7.5 at 0.5 pH unit intervals by addition of either lime or aluminium sulfate (Kemp et al., 1992). The sandy loam soil is under a 8 year crop rotation cycle to minimize the potential effects of vegetation. Replicate samples were taken from the upper 10 cm of each pH plot, passed through a 3.35 mm mesh sieve and stored at -20 °C until further analysis. Soil pH was measured in 1:2 (w/v) soil:deionised water suspensions after shaking (15 min) and settling for 30 min.
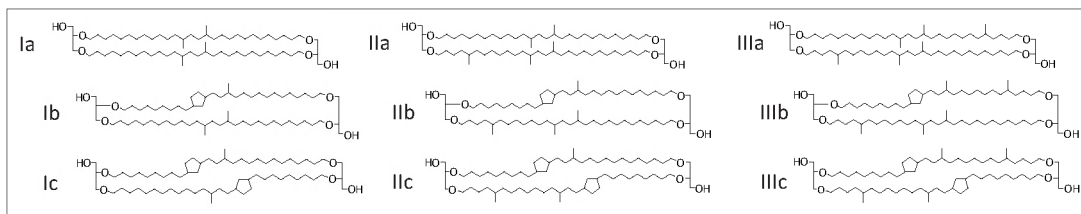
Fig. 2.1. Molecular structures of branched GDGTs.

3.2.2. GDGT analysis

Duplicate soil samples from each pH-controlled plot were freeze dried and extracted (3×) using a modified Bligh and Dyer technique. A solvent mixture (5 ml/g soil) of MeOH:dichloromethane (DCM): phosphate buffer at pH 7.4 (2:1:0.8, v/v/v) was added to ca. 3 g sample in a centrifuge tube and placed in an ultrasonic bath for 10 min. The extract was collected after spinning down the sample. DCM and phosphate buffer were added to the combined extracts to a new volume ratio of 1:1:0.9 (v/v/v) to achieve phase separation. Extract (DCM phase) and residue (MeOH/phosphate buffer phase) were separated by centrifuging at 2500 rpm for 2 min. The DCM phase, containing the GDGTs, was collected in a round bottomed flask. The residue was rinsed twice with DCM, and the combined DCM phases were reduced using a rotary evaporator under near vacuum. The extract was passed over extracted cotton wool to remove any remaining soil particles and completely dried under a N_2 flow.

The extracts were separated into CL and IPL GDGT fractions according to Oba et al. (2006) and Pitcher et al. (2009), except that a hexane:ethyl acetate (1:1, v/v) mixture was used to obtain the CL fractions, and that IPL fractions were retrieved by flushing the silica column with MeOH. A C_{46} GDGT internal standard was added to both CL and IPL fractions following Huguet et al. (2006). The IPL fractions were subjected to acid hydrolysis to cleave the head groups and release the core lipids (hereafter IPL-derived GDGTs; cf. Pitcher et al., 2009).

All fractions were dissolved in hexane:isopropanol (99:1, v/v), filtered over a 0.45 µm PTFE filter, and concentrated to about 3 mg/ml prior to analysis using high performance liquid chromatography/ atmospheric pressure chemical ionization-mass spectrometry (HPLC/APCI-MS) with an Agilent 1100 series LC/MSD SL instrument according to Schouten et al. (2007a), with minor modifications as described by Peterse et al. (2009a). The injection volume was 10 µl for all samples, and selective ion monitoring of the $[M+H]^+$ ions was used to detect and quantify the different GDGTs. Absolute quantification was done according to Huguet et al. (2006). The CBT and MBT indices were calculated as follows (Weijers et al., 2007c):

$$CBT = -LOG ([Ib+IIb]/Ia+IIa]) \qquad (3.1)$$
$$MBT = [Ia+Ib+Ic]/[Ia+Ib+Ic+IIa+IIb+IIc+IIIa+IIIb+IIIc] \qquad (3.2)$$

Roman numerals refer to the structures in *Fig. 3.1*. Soil pH was inferred from CBT using the empirical equation based on the global calibration set of Weijers et al. (2007c):

$$CBT = 3.33 - 0.38 \times pH \qquad (3.3)$$

The reported numbers represent the averaged values for the duplicate soil samples per plot.

3.3. Results and discussion

3.3.1. Abundance of branched GDGTs

Both CL- and IPL-derived branched GDGTs were found in all the plots. The amounts of total CL-GDGTs in the pH-manipulated plots vary between 300 and 640 ng/g soil dry wt, and are generally higher in the low pH soil plots than in those with a higher pH (*Fig. 3.2a*). The amounts of IPL-derived branched GDGTs follow the same trend with soil pH as their CL counterparts, although the average amounts are about 4–10 times lower than those of the CL branched GDGTs (30–150 ng/g soil dry wt; *Fig. 3.2a*). In each plot, IPL-derived GDGTs comprise only 9–19% of the total pool of branched GDGTs. This implies that the largest part of branched GDGTs in soil is not derived from living cells, but is present as fossil branched GDGTs, as recently also suggested by Weijers et al. (2009) and Huguet et al. (2010a).
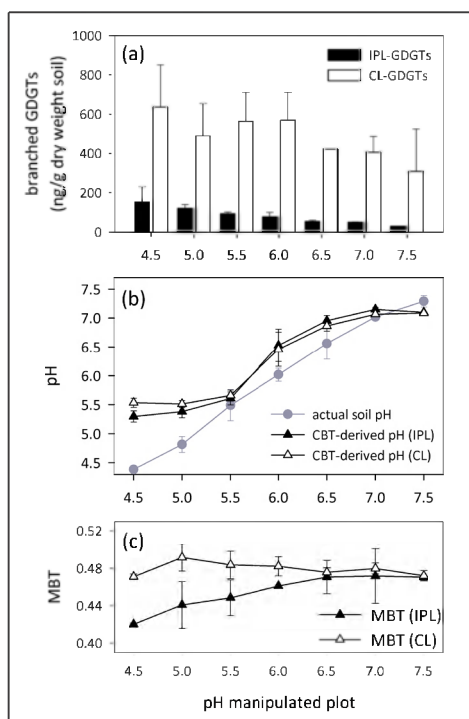
Fig. 3.2. a) Average amounts of CL- and IPL-derived branched GDGTs, b) actual soil pH and CBT-derived pH and c) MBT index values for the soils of long term pH manipulation plots. Error bars are the standard deviation of the mean of duplicate field soil samples for branched GDGT amounts, CBT-derived pH, and MBT index values, and triplicate field soil samples for soil pH. In some cases, the standard deviation in smaller than the symbol.

The decreasing trend in branched GDGT concentration (*Fig. 3.2a*) seems to be principally caused by the variation in pH, as other parameters, such as carbon and nitrogen contents or soil moisture, do not significantly change along the pH transect (Meharg and Killham, 1990; Nicol et al., 2008). This trend has also been observed in the global soil calibration set of Weijers et al. (2007c), where more acidic soils contained the highest amounts of branched GDGTs. Based on a comparison of branched GDGT abundances with 16S rRNA genes in a soil profile from the Saxnäs Mosse peat bog, Sweden, Weijers et al. (2009) suggested that branched GDGTs are likely produced by *Acidobacteria*. The latter are ubiquitous and, after *Proteobacteria*, are the most abundant bacterial phyla in soil (Janssen, 2006). Indeed, the abundance of *Acidobacteria* in soil has been shown to increase with decreasing pH (Saît et al., 2006; Männistö et al., 2007; Hartman et al., 2008; Lauber et al., 2009; Jones et al., 2009), similar to the relationship of branched GDGTs with soil pH. A large scale study of the variation in soil bacterial abundance with changing soil pH showed that the abundance of several soil bacterial phyla correlate with soil pH, but that only *Acidobacteria* abundance decrease with increasing soil

pH (Lauber et al., 2009). Of the 26 distinct *Acidobacteria* subdivisions (Barns et al., 2007), divisions 1, 3, 4, and 6 appear to be most abundant in soil (Barns et al., 1999; Janssen, 2006; Jones et al., 2009), but only relative abundance of subdivision 1 shows a negative relationship with soil pH (Sait et al., 2006; Eichorst et al., 2007; Jones et al., 2009). This suggests that the organisms that produce branched GDGTs may originate from this subgroup. Recently, Oppermann et al. (2010) suggested that producers of branched GDGTs are likely to be heterotrophic organisms, as the $\delta^{13}C$ values of branched GDGT-derived C_{30} and C_{31} alkanes mimic those of the plant derived lipids in the same soil. Currently, cultured representatives of only 5 of the 26 *Acidobacteria* subdivisions exist, most of which are heterotrophs (Ward et al. (2009) and references therein), in agreement with the observation of Oppermann et al. (2010). However, the two *Acidobacteria* cultures that have been analyzed so far, i.e. *Acidobacterium capsulatum* (subgroup 1) and *Holophaga foetida* (subgroup 8), did not contain any branched GDGTs (Weijers et al., 2009).

3.3.2. CBT and MBT indices

The distribution of branched GDGTs changes substantially along the pH transect; both CL- and IPL-derived branched GDGTs with cyclopentane moieties (e.g. Ib, IIb) become more abundant with increasing soil pH, relative to those without cyclopentane moieties (*Fig. 3.3a and b*). The decrease in amount of cyclopentane moieties with lower soil pH supports the empirical relationship between soil pH and the amount of branched GDGTs with cyclopentane moieties found for the global soil calibration set (Weijers et al., 2007c). CBT index values, calculated according to Eq. 3.1, linearly relate with measured actual soil pH ($r^2=0.93$, $P=0.0004$ for CL and $r^2=0.93$, $P=0.0005$ for IPL-derived branched GDGTs). Based on the CBT indices for both CL and IPL-derived fractions, soil pH of each pH manipulated plot was calculated according to Eq. 3.3. CBT-derived pHs generally match well with the measured actual soil pH of each manipulated plot (*Fig. 3.2b*), except at low soil pH (plots with pH 5.0 and 4.5) where the CBT derived pH overestimates the actual soil pH. Possibly, a threshold is reached at pH 5.0, where no further adaptation of the cell membranes to lower soil pH occurs, although lower CBT values are observed in natural soils with pH values as low as 3.3 in the global soil calibration set (Weijers et al., 2007c). Remarkably, the calculated soil pH values for the CL- and IPL-derived fractions in the soils of the pHmanipulated plots show no apparent differences between them. This implies that, in this case, the fossil pool of branched GDGTs has a turnover time of <45 years.
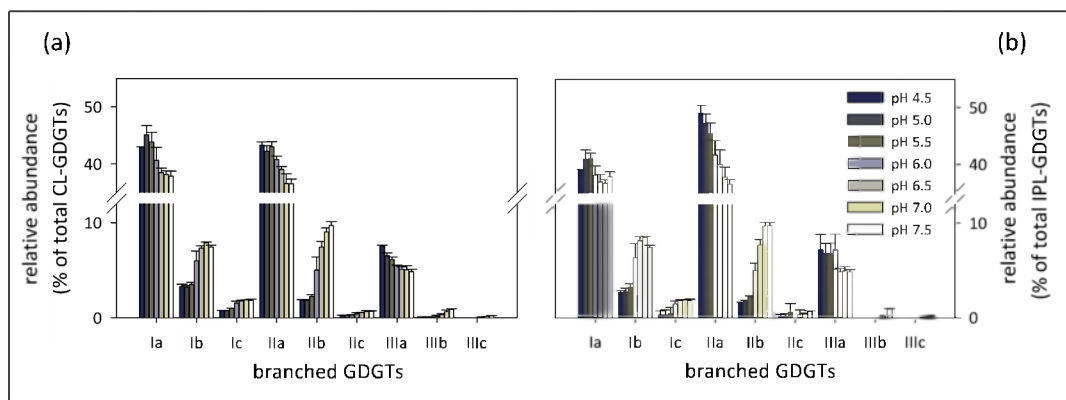
Fig. 3.3. Average distribution of a) CL- and b) IPL-derived branched GDGTs in soils of long term pH manipulation plots. Error bars refer to the standard deviation of the mean of duplicate field soil samples. Roman numerals refer to structures in *Fig. 3.1*.

The controlled character of the Craibstone pH-manipulated plots (with all other measured environmental parameters showing little variation and no gradient) thus unambiguously confirms that pH is an important factor controlling the degree of cyclisation of branched GDGTs in these soils. Likely, the presence of cyclic moieties in lipids in cell membranes influences the permeability and fluidity of the membranes. Generally, a lower membrane permeability helps to protect cells against low pH (Beales, 2004; Yuk and Marshall, 2004). Indeed, archaea containing isoprenoid GDGTs have been shown to increase the amount of cyclopentane moieties in their membranes at high pH (Shimada et al., 2008). Thus, the introduction of cyclopentane moieties in branched GDGTs may increase membrane permeability at higher soil pH (Weijers et al., 2007c).

The global soil calibration also shows that the amount of methyl branches on the alkyl chains of the branched GDGTs, quantified in the MBT index, relates to soil pH, although to a far lesser extent than the CBT index ($r^2 = 0.70$ for the relationship of CBT with pH and $r^2 = 0.37$ for the relationship of MBT and pH; Weijers et al., 2007c). In the manipulated field plots, the abundance of GDGTs Ia, IIa and IIIa decrease with increasing pH (*Fig. 3.3a and b*). However, the MBT index in the pH-manipulated plots remains relatively constant throughout the pH range, with values between 0.47 and 0.49 based on CL-, and between 0.42 and 0.47 based on IPL-derived GDGTs (*Fig. 3.2c*). Only the MBT index based on IPL-derived branched GDGTs shows a weak increase with increasing soil pH, which is, however, opposite to the relationship of MBT and pH for the global soil calibration set of Weijers et al. (2007c). This suggests that soil pH might have only a relatively minor impact on the MBT index at this site.

3.4. Conclusions

The amounts of branched GDGTs decreased with increasing soil pH in long term controlled experimental plots, in agreement with the hypothesis that *Acidobacteria* may be producers of branched GDGTs. A higher number of cyclopentane moieties is introduced in the membrane lipids with increasing soil pH, which is reflected in the CBT index. Consequently, CBT-derived pH resembles the actual soil pH of each manipulated plot, except below pH 5.0, where actual soil pH is overestimated. The changes in soil pH only have a minor impact on the MBT index.

Chapter 4

Assessment of soil *n*-alkane δD and branched tetraether membrane lipid distributions as tools for paleoelevation reconstruction

Francien Peterse, Marcel T.J. van der Meer, Stefan Schouten, Guodong Jia, Jort Ossebaar, Jord Blokker, Jaap S. Sinninghe Damsté, 2009. *Biogeosciences* 6, 2799-2807.

Abstract

$\delta^{18}O$ values of pedogenic minerals forming from soil water are commonly used to reconstruct paleoelevation. To circumvent some of the disadvantages of this method, soil *n*-alkane δD values were recently proposed as a new tool to reconstruct elevation changes, after showing that soil *n*-alkane δD values track the altitude effect on precipitation δD variations (r^2=0.73 along Mt. Gongga, China). To verify the suitability of soil *n*-alkane δD values as a paleoelevation proxy we measured the δD of soil *n*-alkanes along Mt. Kilimanjaro (Tanzania). At midslope, soil *n*-alkane δD values are possibly influenced by the present precipitation belt, causing D-depletion in precipitation, and hence in the soil *n*-alkanes. Consequently, soil *n*-alkane δD values do not linearly relate with altitude (r^2=0.03), suggesting that, in this case, they can not serve as an unambiguous proxy to infer past elevation changes. In contrast, it was recently shown that the MBT-CBT temperature proxy, which is based on the distribution of branched glycerol dialkyl glycerol tetraether (GDGT) membrane lipids, is linearly related with MAT, and thus altitude (r^2=0.77), at Mt. Kilimanjaro. This suggests that this proxy may be more suitable for paleoelevation reconstruction for this region. However, application of the MBT-CBT proxy on the altitude gradient along Mt. Gongga showed that, although the MBT-CBT-derived temperature lapse rate (-5.9 °C/1000 m) resembles the measured temperature lapse rate (-6.0 °C/1000 m), there is a relatively large degree of scatter (r^2=0.55). Our results thus show that both proxies can be subject to relatively large uncertainties in their assessment of past elevation changes, but that a combination of the soil *n*-alkane δD and MBT-CBT proxies can likely result in a more reliable assessment of paleoelevation.

4. 1 Introduction

Stable isotope values of authigenic and pedogenic minerals are a common tool for the reconstruction of paleoelevation changes in mountain ranges (e.g. Poage and Chamberlain, 2001; Rowley and Garzione, 2007, and references therein). $\delta^{18}O$ and δD values of precipitation and meteoric water become more negative with increasing elevation due to rain-out caused by the decrease in temperature and relative humidity, the so-called "altitude effect" (Dansgaard, 1964), a trend that has been recognized in almost all mountain belts of the world (Poage and Chamberlain, 2001). The present day stable oxygen isotope composition of precipitation or meteoric water is well documented in e.g. authigenic carbonates or soil water. This relationship can be used to infer elevation changes of mountain ranges (e.g. Poage and Chamberlain, 2001; Rowley and Garzione, 2007, and references therein). Precipitation and surface water isotopic composition along an altitude gradient provides an isotopic lapse rate that can be used as a reference line for the reconstruction of historical elevation changes. By comparing the reference line with the isotopic values of pedogenic minerals that have formed in the past, such as carbonates, clays, or volcanic glass that, at the time of formation, have formed in equilibrium with surface waters, a paleoelevation record can be obtained. However, there are some disadvantages in using this method. For example, the obtained records are generally very smoothed due to the low formation rate of carbonates, and show a millennial signal at best (Rowley and Garzione, 2007). Furthermore, the mineral isotopic composition can be influenced by different source waters and temperature variations during formation (Dettman and Lohmann, 2000; Rowley and Garzione, 2007). Also, diagenesis and recrystallization can modify the original isotopic composition of pedogenic minerals (Morrill and Koch, 2002; Garzione et al., 2004). Thus, further development of paleoelevation proxies is needed to reduce uncertainties in paleoelevation reconstructions, including developing and validating new proxies, and combining these different proxies in multi-proxy applications.

Recently, Jia et al. (2008) explored the suitability of soil n-alkane δD values as a proxy for paleoelevation as it has been shown previously that hydrogen isotope ratios of leaf wax n-alkanes strongly relate to that of environmental water (e.g. Sessions et al., 1999; Sauer et al., 2001; Sachse et al., 2004; Smith and Freeman, 2006; Rao et al., 2009) and that the hydrogen isotopic composition of environmental water depends on altitude (Dansgaard, 1964). Indeed, the n-alkane δD values for surface soils along the eastern slope of Mt. Gongga (China) record the altitude effect on the precipitation δD well, showing a decreasing trend with altitude (Jia et al., 2008). Based on the relation of n-alkane δD with altitude on the Tibetan Plateau, the uplift of this plateau during the late Eocene and early Miocene was recently reconstructed, the result being consistent with a paleoelevation reconstruction based on carbonate $\delta^{18}O$ (Polissar et al., 2009). An advantage of using n-alkanes hydrogen isotope values instead of those of pedogenic minerals, is that elevations can also be determined at sites where no carbonates are present, but where organic material has been preserved. Furthermore, the production of plant lipids is a relatively short-term process compared to the formation and precipitation of minerals, which makes it possible to increase the resolution of the paleoelevation records. Finally, the uncertainties from the temperature effect during mineral formation that has to be taken into account when using mineral isotope values (Poage and Chamberlain, 2001) can be largely avoided by the use n-alkane δD data, as the apparent isotopic fractionation between water and plant lipids during lipid production is seemingly less temperature dependent than that during carbonate precipitation (Jia et al., 2008). However, a disadvantage of this proxy is that the apparent fractionation may be influenced by physical or vegetation changes along an altitudinal transect, so that soil n-alkane δD values can only be applied as a paleoelevation proxy when the apparent hydrogen isotope fractionation between precipitation

and plant wax *n*-alkanes appears to be independent of elevation, or when changes in apparent fractionation can be reconstructed (Jia et al., 2008).

An alternative method to reconstruct paleoelevation, independent of precipitation, could be the MBT-CBT temperature proxy, which is based on the membrane composition of a yet unknown group of bacteria that occurs ubiquitously in soils worldwide (Weijers et al., 2007c). The membranes of these bacteria are composed of branched glycerol dialkyl glycerol tetraether (GDGT; *Fig. 4.1*) lipids, of which the molecular structure can vary in the amount of methyl branches (4 to 6) attached to the alkyl chain, and in the number of cyclopentane moieties (up to 2) (Sinninghe Damsté et al., 2000; Weijers et al., 2006a). An empirical study showed that the amount of cyclopentane moieties linearly relates with soil pH, whereas the degree of methylation shows a relation with both soil pH and annual mean air temperature (MAT; Weijers et al., 2007c). These relations are expressed in two indices, the Cyclisation of Branched Tetraether (CBT) and the Methylation of Branched Tetraether (MBT) index. By analyzing the distribution of branched GDGTs, which can be determined from the same lipid extract as used for *n*-alkane δD measurements, and using the combination of the CBT and MBT indices, changes in past environmental conditions can be reconstructed (Weijers et al., 2007a, b; Schouten et al., 2008a). Sinninghe Damsté et al. (2008) showed that the distributions of branched GDGTs in surface soils from Mt. Kilimanjaro (Tanzania) change with temperature, and thus with altitude, despite variations in e.g. precipitation or soil type. The temperature lapse rate that was calculated using the MBT-CBT proxy (-6.9±1.0 °C/1000 m; Sinninghe Damsté et al., 2008), approached the lapse rate that was measured in situ (-5.3 °C/1000 m; Hemp, 2006b). Branched GDGTs are generally well preserved, and have been found in sediments as old as the Palaeocene-Eocene thermal maximum (~55 Ma; Weijers et al., 2007b), suggesting that they may be suitable components for paleoelevation studies, when applied to paleosols, for example.

Although these paleoelevation proxies seem promising, more studies are needed to examine potential complicating factors. Both soil *n*-alkane δD and the MBT-CBT proxy are only indirect recorders of altitude, i.e. through the altitude effect on precipitation δD and temperature lapse rate, respectively, and thus other factors besides altitude can potentially affect these proxies. We, therefore, tested these two organicgeochemical proxies on two altitudinal transects to assess their suitability for paleoelevation reconstructions. Soil *n*-alkane δD values were measured along the slope of Mt. Kilimanjaro, and the MBT-CBT temperature proxy was applied along the slope of Mt. Gongga. The same samples were previously analyzed for the MBT-CBT proxy of Mt. Kilimanjaro soils and for soil *n*-alkane δD analysis of Mt. Gongga by Sinninghe Damsté et al. (2008) and Jia et al. (2008), respectively.
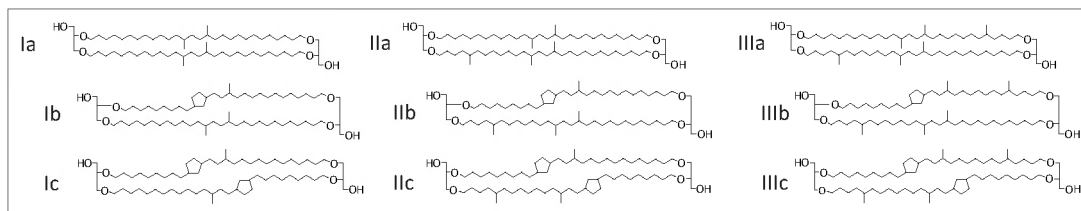
Fig. 2.1. Molecular structures of branched GDGTs.

4.2. Material and methods

4.2.1. Altitudinal transects and soil samples

Mt. Kilimanjaro is located 300 km south of the equator in Tanzania on the border with Kenya (3°S, 37°E). Mt. Kilimanjaro is an ancient volcano, rising from the 700 m elevated savanna plains to a height of 5895 m, which makes it the highest mountain in Africa. Precipitation and temperature vary with altitude and the degree of exposure to wind from the Indian Ocean. Annual precipitation is higher on the southern slope than on the northern slope.

Due to its location close to the equator Mt. Kilimanjaro experiences two distinct rainy seasons; long rains from March to May, and short, but heavy rains in November and December (Hemp, 2006a, b). Rainfall data for the southern slope show an increase in precipitation from about 1900 mm/y at 1400 m to a maximum of about 2700 mm/y at 2200 m altitude, and then decreasing again towards 50% of the maximum rainfall at 3000 m, and only 20% at 4000 m (Hemp, 2006a, b). MAT is 23.4 °C at about 800 m, and decreases linearly upslope with a lapse rate of -5.3 °C/1000 m to a MAT of -7.1 °C at the top (Hemp, 2006b). Also the vegetation on Mt. Kilimanjaro shows a zonated pattern along the slope (Hemp, 2006a, b). Soil n-alkane δD analysis were performed on the same soils as used by Sinninghe Damsté et al. (2008), who sampled 16 surface soils between 1700 m and 3300 m along the southeastern slope of Mt. Kilimanjaro in September 2006. The soil pH for this altitudinal transect ranges from 3.8 to 6.6 (Hemp, 2006b).

Mt. Gongga (7556 m) is located in the Daxue Mountain Range on the eastern side of the Tibetan plateau in Sichuan Province, southwest China (30°N, 102°E). The eastern slope of Mount Gongga drops 6450 m in altitude in only 29 km horizontal distance into the Dadu River valley at 1100 m, the western slope blends into the Tibetan Plateau at 3000–3500 m (Thomas, 1997). Climate characteristics for the eastern and western side of the mountain are substantially different; the east side is influenced by Pacific air masses, whereas the west side is under influence of the Southwest Monsoon. This results in a relatively cool and humid climate with heavy precipitation on the east side of the mountain, and a drier and warmer climate on the west side. Annual precipitation increases with altitude on both sides, with the major part falling during the hottest summer months (May to October; Thomas, 1997, 1999). Weather station data show that MAT declines upward from 11.8 °C at 1600 m to 3.4 °C at 3000 m (Jia et al., 2008). The climatic changes along the altitudinal gradient cause variations in soil and vegetation types, showing a vertical zonated pattern along the slope (Thomas, 1999; Zhong et al., 1999). The soils used for branched GDGT analysis are similar to the ones used in Jia et al. (2008). Our sample set comprises of 36 surface horizons (0–5 cm) along an altitude gradient from 1180 m to 3819 m on the eastern slope of Mt. Gongga, and was sampled in late May 2004. The soils were stored frozen upon arrival in the laboratory in China, and freeze dried before shipping to the laboratory at NIOZ. The pH of the soils was measured in the laboratory in China in a 1:2.5 soil:water (w/v) mixture.

4.2.2. Soil extractions

All soils were freeze dried and powdered with mortar and pestle prior to extraction (3 times for 5 min) with a solvent mixture of dichloromethane (DCM):MeOH (9:1, v/v) using an accelerated solvent extractor (ASE 200, Dionex) at 100 °C and 7.6×10^6 Pa. Each total extract was dried using a rotary evaporator under near vacuum. The extracts were dissolved in DCM and passed over a Na_2SO_4 column to remove all remaining water, dried again under a N_2 flow, and weighed, depending on which 0.1–1.0 µg of a C_{46}

GDGT standard was added to the extracts (cf. Huguet et al., 2006). The extracts were separated by passing them over an activated Al_2O_3 column using hexane:DCM (9:1, v/v) and DCM:MeOH (1:1, v/v) to obtain an apolar and polar fraction, respectively.

4.2.2.1 Soil n-alkane δD analysis

The apolar fractions were each passed over a small silver nitrate impregnated silica column using hexane to further separate the *n*-alkanes. The *n*-alkane containing fractions were analyzed by gas chromatography (GC) using an Agilent 6890 gas chromatograph with a flame ionization detector using a fused silica capillary column (25 m×0.32 mm) coated with CP Sil-5 (film thickness=0.12 μm) with helium as carrier gas. The fractions were dissolved in *n*-hexane, and injected on-column at 70 °C. The oven was programmed to subsequently increase the temperature to 130 °C with 20 °C/min, and then with 4 °C/min to 320 °C at which it was held isothermal for 10 min. Compound-specific hydrogen isotopic compositions of the *n*-alkanes were determined by GC/thermal conversion/isotope ratio monitoring mass spectrometer using a Thermo Electron DELTAPlus XL mass spectrometer. GC conditions were similar to conditions for GC analysis except that the film thickness of the CPSil 5 column was 0.4 μm and that a constant flow of He was used at 1.5 ml/min. Compounds were pyrolyzed at 1450 °C in an empty ceramic tube, which was preactivated by a methane flow of 0.5 ml/min for 5 min. H^+_3-factors were determined daily on the isotope mass spectrometer and decreased slowly from 8.5 to 6 over a 6 week period. H_2 gas with known isotopic composition was used as reference and a mixture of C_{16}–C_{32} *n*-alkanes of known isotopic composition (ranging from -42‰ to -256‰ vs. VSMOW) was used to monitor the performance of the system. The average offsets between the measured hydrogen isotopic composition of the C_{16}–C_{32} *n*-alkanes and their values determined off-line were generally 5‰ or less. Analyses were done at least in duplicate and the reproducibility was always better than 7‰. A squalane standard was co-injected with every sample and its average value was -170.6±3.5‰, which compared favorably with its off-line determined value of -170‰.

4.2.2.2 Branched GDGT analysis

The polar fractions, containing the branched GDGTs, were dried under N_2, ultrasonically dissolved in a hexane:isopropanol (99:1, v/v) mixture, and filtered over a 0.45 μm PTFE filter. All polar fractions were concentrated to about 3 mg/ml prior to analysis by high performance liquid chromatography/atmospheric pressure chemical ionization-mass spectrometry (HPLC/APCI-MS) on an Agilent 1100 series LC/MSD
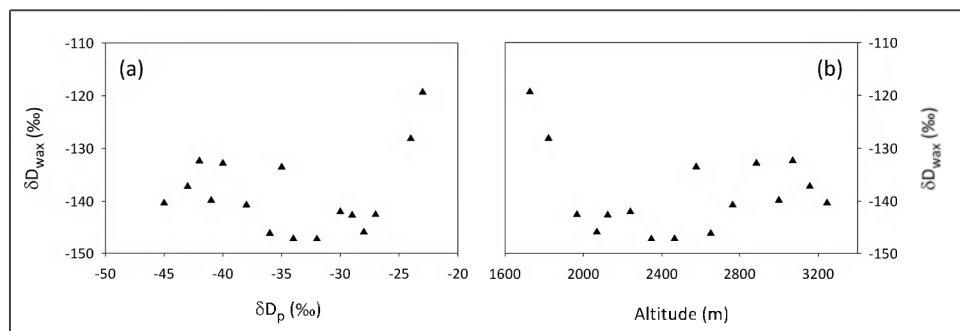
Fig. 4.2. Relations of δD_{wax} with a) modeled δD_p and b) altitude in ‰ versus WSMOW along the southeastern slope of Mt. Kilimanjaro.

SL according to Schouten et al. (2007a), with minor modifications. Briefly, separation of the branched GDGTs was achieved on an Alltech Prevail Cyano column (150 mm×2.1 mm; 3 μm). The compounds were eluted isocratically with 90% A and 10% B for 5 min (flow rate 0.2 ml/min), and then with a linear gradient to 16% B for 34 min, where A=hexane and B=hexane:isopropanol (9:1, v/v). For all samples, the injection volume was 10 μl. Selective ion monitoring of the $[M+H]^+$ was used to detect and quantify the different GDGTs, and absolute quantification of each compound was achieved by calculating the area of its corresponding peak in the chromatogram, comparing it with the peak area of the internal standard, and correcting it for the different response factors (cf. Huguet et al., 2006).

The CBT and MBT indices were calculated according to the following equations:

$$CBT = -LOG\ ([Ib+IIb]/[Ia+IIa]) \tag{4.1}$$
$$MBT = [Ia+Ib+Ic]/[Ia+Ib+Ic+IIa+IIb+IIc+IIIa+IIIb+IIIc] \tag{4.2}$$

Roman numerals refer to the structures in *Fig. 4.1*. The soil pH and MAT were calculated using the empirical equations based on the global calibration set given by (Weijers et al., 2007c):

$$CBT = 3.33 - 0.38×pH \tag{4.3}$$
$$MBT = 0.122 + 0.187×CBT + 0.020×MAT \tag{4.4}$$

Average errors based on duplicate analysis for MBT and CBT on 12 samples are 0.003 and 0.007, respectively.

4.3. Results and discussion

4.3.1. Soil n-alkane δD values along Mt. Kilimanjaro

Soil *n*-alkanes along Mt. Kilimanjaro range from C_{27} to C_{35}, and exhibit an odd-over-even predominance, as is represented by the carbon preference index (CPI) of the *n*-alkanes, which ranges from 5.5 to 15.8. The average chain length (ACL) of the C_{27}-C_{35} *n*-alkanes along the analyzed transect varies between 30.2 and 32.0. C_{29}, C_{31}, and C_{33} *n*-alkanes are most abundant in the soils, and their hydrogen isotope values range from -154‰ to -126‰ for the C_{29}, from -149‰ to -113‰ for the C_{31}, and from -144‰ to -116‰ for the C_{33} *n*-alkane (*Table 4.1*).

To test if the δD of higher plant *n*-alkanes on Mt. Kilimanjaro records precipitation δD (δD_p), one would ideally use directly measured δD_p values. However, for the altitudes that our soil samples were derived from, these data were not available. We therefore used modeled δD_p values according to Bowen and Revenaugh (2003) and Bowen (2009) (*Table 4.1*), noting that only a low density of stations feed the model database for this region. Following the approach of Jia et al. (2008), we plotted the weighed mean of the δD of the most common *n*-alkanes (C_{29}, C_{31} and C_{33}; δD_{wax}) against modeled δD_p and altitude (*Fig. 4.2a, b*). This shows that δD_{wax} values do not strongly correlate with the modeled δD_p, as was found for Mt. Gongga (Jia et al., 2008).

There are several environmental parameters that can potentially have influenced the isotopic values of the *n*-alkanes or precipitation, and may thus explain the absence of the linear relation with altitude. Soil *n*-alkane isotopic values may for example have been influenced by changes in vegetation type (Rommerskirchen et al., 2006), along the slope. However, the absent relation is most likely to be explained by the

Table 4.1. δD values for soil *n*-alkanes and modeled δD values of precipitation (‰) along the southeastern slope of Mt. Kilimanjaro.

Altitude (m)	Soil *n*-alkane				
	$\delta D_{C29} \pm SD$[a]	$\delta D_{C31} \pm SD$	$\delta D_{C33} \pm SD$	δD_{wax}[b]	δD_p[c]
1727	-114±6	-118±2	-129±6	-119.4	-23
1822	-135±2	-125±0	-129±4	-128.2	-24
1967	-156±1	-138±1	-134±2	-142.6	-27
2068	-152±0	-144±2	-137±2	-145.9	-28
2124	-150±1	-140±3	-139±1	-142.7	-29
2239	-154±1	-136±0	-130±2	-142.0	-30
2346	-152±1	-144±1	-144±1	-147.2	-32
2464	-151±2	-147±1	-140±1	-147.2	-34
2578	-139±3	-143±1	-188±1	-133.6	-35
2652	-144±3	-149±1	-137±3	-146.1	-36
2764	-149±4	-143±1	-121±0	-140.8	-38
2885	-138±2	-136±2	-125±2	-132.9	-40
2999	-144±4	-143±1	-135±0	-139.9	-41
3070	-154±3	-133±4	-124±5	-132.4	-42
3157	-143±2	-138±3	-132±4	-137.2	-43
3245	-151±0	-143±1	-134±1	-140.4	-45

[a] Standard deviation of at least duplicate measurements.
[b] Weighed means of C_{29}, C_{31}, and C_{33} *n*-alkanes.
[c] Modeled precipitation δD along Mt. Kilimanjaro according to Bowen and Revenaugh (*2003*) and Bowen (*2009*).

"amount effect", and has been observed in tropical regions before, when the isotopic composition of precipitation is not only related to the condensation temperature, but mainly controlled by local rainout (Rozanski et al., 1992; Rozanski and Araguás Araguás, 1995). The "amount effect" results in more depleted δD_p values with higher amounts of rainfall and/or harder rains, and at Mt. Kilimanjaro, the amount of precipitation and relative humidity are at their highest in the middle montane zone (Hemp, 2006a, b), exactly where δD_{wax} values are most depleted (*Fig. 4.2b*). At the midslope high precipitation belt, the actual δD_p may have shifted to much lower values than the modeled δD_p due to the "amount effect". Indeed, along the western slope of Mt. Kenya (0°S, 37°E), which has a climate similar to Mt. Kilimanjaro, precipitation and lake water δD values were also found to be influenced by the "amount effect" rather than by the "altitude effect" (Rietti-Shati et al., 2000). However, due to the lack of measured source water δD data, we can only speculate about the factors which can explain the absent linear relation.

4.3.2. Branched GDGTs along Mt. Gongga

Branched GDGTs were found in all analyzed surface soils of Mt. Gongga. Their concentrations vary between 0.01 and 5.3 μg/g dry weight (dwt) soil (*Table 4.2*). The distribution of branched GDGTs varies substantially, as is reflected by the CBT and MBT indices, which were calculated according to Eq. 4.1 and Eq. 4.2, respectively (*Table 4.2*). The CBT index for the soils ranges from 0.03 to 1.65. At 1515 m and 1610 m, CBT could not be calculated due to the absence, or too low abundance of branched GDGTs with a cyclopentane moiety (i.e. Ib and IIb; *Fig. 4.1*). MBT values vary between 0.21 and 0.83. The highest values are found at the lower part of the slope in the shrub and grass vegetation zone (1000–1600 m),

Table 4.2. Soil pH, branched GDGT concentrations, MBT and CBT index values, CBT-derived pH, and MBT-CBT-derived MAT for soils along the eastern slope of Mt. Gongga.

Altitude (m)	Soil pH	Total branched GDGTs (mg/g dry weight soil)	CBT	MBT	CBT-derived pH	MBT-CBT-derived MAT (°C)
1180	7.9	0.01	0.72	0.43	6.9	8.7
1220	7.3	0.14	0.61	0.65	7.2	20.9
1515	n.d.[a]	0.62	-[b]	0.83	-	-
1610	7.8	0.01	-	0.25	-	-
1645	7.5	0.42	0.12	0.38	8.4	11.9
1740	6.7	0.01	0.37	0.49	7.8	15.0
1800	7.1	0.72	0.33	0.32	7.9	6.6
1850	7.5	0.15	0.26	0.33	8.1	7.7
1915	6.9	1.17	0.72	0.55	6.9	14.5
1973	7.7	2.69	0.06	0.23	8.6	5.0
2005	7.5	1.30	0.63	0.40	7.1	7.9
2115	7.1	0.46	0.03	0.23	8.7	5.2
2160	7.9	0.51	0.36	0.35	7.8	7.9
2220	6.6	0.26	0.79	0.37	6.7	4.8
2300	6.7	0.86	1.06	0.41	6.0	4.7
2350	6.9	1.28	0.66	0.36	7.0	5.8
2420	7.2	0.47	0.63	0.28	7.1	1.9
2470	7.9	0.66	0.58	0.26	7.2	1.5
2540	7.8	0.13	0.23	0.24	8.1	3.7
2620	6.5	0.16	0.45	0.34	7.6	6.5
2742	4.4	2.86	1.47	0.67	4.9	13.8
2764	5.9	2.68	1.26	0.44	5.4	4.1
2808	5.0	5.29	1.32	0.54	5.3	10.1
2920	5.2	1.22	1.40	0.39	5.1	0.5
2960	7.2	0.67	0.60	0.34	7.2	5.3
3049	4.5	1.96	1.56	0.48	4.7	3.1
3065	6.4	0.34	1.10	0.31	5.9	-1.0
3119	5.6	0.49	1.38	0.39	5.1	0.5
3140	4.9	0.61	1.65	0.57	4.4	7.2
3145	7.3	0.11	0.67	0.21	7.0	-1.8
3188	5.3	0.49	1.44	0.43	5.0	2.0
3209	5.0	0.24	1.44	0.33	5.0	-3.1
3518	4.4	4.69	1.50	0.44	4.8	2.0
3676	6.6	0.33	1.43	0.36	5.0	-1.7
3769	6.3	1.93	1.59	0.37	4.6	-2.5
3819	5.0	1.94	1.48	0.38	4.9	-0.8

[a] Not determined.
[b] Could not be calculated.

above which the MBT values are lower, and remain relatively constant along the rest of the slope.

The variable CBT and MBT values along the altitude gradient suggest that the branched GDGT distribution is influenced by changes in MAT and soil pH. The CBT index shows a linear relation with the measured soil pH (r^2=0.72, n=34; *Fig. 4.3*), and this relation is not significantly different from the global CBT-pH relationship reported by Weijers et al. (2007c), neither for the slope (homogeneity of slopes test: *df*=1,144, *F*=0.01, *P*=0.92), nor for the intercept (ANCOVA: *df*=1,145, *F*=0.36, *P*=0.55). A comparison of the calculated soil pH, derived from the CBT index and Eq. 4.3, and the measured soil pH, varying from 7.9 at the lower slope to 4.4 at higher elevation (*Table 4.2*), shows no significant differences (paired t-test: *t*(33)=-0.072, *P*=0.94), suggesting that changes in soil pH indeed influence the distribution of branched GDGTs, and that the CBT index is a suitable tool to detect those changes.

MAT values along the slope were calculated based on the MBT and CBT indices and Eq. 4.4. MBT-CBT-derived MATs range from 20.9 °C at the lower slope (1220 m) to -3.1 °C at the upper slope (3209 m), and show a linear decrease with altitude (r^2=0.55, n=34; *Fig. 4.4*). The temperature lapse rate based on the MBT-CBT-derived MAT values is -5.9±0.9 °C/1000 m for Mt. Gongga. This calculated lapse rate is identical to the temperature lapse rate of -6.0 °C/1000 m based on the weather station data. Nevertheless, there is a relatively large scatter in the MBT-CBT-derived MAT relationship with altitude, larger than observed for Mt. Kilimanjaro (Sinninghe Damsté et al., 2008). Possibly, other factors than pH or temperature, like soil type or the length of the growing season, have caused the relatively large scatter for this altitude gradient. This suggests that estimations of temperature are associated with relatively large uncertainties, which makes this proxy less suitable for accurate paleoelevation studies in this area.
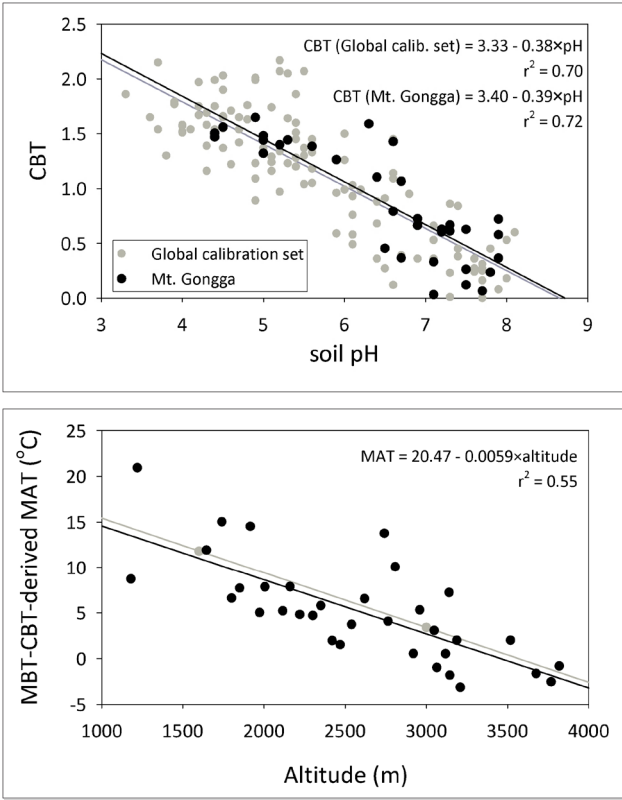
Fig. 4.3. Cross plot of the CBT index vs. measured soil pH for the soils along the eastern slope of Mt. Gongga (black) and for the global soil calibration set of Weijers et al. (*2007c*) (grey).

Fig. 4.4. Relations of MBT-CBT-derived MATs (black) and weather station data (grey) with altitude along the eastern slope of Mt. Gongga.

4.4. Implications and conclusions

Our results for the δD_{wax} in soils of Mt. Kilimanjaro suggest that caution should be taken in deriving a reference record for paleoelevation reconstructions based on n-alkane δD values. Possibly, the relatively high amounts of precipitation in the middle montane belt cause a relative depletion in δD of the plant wax n-alkanes, and therefore mask the relation between δD_{wax} and altitude ($r^2=0.03$, n=16; *Fig. 4.2b*) required for a paleoelevation proxy. Indeed, the calculated "D-lapse rate" along Mt. Kilimanjaro would be $2.6\pm4.2‰/1000$ m, suggesting that, due to both the large error and the absence of a linear relation, δD_{wax} is unlikely to be useful at this location.

In contrast, the MBT-CBT temperature proxy at Mt. Kilimanjaro, which is not influenced by precipitation, shows a good linear relation with altitude ($r^2=0.77$, n=16; Sinninghe Damsté et al., 2008), although the MBT-CBT-based temperature lapse rate (-6.9 ± 1.0 °C/1000 m) is somewhat higher than the measured lapse rate (-5.3 ± 0.1 °C/1000 m; Hemp, 2006a, b). In case of Mt. Gongga, n-alkane δD values relate linearly with altitude (Jia et al., 2008), thereby providing a fairly good proxy to estimate "D-lapse rate" ($17.7\pm1.7‰/1000$ m). Although the MBT-CBT-based MAT estimates also show a linear relation with altitude and provide a temperature lapse rate that resembles the measured lapse rate (respectively -5.9 °C and -6.0 °C/1000 m), there is a large degree of scatter in this correlation.

Thus, it seems that for the two studied mountains, neither potential paleoelevation proxy is working perfectly. However, the combination of soil n-alkane δD values and the MBT-CBT temperature proxy may be a suitable alternative for the more traditional $\delta^{18}O$ based paleoelevation reconstructions. The combination of both organic-geochemical proxies is easily made, as they can be determined from the same lipid extract, yet they are based on fundamentally different principles. Similar paleoelevation estimates from both proxies would yield increased confidence. Compared to the more traditional $\delta^{18}O$ based reconstructions, it should then be possible to obtain higher resolution records, as plant growth and adaptations in bacterial cell membranes are relatively fast processes. Furthermore, branched GDGTs and n-alkanes are relatively more resistant to diagenesis than soil carbonate, and paleoelevation studies may then also be performed in areas where no carbonates or other minerals are present.

Chapter 5

Absence of seasonal patterns in MBT-CBT indices in mid-latitude soils

Johan W.H. Weijers, Beth Bernhardt, Francien Peterse, Josef P. Werne, Jennifer A.J. Dungait, Stefan Schouten, Jaap S. Sinninghe Damsté, 2011. *Geochimica et Cosmochimica Acta* 75, 3179-3190.

Abstract

The degree of methylation and cyclization of bacteria-derived branched glycerol dialkyl glycerol tetraether (GDGT) membrane lipids in soils depends on temperature and soil pH. Expressed in the methylation index of branched tetraethers (MBT) and cyclization ratio of branched tetraethers (CBT), these relationships are used to reconstruct past annual mean air temperature (MAT) based on the distribution of branched GDGTs in ancient sediments; the MBT-CBT proxy. Although it was shown that the best correlation of this proxy is with annual MAT, it remains unknown whether a seasonal bias in temperature reconstructions could occur, such as towards a seasonal period of 'optimal growth' of the, as yet, unidentified soil bacteria which produce branched GDGTs. To investigate this possibility, soils were sampled from eight different plots in the USA (Minnesota and Ohio), The Netherlands (Texel) and the UK (Devon) in time series over 1 year and analyzed for their branched GDGT content. Further analyses of the branched GDGTs present as core lipids (CLs; the presumed fossil pool) and intact polar lipids (IPLs; the presumed extant pool) were undertaken for two of the investigated soil plots. The amount of IPL-derived branched GDGTs is low relative to the branched GDGT CLs, i.e. only 6–9% of the total branched GDGT pool. In all soils, no clear change was apparent in the distribution of branched GDGT lipids (either core or IPL-derived) with seasonal temperature change; the MBT-CBT temperature proxy gave similar temperature estimates year-round, which generally matched the mean annual soil temperature. In addition to a lack of coherent changes in relative distributions, concentrations of the branched GDGTs did not show clear changes over the seasons. For IPL-derived GDGTs these results suggest that their turnover time in soils is in the order of 1 year or more. Thus, our study does not provide evidence for seasonal effects on the distribution of branched GDGTs in soils, at least at mid-latitudes, and therefore, no direct evidence for a bias of MBT-CBT reconstructed temperatures towards a certain season of optimal growth of the source bacteria. If, however, there is a slight seasonal preference of branched GDGT production, which can easily be obscured by natural variability due to the heterogeneity of soils, then a seasonal bias may potentially still develop over time due to the long turnover time of branched GDGTs.

5.1. Introduction

Branched glycerol dialkyl glycerol tetraethers (GDGTs) are core membrane lipids synthesised by as yet unknown bacteria (Weijers et al., 2006a). They occur in peat bogs and soils worldwide (Sinninghe Damsté et al., 2000; Leininger et al., 2006; Weijers et al., 2006b, 2007c; Huguet et al., 2010a,b). Branched GDGTs consist of two alkyl chains ether bound to two glycerol units. The alkyl moieties contain two or three methyl groups each and in some, one of these methyl groups is incorporated into a cyclopentane moiety likely formed via internal cyclization (Weijers et al., 2006a). It has been shown previously that the relative distribution of the different branched GDGTs relates to soil pH and temperature (Weijers et al., 2007c; Peterse et al., 2009b, 2010). The degree of cyclisation of the membrane lipids, expressed in the cyclization ratio of branched tetraethers (CBT) relates to soil pH, and the degree of methylation, expressed in the methylation index of branched tetraethers (MBT) relates to both soil pH and temperature. These relationships are explained as adaptations by the GDGT-synthesizing microbe to ambient conditions in order to maintain the cell membrane in a liquid crystalline state, which is necessary to carry out essential cell membrane functions. In soils, the ambient temperature to which branched GDGT-producing bacteria adapt their cell membrane is most certainly soil temperature. As soil temperature data were not available in the global soil dataset studied by Weijers et al. (2007c), a correlation was made between branched GDGT distributions and annual mean air temperature (MAT), under the assumption that soil and air temperature are strongly related to each other and, on a yearly average basis, do not differ substantially from each other. Since these branched GDGTs are preserved in the sedimentary record, this relationship between MBT-CBT and annual MAT could be used as a proxy to reconstruct past temperatures (Weijers et al., 2007c).

After initial application in the Congo deep sea fan to reconstruct past MATs for tropical Africa since the last deglaciation (Weijers et al., 2007a), the MBT-CBT proxy is increasingly being used to reconstruct past MATs. These include, among others, deglacial Amazonia (Bendle et al., 2010) and East Asia (Peterse et al., 2011), the middle Pleistocene of southwestern North America (Fawcett et al., 2011), the Miocene of northwestern Europe (Donders et al., 2009), the Eocene-Oligocene boundary for East Greenland (Schouten et al., 2008a), the early Eocene of the Sierra Nevada (Hren et al., 2010) and the Palaeocene-Eocene thermal maximum (PETM) in the Arctic (Weijers et al., 2007b). In some cases these palaeotemperature estimates are in agreement with those of other proxies (e.g. Schouten et al., 2008a; Ballantyne et al., 2010), however, a potential bias to summer temperatures could not always be excluded. For example, reconstructed MATs for the Arctic at the PETM are high (ca. 25 °C; Weijers et al., 2007b) and, although comparable to sea surface temperature estimates, the authors suggested that due to 3 months of darkness during polar winter these estimates might be biased towards summer temperature. A comparison with much lower MAT estimates obtained from oxygen isotope ratios of biogenic phosphate led Eberle et al. (2010) to suggest that MBT-CBT temperature estimates for the Arctic during the PETM and early Eocene are indeed seasonally biased, i.e. towards the summer. Nevertheless, a recent study by Pucéat et al. (2010) pointed out that, because of methodological biases, it could in fact be the MAT estimate based on these oxygen isotope ratios of biogenic phosphate that might be underestimated by 4-8 °C. In addition to these deep time applications, Peterse et al. (2009a) showed for high latitude soils at Svalbard that MBT-CBT temperature estimates were equal to measured annual MAT. However, Rueda et al. (2009) compared MBT-CBT derived MAT estimates from a sediment record of the Skagerrak with instrumental temperature data for the last 200 years and found that it best compared with summer temperatures. Thus, there may be a seasonal bias in some MBT-CBT records, although Weijers et al. (2007c) did not find better relationships between MBT-CBT and

seasonal temperatures than with annual mean temperatures.

Soil microbial communities are (indirectly) affected by changes in environmental conditions; temperature being one of them (e.g. Frey et al., 2008, and references therein). In a recent study where soils were incubated at elevated temperatures, Feng and Simpson (2009) observed that, although the biomass and activity of soil microorganisms remained by and large constant, shifts in the overall community composition of microorganisms (i.e. fungi vs. bacteria and gram-negative vs. gram-positive bacteria) might occur as a result of temperature-induced substrate constraints. Similar constraints occur for microbes when temperatures drop below optimum conditions, resulting in limited microbial growth (Nedwell, 1999), and it is generally assumed that microbial activity slows down and shifts to a maintenance-related metabolism when soil freezes. Contrary to this view, however, Drotz et al. (2010) recently reported that both catabolic and anabolic activities of heterotrophic microorganisms proceeded in frozen boreal forest soil, including the biosynthesis of membrane lipids.

It is, therefore, not entirely clear whether the activity of branched-GDGT synthesizing bacteria in soils is dependent on temperature. If this were to be the case, for example via temperature-induced nutrient input to the soil which may vary according to the growing season of vegetation, this could give rise to a preferential period of prosperity of branched-GDGT synthesizing bacteria. Potentially, this might result in a seasonal bias in the temperature 'recorded' in the membrane lipid composition in the soil. In order to investigate this hypothesis, we analyzed the branched GDGT compositions in 1 year-long time series from eight different soil plots in Minnesota and Ohio in the USA, in Devon in the UK and on the island of Texel in The Netherlands. The sites are all located at mid-latitudes where the seasonal contrasts in temperature and growing season are pronounced. In addition to analyzing branched GDGTs as core lipids (CL), i.e. without polar head groups and representing the fossil pool of GDGTs, we also analyzed, in two soil plots, intact polar lipid (IPL)-derived branched GDGTs, i.e. those with a polar head group and presumably derived from living cells. The results were compared with temperature data from local weather stations as well as with *in situ* measured soil temperatures.

5.2. Materials and methods

5.2.1. Soil locations and sampling

5.2.1.1. Itasca State Park and Bath Nature Preserve, USA

Six soils were sampled in the US, three in northwestern Minnesota near Elk Lake in Itasca State Park, Clearwater County, and three in northeastern Ohio near Bath Pond, within Bath Nature Preserve, Summit County. Northwestern Minnesota is characterized by a continental climate with warm, humid summers and very cold winters (Peel et al., 2007). The annual MAT in this part of the state is ca. 4 °C and annual precipitation ca. 700 mm (KNMI, 1997). The climate of northeastern Ohio is typical of humid continental regions with hot summers and cold winters (Peel et al., 2007). The annual MAT in this area is ca. 10 °C and annual precipitation ca. 900 mm (KNMI, 1997). At both sites, soils with three types of vegetation cover were sampled, i.e. pine, deciduous and open field vegetation. The Itasca State Park soils were sampled from September 2008 until August 2009, and the soils in Bath Nature Preserve from October 2008 until September 2009 by colleagues from the University of Akron. Duplicate soil cores were collected at each sampling plot of 3×3 m using a hand auger or, in case of frozen soil, with hammer and chisel. The 0–5 cm interval was used for analysis. All soil samples were stored frozen at -20 °C in ashed glass jars until further processing. Thermistors (NexSens micro-T temperature loggers) were buried at a depth of ca. 15

cm in each of the soil plots in Minnesota and Ohio (slightly deeper than the depth interval used for lipid analysis) to record soil temperature 10 times a day (i.e. every 144 min). An additional thermistor was set ~1.5 m above ground level to record ambient air temperatures at the sites. Thermistors recorded temperature approximately every 2.5 h from September 2008 until October 2009.

5.2.1.2. Rowden Moor, UK

The time series from the UK was obtained from a grassland soil from the long-term experimental research platform site at Rowden Moor near Okehampton (Devon, SW England). Southwestern England is characterized by a humid maritime climate, which means that, in contrast to the USA soils, seasonal extremes in temperature are smaller and that soil temperature is above freezing point virtually all year round. The annual MAT at this site is 9.6 °C and the mean annual precipitation is 1056 mm (Harrod and Hogan, 2008). The soil has a silty clay texture and remains very wet from autumn until early spring due to the virtually impermeable clay layer at 30 cm depth (Harrod and Hogan, 2008). Samples were taken from the control plot, a gently sloping undrained meadow that receives no fertilizer, although cows graze the meadow for a defined period during the year. The vegetation consists of *Lolium perenne* with patches of *Juncus effuses*. The soil was sampled at eighteen time points from November 2008 until November 2009. In order to minimize effects caused by the heterogeneous nature of a soil, sampling was performed by taking five 30 cm long cores with a 3 cm diameter augur in an X-shape over an area of approximately 30×30 m. The short cores were sliced in 10 cm depth increments and stored at -20 °C until sample processing. Upon freeze drying and removal of the grass cover, the 0–10 cm interval increments were pooled and powdered using a ball mill and subsequently extracted. Meteorological data (air temperature, precipitation and soil temperature at 10 cm depth, all at hourly resolution) were obtained from the on-site official UK MET-Office meteorological station.

5.2.1.3. Texel, The Netherlands

A sandy grassland soil was sampled near the Royal NIOZ on the island of Texel, which is in the northwest of The Netherlands. The Netherlands is, like England, characterized by a maritime climate with wet summers and mild winters. The annual MAT near Texel is 9.4 °C and mean annual precipitation is 750 mm (KNMI, 1997). The upper 10 cm of the soil was sampled monthly from March 2008 until February 2009. Three samples were taken in a triangle shape on a 1×1 m plot and merged in order to minimize variability due to soil heterogeneity and stored frozen at -20 °C until further processing. Upon freeze-drying and grinding, the triplicate samples were pooled. In-situ soil temperatures were measured at the time of sampling (always in the morning) using an Ama-Digit ad 20th digital thermometer. Thus, in contrast with the soil plots from the USA and the UK, these soil temperatures do not represent daily averages. Average monthly MATs were obtained from the nearest official weather station at De Kooy, which is located on the mainland ca. 10 km from Texel (KNMI, 1997).

5.2.2. Soil extraction and fractionation

The soils from Elk Lake watershed and Bath Nature Preserve were processed at the Large Lakes Observatory of the University of Minnesota, Duluth. Soils were freezedried and homogenized with mortar and pestle after removal of root clumps and other large pieces of soil debris. Around 10 g of soil were solvent extracted using a DIONEX Accelerated Solvent Extractor (ASE) and *n*-hexane/dichloromethane

(DCM) 9:1 (v/v) at 100 °C and 7.6×10^6 Pa to obtain a total lipid extract (TLE). TLE aliquots were evaporated under nitrogen until dry, re-dissolved in n-hexane/DCM 9:1 (v/v) and applied to an activated Al_2O_3 column. Apolar and polar fractions were eluted with n-hexane/DCM 9:1 (v/v) and DCM/methanol (MeOH) 1:1 (v/v), respectively.

The Texel soil was processed at Royal NIOZ, and the Rowden Moor soil at both Rothamsted Research – North Wyke (extraction) and Utrecht University (hydrolysis). For both soils, samples were extracted using a modified Bligh & Dyer method in order to analyze both IPLs and CLs (Bligh and Dyer, 1959). Freeze dried and powdered soil (ca. 10 g for the Rowden Moor soil and ca. 3 g for the Texel soil) was ultrasonically extracted three times for 10 min. using a single-phase solvent mixture of MeOH/DCM/phosphate buffer 10:5:4 (v/v/v). Upon centrifugation, supernatants were collected and combined. DCM and phosphate buffer were added to the combined extracts to create a new volume ratio of 5:5:4 (v/v/v) and obtain phase separation. The extract (DCM phase) containing the GDGTs was separated from the residue (MeOH/phosphate buffer phase) by centrifugation and collected. The residue phase was extracted twice more with DCM and the combined extracts evaporated to near dryness using a rotary evaporator. The extract was passed over a small column plugged with extracted cotton wool to remove any remaining soil particles and then completely dried under a steady stream of pure N_2. The extract was subsequently separated into a CL and IPL fraction over a small silica gel column according to Pitcher et al. (2009) with minor modifications. The CL fraction was obtained by eluting with 5 column volumes of n-hexane:ethylacetate 1:1 (v/v) and the IPL fraction was obtained by eluting with 5 column volumes of MeOH. A small aliquot of the obtained IPL fraction was analyzed directly using high performance liquid chromatography/mass spectrometry (HPLC/MS) to determine any carry over of CLs into the IPL fraction (see below). In order to analyze IPLs as CLs, the IPL fraction was hydrolyzed to cleave off the polar head groups. To this end the IPL fraction was refluxed for a minimum of 2 h in 1.5 N HCl in MeOH, cooled down and neutralized to ~pH 5. To recover the sample, a small amount of double distilled or extracted demineralized water was added and the mixture was extracted three times with DCM, which was subsequently collected and evaporated to dryness. In addition to this acid hydrolysis, an aliquot of the Rowden Moor soil IPL fraction was subjected to base hydrolysis in order to cleave off phosphate bound head groups only. To this end the sample was refluxed for ca. 2 h in a 1 N KOH in MeOH:H_2O 95:5 (v/v) mixture, cooled down, neutralized and recovered by extraction with DCM similar as for the acid hydrolysis.

All branched GDGTs were quantified against a known amount of a C_{46} GDGT standard (Huguet et al., 2006) that was added to each fraction. Prior to analysis, the samples were ultrasonically dissolved in a n-hexane:2-propanol 99:1 (v/v) solvent mixture in a concentration of ca 2 mg/ml and filtered over an 0.45 μm PTFE filter (Alltech) to remove any particulates.

5.2.3. GDGT analysis

All samples were analyzed at Royal NIOZ. GDGTs were analyzed using high performance liquid chromatography– atmospheric pressure chemical ionization/mass spectrometry (HPLC–APCI/MS) on an Agilent 1100 series LC/MSD SL according to Schouten et al. (2007a) with minor modifications. Briefly, separation was achieved on an analytical Alltech Prevail Cyano column (150×2.1 mm, 3 mm). Branched GDGTs were eluted with 90% A and 10% B, where A = n-hexane and B = n-hexane:2-propanol 9:1 (v/v), isocratically for the first 5 min (flow rate 0.2 ml/min), thereafter with a linear gradient to 18% B in 45 min. Injection volume was 10 μl for all samples. The different GDGTs were detected by scanning for

their [M+H]$^+$ ions (protonated mass) in selected ion monitoring (SIM) mode and the peak area was used for quantification. Absolute quantification was performed according to Huguet et al. (2006). MBT indices and CBT ratios were calculated using peak areas and translated into annual MAT estimates following the soil calibration described in Weijers et al. (2007c).

The standard error of estimate of the calibration formula is 5.5 °C. The instrumental reproducibility of the MAT estimate, based on several duplicate HPLC/MS analyses, was ±0.3 °C. The analytical error due to sample processing and analysis was determined by duplicate processing of all Minnesota soil samples and by triplicate processing of four of the Rowden Moor soil samples. For the Minnesota soils, the average standard deviation of the MAT estimates was 1.1 °C and for the Rowden Moor soil the average standard deviation was 0.4 °C for the CLs and 1.0 °C for the IPLs. For the concentration of GDGTs, the analytical error was ca. 25% for the Minnesota soils and ca. 10% for the Rowden Moor soil.

5.2.4. Correction for carry over of core lipids

As concentrations of IPL-derived branched GDGTs are substantially lower than those of the CL fractions and separation of both fractions over a silica-gel column does not always results in a full separation (likely depending on the extract composition, see Pitcher et al., 2009), small aliquots of the IPL fraction were analyzed using HPLC/MS without further hydrolysis to screen for the presence of branched GDGT CLs. It appeared that the carry over of CLs into the IPL fraction is minor, i.e. ca. 2% of all CLs ended up in the IPL fraction, both for Rowden Moor soil and for the Texel soil. However, given the much lower concentrations of GDGTs in the IPL fraction relative to the CL fraction, this pool of leaked CLs accounted for ca. 23% of all GDGTs measured in the hydrolyzed fraction in Rowden Moor soil and ca. 30% for the Texel soil. Therefore, the reported concentrations of IPL-derived branched GDGTs were corrected for this.

As this (small) fraction of leaked branched GDGT CLs might have a distribution (and thus 'temperature signature') that could deviate from the IPL-derived GDGTs, a correction has also been made for the reconstructed MAT based on the IPL-derived GDGTs. This correction was made by subtracting concentrations of individual branched GDGTs of the leaked CL fraction from the concentrations of branched GDGTs in the IPL-derived fraction, and recalculating MAT based on the new distribution. The resulting correction was minimal in the Rowden Moor soil, i.e. 0.4 °C on average. For the Texel soil this correction is slightly larger, i.e. 1.4 °C on average.

5.3. Results and discussion

5.3.1. Instrumental temperature data

All four sites showed clear differences in seasonal air temperature. Due to the maritime climate of western Europe, however, the maximum difference in monthly mean air temperatures at Texel and Rowden Moor, i.e. 16 and 14 °C, respectively, was lower than at the sites in Itasca State Park (Minnesota) and Bath Nature Preserve (Ohio), i.e. 33 and 26 °C, that experience a continental climate (*Fig. 5.1*). Daily soil temperatures as measured in the Minnesota, Ohio and Rowden Moor soils showed lower extremes than the measured air temperature due to the heat capacity of soils. Among the Minnesota soils, the pine plot showed slightly lower amplitudes in soil temperature than the open field plot and a delayed response to warming in spring, both most likely as a result of the insulating effect of the vegetation cover. This effect was less pronounced for the Ohio soils. Unfortunately, the thermistor from the deciduous plot in Ohio could not be recovered and the one from the deciduous plot in Minnesota malfunctioned, so we

Fig. 5.1. Overview of reconstructed annual mean air temperatures using the MBT–CBT proxy (triangles) and the measured annual mean air (gray horizontal bar) and soil (brown horizontal bar) temperatures among the different soils. The range in monthly average air temperatures is indicated by the gray surface area; the range in monthly average soil temperature is indicated by the vertical brown bars. Note that the vertical bars behind the triangles do not represent the standard error of the mean but represent the total range in temperatures reconstructed with the MBT–CBT proxy during the year. Triangles are color-coded: green represent core lipid (CL) branched GDGTs, red represents intact polar lipid (IPL)-derived branched GDGTs upon acid (H) hydrolysis, and blue represents IPL-derived branched GDGTs derived upon base (OH) hydrolysis, see also bottom axis.

did not obtain *in situ* temperature data for these soils. Under the assumption that the temperature in the deciduous forest soil will not deviate substantially from the temperature in the pine forest soil, the latter was used for comparison with the MBT-CBT derived MATs in the deciduous forest soil. For all soils for which *in situ* soil temperature data were available, the annual mean soil temperature was higher than the annual MAT (*Fig. 5.1*). In the Minnesota and Ohio soils this was mainly due to the fact that winter soil temperatures never reach far below freezing point. For Rowden Moor soil this is principally due to soil temperatures in summer that are about 2 °C higher than air temperatures, probably due to the insulating effect of the grass cover at night. This difference between mean air and mean soil temperature was smallest in the pine forest soil in Ohio (0.4 °C) and largest in the open field soil from Minnesota (4.4 °C). The difference for the open field grassland at Rowden Moor was 1.3 °C.

5.3.2. Branched GDGT core lipids

Concentrations of branched GDGT CLs were determined for all soils and fall within ranges reported in other studies (Kim et al., 2006; Weijers et al., 2006b; Peterse et al., 2009b; Huguet et al., 2010b). For the Minnesota soils, annual averaged concentrations were 240±60 (standard deviation) ng/g dry weight soil (dws) for the open field, 290±70 ng/g1 dws for the pine forest and 430±110 ng/g dws for the deciduous forest time series, respectively (*Fig. 5.2a*). For the Ohio soils the annual averaged concentrations were 170±70 ng/g dws for the open field, 2500±1250 ng/g dws for the pine forest and 310±170 ng/g dws for the deciduous forest (*Fig. 5.2b*). Annual averaged branched GDGT CL concentrations for the Texel and the Rowden Moor grassland soils were 600±120 ng/g dws (*Fig. 5.2c*) and 1600±300 ng/g dws (*Fig. 5.2d*), respectively. In the Minnesota open field soil, the Ohio soils, the Texel soil and the Rowden Moor soil no seasonal trend in branched GDGT CL concentrations was apparent (*Fig. 5.2*). For the Minnesota pine forest and deciduous forest soils somewhat higher concentrations seem to be present in July and August. For the Rowden Moor soil, precipitation data were available, but no relation with precipitation was found.

MBT-CBT reconstructed temperatures (based on the CLs) remained constant throughout the year in all soils, with variations in MAT estimates within the same soil usually <5 °C in the Minnesota and Ohio pine forest soils (*Figs. 5.3 and 5.4*), <3 °C in the deciduous forest and open field soils from the same sites (*Figs. 5.3 and 5.4*), <2 °C in the Texel soil (*Fig. 5.5*) and <1 °C in the Rowden Moor soil (*Fig. 5.6*). The observed variations did not coincide with seasonal variations in soil temperature. The average MBT-CBT derived temperatures for the Minnesota soils were 10.3±1.2 °C (standard deviation) for the open field site and 9.9±1.9 °C for the pine site, which are clearly warmer than the annual MAT of 3.8 °C but closer to the annual mean soil temperature of 8.2 °C at the open field site and 6.0 °C at the pine site (*Fig. 5.1*). For the Ohio soils, the average MBT-CBT derived temperatures were 8.4±0.9 °C for the open field and 12.6±1.6 °C for the pine plot, which are both close to the annual MAT of 9.9 °C and the measured annual mean soil temperature of 10.4 °C at the open field site and 10.0 °C at the pine site (*Fig. 5.1*). Strikingly, MBT-CBT reconstructed temperatures for the deciduous soils in both Minnesota and Ohio were high, i.e. 14.0±0.9 °C and 19.2±1.0 °C, respectively (*Figs. 5.3 and 5.4*). This is 10.2 and 9.6 °C, respectively, higher than measured annual MAT and 8.0 and 9.2 °C, respectively, higher than annual mean soil temperature under pine forest (*Fig. 5.1*). Unfortunately, no soil temperature data were available for both deciduous plots, but it seems unlikely that these would be that much higher than under
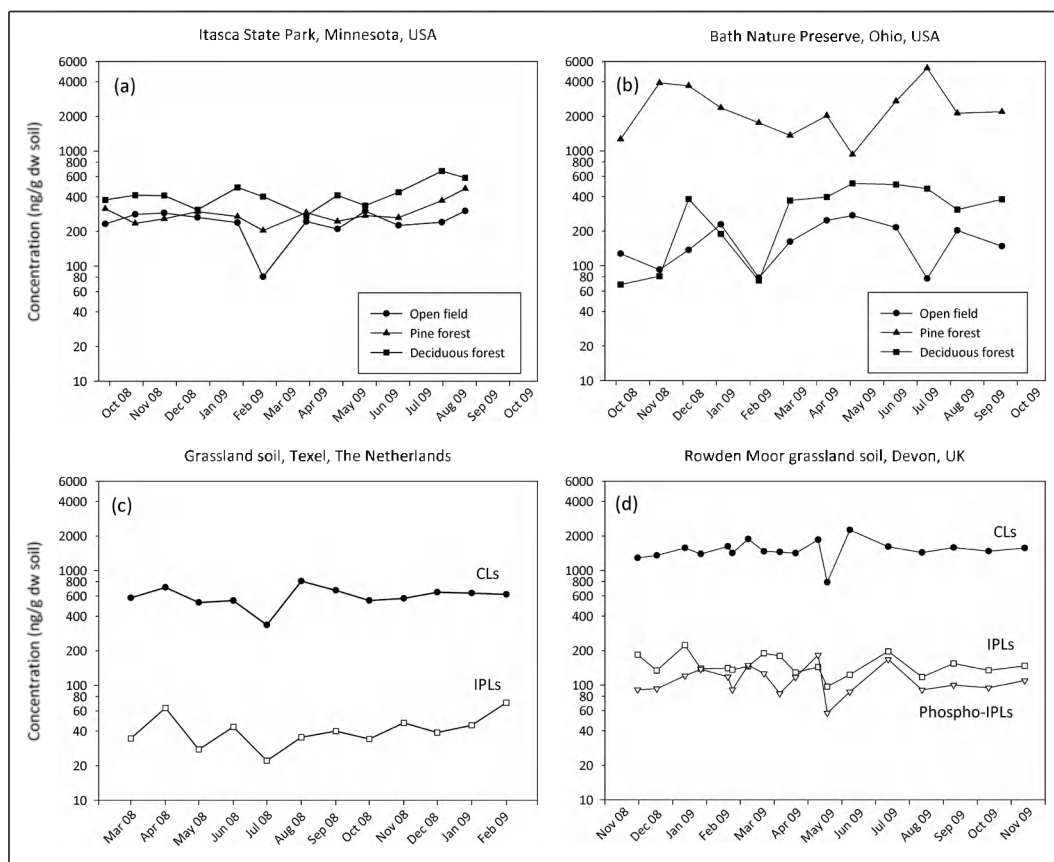
Fig. 5.2. Concentrations of branched GDGTs over the 1-year time series analyzed in the different soils. a) core lipids (CLs) in the soils at Itasca State Park, Minnesota, USA. b) CLs in the soils at Bath Nature Preserve, Ohio, USA. c) CLs and intact polar lipid (IPL)-derived branched GDGTs in the grassland soil at Texel, The Netherlands. d) CLs, total IPL-derived branched GDGTs and branched GDGTs derived from phosphate-bound IPLs in the grassland soil from Rowden Moor, UK.
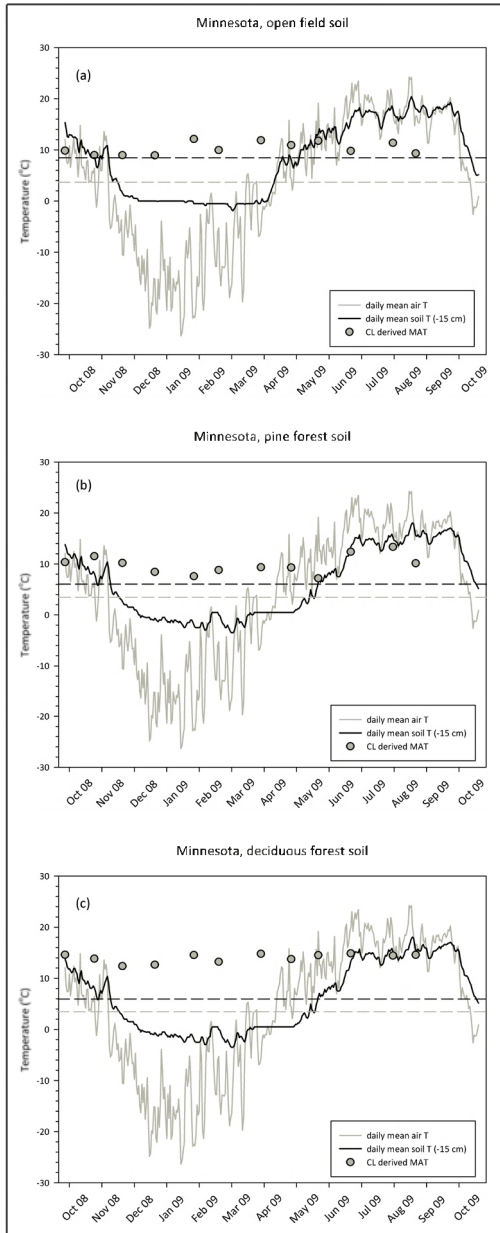
Fig. 5.3. MBT–CBT reconstructed MATs (dots) for a) the open field soil, b) the pine forest soil, and c) the deciduous forest soil at Itasca State Park, Minnesota, USA, plotted against the daily mean air temperature (gray line) and daily mean soil temperature at 15 cm depth (black line). The horizontal gray striped line represents the measured annual MAT and the horizontal black striped line the measured annual mean soil temperature at the site. Note that the soil temperature curve in graph c is actually the soil temperature measured in the pine forest soil (see text).
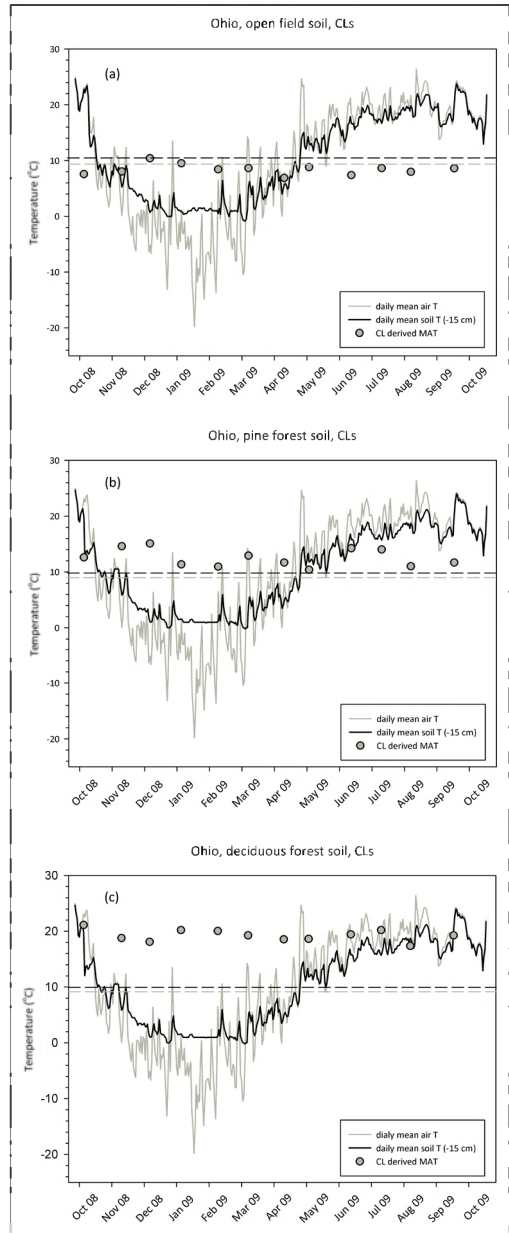
Fig. 5.4. MBT–CBT reconstructed MATs (dots) for a) the open field soil, b) the pine forest soil, and c) the deciduous forest soil at Bath Nature Preserve, Ohio, USA, plotted against the daily mean air temperature (gray line) and daily mean soil temperature at 15 cm depth (black line). The horizontal gray striped line represents the measured annual MAT and the horizontal black striped line the measured annual mean soil temperature at the site. Note that the soil temperature curve in graph c is actually the soil temperature measured in the pine forest soil (see text).

pine forest. This makes these soils the only two in this set of eight to give reconstructed MATs that show offsets to measured temperature larger than the standard error of estimate of the soil calibration dataset of ca. 5.5 °C (Weijers et al., 2007b). The reason for this deviating pattern is, at present, not clear. For the Texel soil, the MBT-CBT reconstructed temperature based on the CLs was 7.1±0.8 °C, which is slightly lower than the annual MAT for this area of 9.4 °C (*Figs. 5.1 and 5.5*). Of the eight soils sampled, the reconstructed temperature based on CLs in the Rowden Moor soil was the most stable throughout the year at 11.1±0.7 °C, which is close to annual MAT of 9.6 °C and equal to the annual mean soil temperature of 11.1 °C (*Figs. 5.2 and 5.6*). One exception is the sample from May 15th that gave a reconstructed temperature of 9 °C. This is clearly lower than the reconstructed temperature for the sample taken a week earlier (May 7th; 11.2 °C) and that of June 4th (11.6 °C). This particular sample is also an outlier in terms of the concentration of branched GDGTs.

In all soils for which continuous soil temperature data are available, i.e. Minnesota open field and pine forest, Ohio open field and pine forest and Rowden Moor soil, the MBT-CBT reconstructed temperature was closer to the measured annual mean soil temperature than to the measured annual MAT. This is surprising as in the soil calibration dataset a calibration was made with annual MAT and not with soil temperature (Weijers et al., 2007c). As is also evident from the temperature data shown here, soil and air
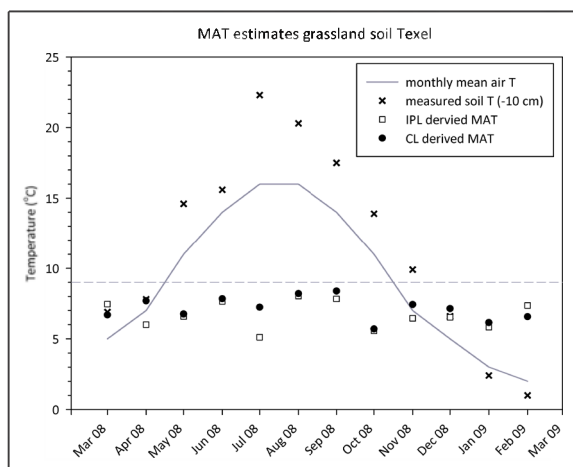
Fig.5.5. MBT–CBT reconstructed MATs based on core lipid (CL, black circles) and intact polar lipid (IPL, white squares)-derived branched GDGTs, for the grassland soil at Texel, The Netherlands, plotted against monthly mean air temperature (black line) and the measured soil temperature at 10 cm depth at the time of sampling (black crosses).
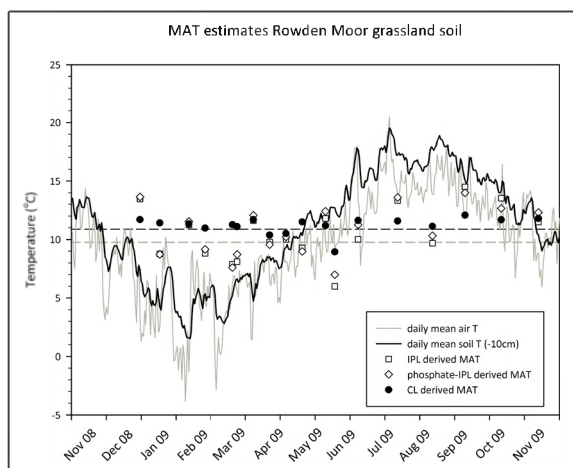
Fig. 5.6. MBT–CBT reconstructed MATs based on branched GDGT core lipids (CL, black circles), IPL-derived branched GDGTs after acid hydrolysis (white squares) and IPL-derived branched GDGTs after base hydrolysis (white diamonds), for the grassland soil at Rowden Moor, UK, plotted against measured daily mean air temperature (gray line) and measured daily mean soil temperature at 10 cm depth (black line).

temperature are not identical, and more importantly, the offset differs with region and type of vegetation. The observed variation depends on a range of factors, including differences in vegetation cover, water content (which determines heat capacity) and latitude (intensity of winter frost conditions) of the soil (e.g. Oliver et al., 1987). The fact that MBT-CBT reconstructed temperatures do not always exactly reflect annual MAT implies that, as suggested by Weijers et al. (2007c), a substantial part of the scatter present in the MBT-CBT calibration may result from this variation in the offset between soil and air temperatures.

The branched GDGT CL assemblages in the eight soils analyzed, clearly showed no response to seasonal changes in temperature. This lack of any seasonal trend may be ascribed to a standing stock of CLs whose abundance is much larger than new production of branched GDGTs over a seasonal cycle. Earlier work, comparing the amount of branched GDGT CLs in a peat core with cell numbers of the most dominant bacteria, suggested the presence of such a standing stock of CLs (Weijers et al., 2009). Indeed, Weijers et al. (2010) showed by means of the stable carbon isotopic composition of the branched alkanes released from branched GDGTs that their turnover time, at least in mid-latitude cropland soils, is near 20 years, and Peterse et al. (2010) showed that the branched GDGT (CLs) composition in a grassland soil had fully adjusted to a manipulated change in pH after 40 years. These studies indicate that the standing stock of branched GDGT CLs turns over on timescales of decades and that, consequently, the distribution of branched GDGT CLs in a given soil is adjusted to new environmental conditions at these time scales. This turnover time of decades for branched GDGT CLs also implies that the variation in CL concentration as found in some soils has to be interpreted with care. It seems unlikely that the pool of CLs is suddenly halved or doubled in a month. These variations are likely to be, at least partly, the result of the well-known spatial heterogeneity of soils. From the work presented here, it is clear that the branched GDGT CL distribution does not adjust to changes in ambient conditions (at least temperature) on time scales <1 year. The turnover time of near 20 years implies that the MAT signal documented by the branched GDGT CLs is a timeintegrated signal over previous years (with the potential for a greater weighting for more recent years, though this remains to be demonstrated).

5.3.3. Branched GDGT intact polar lipids
5.3.3.1. Acid-hydrolyzed IPLs

Since branched GDGT CL distributions did not show a response to seasonal variations, we analyzed IPL-derived branched GDGTs which are presumably a better reflection of the extant soil bacterial population. Therefore, for the Texel soil and Rowden Moor soil, IPL branched GDGTs were separated from the CLs, hydrolyzed and analyzed as CLs. Concentrations of these IPL-derived branched GDGTs varied from ca. 40±15 ng/g dws in the Texel soil (*Fig. 5.2c*) to ca. 150±30 ng/g dws in the Rowden Moor soil (*Fig. 5.2d*). However, as observed for the CLs, no relationship was apparent between the concentration of the IPL-derived branched GDGTs and temperature (*Fig. 5.2*). The IPL fraction of the branched GDGTs in the soils only accounted for 6% (Texel soil) and 9% (Rowden Moor soil) of the total branched GDGT pool, which is only slightly higher than the value of 4% reported by Liu et al. (2010) in a German peat bog. Assuming that all IPLs are derived from extant biomass, this indicates that more than 90% of the branched GDGTs present in the soil are in a fossil (CL) form.

Although temperature estimates reconstructed using branched GDGTs from the IPL fraction were expected to better reflect seasonal temperature, this is not the case. In the Texel soil, temperature reconstructions based on the IPL-derived branched GDGTs showed values that are similar to the estimates

based on the CL fraction (*Fig. 5.5*; average $6.7 \pm 1.0 \,°C$). Except for April and July, the difference between the estimated temperatures from both fractions was <1 °C, i.e. within analytical error. In the Rowden Moor soil, temperature estimates based on GDGTs from the IPL (acid-hydrolyzed) fraction differed slightly more from the estimates based on the CL fraction (*Fig. 5.6*; average $10.6 \pm 2.2 \,°C$). IPL based temperature estimates were either up to 2.4 °C higher (September) or down to 3.4 °C lower (February) than the CL based estimates of the same months. Although these two extremes might suggest some kind of adaptation, it has to be noted that higher IPL-based than CL-based temperature estimates also occurred in winter and lower estimates in summer. A Student's t-test shows that IPL-derived MAT estimates for the warm part of the year (in this case defined as May–October) were not significantly higher than CL-derived MAT estimates, and that IPL-derived MAT estimates for the cool part of the year (November–April) were only just significantly lower than CL-derived MAT estimates, in both cases at a 95% confidence interval. This indicates that the data indeed are scattered and that there is no unambiguous clear trend in IPL-derived MAT related to seasonal changes in temperature (*Fig. 5.6*).

These results suggest that, as with the CL branched GDGTs, the turnover of IPL-derived branched GDGTs in soil is rather slow, albeit perhaps faster than for CL branched GDGTs. One potential cause for this would be if IPLs are also preserved over time scales of months to years, as this would result in a smoothing of the seasonal temperature signal. Harvey et al. (1986) observed that bacterial phospholipids degrade relatively fast, whereas glycosidically bound ether lipids degrade much more slowly. Based on modeling of degradation rates in the marine environment, Schouten et al. (2010) recently proposed that a significant portion of glycosidic GDGTs could indeed be preserved in the sedimentary record. Liu et al. (2010) recently reported the occurrence of branched GDGT IPLs containing glycosidic head groups in a German peat bog, but no IPLs containing a phospho head group, suggesting that glycosidic branched GDGT IPLs may indeed be preserved over time scales longer than those of phospho IPLs.

5.3.3.2. Base-hydrolyzed IPLs

To investigate whether the majority of the branched GDGT IPL pool consisted of glycolipids, an aliquot of the IPL fraction of the Rowden Moor soil samples was subjected to base hydrolysis, which only cleaves ester bound phospho head groups and not ether bound glycosidic head groups. The average concentration of the phospho IPL-derived branched GDGTs was ca. 110 ± 30 ng/g dws (*Fig. 5.2d*). Comparison with the yield of the acid-hydrolyzed IPL aliquot, which was ca. 150 ng/g dws and represents the sum of phospho IPLs and glycosidic IPLs, suggests that the majority of the branched GDGT IPLs contain ester bound phosphate head groups. Given that glycosidic branched GDGTs might even be enriched in abundance over time relative to the phospho IPLs due to their supposedly slower degradation rate, this suggests that the amount of glycolipids produced by the branched-GDGT synthesizing bacteria is small relative to the phospholipids. This is in apparent contradiction with the work of Liu et al. (2010) who only found glycosidic head groups for the branched GDGTs, although it needs to be stressed that this was in a peat bog rather than a soil.

If the branched GDGTs released upon base hydrolysis are derived from (more labile) phospholipid branched GDGTs, then they may be a better reflection of the living bacterial population. However, also in the base-hydrolyzed fraction, GDGT concentrations showed no relationship with temperature over the seasons (*Fig. 5.6*). The MBT–CBT reconstructed MAT based on the base-hydrolyzed IPL fraction (average 10.7 ± 2.1 °C) also showed no noticeable difference with temperatures reconstructed for the

acid-hydrolyzed fraction or the CL fraction (*Fig. 5.6*). Except for June (1.2 °C), the differences between reconstructed MATs in the acid- and base-hydrolyzed samples were within 1 °C, and thus within analytical uncertainty. In fact, this similarity is not strange given that the majority of IPLs seems to consist of phospho bound IPLs, which are measured in both the acid- and the base-hydrolyzed fraction. Thus, the small differences in estimated MAT over the course of a year, based on the acid-hydrolyzed IPL fractions both in the Texel soil and in the Rowden Moor soil, is likely not due to the specific presence of larger amounts of preserved glycosidic IPLs.

Assuming then that IPL-derived branched GDGTs represent living biomass, it might be that branched-GDGT synthesizing bacteria have low cell division rates and exhibit relatively long regeneration times. This would have a similar smoothing effect as with fossil GDGTs in the CL fraction, since part of the IPLs detected at a given point in time could be produced several months earlier. Indeed, many bacteria are known to grow slowly. An extreme example are the anammox bacteria with cell division times up to a month (Van de Graaf et al., 1996; Strous et al., 1998). Also several *Acidobacteria*, the bacterial phylum potentially containing the branched-GDGT synthesizing bacteria (Weijers et al., 2009), are relatively slow growers (Eichorst et al., 2007; Davis et al., 2011). Given that there is no systematic variation over the year in the MBT–CBT reconstructed temperatures for the IPL-derived branched GDGTs, the combined effects of suspected slow regeneration times of the responsible bacteria and the slow degradation rate of IPLs suggest a perceived turnover time of IPLs in these soils in the order of a year.

5.4. Implications

Previous studies have shown that branched GDGT-synthesizing soil microbes adapt their membrane lipid distributions to pH and temperature (Weijers et al., 2007c; Peterse et al., 2009b, 2010). These are the ambient pH and temperature and thus soil pH and soil temperature. Since for the global soil calibration dataset no soil temperature data were available, a calibration was made with annual MAT under the assumption that the two are roughly equal. Although on larger regional and global scales this will be true, on a local scale, as is evident from our study, soil and air temperature are not equal, and more importantly, also the offset between the two is not the same everywhere. It is important to realize, therefore, that, as also indicated by Weijers et al. (2007c), a large part of the scatter in the MBT-CBT calibration with annual MAT (which gives a standard error of estimate of ca. 5 °C) may result from this offset between soil and air temperature. As a consequence, absolute temperatures reconstructed with the MBT-CBT proxy, though calibrated with annual MAT, do not always exactly reflect annual MAT, like in some of the soils studied here. On the larger scale, nevertheless, the MBT-CBT proxy is still thought to be able to provide reasonable estimates of past annual MAT and, especially, of changes therein (e.g. Weijers et al., 2007a). It is the reconstructed absolute temperature that is associated with a slightly larger error (ca. 5 °C). This could only be better constrained when pure cultures of the branched-GDGT synthesizing bacteria are available or when studies like the current one, where soil temperatures are monitored over the annual cycle, are performed on a wide variety of soils.

Our study clearly shows that in mid-latitude soils, no seasonal trends are apparent in the concentration and distribution of branched GDGT CLs. Also in IPL-derived branched GDGT concentration and distribution no clear seasonal trends are apparent. Thus, from the data presented here, it seems that palaeoclimate reconstructions based on branched GDGT CL distributions do not suffer from particular seasonal biases. However, we cannot fully exclude the hypothesis that production of GDGTs in a cer-

tain season could be slightly higher than in others, but that these monthly differences are obscured as they are very small relative to the standing stock of GDGTs. A turnover time of 20 years for CLs implies that ca. 5% of the pool is refreshed in a given year, or ca. 0.4% per month. Monthly variations in this small percentage will not be detectable. Similarly, for the IPL-derived GDGT pool small variations in its turnover rate of ca. 8% per month (based on an assumed turnover time in the order of a year), will likely be obscured by variability due to the heterogeneity of soils. Over the course of 20 years, these small seasonal biases might influence the long term average distribution of branched GDGT CLs and thus the temperature reconstructed using the MBT-CBT proxy. This effect might be expected to be stronger in soils experiencing stronger contrasts between seasons. If such an offset exists, it is, however, not necessarily directed towards a particular season, given that the Texel soil, or the Ohio open field soil, for example, gave reconstructed temperatures lower than annual MAT while the Minnesota soils give reconstructed temperature higher than annual MAT.

The results presented here are derived from soils from mid-latitudes. In the tropics, seasonal contrasts in temperature are much smaller and seasonal biases in MBT-CBT reconstructed MATs are, therefore, expected to be much less of an issue in these climates. Our study, however, cannot completely rule out the presence of a seasonal bias at high latitude sites like the Arctic, as a period of up to 3 months of darkness may have, indirectly via vegetation and nutrient flows, substantial effects on the soil microbial communities. For present-day Svalbard, nevertheless, reconstructed MAT based on branched GDGT CL distributions is close to measured annual MAT (i.e. -4 and -6 °C, respectively; Peterse et al., 2009a). The fact that branched GDGT CLs represent a standing stock that has accumulated over the course of years (ca. 20 years; Weijers et al., 2010) not only explains why the MBT-CBT proxy in soils relates with an annual average temperature, it also implies that the proxy can only be applied on geological time scales with resolutions larger than several decades. Most applications that used the MBT-CBT proxy in obtaining records of MAT estimates have been obtained from sites receiving fluvial transported sedimentsand are, therefore, already considerably temporally smoothed (e.g. Weijers et al., 2007a), but this issue could be important in cases where the proxy is used in high resolution studies of peat or loess deposits.

Acknowledgements

Supplementary Table S5.1. List of MBT and CBT data of all soils analyzed in this study

Soil location	Vegetation type	Lipid fraction	Sample date	MBT	CBT
USA, Minnesota	open field	CL	27-09-08	0.49	0.97
			27-09-08	0.50	0.94
			25-10-08	0.50	1.07
			25-10-08	0.47	0.90
			20-11-08	0.48	0.95
			20-11-08*	0.48	0.96
			20-11-08	0.49	0.99
			20-12-08	0.47	0.93
			20-12-08	0.47	0.89
			20-12-08*	0.47	0.91
			25-01-09	0.56	1.10
			25-01-09	0.54	0.91
			17-02-09	0.47	1.10
			17-02-09	0.53	0.80
			28-03-09	0.52	0.97
			28-03-09	0.58	1.04
			25-04-09	0.57	1.01
			25-04-09	0.50	0.96
			20-05-09	0.48	0.91
			20-05-09	0.56	0.83
			19-06-09	0.50	1.10
			19-06-09	0.54	1.07
			28-07-09	0.56	0.92
			28-07-09	0.49	0.96
			18-08-09	0.49	0.95
			18-08-09	0.50	1.02
USA, Minnesota	pine forest	CL	27-09-08	0.60	1.37
			27-09-08*	0.60	1.41
			27-09-08	0.58	1.44
			25-10-08	0.60	1.42
			25-10-08	0.63	1.36
			25-10-08*	0.62	1.40
			20-11-08	0.62	1.42
			20-11-08	0.55	1.31
			20-12-08	0.53	1.36
			20-12-08	0.56	1.34
			25-01-09	0.58	1.48
			25-01-09	0.48	1.24
			17-02-09	0.58	1.50
			17-02-09	0.55	1.35
			28-03-09	0.51	1.07
			28-03-09	0.56	1.31

			25-04-09	0.62	1.50
			25-04-09	0.50	1.17
			20-05-09	0.51	1.40
			20-05-09	0.50	1.13
			19-06-09	0.67	1.32
			19-06-09	0.60	1.50
			28-07-09	0.64	1.33
			28-07-09	0.66	1.47
			18-08-09	0.59	1.43
			18-08-09	0.58	1.37
USA, Minnesota	deciduous fores	CL	27-09-08	0.47	0.37
			27-09-08	0.50	0.42
			25-10-08	0.50	0.58
			25-10-08	0.47	0.36
			20-11-08	0.45	0.35
			20-11-08	0.47	0.61
			20-12-08	0.43	0.24
			20-12-08	0.42	0.29
			25-01-09	0.46	0.23
			25-01-09*	0.46	0.24
			25-01-09	0.48	0.39
			17-02-09	0.46	0.27
			17-02-09	0.45	0.39
			17-02-09*	0.44	0.39
			28-03-09	0.49	0.28
			25-04-09	0.46	0.30
			25-04-09	0.45	0.31
			20-05-09	0.46	0.30
			20-05-09	0.51	0.45
			19-06-09	0.53	0.56
			19-06-09	0.48	0.37
			28-07-09	0.47	0.31
			28-07-09	0.49	0.41
			18-08-09	0.50	0.37
			18-08-09	0.46	0.34
USA, Ohio	open field	CL	06-10-08	0.30	0.15
			10-11-08	0.31	0.16
			06-12-08	0.36	0.15
			04-01-09	0.34	0.13
			07-02-09	0.32	0.15
			07-03-09	0.32	0.14
			09-04-09	0.29	0.15
			02-05-09	0.32	0.09
			10-06-09	0.30	0.17

			08-07-09	0.32	0.15
			04-08-09	0.30	0.12
			13-09-09	0.33	0.17
USA, Ohio	pine forest	CL	06-10-08	0.65	1.46
			10-11-08	0.67	1.37
			06-12-08	0.69	1.40
			04-01-09	0.63	1.48
			07-02-09	0.62	1.46
			07-03-09	0.65	1.45
			09-04-09	0.63	1.49
			02-05-09	0.60	1.46
			10-06-09	0.67	1.40
			08-07-09	0.66	1.39
			04-08-09	0.62	1.46
			13-09-09	0.63	1.48
USA, Ohio	deciduous forest	CL	06-10-08	0.60	0.28
			10-11-08	0.60	0.55
			06-12-08	0.58	0.52
			04-01-09	0.61	0.47
			07-02-09	0.58	0.28
			07-03-09	0.56	0.30
			09-04-09	0.58	0.47
			02-05-09	0.55	0.32
			10-06-09	0.57	0.33
			08-07-09	0.58	0.29
			04-08-09	0.59	0.64
			13-09-09	0.62	0.57
the Netherlands, Texel	grassland	CL	03-03-08	0.30	0.25
			01-04-08	0.39	0.62
			06-05-08	0.36	0.55
			02-06-08	0.35	0.39
			01-07-08	0.33	0.35
			01-08-08	0.35	0.36
			01-09-08	0.38	0.47
			01-10-08	0.34	0.57
			03-11-08	0.37	0.53
			01-12-08	0.36	0.52
			05-01-09	0.36	0.59
			02-02-09	0.35	0.53
the Netherlands, Texel	grassland	IPL-H	03-03-08	0.32	0.24
			01-04-08	0.35	0.57
			06-05-08	0.34	0.46
			02-06-08	0.34	0.35
			01-07-08	0.28	0.29

			01-08-08	0.34	0.31
			01-09-08	0.35	0.38
			01-10-08	0.32	0.47
			03-11-08	0.34	0.44
			01-12-08	0.33	0.43
			05-01-09	0.33	0.49
			02-02-09	0.36	0.50
England, Devon	grassland	CL	28-11-08	0.43	0.39
			15-12-08	0.42	0.40
			09-01-09	0.43	0.41
			23-01-09	0.42	0.44
			16-02-09	0.43	0.47
			06-03-09	0.42	0.35
			20-03-09	0.42	0.50
			03-04-09	0.42	0.47
			17-04-09	0.44	0.48
			15-05-09	0.46	0.86
			04-06-09	0.43	0.40
			08-07-09	0.43	0.43
			04-09-09	0.44	0.40
			05-10-09	0.44	0.46
			20-02-09	0.43	0.44
			20-02-09	0.42	0.45
			20-02-09	0.42	0.44
			07-05-09	0.44	0.51
			07-05-09	0.43	0.52
			07-05-09	0.41	0.51
			07-08-09	0.44	0.46
			07-08-09	0.43	0.43
			07-08-09	0.43	0.43
			06-11-09	0.43	0.40
			06-11-09	0.43	0.40
			06-11-09	0.42	0.41
England, Devon	grassland	IPL-H	28-11-08	0.42	0.17
			15-12-08	0.36	0.32
			09-01-09	0.39	0.25
			23-01-09	0.36	0.34
			16-02-09	0.35	0.39
			06-03-09	0.41	0.27
			20-03-09	0.39	0.42
			03-04-09	0.39	0.40
			17-04-09	0.38	0.34
			15-05-09	0.38	0.75
			04-06-09	0.37	0.32

			08-07-09	0.44	0.28
			04-09-09	0.46	0.28
			05-10-09	0.45	0.34
			20-02-09	0.35	0.37
			20-02-09	0.39	0.36
			20-02-09	0.36	0.36
			07-05-09	0.41	0.33
			07-05-09	0.43	0.35
			07-05-09	0.43	0.40
			07-08-09	0.37	0.32
			07-08-09	0.43	0.32
			07-08-09	0.43	0.35
			06-11-09	0.40	0.29
			06-11-09	0.42	0.27
			06-11-09	0.44	0.27
England, Devon	grassland	IPL-OH	28-11-08	0.42	0.18
			15-12-08	0.36	0.33
			09-01-09	0.39	0.24
			23-01-09	0.36	0.34
			16-02-09	0.35	0.39
			06-03-09	0.42	0.27
			20-03-09	0.39	0.44
			03-04-09	0.39	0.41
			17-04-09	0.38	0.36
			15-05-09	0.40	0.74
			04-06-09	0.39	0.32
			08-07-09	0.44	0.29
			04-09-09	0.46	0.29
			05-10-09	0.43	0.34
			20-02-09	0.36	0.37
			20-02-09	0.40	0.34
			20-02-09	0.37	0.38
			07-05-09	0.43	0.35
			07-05-09	0.42	0.36
			07-05-09	0.43	0.39
			07-08-09	0.38	0.39
			07-08-09	0.42	0.34
			07-08-09	0.44	0.33
			06-11-09	0.42	0.27
			06-11-09	0.43	0.26
			06-11-09	0.44	0.31

* denotes duplicate injection; all other replicate dates represent results of duplicate or triplicate sample processing.

Chapter 6

Constraints on the application of the MBT-CBT paleothermometer at high latitude environments (Svalbard, Norway)

Francien Peterse, Jung-Hyun Kim, Stefan Schouten, Dorthe Klitgaard Kristensen, Nalân Koç, Jaap S. Sinninghe Damsté, 2009. *Organic Geochemistry* 40, 692-699.

Abstract

Branched glycerol dialkyl glycerol tetraethers (GDGTs) are membrane lipids of unknown bacteria that are ubiquitous in soil and peat. Two indices based on the distribution of these lipids in soils, the Cyclization of Branched Tetraethers (CBT) and the Methylation of Branched Tetraethers (MBT) indices have been shown to correlate with soil pH, and mean annual air temperature (MAT) and soil pH, respectively, and can be used to reconstruct MAT in palaeoenvironments. To verify the extent to which branched GDGTs in marine sediments reflect the distribution pattern on land and whether these proxies are applicable for palaeo-climate reconstruction in high latitude environments with a MAT of <0 °C, we compared the branched GDGT distribution in Svalbard soils and nearby fjord sediments. Although branched GDGT concentrations in the soil are relatively low (0.02–0.95 µg/g dry weight (dw)) because of the cold climate and the short growing season, reconstructed MATs based on the MBT-CBT proxy are ca. -4 °C, close to the measured MAT (ca. -6 °C). Concentrations of branched GDGTs (0.01–0.20 µg/g dw) in fjord sediments increased towards the open ocean and the distribution was strikingly different from that in soil, i.e. dominated by GDGTs with one cyclopentane moiety. This resulted in MBT-CBT-reconstructed MAT values of 11-19 °C, well above measured MAT. The results suggest that at least part of the branched GDGTs in marine sediments in settings with a low soil organic matter (OM) input may be produced in situ. In these cases, the application of the MBT-CBT palaeothermometer will generate unrealistic MAT reconstructions. The MBT-CBT proxy should therefore only be used at sites with a substantial input of soil OM relative to the amount of marine OM, i.e. at sites close to the mouth of rivers with a catchment area where sufficient soil formation takes place and the soil thus contains substantial amounts of branched GDGTs.

6.1. Introduction

Branched glycerol dialkyl glycerol tetraether lipids (GDGTs; I–III, *Fig. 6.1*) as such were discovered in a Dutch Holocene peat deposit and identified by Sinninghe Damsté et al. (2000) using nuclear magnetic resonance (NMR) spectroscopy, their branched alkyl chain building blocks being first identified in the Messel shale by Chappe et al. (1980) using ether cleavage of the organic matter (OM). Branched GDGTs differ from archaeal GDGT lipids in that their carbon skeletons are not isoprenoid, but comprise branched carbon chains. Branched GDGTs possess 4–6 methyl groups and can contain up to two cyclopentane moieties that are likely formed by internal cyclization (Weijers et al., 2006a). The assignment of the exact origin of the branched GDGTs was ambiguous because of their mixed bacterial (branched carbon chains) and archaeal (membrane-spanning tetraethers, ether lipids) structural characteristics. Weijers et al. (2006a) examined the stereo configuration of the glycerol moieties of the membrane lipids and found them to be identical to those in glycerol moieties synthesized by bacteria. In combination with the fact that branched dialkyl glycerol diethers have been found in thermophilic bacteria (Langworthy et al., 1983; Huber et al., 1992; Sinninghe Damsté et al., 2007) and that they contain characteristic branched alkyl chains, it is likely that the branched GDGTs are produced by bacteria. However, the exact phylogenetic position of these bacteria is unknown.

Branched GDGTs occur ubiquitously in soils worldwide (Weijers et al., 2006b), but have also been found in coastal marine sediments, where they have been deposited after transportation by rivers from land (Schouten et al., 2000; Hopmans et al., 2004; Weijers et al., 2006b; Kim et al., 2006; Walsh et al., 2008; Rueda et al., 2009). Their abundance in sediments from coastal zones has been proposed to indicate the input of soil OM to a marine system and is quantified in the Branched and Isoprenoid Tetraether (BIT) index (Hopmans et al., 2004). In this index, the amount of the branched GDGTs, representing soil OM in the sediment, is compared with the amount of crenarchaeol (IV, *Fig. 6.1*), an isoprenoid GDGT derived predominantly from marine planktonic archaea (Sinninghe Damsté et al., 2002; Schouten et al., 2008b):

$$BIT = [Ia+IIa+IIIa]/[Ia+IIa+IIIa+IV] \qquad (6.1)$$

The Roman numerals refer to the structures in *Fig. 6.1*. Consequently, a BIT index of 1 represents soil OM alone, whereas an index of 0 represents fully marine derived OM. In addition to marine sediments, branched GDGTs have also been found in lakes where they likely originate from soil erosion (Powers et al., 2004; Blaga et al., 2009).
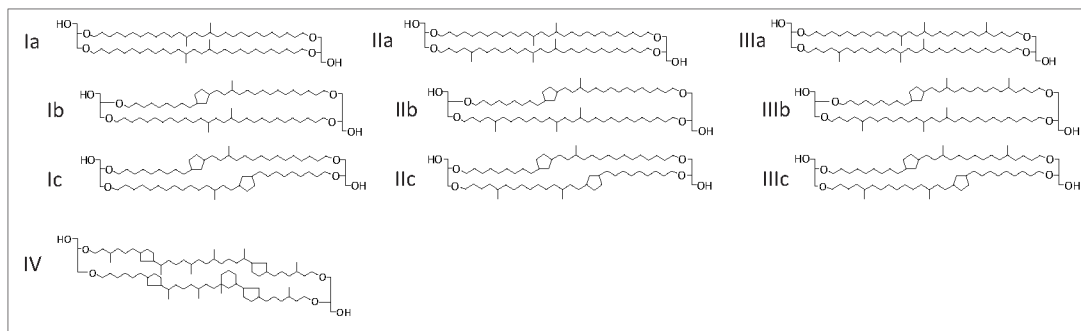

Fig. 6.1. Molecular structures of branched GDGTs and crenarchaeol.

Weijers et al. (2007c) analyzed the relative distribution of branched GDGTs for a dataset comprising 130 globally distributed soils and showed that MAT and soil pH were major factors controlling the GDGT distribution. The number of cyclopentane moieties in the branched GDGTs is related to soil pH, whereas the number of methyl groups is related to both MAT and soil pH. Based on these relationships, two indices were proposed to quantify the changes in branched GDGT distribution: the CBT index, reflecting soil pH, and the MBT index for both MAT and soil pH. The indices are defined as:

$$MBT = [Ia+Ib+Ic]/[Ia+Ib+Ic+IIa+IIb+IIc+IIIa+IIIb+IIIc] \tag{6.2}$$

$$CBT = -LOG ([Ib+IIb]/[Ia+IIa]) \tag{6.3}$$

The Roman numbers again refer to the structures given in *Fig. 6.1*. In order to reconstruct palaeotemperatures and past soil pH on the basis of the distribution of branched GDGTs, the relationships of the two indices with pH and MAT can be combined, resulting in Eq. 6.4:

$$MBT = 0.122 + 0.187 \times CBT + 0:020 \times MAT \qquad (r^2=0.77) \tag{6.4}$$

Recently, analysis of the branched GDGT distribution in geothermally heated soils confirmed that the MBT index is strongly related to temperature (Peterse et al., 2009b). The MBT-CBT proxy has been applied to marine sediments from several areas and geological ages (Weijers et al., 2007a,b; Schouten et al., 2008a; Rueda et al., 2009). For example, based on the distribution of branched GDGTs in a sediment core from the Congo River fan, changes in the continental air temperature of tropical Africa over the last 25,000 yr could be reconstructed (Weijers et al., 2007a).

Despite these promising results, many issues regarding the proxies remain to be resolved. First, the MBT-CBT proxy has been mainly applied to tropical areas and its applicability to high latitude environments with a MAT below 0 °C has not been assessed. In high latitude areas the growing season is short and the rate of soil formation is low, in contrast to the relatively constant environmental conditions in the humid tropics, and this might potentially affect the MBT-CBT proxy. Furthermore, it has been applied to areas where large amounts of branched GDGTs were transported from land to sea, e.g. by rivers (Hopmans et al., 2004; Weijers et al., 2007a), or ice rafting events (Schouten et al., 2007b, 2008a,b), but not to high latitude areas where soils are poorly developed, the land is covered with snow for most of the year and glaciers and spring snow melt are the main mechanisms for transport of soil OM to the marine environment. Lastly, the distributions of branched GDGT in soils and nearby marine sediments have not been directly compared, so the extent to which the continental climate signal is reflected in nearby marine sediments is not clear. To address these issues, we analyzed the branched GDGT distribution in soils from Svalbard, an archipelago in the northern Atlantic Ocean between 74°N and 81°N, and in nearby fjord and ocean sediments.

6.2. Material and methods

6.2.1. Environmental setting

Svalbard is an archipelago in the northern Atlantic Ocean, between Norway and the North Pole. About 60% of the land is covered by glaciers. The largest ice-free zones can be found in the central and western areas. At the latter site, an arm of the Gulf Stream (West Spitsbergen Current) flows northwards,

resulting in a milder climate and longer ice-free periods relative to eastern Svalbard, where the cold East Spitsbergen Current influences the formation of sea ice (*Fig. 6.2a*). An overview of the climate is given by Birks et al. (2004). In short, Svalbard has a permafrost layer that can be up to 450 m thick, but this layer may be defrosted up to 1 m from the surface during summer. The mean annual precipitation is about 400 mm along the west coast and decreases to 200–300 mm towards the heads of the fjords and inland. Much of the precipitation falls as snow and western Svalbard is generally snow covered between early September to late May/early June. The growing season is therefore short, only 6–8 weeks, and the MAT for Ny Ålesund, located in our study area, is 5.8 °C (Birks et al., 2004).

6.2.2. Soil and marine surface sediment sampling

In total, nine soils were sampled from three different locations on Svalbard in September 2007. The sampling sites at each location were selected according to their variation in topographic position or vegetation type (*Table 6.1*). Around Longyearbyen one site was sampled, around Ny Ålesund two sites and on the Mitra Peninsula soils were sampled at six sites along a small river flowing from Lake Dieset to the ocean (*Fig. 6.2a and b*). Depending on the depth at which permafrost or bedrock were encountered, the upper 5–10 cm of the soil were collected with a small scoop and stored in geochemical bags. Besides the soils, a coal seam (NA3) and beach sand (NA4) were sampled around Ny Ålesund and freshly weathered rock (LB2) was sampled close to Longyearbyen.

The sediments were retrieved from the relatively ice free Kongsfjorden and Krossfjorden, situated in the western part of Svalbard (*Fig. 6.2a and b*). Twenty nine surface sediments (0–1 cm) were sub-sampled from cores that were collected with a multicorer during a SciencePub IPY-cruise on the R/V Lance in September 2007 (*Fig. 6.2b*). All samples were stored at -20 °C, transported to the Royal NIOZ and upon arrival at the laboratory kept at -40 °C until further analysis.
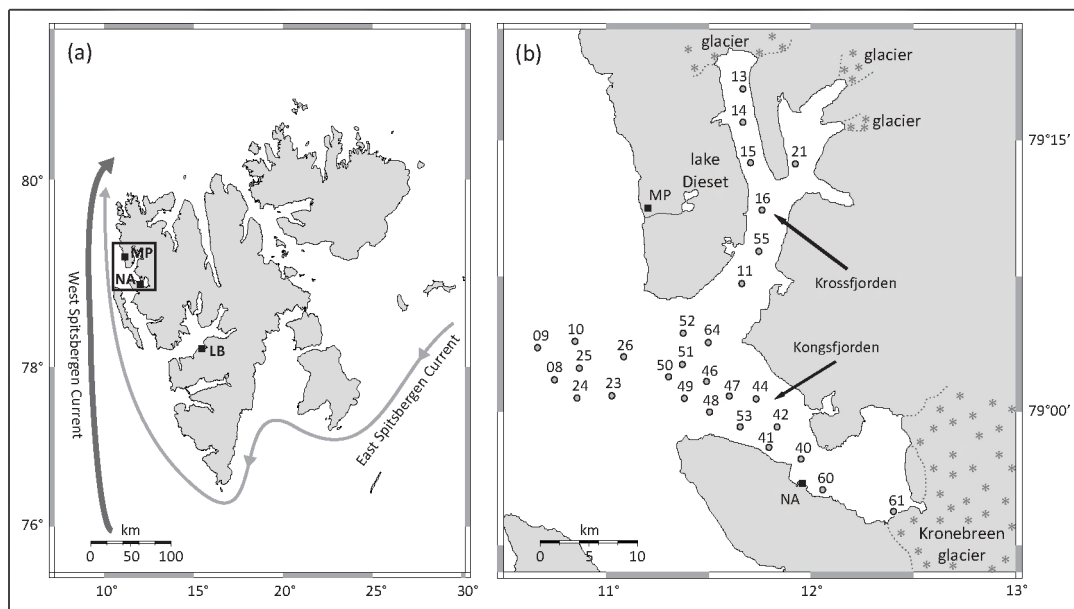

Fig. 6.2. Map of a' Svalbard showing locations of soil sampling sites; LB, Longyearbyen; NA, Ny Ålesund; MP, Mitra Peninsula and b) Krossfjorden and Kongsfjorden showing locations of marine sediment sampling sites (see also *Table 2*, sample labels with prefix NP-07-13).

6.2.3. Organic carbon content and soil pH

All samples were freeze dried and powdered with a mortar and pestle, and about 30 mg of each were weighed and decalcified using HCl. The decalcified samples were analyzed for organic carbon content (C_{org}) using a Flash EA 1112 Thermo elemental analyzer. The pH of the soil samples was measured with a WTW pH 315i meter in a 1:2.5 soil:water (w/v) mixture.

6.2.4. GDGT analysis

Lipids were extracted ($3\times$) from the freeze-dried and powdered soils and sediments using a DIONEX accelerated solvent extractor (ASE 200) at 100 °C and a pressure of 7.6×10^6 Pa for 5 min with a mixture of dichloromethane (DCM):MeOH 9:1 (v/v). The extracts were dried using a rotary evaporator under near vacuum. The samples were dissolved in DCM and passed over a Na_2SO_4 column to remove remaining water. All samples were dried again under N_2 and weighed, after which an internal C_{46} GDGT standard was added (cf. Huguet et al., 2006). Depending on weight, 0.05–1.0 µg C_{46} GDGT standard was added to the extracts. The extracts were separated into apolar and polar fractions over an activated Al_2O_3 column, using hexane:DCM 9:1 (v/v) and DCM:MeOH 1:1 (v/v) mixtures, respectively. The polar fraction (containing GDGTs) was dried under N_2, ultrasonically dissolved in hexane:isopropanol (99:1, v/v) and filtered over a 0.45 µm PTFE filter. The polar fractions were concentrated to 3 mg/ml prior to analysis using high performance liquid chromatography – atmospheric pressure chemical ionization/mass spectrometry (HPLC/APCI-MS).

6.2.5. HPLC/APCI-MS

The branched GDGTs were analyzed using HPLC/APCI-MS with an Agilent 1100 series instrument equipped with automatic injector and Chemstation software according to Schouten et al. (2007a), with minor modifications. Briefly, component separation was achieved with an Alltech Prevail Cyano column (150 mm×2.1 mm; 3 µm). The branched GDGTs were eluted isocratically with 90% A and 10% B for 5 min and then with a linear gradient to 16% B for 34 min, where A = hexane and B = hexane:isopropanol 9:1 (v/v). The injection volume for all samples was 10 µl. To detect and quantify the different GDGTs, single ion monitoring of [M+H]$^+$ -ions was used. Absolute quantification was achieved by calculating the area of its corresponding peak in the chromatogram, comparing it with the peak area of the internal standard and correcting for the different response factors (cf. Huguet et al., 2006). BIT, MBT and CBT indices were calculated according to Eqs. 6.1-6.3, respectively. The average reproducibility of the indices, based on duplicate analysis of a selected number of soils and sediments, is 0.002 for the BIT, 0.003 for the MBT and 0.01 for the CBT index.

6.3. Results

6.3.1. Soils

The C_{org} (wt%) content of the soils varies between 0.6%, for two relatively undeveloped soils under little vegetation on the Mitra Peninsula (MP2, MP5), and 7.8% for a soil under a thick moss layer at Longyearbyen (LB1). C_{org} contents for the non-soil samples are 0.08% for beach sand (NA4), 1.8% for the freshly weathered rock (LB2) and 42.9% for a coal seam close to Ny Ålesund (NA3; *Table 6.1*). Soil pH values are between 4.4 for Longyearbyen soil (LB1) and 9.3 for a soil from the shore of Lake Dieset (MP6; *Table 6.1*). Both the coal seam and the freshly weathered rock have a pH of 7.5 and the pH of

Table 6.1. Description and general properties of Svalbard soils, coal seam, beach sand, and freshly weathered rock.

Sample	Site description	Latitude	Longitude	C_{org} (%)	pH
NA1	Thick layer of green mosses	78°55′31 N	011°56′03 E	5.4	7.4
NA2	Moss patches	78°55′24 N	011°55′10 E	2.2	6.3
NA3	Coal seam	78°55′37 N	011°55′03 E	42.9	7.5
NA4	Beach sand	78°55′39 N	011°56′16 E	0.08	9.5
MP1	Close to river mouth, stones and pebbles, patches of lichens	79°11′12 N	011°10′13 E	1.5	7.1
MP2	River bank, probably flooded during ice melting in spring, mainly stones with patches of moss and lichens	79°11′34 N	011°11′59 E	0.6	8.3
MP3	River bank, probably flooded during ice melting in spring, mainly stones with small patches of mosses and lichens	79°12′04 N	011°16′01 E	1.8	5.5
MP4	Stones and pebbles, patches of mosses and lichens	79°12′13 N	011°18′15 E	1.4	8.3
MP5	Lake shore, stones and pebbles, occasional patches of mosses	79°12′01 N	011°19′01 E	0.6	8.3
MP6	Lake shore, stones and pebbles, no vegetation	79°12′22 N	011°19′02 E	n.d.[a]	9.3
LB1	Thick moss layer	78°12′57 N	015°36′43 E	7.8	4.4
LB2	Freshly weathered rock	78°12′36 N	015°37′54 E	1.8	7.5

[a] Not determined.

Table 6.2. Branched GDGT concentrations and proxy values for Svalbard soils, coal seams, beach sand and freshly weathered rock.

Sample	Branched GDGT concentration (ng/g dry wt soil)[a]									Total branched GDGTs (mg/g dry wt soil)	BIT	CBT	MBT	MBT-CBT-derived MAT (°C)
	Ia	Ib	Ic	IIa	IIb	IIc	IIIa	IIIb	IIIc					
NA1	107	25	n.d.[b]	391	76	n.d.	347	n.d.	n.d.	0.95	1.00	0.69	0.14	-5.6
NA2	18	1	n.d.	40	1	0.3	10	n.d.	n.d.	0.07	0.98	1.54	0.27	-6.9
NA3	n.d.	n.d.	n.d.	n.d.	n.d.	n.d.	n.d.	n.d.	n.d.	n.d.	-[c]	-	-	-
NA4	n.d.	n.d.	n.d.	n.d.	n.d.	n.d.	n.d.	n.d.	n.d.	n.d.	-	-	-	-
MP1	42	3	0.3	82	6	1	2	n.d.	n.d.	0.15	0.96	1.14	0.29	-2.1
MP2	12	4	0.4	41	13	1	34	2	0.3	011	0.79	-.49	0.15	-3.3
MP3	43	1	1	86	3	1	20	1	n.d.	0.16	0.98	1.46	0.29	-5.4
MP4	8	3	1	37	16	1	23	1	n.d.	0.09	0.95	0.37	0.14	-2.7
MP5	5	2	0.3	19	8	1	15	1	n.d.	0.05	0.90	0.35	0.15	-2.1
MP6	2	1	0.1	7	2	0.3	6	0.3	0.2	0.02	0.86	0.44	0.14	-3.1
LB1	39	7	n.d.	117	12	n.d.	29	n.d.	n.d.	0.20	0.99	0.92	0.22	-3.6
LB2	n.d.	n.d.	n.d.	n.d.	n.d.	n.d.	n.d.	n.d.	n.d.	n.d.	-	-	-	-

[a] Roman numbers refer to structures in *Fig. 6.1*.
[b] Below detection limit.
[c] Could not be calculated.

the beach sand is 9.5.

Branched GDGTs are present in all 9 soils. For the beach sand, freshly weathered rock and coal seam (NA4, LB2 and NA3, respectively) they were not detected. The concentration in the soils varies between 0.02 and 0.95 µg/g soil dw (*Table 6.2*). GDGT II is most abundant in these soils and GDGTs I and III are present in smaller amount (*Fig. 6.3a*). The branched GDGTs without cyclopentane moieties (Ia, IIa and IIIa) are always more abundant than their counterparts possessing one or two cyclopentane moieties.

The average distribution pattern is similar to that of a Svalbard soil reported by Weijers et al. (2007c). The MBT index, calculated using Eq. 6.2, varies between 0.14 and 0.29 and the CBT index, calculated using Eq. 6.3, varies between 0.35 and 1.54 (*Table 6.2*). BIT values, calculated according to Eq. 6.1, vary between 0.79 and 1.00 (*Table 6.2*). For the beach sand, freshly weathered rock and coal seam MBT, CBT and BIT indices could not be calculated, as they do not contain any branched GDGTs.

6.3.2. Surface sediments

The surface sediments from Kongsfjorden and Krossfjorden vary in C_{org} content from 0.2% close to the glacier mouth at Kongsfjorden to 2.3% in the open ocean. Values for both fjords are about 1%, increasing to more than 1.5% towards the entrance and finally increasing to 2.3% for the open ocean sediments (*Table 6.3, Fig. 6.4a*).

Branched GDGTs occur in all the fjord sediments. The amounts vary from 0.01 to 0.20 μg/g sediment dw (*Table 6.3*). The lowest concentrations are in both fjords, but increase from the fjords towards the open ocean, where the largest amounts are present (*Fig. 6.4b*). The branched GDGTs are generally dominated by GDGT II (40–49% of total branched GDGTs). Strikingly, those with one cyclopentane moiety (Ib and IIb) are present in higher amount (*Fig. 6.3b*) than those without cyclopentane moieties (Ia and IIa). The MBT values for the marine sediments vary from 0.26 to 0.47 (*Table 6.3*). In general, MBT values decrease from the fjord towards the open ocean (*Fig. 6.4d*). The highest range of MBT values is found for the Krossfjorden sediments, where they vary between 0.40 and 0.46. For Kongsfjorden, the values range between 0.34 and 0.39, except for the sediment close to the glacier mouth (NP-07-13-61) where the value is 0.26. The domination of branched GDGTs with one cyclopentane moiety over those without cyclopentane moieties results in negative CBT values for nearly all the marine sediments. The CBT values range between 0.35 and 0.18 and their spatial distribution does not show a clear pattern (*Fig. 6.4e*). The sample taken in front of the glacier is again distinctly different and has a positive CBT value of 0.16. BIT indices vary between 0.01 and 0.02, where 0.01 is found for the fjord sediments and 0.02 for the open ocean sediments (*Table 6.3*). The sediment at the glacier front differs from the rest and has a BIT index of 0.12.
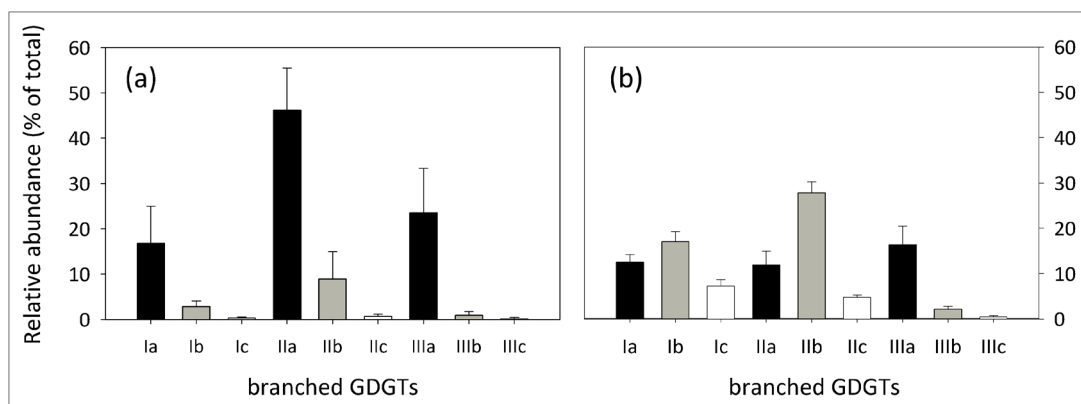

Fig. 6.3. Bar plots with standard deviation of average branched GDGT distributions in a) Svalbard soils (n=9) and b) Svalbard marine surface sediments (n=29). Roman numerals refer to structures in *Fig. 6.1*.

Sample	Latitude	Longitude	C_{org} (%)	Branched GDGT concentration (ng/g dry wt sediment)[a]									Total branched GDGTs (mg/g dry wt sediment)	BIT	CBT	MBT	MBT-CBT-derived MAT (°C)
				Ia	Ib	Ic	IIa	IIb	IIc	IIIa	IIIb	IIIc					
NP-07-13-08	79°01.77'N	010°44.95'E	2.3	23	30	12	21	52	9	35	5	1	0.19	0.02	-0.28	0.35	13.8
NP-07-13-09	79°03.57'N	010°39.91'E	1.6	21	26	10	22	48	9	39	5	1	0.18	0.02	-0.24	0.32	11.9
NP-07-13-10	79°03.92'N	010°50.90'E	2.1	19	24	9	17	41	8	35	4	1	0.16	0.02	-0.26	0.33	12.6
NP-07-13-11	79°07.11'N	011°39.75'E	0.8	5	6	3	4	11	2	5	1	0.3	0.04	0.01	-0.27	0.38	15.3
NP-07-13-13	79°17.78'N	011°40.09'E	0.5	1	2	1	1	2	0.3	1	n.d.[b]	n.d.	0.01	0.01	-0.23	0.46	18.9
NP-07-13-14	79°15.97'N	011°40.09'E	0.6	2	2	1	1	3	0.5	1	0.2	n.d.	0.01	0.01	-0.21	0.42	16.8
NP-07-13-15	79°13.75'N	011°42.35'E	0.7	3	4	2	2	6	1	2	0.4	n.d.	0.02	0.01	-0.26	0.43	17.7
NP-07-13-16	79°11.16'N	011°45.68'E	1.0	8	12	5	7	19	3	8	n.d.	n.d.	0.06	0.01	-0.29	0.40	16.7
NP-07-13-21	79°13.70'N	011°55.41'E	1.0	4	6	3	3	9	1	2	0.5	n.d.	0.03	0.01	-0.35	0.44	19.0
NP-07-13-23	79°00.89'N	011°01.66'E	2.1	17	23	9	18	43	8	36	4	1	0.16	0.02	-0.27	0.31	21.1
NP-07-13-24	79°00.76'N	010°51.53'E	2.1	19	23	9	18	40	8	34	4	1	0.15	0.02	-0.22	0.33	12.6
NP-07-13-25	79°02.43'N	010°52.19'E	2.1	24	30	12	24	49	9	39	5	1	0.19	0.02	-0.22	-/34	12.9
NP-07-13-26	79°03.06'N	011°05.20'E	1.9	17	22	9	16	38	7	29	3	1	0.14	0.02	-0.26	0.34	13.2
NP-07-13-40	78°57.35'N	011°57.11'E	1.0	8	12	5	9	22	4	11	2	0.4	0.07	0.01	-0.33	0.35	14.4
NP-07-13-41	78°58.00'N	011°47.68'E	1.2	11	18	8	12	32	6	19	3	1	0.11	0.01	-0.33	0.34	14.1
NP-07-13-42	78°59.16'N	011°50.10'E	1.2	9	14	6	9	23	4	12	2	0.4	0.08	0.01	-0.31	0.36	15.0
NP-07-13-44	79°00.72'N	011°43.89'E	1.3	10	16	7	9	25	5	12	2	1	0.08	0.01	-0.33	0.38	15.9
NP-07-13-46	79°01.69'N	011°29.43'E	1.5	10	15	6	9	22	4	13	2	0.5	0.08	0.02	-0.29	0.39	16.3
NP-07-13-47	79°00.87'N	011°36.10'E	1.3	7	11	5	7	17	3	10	1	0.4	0.06	0.01	-0.31	0.37	15.3
NP-07-13-48	78°59.99'N	011°30.33'E	1.8	12	17	7	12	29	5	20	2	1	0.11	0.01	-0.29	0.34	13.6
NP-07-13-49	79°00.74'N	011°22.92'E	1.9	13	18	7	12	31	5	20	3	1	0.11	0.01	-0.29	0.35	13.9
NP-07-13-50	79°01.95'N	011°18.35'E	1.7	14	20	8	14	34	6	22	3	1	0.12	0.01	-0.29	0.35	14.2
NP-07-13-51	79°02.64'N	011°22.30'E	1.6	23	34	14	22	56	11	38	5	n.d.	0.20	0.01	-0.31	0.35	14.3
NP-07-13-52	79°04.38'N	011°22.58'E	1.5	6	6	3	3	8	1	4	0.5	n.d.	0.03	0.01	-0.18	0.47	18.9
NP-07-13-53	78°59.15'N	011°39.21'E	1.5	12	18	7	11	27	5	15	2	1	0.10	0.01	-0.31	0.38	15.9
NP-07-13-55	79°08.90'N	011°44.78'E	0.9	7	10	4	7	17	3	7	1	0.4	0.06	0.01	-0.31	0.37	15.4
NP-07-13-60	78°55.63'N	012°03.38'E	0.6	4	6	3	4	10	2	4	1	n.d.	0.03	0.01	-0.32	0.37	15.4
NP-07-13-61	78°54.41'N	012°24.20'E	0.2	1	1	0.3	2	2	0.2	2	0.3	n.d.	0.01	0.12	0.16	0.26	5.3
NP-07-13-64	79°03.86'N	011°29.88'E	1.5	9	13	5	7	20	4	11	2	0.4	0.07	0.01	-0.31	0.38	15.9

6.4. Discussion

6.4.1. Branched GDGTs in Svalbard soils

During the process of soil formation, physical and chemical characteristics of the soil change. In general C_{org}, total N and soil moisture increase, whereas soil pH and particle size decrease with time (Bekku et al., 1999; Hodkinson et al., 2003). The low C_{org} values for the Svalbard soils with a high pH (i.e. C_{org} <1.5% and pH >8; *Table 6.1*) suggest that little soil formation has taken place at these sites. The low rate of soil formation on Svalbard results in lower growth rate for the microbial biomass (Bekku et al., 1999), which may explain why the branched GDGT concentrations in the soils are relatively low. For example, their amounts are comparable to those in similar environments like Alaska (0.07 µg/g soil dw), Greenland (0.10 µg/g soil dw) and Canada (0.07 µg/g soil dw), but lower than those from temperate environments (e.g. France, 1.6 µg/g soil dw; Weijers et al., 2006b). Accordingly, it seems that the rate and duration of soil formation are important for the amount of branched GDGTs in a soil. This may also explain the absence of branched GDGTs from the freshly weathered bedrock and the beach sand, as soil forming processes have not yet taken place there. The absence of branched GDGTs from the coal seam may be explained by the high maturity of the coal, resulting in thermal destruction of fossil branched GDGTs (cf. Schouten et al., 2004). The fact that some Svalbard soils with a high C_{org} content have a low concentration of branched GDGTs may be caused by the type of vegetation and OM at those sites, i.e. soils NA1 and LB1 were under a thick layer of moss, which contains recalcitrant compounds that decompose slowly (e.g. Hobbie, 1996, 2000). Furthermore, the low soil temperature and the short growing season slow down decomposition, resulting in an accumulation of non-decomposable compounds and thus an increase in C_{org}, while microbial activity remains limited (Hobbie et al., 2000).

Despite the generally low concentrations of branched GDGTs, they are sufficient to reliably determine BIT, CBT and MBT indices. The CBT index relates to in situ soil pH (r^2=0.51), but to a lesser extent than observed for the global soil calibration (r^2=0.70; Weijers et al., 2007c) or geothermally heated soils (r^2=0.76; Peterse et al., 2009b). MAT estimates based on the MBT-CBT indices and the transfer function (Eq. 6.4) result in reconstructed temperatures between -6.9 °C and -2.1 °C (*Table 6.2*). Thus, even though the growing season on Svalbard is short and soil formation is limited, resulting in relatively low branched GDGT concentrations in the soils, the distribution closely reflects the measured MAT of about -6 °C for Svalbard (Birks et al., 2004). This supports the applicability of the MBT-CBT temperature proxy for high latitudinal soils with a MAT <0 °C.

6.4.2. Branched GDGTs in marine surface sediments

If branched GDGTs are primarily derived from soil and are transported from land to the sea by, e.g. rivers, it would be expected that they would decrease in concentration from land to the open ocean. However, an opposite pattern is observed for Kongsfjorden and Krossfjorden (*Fig. 6.4b*), in contrast with earlier results obtained by Hopmans et al. (2004), Kim et al. (2006) and Walsh et al. (2008), who all found that branched GDGT concentrations decrease with increasing distance from the shore. The C_{org} content of the sediments follows the same trend as the branched GDGTs and is also higher in the open ocean than in the fjord sediments (*Fig. 6.4a*). To distinguish between high branched GDGT concentrations re-

---

Table 6.3. General properties, branched GDGT concentrations and proxy values for marine surface sediments in Kongsfjorden and Krossfjorden.
[a] Roman numbers refer to structures in *Fig. 6.1*.
[b] Below detection limit.

sulting from high C_{org} content and high branched GDGT concentrations resulting from an actual elevated branched GDGT input, the amounts of branched GDGTs are normalized to C_{org}. However, the overall pattern does not change substantially, i.e. the C_{org}-normalized branched GDGT concentrations are still somewhat higher in the open ocean than in the fjords (*Fig. 6.4c*). These results suggest that in Svalbard, the input of soil OM, and thus branched GDGTs, to the fjords is limited. This is likely due to a combination of factors, i.e. (i) the limited development of soil on Svalbard, (ii) the low abundance of branched GDGTs in the soil and (iii) the terrestrial material transported to the fjords by glaciers or spring snow melt is low in soil OM content, because the growth of plants and soil development is limited on the heavily glaciated land surrounding the fjords (Winkelmann and Knies, 2005).

The low BIT index values for the sediments indicate that marine OM dominates over soil OM in the fjords. This agrees with results of Winkelmann and Knies (2005), who found that up to 90% of OM in the sediments of these fjords was of marine origin, on the basis of $\delta^{13}C$ values of C_{org}. They attributed this to an increased production of marine OM as a result of local upwelling of nutrient rich Atlantic water specifically in Kongsfjorden and Krossfjorden. The only site in our study area where there is an indication of significant input of soil OM was in front of the Kronebreen glacier in Kongsfjorden (NP-07-13-61; *Fig. 6.2b*). The BIT index for the sediment from this site is 0.12 and the branched GDGT distribution differs substantially from the other sediments, being more like the distribution in the soils. We conclude that, in this specific case, the glacier was likely responsible for the transport of some soil material to the fjord.

6.4.3. MBT-CBT proxy for marine surface sediments

The branched GDGT distribution in all but one marine surface sediment differs strongly from that in the soils (*Fig. 6.3a and b*). For example, the relative amount of GDGT IIa is clearly lower in the sediments than in the soils. Another difference is the high abundance of branched GDGTs with one cyclopentane moiety (Ib and IIb; *Fig. 6.3b*) in the marine sediments, while branched GDGTs without cyclopentane moieties are most abundant in soils (*Fig. 6.3a*). To the best of our knowledge, this domination of branched GDGTs with a cyclopentane moiety over branched GDGTs without cyclopentane moieties has not been reported for soils (e.g. Weijers et al., 2007c) or marine sediments (e.g. Weijers et al., 2007a,b; Schouten et al., 2008a). An explanation for the distribution could be the preferential degradation of branched GDGTs without rings upon transport from land to the ocean. However, this is not observed for other sites where large amounts of soil OM are deposited in marine sediments (e.g. Weijers et al., 2007a). Instead, we suggest that the different distribution in marine sediments is caused by *in situ* production of branched GDGTs, especially those containing a cyclopentane moiety. This is supported by the observation that branched GDGT concentrations actually increase towards the open ocean (*Fig. 6.4b*), rather than decreasing or remaining at a similar level.

The MBT-CBT-based MAT estimates based on the branched GDGT distributions in the marine sediments vary between 12 °C and 19 °C (*Table 6.3*), which is much higher than the reconstructed MAT based on the branched GDGT distribution in the soils and the measured MAT for the Kongsfjorden and Krossfjorden area of about -6 °C. The highest reconstructed temperatures are for the fjord sediments and these decrease towards the open ocean. Although the sediments have high MBT values compared to the Svalbard soils (*Tables 6.2 and 6.3*), the main cause for the large overestimate of MAT is the relatively high abundance of branched GDGTs with one cyclopentane moiety; the negative CBT indices for the marine sediments cause an overestimate of MAT upon application of the transfer function (Eq. 6.4). From
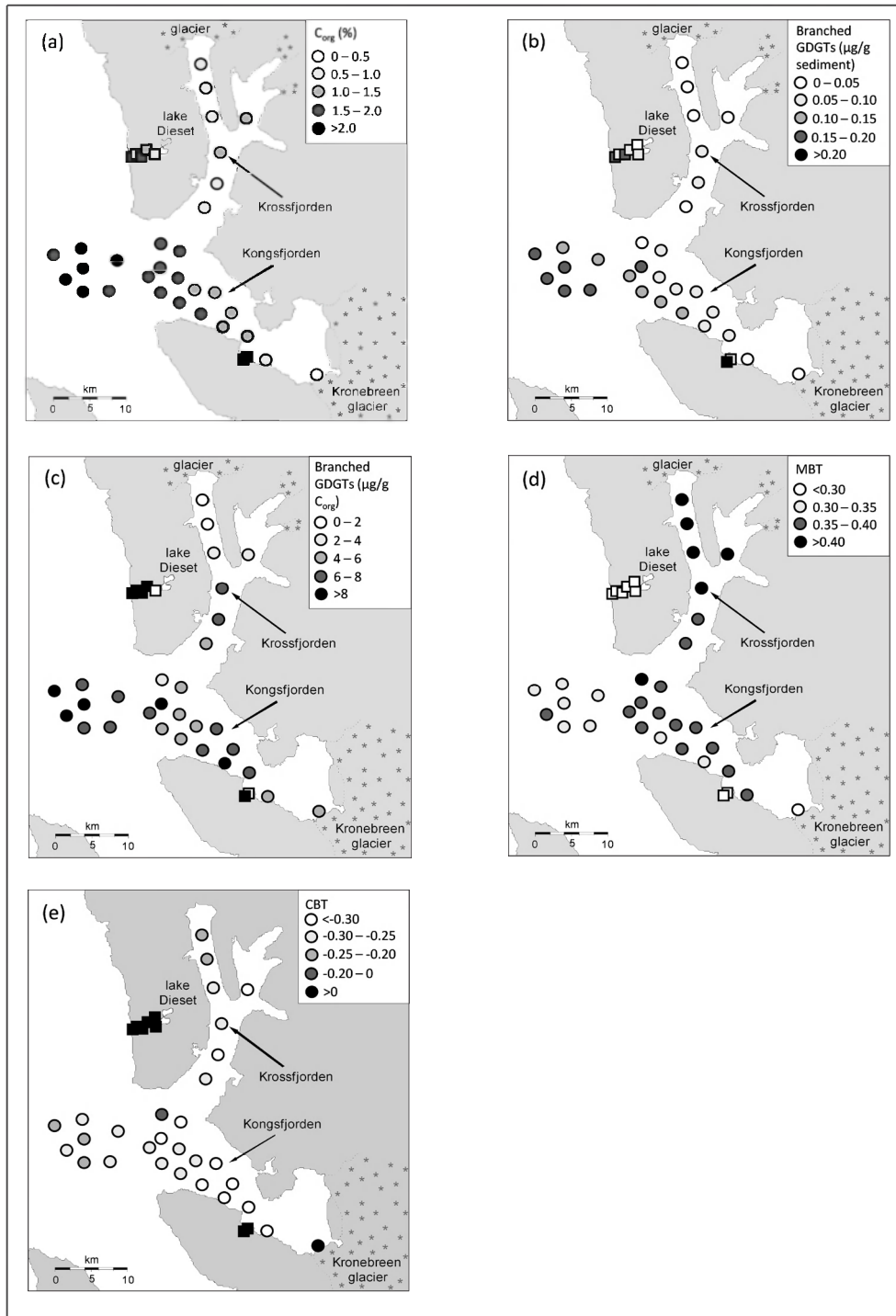
Fig. 6.4. Spatial distribution of a) C$_{org}$, b) branched GDGT concentration, c) branched GDGT concentration normalized to C$_{org}$, d) MBT index, and e) CBT index for marine surface sediments (dots) in Kongsfjorden an Krossfjorden and soils (squares) in Mitra Peninslula and Ny Ålesund.

these results it seems that the application of the MBT-CBT proxy to marine surface sediments is not valid for this particular environment. Only in front of the glacier mouth in Kongsfjorden, where we detected significant soil OM input, does MAT reconstruction result in a slightly cooler temperature of 5.3 °C. The branched GDGT distribution in this sediment is not dominated by cyclopentane-bearing branched GDGTs and therefore has a positive CBT value, just as for the Svalbard soils. Also the MBT value for this sediment lies in the range of the MBT values for the soils (*Tables 6.2 and 6.3*).

If we extrapolate our results to other environments, then it may be that in marine sediments with a low input of soil OM and a high production of marine OM at least part of the branched GDGTs may be produced in situ. Application of the MBT-CBT proxy using the transfer function based on the global soil calibration (Weijers et al., 2007c) will then result in unrealistic MAT reconstructions. It is therefore recommended that the MBT-CBT indices should only be used as a palaeothermometer at sites where a substantial input of soil OM relative to the amount of marine OM can be expected, e.g. those close to the mouth of rivers with well developed soils containing substantial amounts of branched GDGTs in their catchment areas. The critical limit of the BIT index for which the MBT-CBT proxy should not be used for marine sediments to reconstruct continental temperatures remains to be determined. Recently, Rueda et al. (2009) reported, however, realistic air temperature reconstructions using the MBT-CBT paleothermometer for marine sediments from the Skagerak with BIT values of ca. 0.07.

6.5. Conclusions

Branched GDGT concentrations in soils on Svalbard and those from similar other high latitude environments are low, likely due to limited soil formation and soil microbial activity. Despite these low amounts, the distribution still reflects the measured MAT. This confirms the applicability of the MBT-CBT temperature proxy for high latitude soils. However, the branched GDGT distribution in marine sediments from nearby fjords shows a strikingly different pattern from the Svalbard soils. This difference is likely due to a limited input of soil OM to the marine system and the low concentration of branched GDGTs in the soil OM. In addition, it seems that a part of the branched GDGTs, such as those with one cyclopentane moiety, may be produced in situ in the marine sediments. Thus, our results suggest that, in principle, the MBT-CBT proxy can be applied at terrestrial sites with a MAT <0 °C, but that MAT estimates based on the branched GDGT distribution in marine sediments can only be applied when large amounts of soil OM are present relative to marine OM.

Chapter 7

Identification and distribution of intact polar branched tetraether lipids in peat and soils

Abstract

Branched glycerol dialkyl glycerol tetraether lipids (GDGTs) are membrane lipids of soil bacteria that occur ubiquitously in soil, but their occurrence as intact polar lipids (IPLs) has not been well studied. Here we report the identification and distribution of IPL-branched GDGTs throughout a depth profile of a Swedish peat bog. In addition to two reported glycosidic IPL-branched GDGTs, we identified IPL-branched GDGTs with a hexose-glucuronyl, phospho-hexose, phospho-inositol, or hexose phosphoglycerol head group, based on mass spectrometry. A selected reaction monitoring (SRM) assay was developed to monitor changes in head group distribution with depth. The abundance of all monitored IPL-branched GDGTs increased below the water table, suggesting that they are primarily produced in this part of the peat. This is supported by the concentrations of CL and IPL-derived branched GDGTs, which also substantially increase below the water table. However, individual IPL trends differ; phospholipids in particular show a greater increase with depth than glycosidic IPLs. This implies that branched GDGTs are primarily produced in the anoxic part by anaerobic bacteria, since phospholipids are less stable than glycolipids and therefore serve as better marker for in situ production. The SRM method was also applied to two different soil types, which showed that most IPL-branched GDGTs were present in these, albeit in different distributions.

7.1. Introduction

Branched glycerol dialkyl glycerol tetraether (GDGT) lipids are membrane spanning components that occur ubiquitously in soil and peat (Sinninghe Damsté et al., 2000; Weijers et al., 2006b). Despite having archaeal traits (i.e. membrane spanning properties, ether bonds), the branched GDGTs are presumed to be of bacterial origin, based on their branched carbon chains and the typical bacterial stereo configuration of the glycerol backbone (Weijers et al., 2006a). Several proxies are based on the distributions of these branched GDGTs, i.e. the BIT (branched and isoprenoid tetraether) index, used to determine the relative input of soil organic matter (OM) to marine sediments (Hopmans et al., 2004), and the MBT-CBT (methylation of branched tetraethers/cyclisation of branched tetraethers) proxy used for the reconstruction of continental air temperatures and past soil pH (Weijers et al., 2007c). The exact type of bacteria that produces these GDGTs has not been identified, although it has been suggested that they are likely to be heterotrophic bacteria (Pancost and Sinninghe Damsté, 2003; Oppermann et al., 2010; Weijers et al., 2010) and bacteria of the phylum *Acidobacteria* have been proposed as potential producers (Weijers et al., 2009; Peterse et al., 2010).

Most branched GDGT studies have focussed only on the occurrence of core lipids (CLs) in the environment. However, such studies only investigate the pool of fossil material in a soil. In living cells, the branched GDGTs will most likely occur as intact polar lipids (IPLs), i.e. with polar head groups attached to the CLs. These IPLs are considered to be markers for living cells, as the head groups are thought to be quickly lost upon cell lysis (White et al., 1979; Harvey et al., 1986). IPLs can be measured indirectly after separating CLs from IPLs by way of column chromatography and subsequent acid hydrolysis of the IPL fraction to cleave the headgroups and release the CLs (e.g. Oba et al., 2006; Pitcher et al., 2009). Although useful, the method does not provide any information on the type of head group. To analyze IPLs as such, high performance liquid chromatography/electrospray ionization-mass spectrometry (HPLC/ESI-MS) can be used (Zink et al. 2003; Sturt et al. 2004). Using this method, Liu et al. (2010) recently identified two glycosidic IPL branched GDGTs, with a glucose (Glc) and with a glucuronyl (GlcA) head group, in the water saturated part of a German peat bog. They found that the IPL-branched GDGTs accounted for only 4-7% of the total IPLs in the peat bog, and suggested that their producers were likely not to be a major contributor to the microbial community. The concentration of the two IPL-branched GDGTs decreased with depth, whereas the amount of CLs increased, which was interpreted as an indication of accumulation of fossil branched GDGTs. However, it was unclear if these two IPL-branched GDGTs covered the full diversity of structures of IPL branched GDGT components, and how widespread they were.

We have analyzed the IPL-branched GDGTs in the acrotelm and catotelm of the Saxnäs Mosse peat bog in Sweden, previously examined for CL-GDGTs and 16S rRNA genes by Weijers et al. (2009). In addition, we examined two different soils and compared the IPL-branched GDGTs distributions with those of the peat bog.

7.2. Materials and methods

7.2.1. Sample collection and extraction

The Saxnäs Mosse is a raised bog in the south of Sweden (56° 51'20.78''N, 13 27'39.62''E) and is composed mainly of *Sphagnum magellanicum* and *Sphagnum papillosum*. The sampling site and sample collection have been described by Weijers et al. (2004, 2009). The peat bog is water saturated, and thus primarily anoxic, up to 25 cm depth. The upper 25 cm of the peat experiences alternating oxic and anoxic conditions as a result of changes in the water table level. At the time of sampling, (autumn

2003) the water table level was at ca. 14 cm. We used subsamples that were, at the time, taken at a 2 cm depth interval and stored frozen at -40 °C upon arrival at the Royal NIOZ. In addition, we analyzed *S. magellanicum*, sampled at the Bargerveen peat bog in The Netherlands in 1999, freeze dried, and stored at -20 °C until analysis.

The peat samples were freeze dried and, together with *S. magellanicum*, extracted (3×) using a modified Bligh and Dyer technique (Bligh and Dyer, 1959). A solvent mixture (5 ml/g dry wt. peat) of MeOH: dichloromethane (DCM):K phosphate buffer at pH 7.4 (2:1:0.8, v/v/v) was added to ca. 0.3-1.3 g dry wt. peat in a centrifuge tube and placed in an ultrasonic bath for 10 min. The extract was collected after centrifuging the sample at 2500 rpm for 2 min. DCM and phosphate buffer were added to the combined extracts to a volume ratio of 1:1:0.9 (v/v/v) to achieve phase separation. The DCM phase and aqueous MeOH/phosphate buffer phase were separated by centrifuging at 2500 rpm for 2 min. The DCM phase, containing the IPLs, was passed over extracted cotton wool to remove any remaining particles and collected in a glass tube. The aqueous phase was rinsed (2×) with DCM and all the DCM phases were combined and dried under a N_2 flow and stored at -20 ˚C until analysis.

An aliquot of the Bligh and Dyer extract (BDE) from 30 cm depth was subjected to base hydrolysis to cleave off phospho headgroups only, leaving the glycolipids intact (cf. Pitcher et al., 2009). To this end, the aliquot was refluxed for 1 h in 1N KOH in MeOH:water (24:1, v/v). The cooled solution was adjusted to pH 5 with 2N HCl:MeOH (1:1, v/v) and bidistilled water added to achieve a ratio of H2O:MeOH (1:1, v/v), after which the mixture was washed (3×) with DCM. The resulting fraction was dried under N_2 and analyzed for glycolipids using HPLC/ESI-MS.

7.2.2. IPL analysis

An aliquot of each BDE, as well as of the glycolipid fraction, in hexane:2-propanol:water (72:27:1) at a concentration of 3.5-6.5 mg/ml was filtered through a 0.45 μm regenerated cellulose (RC) filter (Alltech Associates Inc., Deerfield, IL) prior to HPLC/ESI-MS analysis.

IPLs were analyzed according to Sturt et al. (2004), with some modifications. An Agilent 1200 series LC instrument (Agilent, San Jose, CA), equipped with thermostatted auto-injector and column oven, coupled to a Thermo LTQ XL linear ion trap with Ion Max source with electrospray ionization (ESI) probe (Thermo Scientific, Waltham, MA), was used. Separation was achieved with a Lichrosphere diol column (250×2.1 μm, 5 μm particles; Alltech Associates Inc., Deerfield, IL) maintained at 30 °C. The following elution programme was used (flow rate 0.2 ml/min): 100% A (1 min), followed by a linear gradient to 66% A: 34% B in 17 min, held 12 min, followed by a linear gradient to 35% A: 65% B in 15 min, where A = hexane/2-propanol/formic acid/14.8 M NH_{3aq} [79:20:0.12:0.04 (v/v/v/v) and B = 2-propanol/water/formic acid/14.8 M NH_{3aq} [88:10:0.12:0.04 (v/v/v/v)]. Total run time was 60 min with a re-equilibration period of 20 min between runs. For MS detection source parameters were optimized using loop injections of standard IPLs [1,2-dipalmitoyl-*sn*-glycero-3-phosphocholine, 1,2-dipalmitoyl-*sn*-glycero-3-phosphoethanolamine, 1,2-dipalmitoyl-*sn*-glycero-3-phospho-L-serine, 1,2-dipalmitoyl-*sn*-glycero-3-phospho-*rac*-glycerol, 1,2-dipalmitoyl-*sn*-glycero-3-phosphate, soy L-a-phosphatidylinositol (Avanti Polar Lipids, Alabaster, AL) and 1,2-distearoyl-3-O-β-D-galactosyl-*sn*-glycerol, 1,2-distearoyl-3-O-(α-D-galactosyl1-6)-β-D-galactosyl-*sn*-glycerol, the main phospholipid of *Thermoplasma acidophilum* (Matreya LCC, Pleasant Gap PA)] into a stream of 0.2 ml/min of 60% A: 40% B. ESI settings were as follows: capillary 275 °C, sheath gas (N_2) pressure 25 (arbitrary units), auxiliary gas (N_2) pressure 15

(arbitrary units), sweep gas (N_2) pressure 20 (arbitrary units), spray 4.5 kV (positive ion ESI) or -5.5 kV (negative ion ESI).

Each BDE was analyzed by way of a routine where a positive ion scan (*m/z* 400-2000 or 1000-2000) was followed by a data dependent MS^2 experiment where the base peak in the spectrum was fragmented [normalized collision energy (NCE) 25, isolation width 5.0, activation Q 0.175]. This was followed by a data dependent MS^3 experiment where the base peak in the MS^2 spectrum was fragmented under identical conditions. The procedure was repeated on the 2nd to 4th most abundant ions in the initial spectrum.

7.2.3. CL and IPL-derived GDGT analysis

The remainder of the BDE was separated into a CL fraction and an IPL fraction over an activated silica column according to Oba et al. (2006) and Pitcher et al. (2009), except that hexane:EtAc (1:1, v/v) was used to retrieve the CL branched GDGTs and that MeOH was used to obtain the IPLs. A C_{46} internal GDGT standard (0.1 µg) was added to the CL fraction and an aliquot of the IPL fraction according to Huguet et al. (2006), after which the IPL aliquot was subjected to acid hydrolysis to cleave all ether-bound and most of the ester-bound head groups and release the core lipids (IPL-derived GDGTs; cf. Picher et al., 2009). Additionally, IPL aliquots of three selected samples (6, 32 and 42 cm depth) were, after addition of 0.1 µg internal GDGT standard, subjected to base hydrolysis to cleave off only phospho head groups, as described above for a BDE aliquot.

The CL, IPL-derived, and phospholipid-derived CL fractions were dissolved in hexane:isopropanol (99:1, v/v) and filtered over a 0.45 µm PTFE filter and concentrated to ca. 3 mg/ml prior to HPLC/atmospheric pressure chemical ionization (APCI)-MS analysis with an Agilent 1100 series LC/MSD SL according to Schouten et al. (2007a), with minor modifications. In short, component separation was achieved with an Alltech Prevail Cyano column (150 mm×2.1 mm; 3 µm). The branched GDGTs were eluted isocratically with 90% A and 10% B for 5 min and then with a linear gradient to 16% B for 34 min, where A = hexane and B = hexane:isopropanol (9:1, v/v). The injection volume was 10 µl. Single ion monitoring of $(M+H)^+$ ions was used to detect and quantify the branched GDGTs. Absolute quantification was carried out as described by Huguet et al. (2006).

7.3. Results and discussion
7.3.1. Concentrations of CL and IPL-derived branched GDGTs

Although the Saxnäs Mosse had been investigated for branched GDGT CLs (Weijers et al., 2009), the presence of IPL-branched GDGTs had not been established. We therefore analyzed and quantified the amounts of IPL-derived branched GDGTs following the approach of Pitcher et al. (2009). IPL-derived branched GDGTs were present throughout the whole depth profile, the concentration varying between 1 and 31 µg/g dry wt. (dwt) peat (open squares, *Fig. 7.1*). This is substantially lower than that of the CL-GDGTs (5 to 180 µg/g dwt peat; filled black squares, *Fig. 7.1*). Importantly, the data show that IPL-derived branched GDGTs are most abundant below the water table, supporting the hypothesis that they are likely to be produced primarily in the anoxic part of the bog (Weijers et al., 2009).

The relative distribution of branched GDGTs throughout the profile is generally similar for CL and IPL-derived branched GDGTs. Branched GDGT-I is the most abundant type throughout the whole profile and contributes between 50% and 65% to the total branched GDGT pool. Branched GDGT-II contributes
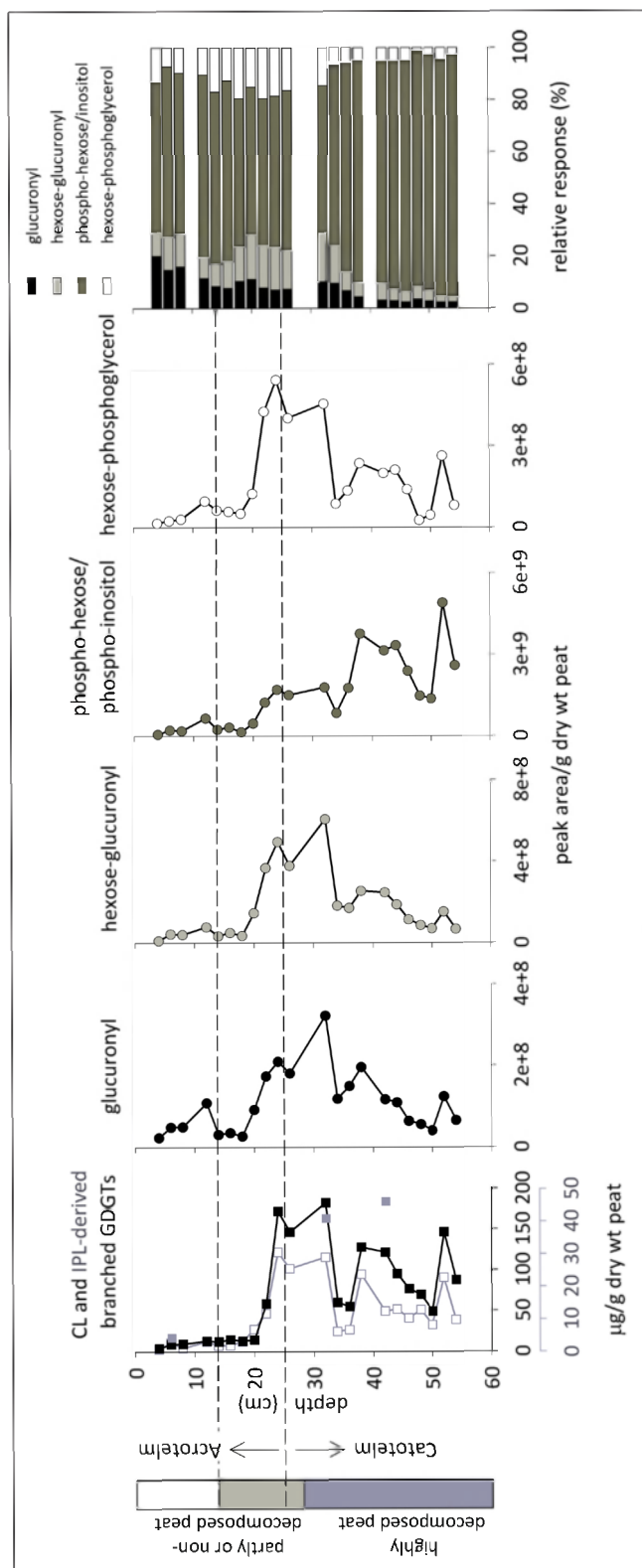
Fig. 7.1. Dept profiles of the Saxnäs Mosse peat bog showing the concentrations of CL, IPL-derived and phospho-branched GDGTs In respectively solid black, open grey, and solid grey squares, the peak areas per gram dry weight peat for the IPL-branched GDGTs included in the SRM assay, and the trends in relative response of the different IPL-branched GDGTs with depth. The horizontal dotted lines indicate the level of the water table at the time of sampling (14 cm), and at its lowest point (25 cm). The state of decomposition of the peat is indicated in the profile on the left.

30-45%, and branched GDGTs of type III contributes ca. 5%.

7.3.2. Identification of IPL-branched GDGTs

Given that the highest concentrations of IPL-derived branched GDGTs occur below the water table, we initially focussed our study on the anoxic part of the peat. An aliquot of the BDE from 30 cm was analyzed in detail by way of HPLC-ESI-MS[n] to search for mass spectra indicative of IPL-branched GDGTs. Although peaks with MS[1] spectra containing ions in the expected m/z range for IPL-branched GDGTs (i.e. m/z >1050) were observed, the IPL profile was dominated by betaine lipids, i.e diacylglycerols with β-alanine (DGTA) and homoserine (DGTS) head groups, as well as diacylglycerols with phosphocholine (DAG-PC) and phosphatidyl-(N)-methylethanolamine (DAG-PME) head groups, dietherglycerols with a phosphatidylethanolamine (DEG-PE) head group and two unknown IPLs (*Fig. 7.2a*). PEs and PMEs, together with PCs, are IPLs which occur in many bacteria, such as methanotrophic bacteria (e.g. Fang et al., 2000), but also ocur as minor IPLs in plants. Betaine lipids, on the other hand, are mainly associated with algae, fungi and spore-producing plants (e.g. Dembitsky, 1996) and a limited number of bacteria. To differentiate between bacterial and plant IPLs in the peat, we determined the IPL composition of *S. magellanicum*, the dominant *Sphagnum* species at 30 cm depth in the bog (Weijers et al., 2009). The IPLs were dominated by betaine lipids DGTA and DGTS, with a smaller contribution of PCs (*Fig. 7.2b*). This
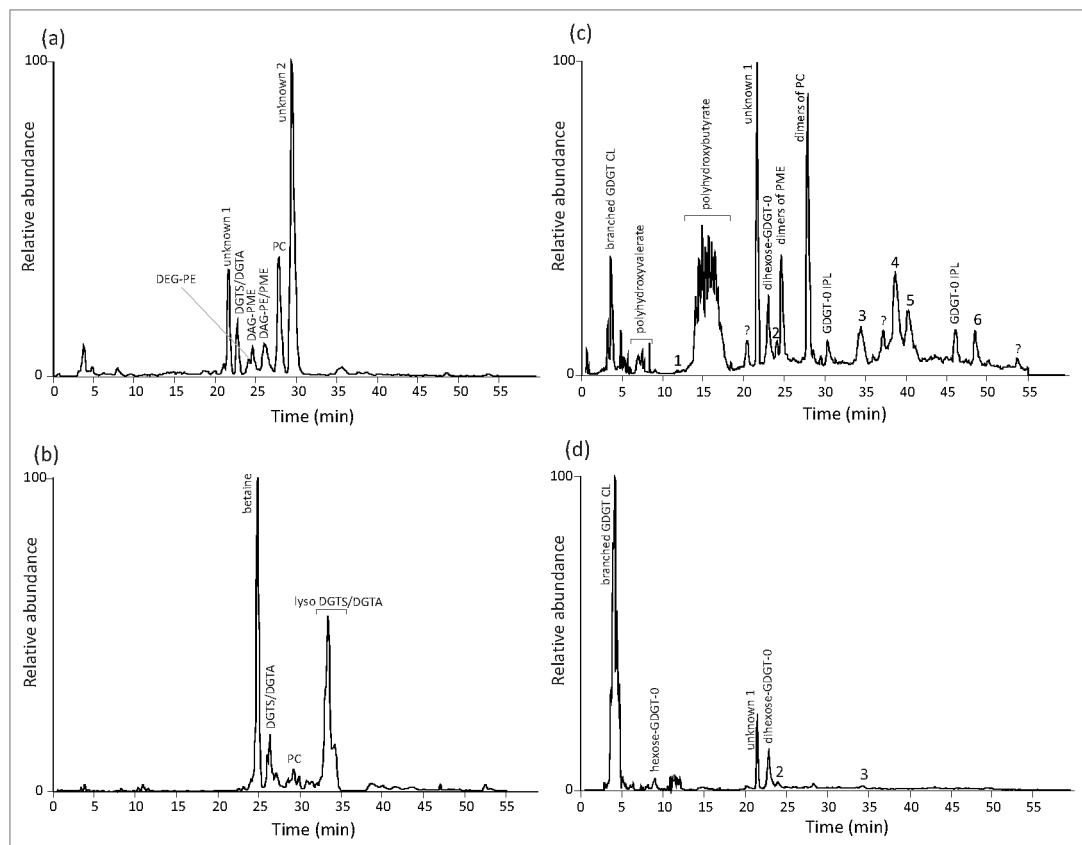
Fig. 7.2. HPLC/ESI-MS base peak chromatograms for the Bligh and Dyer extracts of a) the Saxnäs Mosse peat at 30 cm depth and b) *Sphagnum magellanicum*, both scanned with an analytical window of *m/z* 400-2000, c) the Saxnäs Mosse peat at 30 cm scanned with an analytical window of *m/z* 1000-2000, and d) scanned ar *m/z* after base hydrolysis.

implies that the major part of the betaine lipids in the peat are likely derived from *Sphagnum*, while the PCs, as well as the PEs and PMEs at 30 cm have a bacterial origin.

Careful inspection of the base peak chromatogram revealed no spectra that could be attributed to IPL-branched GDGTs. The BDE was therefore re-analyzed using a restricted range from *m/z* 1000-2000, to enhance specificity (*Fig. 7.2c*). This resulted in the appearance of known IPL-isoprenoid GDGTs such as GDGT-0 with mono- and dihexose moieties (*Fig. 7.2c*; Sturt et al., 2004), as well as two GDGT-0 based IPLs with unknown head groups. The spectra of these unknown IPLs ([M+H]$^+$ at *m/z* 1691 and 1853, respectively) showed one or two losses of 162 Da (representing 1 or 2 hexose moieties) and, in both cases, losses of 147 and 80 Da (representing a phospho-moiety) generating an ion at *m/z* 1302. We also detected a range of IPL-branched GDGTs and discuss their identification in more detail below.

The two IPL-branched GDGTs reported by Liu et al. (2010), i.e. a branched GDGT core lipid of 1022 Da (branched GDGT-I; cf. the numbering in Weijers et al., 2009) with either a glucose (Glc) or glucuronyl (GlcA) head group, were tentatively assigned in the peat, albeit at relatively low levels (labelled 1 and 2 in *Fig. 7.2c*). In case of the GlcA-branched GDGT, ions at *m/z* 1215 and 1220 correspond to the ammoniated and sodiated versions of branched GDGT-I. Confirmation came from the corresponding MS^2 spectra showing the diagnostic losses of 193 (glucuronyl and NH$_3$) from the ammoniated species, and 176 from the sodiated species (generating an ion at *m/z* 1044, corresponding to the sodiated version of branched GDGT-I). For the Glc-branched GDGT, the tentative assignment was based solely on observation of the ammoniated molecular ion of the branched GDGT-I with a glucose head group in MS^1 (*m/z* 1201), as the abundance was too low for MS^2 data to be acquired.

In addition to the two reported IPL-branched GDGTs, we identified, based on fragmentation patterns in MS^2 and MS^3, a number of other IPL-branched GDGTs. Peak 3 in *Fig. 7.2c* was tentatively assigned as a branched GDGT-I with a hexose and a GlcA moiety (*Fig. 7.3a*). The spectrum revealed a sodiated molecular ion at *m/z* 1382, which, on fragmentation, generated major fragments at *m/z* 1220 (loss of 162 Da) and 1044 (loss of 338 Da), which represent neutral losses of a hexose moiety and the combined neutral loss of a hexose and glucuronyl moiety (162 + 176 = 338), respectively. The ion at *m/z* 1044 represents the sodiated form ([M+Na]$^+$) of branched GDGT-I. From the spectrum it can not be assessed whether the two moieties are combined in one head group, or that they represent two separate head groups attached to either end of the tetraether. The spectrum shows only the loss of the hexose moiety from the IPL (loss of 162), and the subsequent loss of the glucuronyl moiety then generates the core GDGT. This suggests that the glucuronyl is attached to the core GDGT, and that the hexose unit is in turn attached to the glucuronyl. However, if that were the case, losses representing the hydroxyl and/or glycerol moieties at the other end of the GDGT (i.e. -18 and -74) would be expected, and these are not observed. Although in MS^1 some ions were observed that matched the expected *m/z* for IPLs with hexose and/or glucuronyl headgroups with a branched GDGT-II as the core, this could not be confirmed from corresponding MS^2 spectra.

Further inspection of the chromatogram revealed several more peaks that generated diagnostic fragments for either the protonated or sodiated form of the branched GDGT-I core lipids (peaks 4 and 5; *Fig. 7.3c*). The MS^1 spectrum of peak 4 shows two major ions at *m/z* 1264 and 1286 respectively. The main neutral losses in the MS^2 spectrum of *m/z* 1264 were of 18, 74, 162, 242, 260 and 316 Da (*Fig. 7.3b*). The neutral losses of 162, 242, and 260 are diagnostic for a phospho-hexose head group, with the loss of 162 representing the loss of just the hexose moiety, while the losses of 242 (generating *m/z* 1022, the

[M+H]$^+$ of branched GDGT-I) and 260 represent the loss of the complete phospho-hexose head group. The loss of 316 represents the combined loss of both the phospho-hexose and a glycerol moiety, the latter loss being commonly observed for GDGT CLs. The observation of the diagnostic losses for a glycerol moiety (of 18 and 74 Da, respectively) directly from the parent ion, confirms that the phospho- and hexose moieties are combined in one head group, as discussed above for the hexose-GlcA IPL. Consequently, this component was tentatively assigned as a phospho-hexose IPL with a branched GDGT-I core lipid, with the ion at m/z 1264 representing the [M+H]$^+$ ion while the ion at m/z 1286 represents the [M+Na]$^+$. This is confirmed by MS^2 of the latter ion (*Fig. 7.3c*), with major fragments at m/z 1106 (neutral loss of 180 representing a hexose moiety) and 1044 (neutral loss of 242 representing loss of a phospho-hexose). A phospho-hexose IPL with a branched GDGT-II as its core was also detected, based on a parent ion at m/z 1278, which represents [M+H]$^+$, and the analogous fragmentation to the phospho-hexose branched GDGT-I (*Fig. 7.3d*).

Another IPL (Peak 5) also showed major ions at m/z 1264 and 1286 in MS^1, like the earlier eluting phospho-hexose branched GDGT-I (peak 4, *Fig. 7.2c*). The spectrum generated in MS^2 of the parent ion at m/z 1286 is identical to that for the same ion of the phospho-hexose branched GDGT-I. The MS^2 spectrum of the parent ion at m/z 1264 was also nearly identical, but differed in the relative abundances of the various fragment ions (*Fig. 7.3e*). The fragment representing the loss of a hexose moiety (m/z 1102) is suppressed in relative intensity, while fragment ions relating to neutral losses of one or more water molecules (subsequent losses of 18 Da), from either the parent ion or GDGT-I core lipid, were much more prominent. However, the fragment ion representative of the loss of a glycerol moiety from the GDGT-I core lipid (m/z 948 and 966 resulting from neutral losses of 74 and 56 Da from m/z 1022, respectively), was absent. Instead, fragment ions at m/z 950 and 968 are observed, which can be formed after three and four subsequent losses of hydroxyl groups in the form of water (losses of 54 and 72). The shift in retention time, combined with the differences in fragmentation pattern, point towards a different, and slightly more polar, moiety attached to the phospho group, but with identical molecular weight to that of the phospho-hexose branched GDGT-I. Substitution of a hexose by an inositol moiety might explain both the slight shift in retention time and the subtle difference in fragmentation pattern. Inositol contains 5 hydroxyl moieties, possibly leading to the prominent fragments representing subsequent losses of water. The less abundant formation of the fragment at m/z 1102 can be explained by the somewhat more stable nature of the ether bond of the inositol to the phospho-group as opposed to the glycosidic bond of a hexose moiety. However, as there was insufficient material for a sugar analysis after compound isolation, this assignment remains speculative. The presence of the analogue IPL with the GDGT-II as the core lipid could also confirmed based on its fragmentation in MS^2.

Lastly, an IPL which appears to be based on the branched GDGT-I core lipid (*Fig. 7.2c*, peak 6) has a parent ion at m/z 1338, and generates one main fragment ion in MS^2 at m/z 1264 (loss of 74 Da), which is identical to the [M+H]$^+$ of the branched GDGT-I-phospho-hexose (*Fig. 7.3f*). The loss of 74 Da is typical for the loss of a glycerol moiety from a phosphoglycerol attached to an ether lipid. Therefore, the combined head group appears to consist of three moieties: a phosphatidic acid, a hexose and a glycerol. Whether these moieties are combined in one head group or distributed over either end of the tetraether cannot be concluded from this spectrum. However, based on commonly occurring head groups, a structure with a hexose representing one head group and a phosphoglycerol representing the other is proposed.
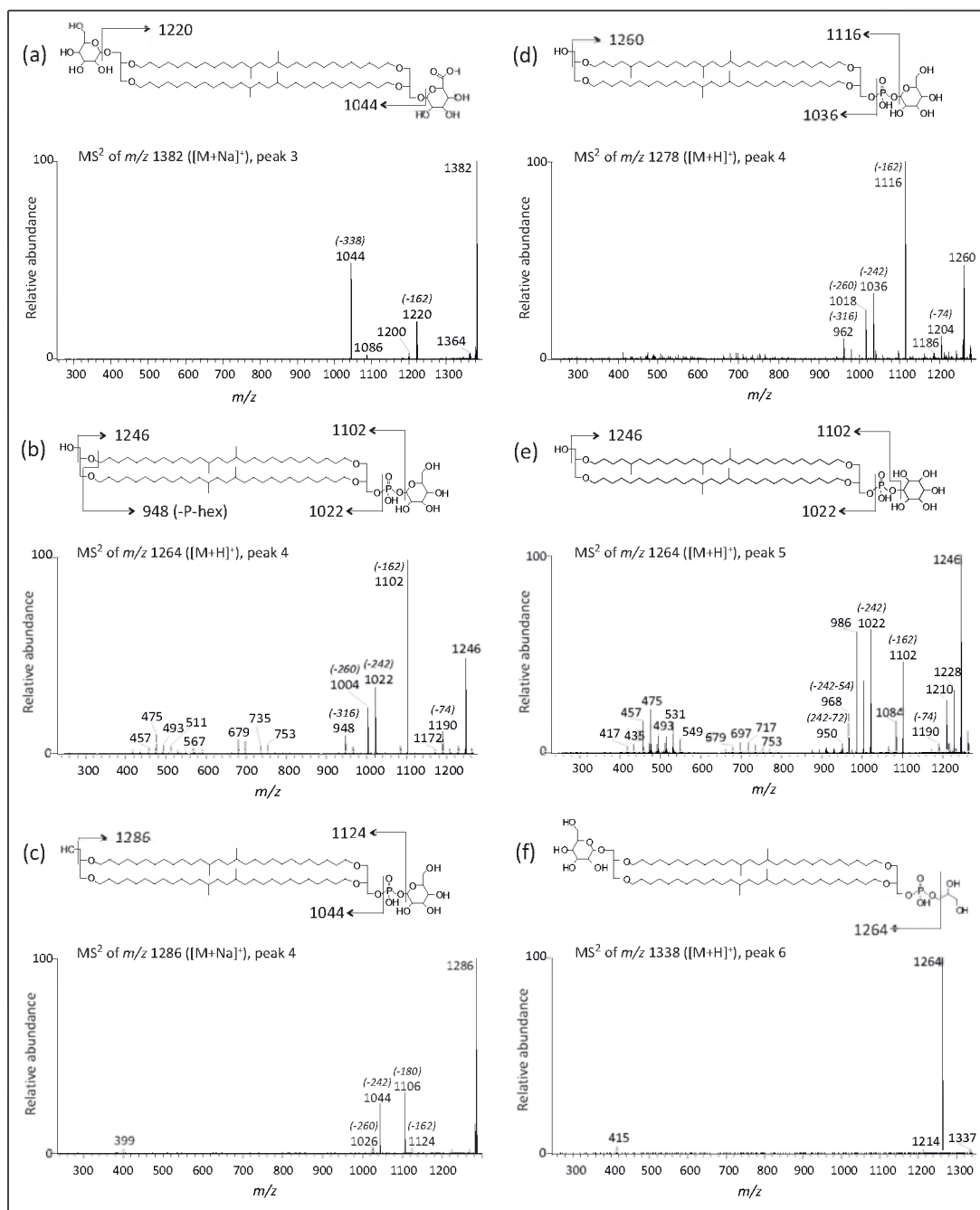
Fig. 7.3. MS² spectra and molecular structures with characteristic losses of the tentatively identified IPL-branched GDGTs: a) sodium adduct of hexose-GlcA-branched GDGT-I, b) phospho-hexose-branched GDGT-I, c) sodium adduct of phospho-hexose-branched GDGT-I, d) phospho-hexose-branched GDGT-II, e) phospho-inositol-branched GDGT-I, and f) hexose-phosphoglycerol-branched GDGT-I. The peak numbers indicated in the spectra correspond to those in Fig. 7.2.

Support for the tentative assignmentss of the novel phospho-containing IPL-branched GDGTs (peaks 4-6) was obtained from IPL analysis of the peat BDE after base hydrolysis. The latter results in hydrolysis of ester bonds but leaves glycosidic bonds intact. Indeed, the peaks representing the IPLs of branched GDGTs with a putative phospho-containing head group were not observed in the base hydrolyzed BDE, in contrast to those with glycosidic head group (*Fig. 7.2d*). Furthermore, the phospholipid derived CLs released on hydrolysis caused a substantial increase in the MS-response of branched GDGT CLs, which suggests that the largest part of the IPL-branched GDGTs has a phospho head group directly connected to their CL.

7.3.3. IPL-GDGT distribution with depth

To monitor the changes in IPL-GDGT composition throughout a depth profile of the bog, we developed a selective reaction monitoring (SRM) method based on the spectra of the distinct IPL-GDGTs, using the transitions described in *Table 7.1*. The transitions are based on IPLs with a branched GDGT-I CL, the most abundant type in the Saxnäs Mosse (see above and Weijers et al., 2009). The method includes the branched GDGT-I CL, the IPL-branched GDGTs identified here and the GlcA-branched GDGT. Also an IPL of an isoprenoid GDGT, a dihexose-GDGT-0, was added to the study. Because of the poor response in full scan mode, the Glc-branched GDGT was not included.

Application of the SRM method clearly improved detection of the different IPLs vs. the full scans (*Fig. 7.4*). Application of the method to the peat profile shows that the IPL-branched GDGT distribution, quantified as peak area per gram dwt peat, in the anoxic part of the peat (*Fig. 7.4a*) is different from that in the oxic part (*Fig. 7.4b*), although all IPLs occur throughout the profile (*Fig. 7.1*). The concentration of phospho-hexose-branched GDGTs shows a strong increase in the anoxic part, whereas the highest concentrations of GlcA-, hexose-GlcA-, and hexose-phosphoglycerol-branched GDGTs occur right below the water table at the time of sampling.

Table 7.1. Parent and selected fragment ions for the IPL-branched GDGTs included in the HPLC/SRM-MS method. GDGT numbers correspond to the molecular structures in Weijers et al. (*2009*).

Lipid monitored	Parent (m/z)	Product (and loss) (m/z)
branched GDGT-I CL	1022 [M+H]$^+$	948 (*-74*)
di-hexose-GDGT-0	1643 [M+NH$_4$]$^+$	1302 (*-341*)
glucuronyl-branched GDGT-I	1215 [M+NH$_4$]$^+$	1180 (*-35*), 1022 (*-193*)
hexose-glucuronyl-branched GDGT-I	1382 [M+Na]$^+$	1220 (*-162*), 1044 (*-338*)
phospho-hexose-branched GDGT-I	1264 [M+H]$^+$	1102 (*-162*), 1022 (*-242*)
hexose-phosphoglycerol-branched GDGT-I	1338 [M+H]$^+$	1264 (*-74*)

Although all IPL-branched GDGTs are more abundant in the anoxic than in the oxic layer, suggesting that they are mainly produced in this part of the peat, there clearly are different trends in relative response of IPL-branched GDGTs with glycosidic and phospho head groups with depth (last panel in *Fig. 7.1*). The IPL-branched GDGTs with phospho head groups are more dominant below the water table, whereas glycolipid branched GDGTs are relatively more dominant above the it. Laboratory (Harvey et al., 1986) and theoretical (Schouten et al., 2010) studies suggest that phospholipids are better indicators of *in situ* production and/or the presence of living cells in sediments than glycolipids. Glycolipids are potentially more recalcitrant than phospholipids, and may even be preserved on geological time scales (Schouten et al.,

2010; Bauersachs et al., 2010). Furthermore, since oligotrophic peat bogs, like the Saxnäs Mosse, are limited in nutrients, especially N and P (Aerts et al., 1992), preferential degradation of phospho head groups may take place in the oxic part to free the phosphorus for consumption.

Our observations are in agreement with the more recalcitrant nature of glycolipids. The oxic part of the bog contains much less of the IPL-branched GDGTs, probably due to rapid oxic degradation of any material produced at times of high water level and anaerobic conditions. It is also in this part that we observe a much stronger decrease in phospholipid concentration compared to the anoxic part than for glycolipid concentrations. This trend is confirmed by the comparison of branched GDGT CLs released after base hydrolysis (phospholipid-derived), and after acid hydrolysis (mostly glycolipid-derived) of the IPL fractions from selected depths. Base hydrolysis released 1.3 (at 6 cm) to 3.6 (at 42 cm) times as much branched GDGT CLs as acid hydrolysis in the oxygenated and the anoxic part of the peat, respectively (filled grey squares, *Fig. 7.1*). This confirms that the greatest part of the IPL-branched GDGTs indeed consists of those with phospho-containing head groups, particularly in the anoxic part. It therefore seems that the best markers for in situ production of branched GDGTs in the bog are IPL-branched GDGTs with a phospho head group, i.e. phospho-hexose branched GDGTs. Their increase in relative response below the water table furthermore supports previous suggestions that branched GDGTs are produced by anaerobic bacteria.

The isoprenoid GDGT IPL included in the SRM study, a dihexose-GDGT-0, also gives a substantially higher response in the anoxic part below the water table than in the oxic section above the water table (data not shown). Based on the GDGT-0 CL distribution, its origin was ascribed to methanogenic archaea (Weijers et al., 2009). The higher abundance of this IPL in the anoxic part therefore supports methanogens as likely source organisms.

7.3.4. IPL-branched GDGTs in soil

Apart from peat, branched GDGT CLs have been reported in a large number of different soil types (e.g. Huguet et al. 2010b; Kim et al., 2010b; Peterse et al., 2009a,b,c, 2010; Weijers et al., 2006b, 2007c), but branched GDGTs in their intact form have not been reported. We therefore applied our SRM method (*Figs. 7.5a, b*) to two different soils, i.e. a sandy soil from Texel, The Netherlands, and a sandy loam from Craibstone, Scotland (*Figs. 7.5a and b*). Both contain IPL-branched GDGTs with phospho-hexose (peak 4) and hexose-phosphoglycerol (peak 6), but with a different distribution from the Saxnäs Mosse bog. Although the chromatograms suggest that the soils also contain hexose-GlcA-branched GDGTs, the peaks have a later retention time than in the peat. Inspection of the chromatograms from the data dependent full scan for both soils could not reveal a MS^2 spectrum of these components at the later retention time. The observed peaks can therefore not be interpreted as hexose-GlcA-branched GDGTs.

The hexose-phosphoglycerol-branched GDGTs appear to be more predominant in the soils than the peat, while the contribution of branched GDGTs with a phospho-hexose head group appears to be smaller. The presence of phospho IPL-branched GDGTs implies that the branched GDGTs in the soils are likely also produced in situ. Compared to the Swedish peat, the soils contain a relatively larger amount of glycosidic IPL-branched GDGTs, suggesting that the pool of fossil lipids may be larger than in the peat. Indeed, the proportion of IPL-derived branched GDGTs is 17% for the Scottish sandy loam, and only 6% in the Texel sandy soil , whereas IPL-derived branched GDGTs can make up to 30% of the total branched GDGT pool in the Saxnäs Mosse bog.
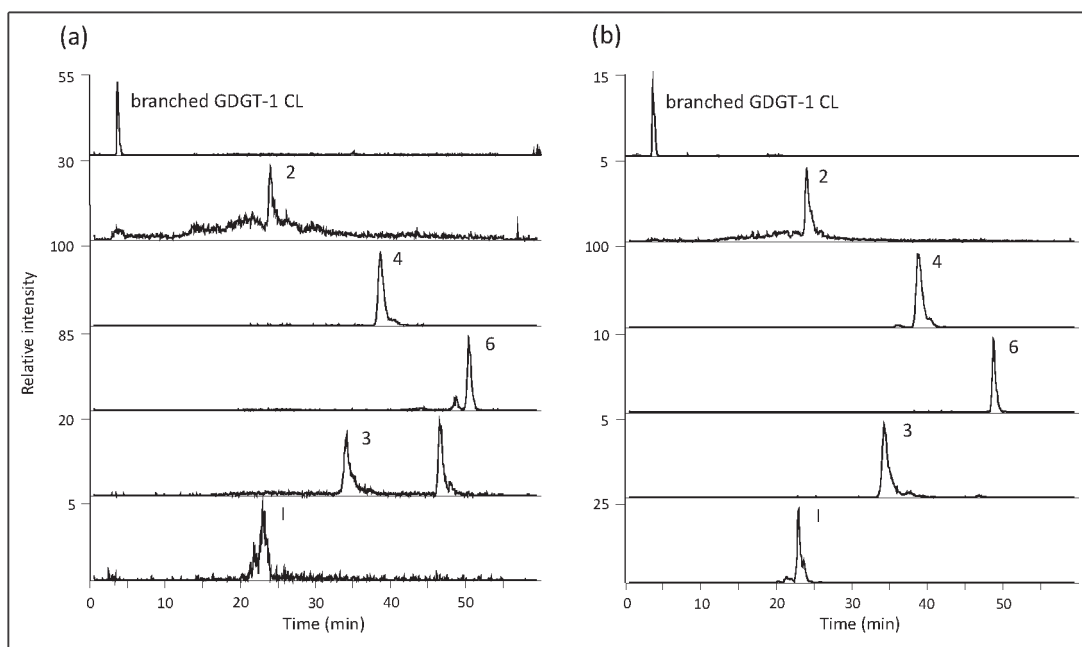
Fig. 7.4. SRM assay results for the Saxnäs Mosse peat at a) 42 cm (anoxic), and b) 6 cm (oxic) depth. The peak numbers correspond to those in *Fig. 7.2.*

7.3.5. Implications for the source (s) of branched GDGTs

The highest amounts of branched GDGTs in all the samples analyzed to date are found in peat bogs, which presumably provide the most suitable living conditions for the organisms producing these compounds (Weijers et al., 2004; 2009). However, as shown in *Fig. 7.2a*, the IPL pool in the peat studied here, is dominated by plant and other bacterial IPLs, and IPL-branched GDGTs are at first glance barely detectable. Although the response factors for the IPLs can vary widely, this does suggest that branched GDGTs are not among the most abundant IPLs in the peat bog. Weijers et al. (2009) showed that the bacterial community in the Saxnäs Mosse, determined with 16S rRNA gene sequencing, consists almost solely of *Acidobacteria*, except for a small contribution of *Proteobacteria* at 26 cm depth. *Acidobacteria* were, therefore, suggested as potential source organism for the branched GDGTs. However, the phylum of *Acidobacteria* is one of the most diverse bacterial phyla in soil (Janssen, 2006) and contains a large number of subdivisions with different characteristics. If indeed only one, or perhaps a few subdivisions actually synthesize branched GDGTs, this could explain the relatively limited, but at the same time ubiquitous, presence of branched GDGTs in soils and peats. Alternatively, the relatively low concentrations of IPL-branched GDGTs vs. other IPLs could be explained by strong bonds between the IPL-branched GDGTs and the peat or soil matrix, hindering efficient extraction with the Bligh and Dyer technique. However, Huguet et al. (2010a) found that acid hydrolysis of the residue after Bligh and Dyer extraction released only low amounts of additional branched GDGTs from a French peat.

The IPL-branched GDGTs in the soils are structurally mainly similar to those in the peat bog, and thus likely have the same bacterial source. The variation in relative abundance and distribution between soils and peat may be caused by the diversity within the bacterial sources, or by differences in soil types and properties.
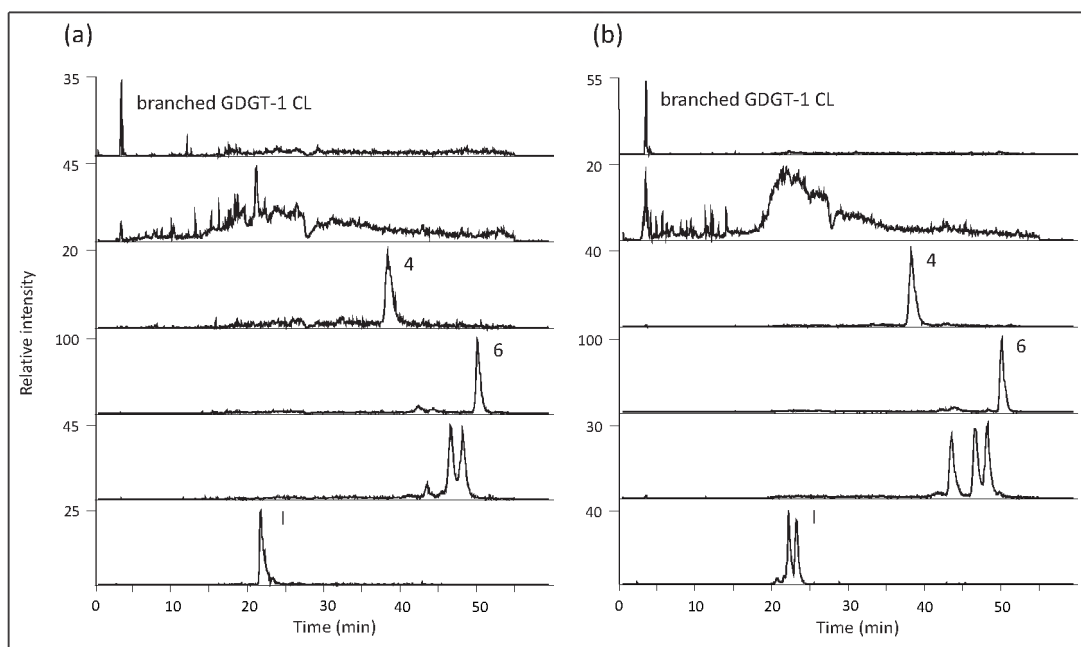
Fig. 7.5. SRM assay results for a) Sandy soil, Texel (the Netherlands), and b) Sandy loam soil, Craibstone (Scotland). The peak numbers correspond to those in *Fig. 7.2*.

7.4. Conclusions

IPL-branched GDGTs, with hexose-glucuronyl, phospho-hexose, phospho-inositol, or hexose-phosphoglycerol head groups have been identified in the Saxnäs Mosse peat bog (Sweden). In addition to the branched GDGTs with a glycosidic head group that were previously identified in the catotelm of a German peat bog by Liu et al. (2010), these newly identified IPLs also contain phospho-head groups. The distribution of IPL-branched GDGTs with depth is different for IPL-branched GDGTs with phospho and glycosidic head groups, which seems to be primarily controlled by the change in oxygen concentration above and below the water table. When phospholipids are considered as an indicator for living cells, and thus in situ production, then the increase of especially phospho-hexose-branched GDGTs below the water table would suggest that branched GDGT production mainly takes place under anoxic conditions. Comparison of trends in IPL-branched GDGTs with changes in absolute amounts of IPL-derived and CL branched GDGTs with depth indeed supports that branched GDGTs are mainly produced by anaerobic bacteria, possibly from a subdivision of the phylum *Acidobacteria*, in the anoxic part of the peat. Similar IPL-branched GDGTs are also present in soils, although their distributions differ somewhat from that in the peat profile.

Chapter 8

Revised calibration of the MBT-CBT paleotemperature proxy based on branched tetraether membrane lipids in surface soils

Francien Peterse, Jaap van der Meer, Stefan Schouten, Johan W.H. Weijers, Noah Fierer, Robert B. Jackson, Jaap S. Sinninghe Damsté. Submitted in modified form to *Geochimica et Cosmochimica Acta*.

Abstract

The MBT-CBT proxy for the reconstruction of paleotemperatures and past soil pH is based on the distribution of branched glycerol dialkyl glycerol tetraether (GDGT) membrane lipids. The Methylation of Branched Tetraether (MBT) and the Cyclisation of Branched Tetraether (CBT) indices were developed to quantify these distributions, and significant empirical relations with annual mean air temperature (MAT) and/or soil pH were found in a large data set of soils. In this study, we extended this soil dataset to 278 globally distributed surface soils. Of these soils, 26% contains all nine branched GDGTs, while in 63% of the soils the seven most common branched GDGTs (i.e. Ia, Ib, Ic, IIa, IIb, IIc, and IIIa) were detected, which were selected for calibration purposes. This resulted in a new transfer functions for the reconstruction of pH based on the CBT index: $pH = 7.90 - 1.97 \times CBT$ ($r^2 = 0.70$; RMSE=0.8; n=176), as well as for MAT based on the CBT index and adjusted MBT index (MBT'): $MAT = 0.81 - 5.67 \times CBT + 31.0 \times MBT'$ ($r^2 = 0.59$; RMSE=5.0 °C; n=176). The new transfer function for MAT has a substantially lower correlation coefficient than the original equation. To investigate possible improvement of the correlation, we used the same extended dataset to statistically derive the indices that best describe the relations of branched GDGTs with MAT and soil pH. These new indices, however, resulted in only a relatively minor increase in correlation coefficients while they cannot be explained straightforwardly by physiological mechanisms. The large scatter in the calibration cannot be fully explained by local factors or by seasonality, but MAT for soils from arid regions are generally substantially underestimated, up to 20 °C, suggesting that absolute branched GDGT-based temperature records for these areas should be interpreted with caution. The applicability of the new MBT'-CBT calibration function was tested using previously published MBT-CBT-derived paleotemperature records covering the last deglaciation in Central Africa and East Asia, the Eocene-Oligocene boundary and the Paleocene Eocene thermal maximum. The results show that trends remain similar in all records, but that absolute temperature estimates and the amplitude of temperature changes are lower for most records, and generally in better agreement with independent proxy data.

8.1. Introduction

The reconstruction of paleotemperatures provides a valuable contribution to our understanding of the climatic changes in the past. The number of proxies that can estimate past continental air temperatures is, however, relatively limited. A large part of the continental temperature records is retrieved from lake sediments, where climate indicators like pollen, chironomids, or diatoms may be preserved (e.g. Colinvaux et al., 1996; Kurek et al., 2009; Lotter et al., 1997). However, many of the available proxies are, besides temperature, also sensitive to changes in other environmental parameters, which can disturb their temperature signal.

The distribution of a particular suite of globally occurring molecules, i.e. branched glycerol dialkyl glycerol tetraethers (GDGTs; *Fig. 8.1*), shows potential as a tool to obtain high resolution continental temperature reconstructions (Weijers et al., 2007c). These branched GDGTs vary in the amount of methyl branches (4 to 6) and can contain up to two cyclopentane moieties (Sinninghe Damsté et al 2000; Weijers et al 2006a). The stereochemistry of their glycerol moieties indicates that they have a bacterial origin (Weijers et al., 2006a), although the exact type of bacteria that synthesizes branched GDGTs is unknown.

An empirical study of 134 soils from over 90 locations worldwide showed that the distribution of the different branched GDGTs varies with annual mean air temperature (MAT) and soil pH; the number of cyclopentane moieties relates with soil pH, whereas the number of methyl branches is related to MAT and, to a lesser extent, also to soil pH (Weijers et al 2007c). To quantify those changes, the Cyclisation of Branched Tetraethers (CBT) and Methylation of Branched Tetraethers (MBT) indices were developed, and defined as:

$$CBT = -LOG ((Ib+IIb)/(Ia+IIa)) \qquad (8.1)$$
$$MBT = (Ia+Ib+Ic)/(Ia+Ib+Ic+IIa+IIb+IIc+IIIa+IIIb+IIIc) \qquad (8.2)$$

Roman numerals in the equations refer to the relative abundance of the molecules in *Fig. 8.1*. Based on the branched GDGT distributions in a globally distributed soil calibration dataset, an equation to express CBT as function of soil pH was derived:

$$CBT = 3.33 - 0.38 \times pH \qquad (n=114; r^2=0.70) \qquad (8.3)$$

Similarly, an equation for the relation of MBT with MAT and pH was derived:

$$MBT = 0.867 - 0.096 \times pH + 0.021 \times MAT \qquad (n=114; r^2=0.82) \qquad (8.4)$$

Substitution of pH by the CBT index consequently results in a function to derive MAT based on the distribution of branched GDGTs only:

$$MBT = 0.122 + 0.187 \times CBT + 0.020 \times MAT \qquad (n=114; r^2=0.77) \qquad (8.5)$$

The error of estimate for soil pH and MAT is 0.7 and 4.8 °C, respectively. These relatively large errors indicated that care had to be taken with the interpretation of the absolute values that are reconstructed with these proxies.

While based and calibrated on soils, the MBT-CBT paleotemperature proxy (i.e. Eq. 8.5) has so far mostly been applied on coastal marine sediment cores, where branched GDGTs are likely deposited as part of river transported soil organic matter (Hopmans et al., 2004). Hence, down-core analysis of branched GDGT distributions in river fan sediments results in an integrated climate record of the river basin. In this way, paleoclimate reconstructions have been made for e.g. tropical central Africa (Weijers et al., 2007a), the Arctic continent (Weijers et al., 2007b), Greenland (Schouten et al., 2008a), the Skagerak (Rueda et al., 2009), and the Amazon basin (Bendle et al., 2010). The MBT-CBT proxy has also been applied on the terrestrial realm. Analysis of branched GDGTs in a Pliocene peat deposit in the Canadian Arctic provided insight in Arctic air temperatures during this time (Ballantyne et al., 2010), whereas branched GDGTs in a loess-paleosol sequence from the Chinese loess plateau revealed the timing and magnitude of deglacial atmospheric warming in East Asia (Peterse et al., 2011). Application of this proxy on lake sediments, however, showed that the distribution of branched GDGTs in the sediments from Lake Challa in Tanzania, and lake Towuti in Indonesia differs from that in the surrounding soils (Sinninghe Damsté et al., 2009; Tierney and Russel, 2009). Therefore, in situ production was suggested as a source of branched GDGTs, in addition to those derived from erosion of soils in the lake catchment. The mixed provenance of branched GDGTs in lakes complicates the application of the MBT-CBT proxy in these settings, and tends to result in underestimated MATs (Blaga et al., 2010; Tierney et al., 2010b; Zink et al., 2010).

In this study, we extended the original soil data set of Weijers et al. (2007c), and combined it with previously reported branched GDGT distributions in soils from China (Peterse et al., 2009c), France (Kim et al., 2010b), and Svalbard (Peterse et al., 2009a). Besides recalibration of the MBT-CBT index, we also tested other combinations of branched GDGTs that may improve their relation with temperature and soil pH. Finally, the new calibration function was tested by applying them on previously published MBT-CBT records.
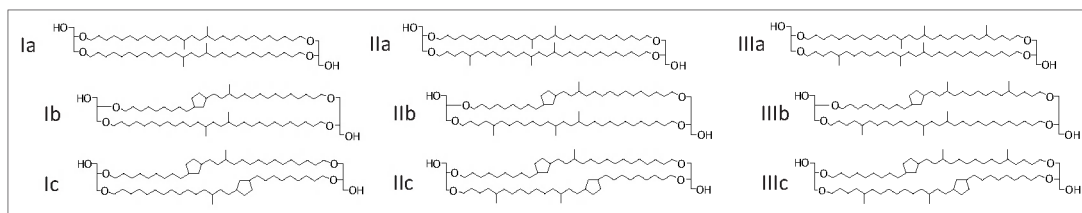
Fig. 8.1. Molecular structures of branched GDGTs.

8.2. Material and methods
8.2.1 Soil data set compilation
Of the initial global soil calibration set published by Weijers et al. (2007c), only the surface soils (0-10 cm) were selected for the new calibration set as these are likely to be under direct influence of MAT. This set was extended with newly analyzed surface soils from North-America, Brazil, Peru, Colombia, Ecuador, Chile, the Netherlands, Egypt and Uganda. Previously reported branched GDGT distributions in soils from France (Kim et al., 2010b), Svalbard (Peterse et al., 2009a) and China (Peterse et al., 2009c) were re-evaluated and added to complete the data set. The final soil collection is composed of 278 globally distributed surface soils (*Fig. 8.2; Supplementary Table S8.1*).
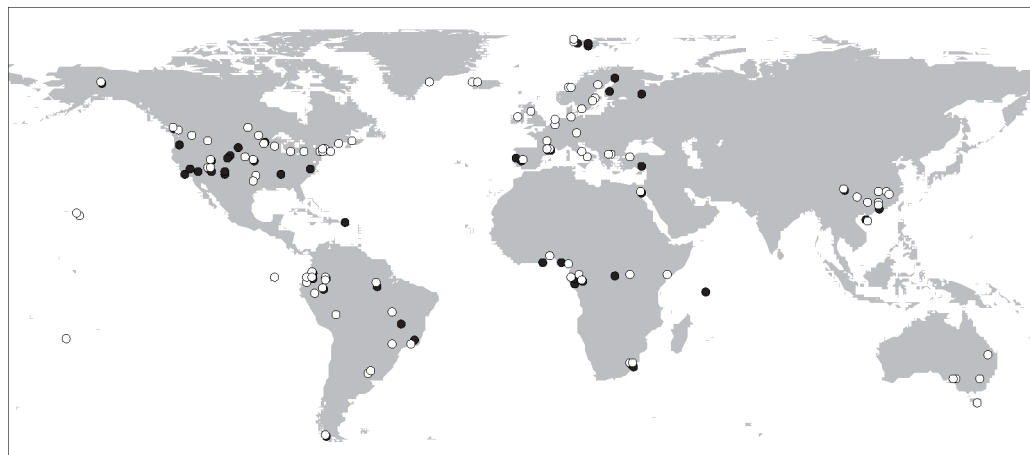
Fig. 8.2. Global overview map of the locations of surface soils used in this study. Open circles are soils included in the new calibration set (n=176). The filled circles indicate soils that are excluded from the calibration set (n=102) because one or more of the branched GDGTs are below detection limit.

8.2.2 Branched GDGT analysis

The surface soils were freeze dried, powdered, and extracted (3×) with a mixture of dichloromethane (DCM):MeOH 9:1 (v/v), using a DIONEX accelerated solvent extractor (ASE 200) at 100°C and a pressure of 7.6×10^6 Pa for 5 min. The extracts were dried under near vacuum using a rotary evaporator, then dissolved in DCM and passed over a Na_2SO_4 column to remove any remaining water. Separation of the extracts in apolar and polar fraction was done by passing them over an activated Al_2O_3 column using hexane:DCM 9:1 (v/v) and DCM:MeOH 1:1 (v/v), respectively. The polar fraction, containing the branched GDGTs, was dried under N_2, dissolved in hexane:isopropanol 99:1 (v/v), and filtered through a 0.45 μm PTFE filter. The polar fractions were concentrated to about 3 mg/ml prior to analysis by high performance liquid chromatography/atmospheric pressure chemical ionization-mass spectrometry (HPLC/APCE-MS) on an Agilent 1100 series LC/MSD SL according to Schouten et al. (2007a). Separation of the branched GDGTs was achieved on an Alltech Prevail Cyano column (150 mm×2.1 mm; 3 μm) as described by Schouten et al. (2007a), with minor modifications. In short, the compounds were eluted isocratically with 90% A and 10% B for 5 min at a flow rate of 0.2 ml/min, and then with a linear gradient to 16% B for 34 min, where A=hexane and B=hexane:isopropanol 9:1 (v/v). The injection volume was 10 μl per sample. Selective ion monitoring of the $[M+H]^+$ of the different branched GDGTs was used to detect and quantify them.

8.2.3 Statistical analyses

A Principal Component Analysis (PCA) was performed on the relative abundances of the branched GDGTs in the 176 surface soils of the new calibration dataset to identify possible outliers. Subsequently, this dataset was used to derive new indices to describe the relations of branched GDGT distributions with MAT and with soil pH with linear regression analysis, following the approach used for the TEX_{86} calibration by Kim et al. (2010a). In short, for each relation, the top hundred indices with the highest correlation coefficient were obtained according to the following format:

$$\text{Index} = \text{LOG} \left(\sum k_1 X / \sum k_2 X \right) \qquad (8.6)$$

In this index, *X* refers to the relative abundance of one of branched GDGTs Ia, Ib, Ic, IIa, IIb, IIc, or IIIa. The sets of branched GDGTs are represented by k_1 and k_2, the summation describes of which describes the numerator and the denominator, respectively. For each MAT and pH, the index with the highest correlation coefficient was selected for further testing.

Another set of equations to predict pH and MAT based on the distribution of branched GDGTs was derived using least squares multiple linear regression analysis. This method assigns weighing factors to the fractional abundance of the individual branched GDGTs to obtain the equations with the highest coefficient of determination.

A Moran's I test was performed to test the spatial autocorrelation of MAT and pH estimates in our set of surface soils. All statistical analyses were performed with the R package, except for the multiple linear regression analysis, which was performed using SYSTAT 12.

8.3. Results and discussion

8.3.1 Branched GDGT abundances

Branched GDGTs were detected in all soils, although not every soil contains the complete suite of branched GDGTs, i.e. only 74 (26%) of the soils contains detectable amounts of all nine branched GDGTs (*Supplementary Table S8.1*). In particular, branched GDGTs IIIb and IIIc (*Fig. 8.1*) are frequently below detection limit and if present do not comprise more than 1% of total branched GDGTs on average. The most dominant branched GDGTs are Ia, IIa and IIIa, while branched GDGTs with cyclopentane moieties are generally present in lower amounts.

For the assessment of the relationship between environmental parameters and GDGT distributions it would be preferable to use only those soils that contain all branched GDGTs. However, since this data set comprises only 74 soils, we excluded branched GDGT-IIIb and IIIc, since they are generally below the detection limit and, if detected, occur only in low abundance. This leaves 176 (or 63%) of the surface soils that contain quantifiable amounts of the seven remaining GDGT isomers for the calibration (filled circles, *Fig. 8.2*).

To examine the relationships of the relative abundances of the different branched GDGT types with the environmental parameters, we plotted their individual abundances (as a percentage of total branched GDGTs) versus MAT and pH, respectively (*Figs. 8.3 and 8.4*). Branched GDGTs without cyclopentane moieties show the strongest linear relation with MAT. Branched GDGT-IIa and IIIa negatively relate with MAT, while branched GDGT-Ia shows a positive relation. This confirms that the number of methyl branches attached to the tetraether backbone of the GDGTs increases with increasing MAT (Weijers et al., 2007c; Peterse et al., 2009b). The other branched GDGTs show mainly scatter or a weak relation with MAT (e.g. branched GDGT-Ic, *Fig. 8.3c*).

The relations of the different branched GDGTs with pH are generally stronger than those with MAT (*Fig. 8.4*). Most of the branched GDGTs with cyclopentane moieties show a positive exponential relation with pH, whereas branched GDGT-Ia is the only type that is negatively related with pH, and branched GDGTs Ic and IIa show no clear relation. As pH is a logarithmic function of the proton concentration in a soil, the exponential relations of the branched GDGTs with cyclopentane rings support the idea that soil pH influences the degree of cyclisation of branched GDGTs (cf. Weijers et al., 2007c; Peterse et al., 2010). The relatively strong relation between branched GDGT-Ia and pH indicates that also the degree of methylation is, to some extent, dependent on pH (cf. Weijers et al., 2007c).
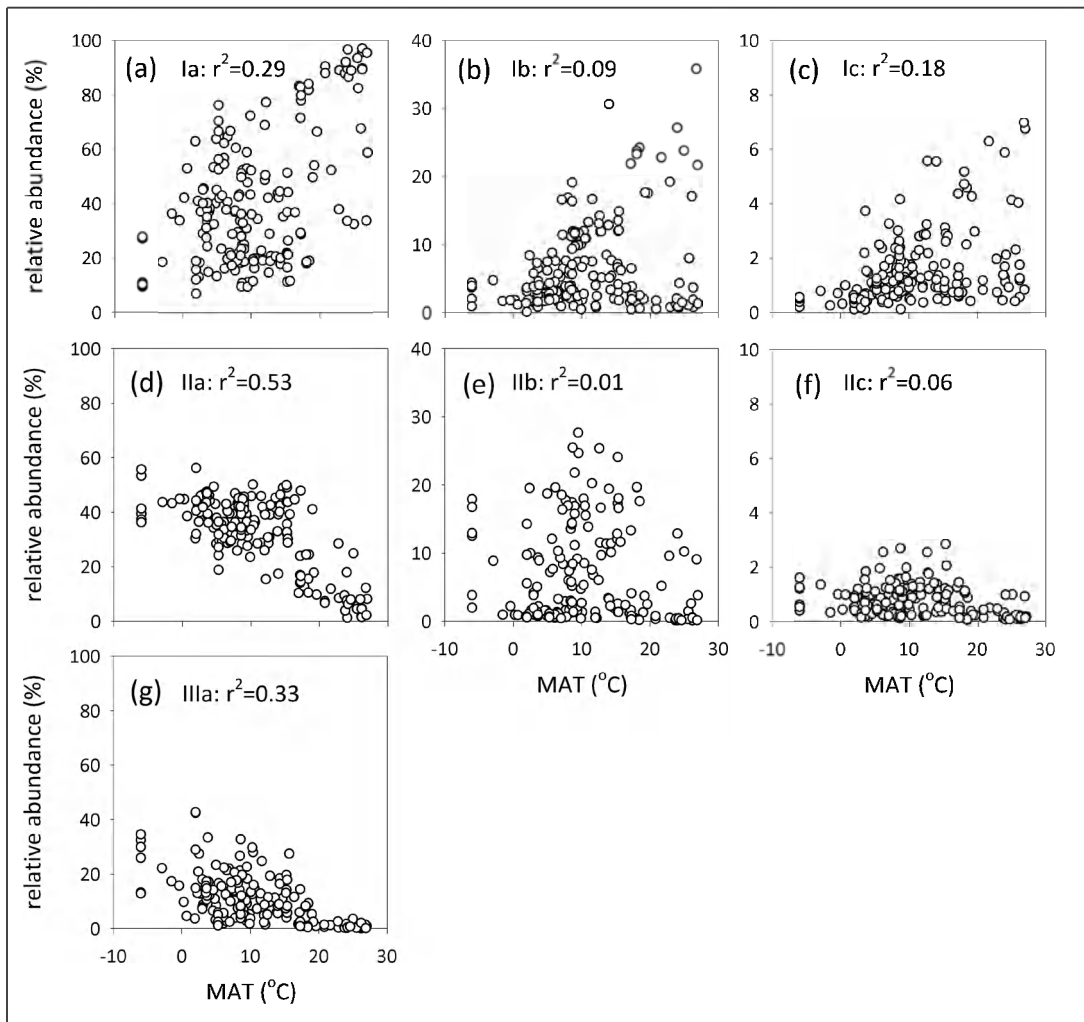
Fig. 8.3. Plots of the relative abundance of each individual branched GDGT (as a percentage of the sum of the seven selected branched GDGTs) versus MAT; a) Ia, b) Ib, c) Ic, d) IIa, e) IIb, f) IIc, g) IIIa. Determination coefficients indicate those of a linear regression.

Principal component analysis (PCA) on the relative abundances of the branched GDGTs in these surface soils shows that the first two axes explain a cumulative of 81.5% of the variance in the data (*Fig. 8.5*). On the first component, explaining 49.0% of the variance, the score of GDGT-Ia is opposite to that of all other branched GDGTs, especially GDGTs-IIb and IIc. Branched GDGTs-IIc and IIb stand out on the positive side of the second factor (explaining 32.5% of the variance), against branched GDGTs-IIa and IIIa, which have the highest negative scores on this factor. Based on the distribution of the soils in the PCA plot, no outliers can be defined, so that all 176 soils were used for calibration purposes.

8.3.2 Recalibration of the MBT-CBT proxy

Based on the relative abundance of the branched GDGTs in the surface soils in the new dataset, we recalibrated the MBT and CBT indices. Since branched GDGTs-IIIb and IIIc were excluded in this dataset, we redefined the MBT index as follows:

Fig. 8.4. Plots of the relative abundance of each individual branched GDGT (as a percentage of the sum of the seven selected branched GDGTs) versus soil pH; a) Ia, b) Ib, c) Ic, d) IIa, e) IIb, f) IIc, g) IIIa. Determination coefficients indicate those of an exponential regression.

$$\text{MBT'} = (\text{Ia}+\text{Ib}+\text{Ic})/(\text{Ia}+\text{Ib}+\text{Ic}+\text{IIa}+\text{IIb}+\text{IIc}+\text{IIIa}) \qquad (8.7)$$

Correlation of the MBT' and CBT indices with MAT and soil pH resulted in the following equations (*Fig. 8.6a, b*):

$$\text{pH} = 7.90 - 1.97 \times \text{CBT} \qquad (n=176; r^2=0.70; \text{RMSE}=0.8) \qquad (8.8)$$
$$\text{MAT} = -0.64 + 22.9 \times \text{MBT'} \qquad (n=176; r^2=0.47; \text{RMSE}=5.7 \ ^\circ\text{C}) \qquad (8.9)$$

Similar to the original calibration set, no strong relation was observed between CBT and MAT, but MBT' also relates with soil pH:

$$\text{pH} = 7.88 - 3.80 \times \text{MBT'} \qquad (n=176; r^2=0.40; \text{RMSE}=1.1) \qquad (8.10)$$

101

Thus, substitution of pH in Eq. 8.10 by the CBT index (cf. Weijers et al., 2007c) results in an equation that enables the estimation of MAT based on the CBT and MBT' indices (Eqs. 8.1 and 8.7; *Fig. 8.6c*), i.e. the distribution of branched GDGTs:

$$MAT = 0.81 - 5.67 \times CBT + 31.0 \times MBT' \qquad (n=176; r^2=0.59; RMSE=5.0\ °C) \qquad (8.11)$$

The correlation coefficients of these new transfer functions are considerably lower than those of the original equations, i.e. Eqs. 8.3-8.5 (Weijers et al., 2007c), and the new MBT'-CBT calibration shows a relatively large amount of scatter (*Fig. 8.6c*).
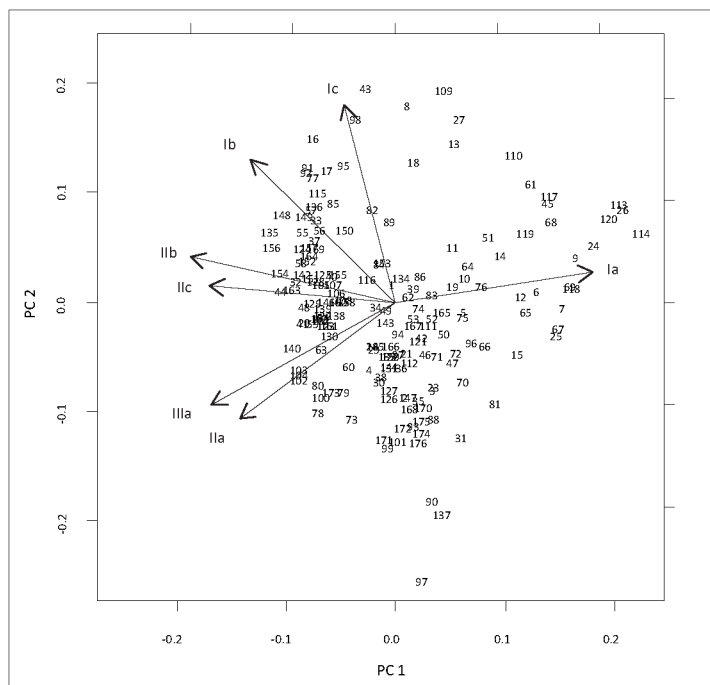
Fig. 8.5. Principal components analysis (PCA) biplot of the branched GDGT distributions in the surface soils of the extended global calibration set (n=176). The first compnent explains 49.0%, and 32.5% of the variation is explained by the second component.

8.3.3 Statistical reevaluation of the relations between branched GDGT distributions with MAT and soil pH

The original MBT and CBT indices were defined by empirically linking environmental controls with a presumed physiological mechanism of membrane adaptation by the soil bacteria producing the branched GDGTs, i.e. an increase in the number of methyl branches with decreasing MATs, and the formation of additional cyclopentane moieties with increasing soil pH (Weijers et al., 2007c). An objective statistical approach for determining the best indices to describe the relations between branched GDGTs, MAT and pH has so far been lacking. To examine this, we used linear regression analysis to compute the best combinations to describe MAT and pH based on the relative abundance of the previously selected seven branched GDGTs in the extended global surface soil calibration set. The following index gave the best relation with MAT:

$$Index\text{-}1 = LOG\ (Ic/IIIa) \qquad\qquad\qquad (8.12)$$

$$MAT = 16.5 + 7.96 \times Index\text{-}1 \qquad\qquad (n=176; r^2=0.60; RMSE=4.9\ °C) \quad (8.13)$$

For soil pH, the following index and equation were obtained:

$$Index\text{-}2 = LOG\ ((Ic+IIb)/(Ia+Ib+Ic+IIc)) \qquad\qquad\qquad\qquad (8.14)$$
$$pH = 7.94 + 2.00 \times Index\text{-}2 \qquad\qquad (n=176; r^2=0.78; RMSE=0.7) \quad (8.15)$$

Strikingly, index-1 is much simplified over the MBT' index, while index-2 uses more individual branched GDGTs compared to the CBT index. However, although the determination coefficients for these new indices are slightly higher compared to the MBT' and CBT index, the accuracy of the MAT and pH estimates is only marginally improved. Both indices heavily rely on the relative abundance of branched GDGT-Ic, which often comprises less than 2% of the total amount of branched GDGTs, with maxima of 6% in a few soils from the humid tropics (*Fig. 8.3c; Supplementary Table S8.1*). Furthermore, these new indices lead to a disconnection with the presumed mechanism of adaptation of the cell membrane, i.e. variation in the degree of methylation and cyclisation of the membrane to adjust its fluidity and permeability. We, therefore, fail to see a significant advance in using these new indices.

Another method that can potentially improve the empirical relation between branched GDGT distribution and environmental parameters is least squares multiple linear regression analysis. A recent application of this method on branched GDGT distributions in East African lakes showed that the accuracy of MAT estimates improved considerably relative to those derived with the original MBT-CBT proxy (Tierney et al., 2010b). The method assigns weighing factors to the fractional abundance of the individual branched
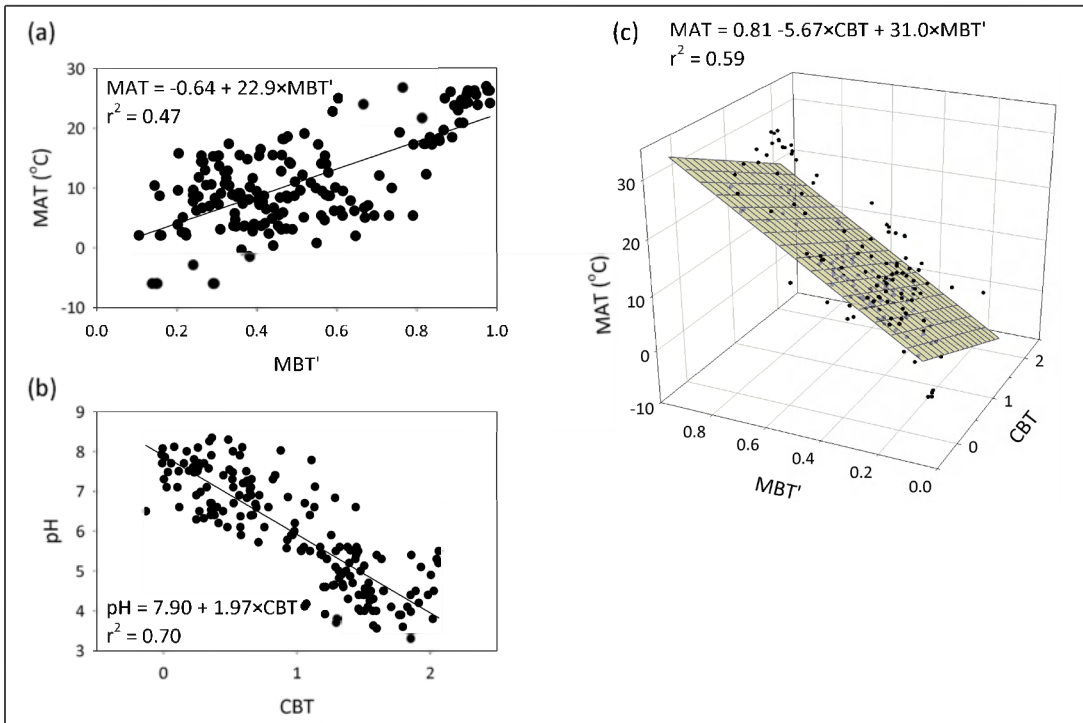
Fig. 8.6. Linear regression plots of a) MAT and MBT´, and b) pH and CBT based on application of Eqs. 8.7 and 8.1, respectively, on the new global surface soil calibration set, and c) 3D regression plot for the MBT´-CBT calibration on MAT (Eq. 8.11).

GDGTs to obtain the equation with the highest coefficient of determination for the estimation of MAT or pH. Application to our dataset resulted in the following equations:

$$pH = 8.49 - 0.043 \times Ia + 0.013 \times Ib + 0.019 \times Ic - 0.037 \times IIa + 0.045 \times IIb - 0.18 \times IIc + 0.020 \times IIIa$$
$$(n=176; r^2=0.72; RMSE=0.7) \qquad (8.16)$$

$$MAT = 192.7 - 1.7 \times Ia - 1.6 \times Ib - 1.2 \times Ic - 2.0 \times IIa - 1.7 \times IIb - 3.3 \times IIc - 1.9 \times IIIa$$
$$(n=176; r^2=0.60; RMSE=4.9 \ ^{\circ}C) \quad (8.17)$$

Again, the determination coefficients show only marginal improvements on the revised MBT' and CBT relations. Furthermore, also this method neglects the mechanisms that are supposedly underlying the synthesis of branched GDGTs in soils. Therefore, we propose to use the MBT' and CBT indices with their revised calibrations as proxies for paleotemperature and past soil pH.

8.3.4 Accuracy of MAT and pH estimates

The 3D calibration plot of the MBT'-CBT proxy has a considerable amount of scatter (*Fig. 8.6c*). Weijers et al. (2007c) ascribed the scatter in their calibration plot to the use of air temperature instead of in situ soil temperature, as well as to the heterogeneity of soils. It has been suggested that application of a local rather than the global calibration may improve the accuracy of branched GDGT-derived temperature estimates (e.g. Sinninghe Damsté et al., 2008; Peterse et al., 2009b; Bendle et al., 2010). We, therefore, performed a Moran's I test, which analyzes the degree of dependence in a geographical space, and thus indicates whether two soils that are located in each others vicinity have a similar offset between estimated and measured MAT. Hence, application of local calibrations would become beneficial when soils from one geographical location all have the same temperature deviation. However, the test results show no indication of such a relation, which implies that a local calibration will not likely lead to substantially improved accuracy. Also the accuracy of the relation between pH and CBT does not benefit from a local calibration.

Secondly, seasonality has been put forward to explain part of the scatter (e.g. Peterse et al., 2011; Rueda et al., 2009; Weijers et al., 2007b). However, Weijers et al. (2007c) did not find better relations between seasonal temperatures and the MBT index than with MAT. Furthermore, no apparent seasonal pattern in the distribution of branched GDGTs was found in mid-latitude soils (Weijers et al., 2011). Hence, the remaining scatter is unlikely to be fully explained by seasonality.

Another environmental parameter that has been suggested to affect branched GDGT distributions is soil moisture, or precipitation (Weijers et al., 2007c). The relative abundance of some of the branched GDGTs indeed relates with MAP (*Fig. 8.7*), especially GDGTs Ia ($r^2=0.36$) and IIa ($r^2=0.41$). These branched GDGTs contribute to the CBT index as well as the MBT' index, suggesting that variations in MAP may possibly affect the index values. However, like in the original calibration set of Weijers et al. (2007c), MAP and MAT are correlated with each other ($r^2=0.31$), which makes it impossible to statistically separate influences of MAP and MAT on branched GDGT distributions. However, the possible influence of MAP becomes visible when we plot MBT'-CBT-derived MATs using the revised soil calibration (Eq. 8.11) versus measured MAT for all soils of this study (*Fig. 8.8a*), thereby assuming a relative abundance of 0% for the branched GDGTs which were below detection limit. The MAT scatter plot shows one cluster of soils for
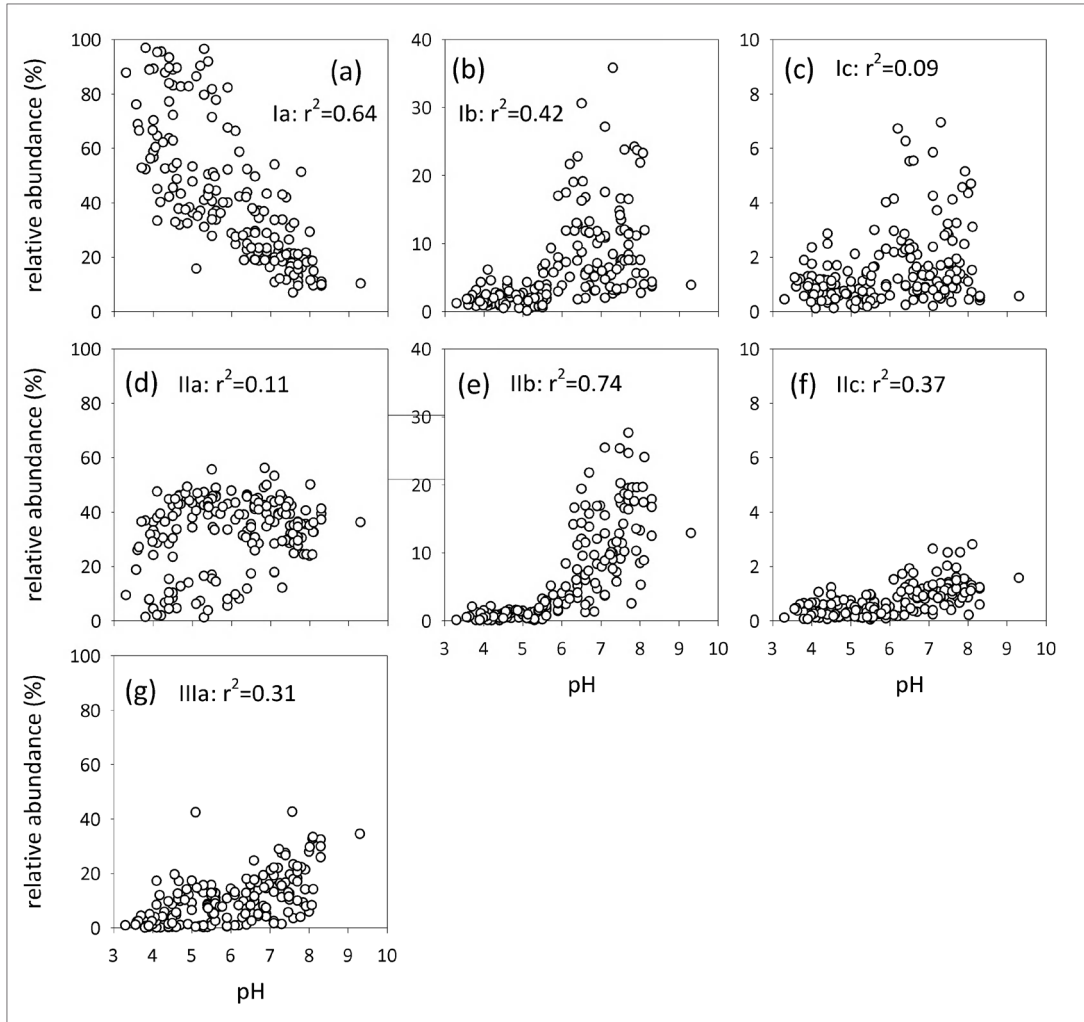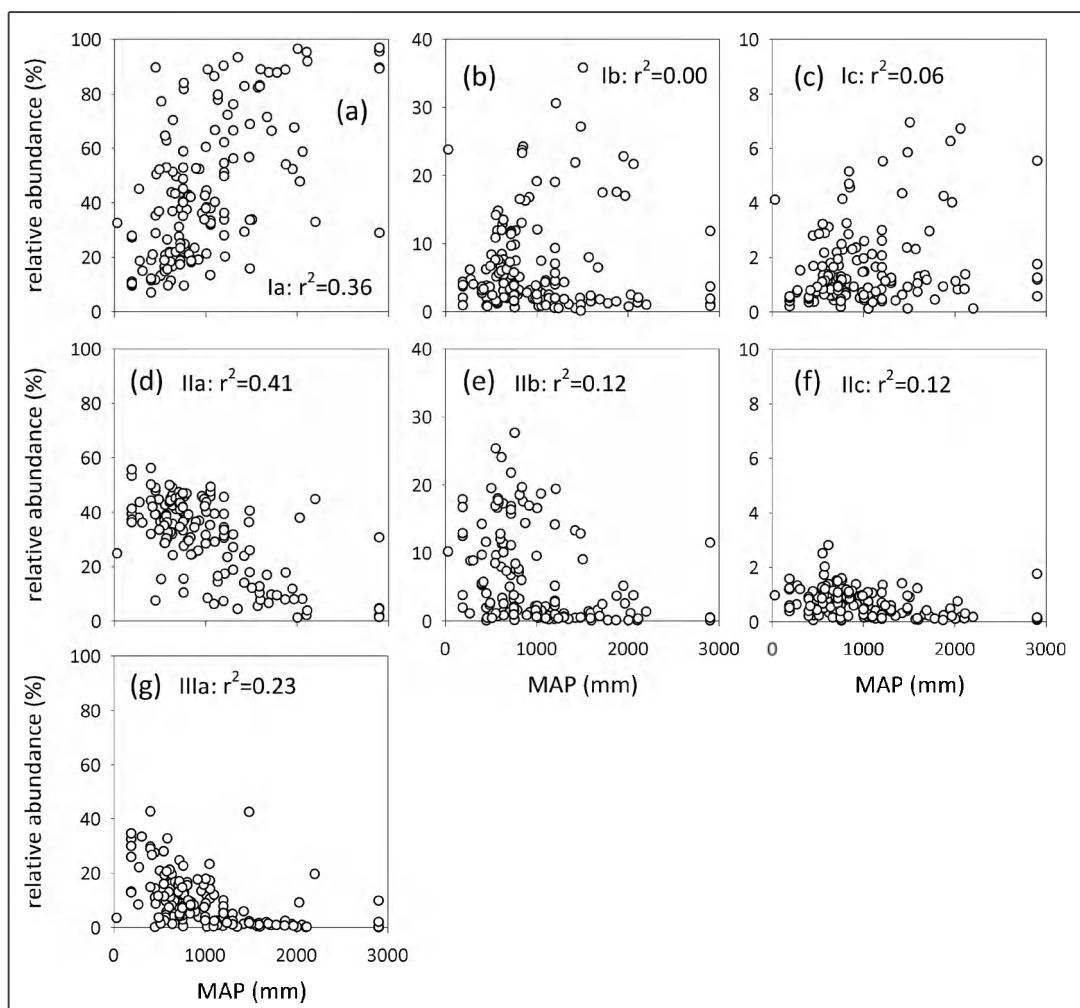
Fig. 8.7. Plots of the relative abundance of each individual branched GDGT (as a percentage of the sum of the seven selected branched GDGTs) versus MAP; a) Ia, b) Ib, c) Ic, d) IIa, e) IIb, f) IIc, g) IIIa. Determination coefficients indicate those of a linear regression.

which the reconstructed MAT strongly underestimates actual MAT up to 20 °C (*Fig. 8.8a*). The addition of precipitation data to this plot shows that this cluster mainly comprises alkaline soils from arid regions (MAP ≤ 500 mm; *Fig. 8.8b*) that are generally low in organic matter. This suggests that in these soil types, temperature is apparently no longer an important control on the distribution of branched GDGTs. Although it is not possible to define an exact precipitation threshold or soil type for which the MBT'-CBT proxy should not be utilized, we suggest that MAT reconstructions for arid regions should be interpreted with care.

In summary, several factors may contribute to the scatter in the calibration between branched GDGT distributions with MAT and pH. However, the relatively large uncertainty in absolute temperature estimates is likely to be mainly systematic. Hence, application of the proxy on a local scale, e.g. down core, results in temperature estimates with the same systematic error. As a consequence, the uncertainty on the trends in these paleotemperature records is likely to be much smaller (e.g., Tierney et al., 2010a; Peterse et al., 2011).
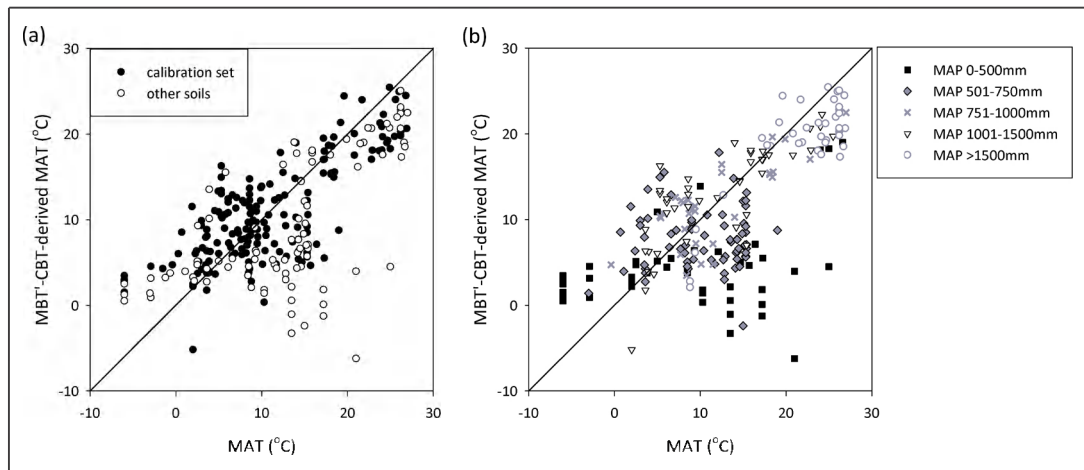
Fig. 8.8. MBT'-CBT-derived MAT estimates versus measured MAT for a) the surface soils included in the MBT'-CBT global calibration set (filled circles, n=176) as well as the soils that were excluded from the calibration set for which MAT was estimated by taking 0% for branched GDGTs below the detection limit (open circles; n=94), and b) soils for which MAP data were available (n=234) divided in different precipitation classes.

8.4. Implications for paleoclimate reconstruction

To test the impact of the new MBT' and CBT indices on paleotemperature reconstructions, we derived new temperature records for the atmospheric warming in tropical Africa (Weijers et al., 2007a) and southeast Asia (Peterse et al., 2011) over the last deglaciation, the onset of long-term cooling near the Eocene-Oligocene (E-O) boundary (Schouten et al 2008a), and the period of extreme warmth during the PETM (Weijers et al., 2007b), and compared them with the records based on the original MBT-CBT calibration.

8.4.1 Deglacial atmospheric warming of tropical Africa

Application of the original MBT-CBT calibration in a sediment core recovered close to the Congo River outflow suggested that MATs increased with ~0.7 °C/kyr from 20-21 °C during the Last Glacial Maximum (LGM) to a maximum of 25 °C in the first half of the Holocene (*Fig. 8.9a*, filled circles; Weijers et al 2007a). The 24.5 °C that was reconstructed from the core-top sediment was similar to the present day MAAT of the Congo River Basin (23.7 °C; Weijers et al., 2007a). Application of the newly calibrated MBT'-CBT shows the same temperature trends as the original MBT-CBT record (*Fig. 8.9a*, open circles), although absolute MAAT estimates are lower, and now suggest MATs of 17.5 °C during the LGM, increasing to 20.5 °C during the Holocene. The branched GDGT distribution in the surface sediment now suggests an air temperature of 20.5 °C, which is somewhat lower than the measured modern air temperature, although still well within the calibration error of the proxy. The LGM-Holocene temperature difference of ~3 °C is still within the range indicated by other proxy records based on e.g. pollen assemblages and TEX$_{86}$-derived lake surface temperature as cited by Weijers et al. (2007a). Weijers et al. (2007a) also used the CBT-derived pH record to reconstruct humidity changes in central Africa. The pH record based on the newly calibrated CBT index is very similar to the original pH record, both in trend as in absolute values (*Fig. 8.9b*).

8.4.2 Deglacial atmospheric warming of East Asia

A continuous air temperature record for East Asia covering the last 34,000 years was derived from branched GDGT distributions in a loess-paleosol sequence from the Mangshan loess plateau in China

(*Fig. 8.9c*, filled circles; Peterse et al., 2011). The original record suggested a large increase in air temperature over the deglaciation with MAT estimates increasing from ~17 °C during the last glacial period to a maximum of ~27 °C during the Holocene climatic optimum. The temperature record was considered to be biased towards the summer, as the branched GDGTs in the surface loess layer reflected average present day air temperatures of the monsoon and summer season (~24 °C). The air temperatures that are derived with the new MBT'-CBT calibration are lower than the original record, and now suggest air temperatures of ~15 °C for the LGM, increasing towards 21 °C in the Holocene (*Fig. 8.9c*, open circles). A deglacial warming of 6-7 °C, as indicated by the new record, falls in the temperature range based on the pollen and phytolith-derived reconstructions for this region as cited by Peterse et al. (2011). The temperature estimate of the surface layer, ~19 °C, suggests that the record is less biased towards summer temperatures, although it is still well above the present day MAT in this area of 13 °C. Irrespective of the lower absolute MAT estimates, which fall within the error of the proxies, the timing of the onset of deglacial atmospheric warming, and consequently the main conclusions of the original study, remain unaffected.

8.4.3 Oligocene-Eocene cooling of Greenland landmass

The climatic transition from a 'greenhouse' world to an 'icehouse' world took place around the E-O boundary (33.7 kyr BP), when the East Antarctic Ice Sheet first expanded. Branched GDGTs from Greenland landmass, preserved in a marine sediment core from the Greenland Basin (ODP Site 913B), provided insight in the extent of atmospheric cooling in high-latitudes during this period (Schouten et al., 2008a). Application of the original MBT-CBT proxy suggested late Eocene air temperatures of 12-16 °C, dropping to 8-10 °C during the early Oligocene (*Fig. 8.9d*, filled circles), indicating a cooling of ~3-5 °C of the Greenland landmass. The absolute temperatures derived from the new MBT'-CBT calibration are similar to those reconstructed using the original indices, although the extent of the cooling is now slightly lower, i.e. ~2 °C (*Fig. 8.9d*, open circles). Application of Eq. 8.11 results in temperature estimates of 14±1 °C for the Eocene, and 12±1 °C for the early Oligocene, which fits independent temperature estimates based on pollen assemblages in the same, and nearby-located sediment cores, that indicate air temperatures of 14±3 °C, decreasing to 10-11±3 °C for the latest Eocene to Oligocene (Eldrett et al., 2009). Hence, the use of the new calibration does not affect the interpretation of high latitude climate development across the Eocene-Oligocene boundary.

8.4.4 Paleocene-Eocene thermal maximum at the Arctic

Branched GDGTs originating from the high latitude continents surrounding the Arctic Ocean during the PETM have been analyzed in a sediment core from the Lomonosov Ridge (IODP Hole 302-4A) and indicate an atmospheric warming of ~8 °C during the PETM, above background values of ~17 °C (*Fig. 8.9e*, filled circles; Weijers et al., 2007b). These temperatures are considered to be relatively high, but were ascribed to a summer biases (Weijers et al., 2007b). The new MAT estimations based on the MBT'-CBT proxies are 2 °C lower (~17 °C) during the late Paleocene and 3 °C lower (~21 °C) for the PETM compared to the original record (*Fig. 8.9e*, open circles). The previously observed trends in the temperature record remain unaffected but the magnitude of the warming decreases from 8 to 6 °C. The lower absolute MAT estimates and reduced amplitude of the record are more in line with the temperature estimates based on other proxies, i.e. pollen assemblages and oxygen isotopic compositions of fossil teeth and bones (e.g.
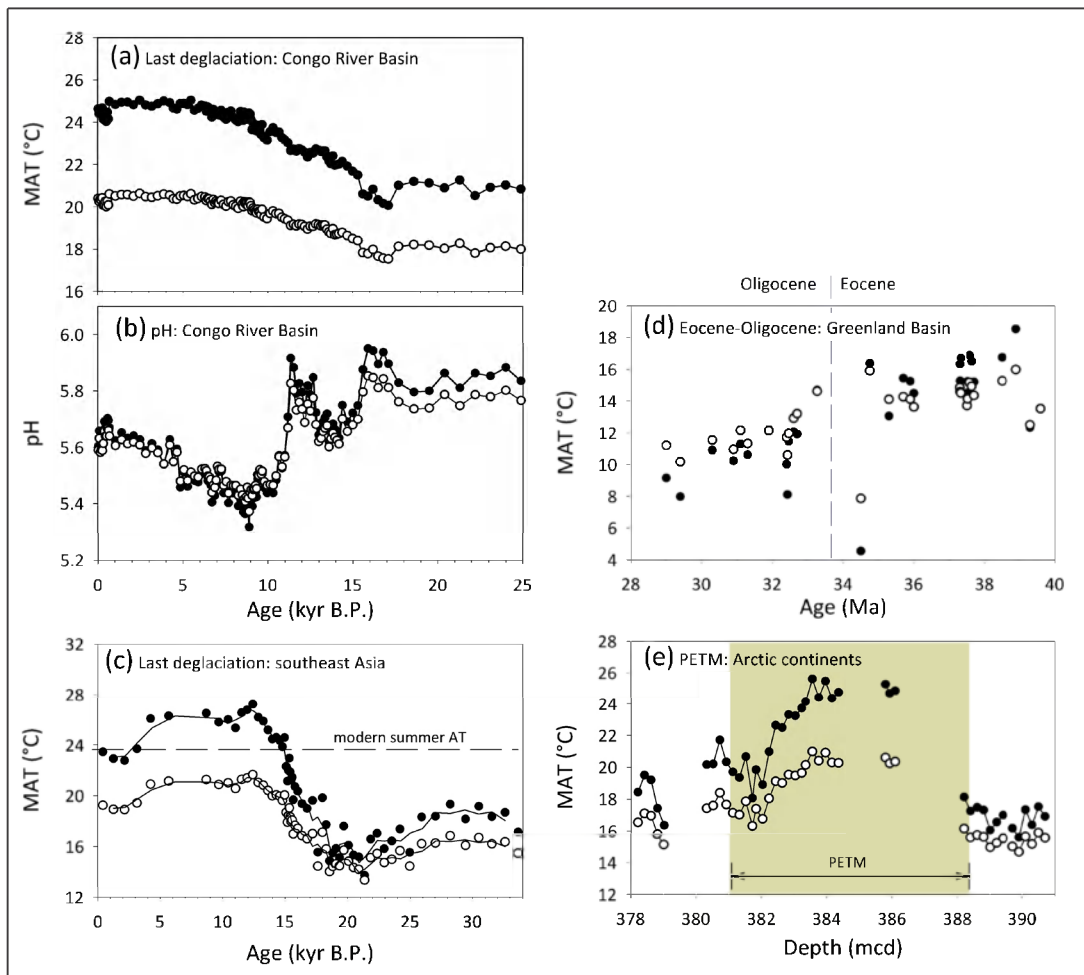
Fig. 8.9. Comparison of climate reconstructions based on the original MBT-CBT paleothermometer (*Weijers et al., 2007c*; filled circles) and based on the MBT'-CBT calibration (open circles) for a) the deglacial atmospheric warming and b) pH record of tropical central Africa (*Weijers et al., 2007a*), c) deglacial atmospheric warming in East Asia (*Peterse et al., 2011*), d) the onset of long-term cooling of Greenland around the Eocene-Oligocene boundary (*Schouten et al., 2008a*), and e) the episode of extreme warmth during the PETM for high latitude continents surrounding the Arctic Ocean (*Weijers et al., 2007b*).

Eberle et al., 2010). This suggests that the use of the newly calibrated MBT'-CBT proxy results in improved MAT estimates for this ancient greenhouse period.

8.5. Conclusions

Extension of the global calibration set and excluding rarely detected branched GDGTs from the MBT index has lead to new transfer functions to predict MAT and soil pH. Attempts to improve the accuracy of the transfer functions with a statistical approach resulted in only marginally better correlation coefficients for the relations with MAT and pH, while their definition does not relate to the presumed physiological processes that are underlying the mechanism of the original MBT-CBT proxy. Thus, we propose to use the recalibrated MBT-CBT indices as originally defined by Weijers et al. (2007c), although in a slightly modified form (MBT'). Inspection of the large scatter in the MBT'-CBT calibration plot (*Fig. 8.6c*) indicated that branched GDGT-based temperature estimates for arid soils may be underestimated by as much as 20

°C, and care should be taken with the interpretation of absolute temperature for arid regions.

Application of the new MBT'-CBT transfer function on previously published paleotemperature records from different locations and geological eras showed that the trends in the temperature reconstructions remain unchanged. The absolute temperature estimates, however, are generally lower, and often better match with temperature estimates for the same region and time interval based on independent proxies.

Supplementary Table S8.1. Overview of the relative abundance of individual branched GDGTs, MAT, pH, MAP, MBT' and CBT index values, and coordinates for the surface soils of this study. The first part of the table comprises the soils that are included in the new global calibration set. The soils that were excluded from the calibration set are mentioned in the second part of the table. Branched GDGT below detection limit are set to 0%.

| Sample name | relative abundance (%) | | | | | | | measured MAT (°C) | soil pH | MAP (mm) | MBT' | CBT | Coordinates (X,Y) | Study |
	IIIa	IIa	IIb	IIc	Ia	Ib	Ic							
Australia-17	5.9	32.9	3.4	0.3	43.7	12.8	0.9	13.9	6.4	624	0.57	0.68	148.33, -34.72	Weijers et al., 2007c
Australia-25	11.0	48.9	1.9	0.3	35.3	2.0	0.5	14.7	5.6	450	0.38	1.33	139.67, -34.7	Weijers et al., 2007c
Australia-4	5.3	41.1	1.3	0.4	49.7	2.0	0.4	19.0	6.6	677	0.52	1.45	150.6, -26.72	Weijers et al., 2007c
Australia-9	14.4	47.9	4.1	0.5	28.7	3.8	0.6	17.3	6.0	450	0.33	0.99	138.65, -34.97	Weijers et al., 2007c
Australia-T	1.5	15.4	0.5	0.2	77.2	2.4	2.9	12.2	4.4	513	0.82	1.51	147.5, -42.83	Weijers et al., 2007c
Brazil-1	0.3	8.4	0.5	0.4	88.9	0.8	0.7	22.9	4.5	1021	0.90	1.90	-43.68, -22.75	Weijers et al., 2007c
Brazil-6	0.6	7.3	0.3	0.1	90.3	0.5	0.8	20.8	5.2	1194	0.92	2.07	-50.32, -22.55	Weijers et al., 2007c
Cameroon-1	1.2	11.9	5.1	0.5	52.3	22.8	6.3	21.7	6.4	1950	0.81	0.36	9.33, 4.23	Weijers et al., 2007c
Canada-14	1.8	36.3	0.5	0.4	56.7	2.0	2.4	6.1	4.0	1474	0.61	1.57	-63.42, 45.42	Weijers et al., 2007c
Canada-17	20.8	36.4	19.5	0.9	13.1	8.4	0.9	2.4	7.7	505	0.22	0.25	-98.18, 49.95	Weijers et al., 2007c
Canada-24	9.2	37.9	1.1	0.7	47.7	2.5	0.8	9.5	5.0	2031	0.51	1.37	-122.38, 49.25	Weijers et al., 2007c
China-20	0.3	7.7	0.1	0.1	89.0	1.5	1.3	24.7	3.9	1600	0.92	1.77	110.33, 18.77	Weijers et al., 2007c
China-23	1.7	10.3	1.2	1.2	83.1	1.5	1.0	18.2	4.5	1590	0.86	1.55	116.92, 28.22	Weijers et al., 2007c
China-25	2.0	16.9	1.6	0.3	71.4	6.5	1.3	17.2	5.5	1670	0.79	1.04	116.27, 28.48	Weijers et al., 2007c
China-27	1.0	12.7	0.4	0.1	82.7	2.3	0.7	17.8	4.7	1590	0.86	1.54	117.75, 27.09	Weijers et al., 2007c
China-31	0.8	9.7	2.5	0.2	66.4	17.5	3.0	19.6	6.1	1720	0.87	0.58	114.28, 24.38	Weijers et al., 2007c
China-32	1.4	6.7	0.7	0.4	87.9	1.8	1.2	20.8	4.3	1690	0.91	1.58	113.65, 23.65	Weijers et al., 2007c
China-4	1.3	14.0	0.5	0.3	82.8	0.5	0.6	17.2	4.9	1422	0.84	2.01	113.83, 28.2	Weijers et al., 2007c
China-49	5.6	17.4	19.4	1.4	20.1	30.6	5.5	14.0	6.5	1210	0.56	-0.12	106.43, 26.38	Weijers et al., 2007c
China-5	5.9	23.9	13.3	1.4	29.3	21.9	4.3	17.2	8.0	1422	0.55	0.18	113.9, 28.2	Weijers et al., 2007c
China-6	2.4	17.8	3.7	0.2	54.0	17.6	4.3	19.2	7.1	1876	0.76	0.53	110.52, 24.82	Weijers et al., 2007c
France-15	9.8	42.9	1.1	0.2	43.3	2.1	0.6	8.3	4.7	664	0.46	1.42	2.55, 45.05	Weijers et al., 2007c
Gabon-1	0.9	9.4	0.1	0.1	87.8	1.2	0.5	23.7	3.3	1781	0.89	1.86	12.8, 0.52	Weijers et al., 2007c
Gabon-2	0.2	1.2	0.1	0.1	96.5	0.7	1.1	24.1	5.3	2007	0.98	2.06	14.12, -1.52	Weijers et al., 2007c
Gabon-6	0.7	8.0	2.6	0.2	67.5	17.0	4.0	26.0	5.9	1969	0.89	0.59	10.28, -0.52	Weijers et al., 2007c
Galapagos	0.1	7.5	0.1	0.1	89.6	0.9	1.7	24.0	4.4	451	0.92	1.99	-89.75, -0.85	Weijers et al., 2007c
Germany-G1	16.6	29.6	7.2	0.9	42.0	3.1	0.7	5.4	7.4	805	0.46	0.84	12, 48	Weijers et al., 2007c

Location														Reference
Germany-G2	15.5	29.3	7.6	0.8	42.9	3.2	0.6	5.8	7.3	805	0.47	0.83	12, 48	Weijers et al., 2007c
Germany-H1	12.0	37.3	8.4	1.5	24.8	11.9	4.1	8.7	6.1	768	0.41	0.49	9.98, 53.63	Weijers et al., 2007c
Greece-13	8.7	39.0	0.5	0.2	50.4	0.8	0.4	12.1	5.4	458	0.52	1.86	23.55, 40.5	Weijers et al., 2007c
Greece-5	27.4	39.2	11.6	1.1	11.6	6.2	2.8	15.7	7.4	446	0.21	0.45	22.5, 40.58	Weijers et al., 2007c
Greenland-5	15.7	44.8	2.2	1.0	33.8	1.8	0.7	-0.4	5.5	984	0.36	1.30	-37.67, 65.62	Weijers et al., 2007c
Iceland-3a	15.7	47.3	1.3	0.7	31.1	3.3	0.6	3.5	5.3	706	0.35	1.23	-22.75, 65.08	Weijers et al., 2007c
Iceland-6	13.1	43.5	5.0	1.5	27.5	7.3	2.2	3.5	6.1	706	0.37	0.76	-20.88, 65.35	Weijers et al., 2007c
Ireland-9	3.8	36.9	1.3	0.6	52.3	3.2	1.9	8.8	3.8	928	0.57	1.30	-7.8, 53.9	Weijers et al., 2007c
Italy-1	8.2	39.1	3.2	0.9	42.3	5.1	1.2	14.0	6.2	811	0.49	0.99	16.15, 39.67	Weijers et al., 2007c
Italy-11	8.2	43.6	1.3	0.5	44.2	1.8	0.4	15.4	5.4	1007	0.46	1.45	13.52, 41.48	Weijers et al., 2007c
Italy-14	8.9	40.1	2.2	0.5	44.5	3.3	0.5	14.2	5.6	1007	0.48	1.18	13.53, 41.48	Weijers et al., 2007c
Italy-17	17.8	28.8	16.6	1.0	21.3	12.0	2.6	15.4	7.6	1007	0.36	0.24	13.62, 41.45	Weijers et al., 2007c
Nigeria-19	1.4	12.2	9.0	0.9	33.7	35.8	7.0	26.8	7.3	1507	0.77	0.01	3.5, 6.62	Weijers et al., 2007c
Norway-1	23.3	35.2	18.7	1.1	13.4	7.5	0.9	5.0	7.6	1048	0.22	0.27	9.68, 63.82	Weijers et al., 2007c
Norway-3	5.8	36.5	0.9	0.6	52.6	2.8	0.9	5.3	4.3	892	0.56	1.39	10.68, 63.43	Weijers et al., 2007c
Rarotonga	0.2	3.8	0.4	0.3	91.9	2.0	1.4	23.8	5.4	2112	0.95	1.60	-159.82, -21.2	Weijers et al., 2007c
Scotland-D	7.4	42.2	1.6	1.0	42.6	3.8	1.5	8.2	5.4	991	0.48	1.20	-3.33, 54.92	Weijers et al., 2007c
South Africa-12	0.8	15.5	0.2	0.0	81.7	0.6	1.1	18.4	5.5	759	0.83	2.07	30.27, -29.52	Weijers et al., 2007c
South Africa-3	0.4	10.4	0.2	0.1	83.9	2.5	2.5	18.4	4.4	759	0.89	1.54	30.92, -29.5	Weijers et al., 2007c
Spain-6	11.5	44.6	2.3	0.4	36.8	3.6	0.7	16.4	6.6	486	0.41	1.14	-6.27, 38.9	Weijers et al., 2007c
Sweden-15	4.6	38.5	0.9	1.0	52.9	1.2	1.0	0.7	4.5	569	0.55	1.65	19.57, 64.18	Weijers et al., 2007c
Sweden-17	3.7	30.3	0.7	0.5	62.8	1.4	0.6	1.9	4.5	569	0.65	1.66	19.48, 64.2	Weijers et al., 2007c
Sweden-4	20.6	36.2	17.7	1.2	15.5	7.6	1.1	7.7	7.7	578	0.24	0.31	14.07, 55.82	Weijers et al., 2007c
Sweden-B	1.3	24.1	0.8	0.5	70.3	2.1	0.8	5.3	4.0	641	0.73	1.51	18.43, 59.63	Weijers et al., 2007c
Sweden-S	2.6	28.6	1.1	0.7	64.6	1.6	0.8	6.6	4.1	555	0.67	1.54	17.95, 59.35	Weijers et al., 2007c
the Netherlands-B	22.7	27.6	27.6	1.6	9.5	9.8	1.2	9.5	7.7	761	0.21	0.00	4.75, 50.92	Weijers et al., 2007c
the Netherlands-T5	2.9	33.2	1.5	0.7	58.9	1.5	1.3	9.4	4.0	752	0.62	1.48	4.75, 53.08	Weijers et al., 2007c
the Netherlands-T7	4.4	36.4	2.1	0.6	52.8	2.4	1.2	9.4	3.7	752	0.56	1.30	4.75, 53.08	Weijers et al., 2007c
Turkey-12	28.0	35.1	8.5	0.9	18.8	7.6	1.1	10.4	8.0	547	0.28	0.53	29.93, 39.92	Weijers et al., 2007c
Uruguay-7	2.5	14.4	0.8	0.4	77.8	2.5	1.7	17.3	5.6	1133	0.82	1.45	-57.83, -32.67	Weijers et al., 2007c
Uruguay-8	0.8	16.5	0.3	0.1	79.6	1.9	0.7	17.3	5.3	1133	0.82	1.64	-57.5, -32.0	Weijers et al., 2007c
USA-10	0.3	6.2	0.4	0.2	86.5	4.3	2.1	24.2	5.1	1093	0.93	1.29	-159.4, 22.67	Weijers et al., 2007c

USA-13	3.6	33.5	2.6	0.4	52.2	6.7	0.9	10.0	5.9	493	0.60	0.96	-99.47, 40.47	Weijers et al., 2007c
USA-17	22.1	43.7	8.8	1.3	18.6	4.7	0.8	-2.9	7.1	277	0.24	0.66	-147.83, 64.87	Weijers et al., 2007c
USA-R-1	17.7	25.9	16.9	1.4	19.0	16.8	2.4	8.0	6.6	918	0.38	0.12	-73.8, 42.75	Weijers et al., 2007c
USA-R-2	8.2	34.3	14.4	1.1	23.3	16.3	2.3	8.6	6.5	876	0.42	0.27	-84.6, 41.58	Weijers et al., 2007c
USA-R-3	9.9	29.5	18.5	1.2	21.1	16.5	3.3	7.1	7.7	815	0.41	0.16	-89.25, 43.31	Weijers et al., 2007c
USA-R-4	17.0	34.6	16.4	1.5	17.3	11.4	1.9	7.2	7.7	719	0.31	0.27	-93.13, 44.53	Weijers et al., 2007c
USA-R-5	33.4	36.1	8.9	1.2	14.9	4.0	1.5	3.8	8.1	307	0.20	0.60	-112.29, 45.57	Weijers et al., 2007c
USA-R-6	26.7	42.0	5.8	0.6	21.0	3.3	0.8	8.5	7.4	419	0.25	0.84	-117.32, 47.38	Weijers et al., 2007c
USA-W	1.7	23.5	0.4	0.6	72.2	0.5	1.1	9.9	4.5	1239	0.74	2.03	-70.65, 41.54	Weijers et al., 2007c
Zaire-1	0.7	7.9	0.1	0.1	88.8	1.5	0.9	24.6	3.9	1871	0.91	1.79	42.47, 0.87	Weijers et al., 2007c
Brazil-12	0.9	8.1	3.8	0.2	58.7	21.7	6.7	24.9	6.2	2060	0.87	0.42	-54.95, -2.6	This study
Brazil-28	0.4	5.5	1.4	0.1	82.3	8.0	2.3	25.6	5.9	1570	0.93	0.97	-50, -12	This study
Chile-1	8.4	37.9	1.1	0.6	45.0	6.1	0.7	5.0	4.1	268	0.52	1.06	-72.8, -53.47	This study
Colombia-11	4.8	40.0	1.4	0.2	48.7	4.0	1.0	10.8	4.6	750	0.54	1.22	-77.37, 1.12	This study
Colombia-14	11.9	40.3	3.2	0.2	40.6	3.1	0.7	6.6	5.5	750	0.44	1.10	-77.37, 1.17	This study
Colombia-7	0.1	1.9	0.1	0.1	95.5	1.1	1.2	26.2	4.2	2900	0.98	1.92	-72.23, -0.47	This study
Colombia-9	0.1	1.5	0.1	0.1	96.9	0.8	0.6	26.2	3.8	2900	0.98	2.02	-72.22, -1.47	This study
Ecuador-19	9.8	30.7	11.5	1.8	28.9	11.8	5.5	12.7	6.6	2900	0.46	0.41	-78.72, -2.12	This study
Ecuador-3	10.0	45.6	3.0	0.7	33.8	4.0	3.0	8.4	5.6	1200	0.41	1.06	-78.63, -0.53	This study
Ecuador-7	0.2	4.6	0.5	0.1	89.6	3.7	1.3	26.2	4.6	2900	0.95	1.35	-76.83, -0.32	This study
Egypt-1	3.5	24.9	10.2	1.0	32.5	23.8	4.1	25.0	7.6	30	0.60	0.23	33.97, 28.53	This study
Peru-10	0.2	4.4	0.3	0.2	93.4	1.1	0.4	25.5	4.4	1350	0.95	1.86	-69.13, -12.68	This study
Peru-4	2.0	4.5	0.5	0.2	89.2	1.9	1.7	26.2	4.0	2900	0.93	1.60	-73.27, -3.85	This study
Peru-6	0.1	2.2	0.1	0.1	95.3	1.3	0.8	26.9	4.1	2104	0.97	1.83	-76.08, -5.77	This study
the Netherlands-A	4.1	42.1	16.9	1.0	23.3	11.8	0.9	9.0	6.7	720	0.36	0.36	4.75, 53.08	This study
the Netherlands-F	7.0	45.7	11.1	0.7	25.0	9.7	1.0	9.0	6.7	720	0.36	0.53	4.75, 53.08	This study
the Netherlands-J	4.3	43.4	15.8	0.9	23.4	11.5	0.8	9.0	6.4	720	0.36	0.39	4.75, 53.08	This study
the Netherlands-M	5.0	40.9	21.8	1.1	18.7	11.6	0.9	9.0	6.9	720	0.31	0.25	4.75, 53.08	This study
Uganda-1	2.3	26.0	0.5	0.5	68.8	1.0	0.9	12.0	3.6	1483	0.71	1.80	29.97, 0.35	This study
Uganda-2	42.4	40.5	0.5	0.5	15.8	0.1	0.1	2.0	5.1	1483	0.16	1.93	29.88, 0.38	This study
Uganda-3	1.6	17.9	12.8	1.0	33.6	27.2	5.8	24.0	7.1	1483	0.67	0.11	30.05, 0.83	This study
USA-BB1	4.1	30.5	0.6	0.3	62.2	2.0	0.4	6.1	4.3	1200	0.65	1.55	-68.1, 44.9	This study

USA-BB2	5.7	33.6	1.0	0.2	54.5	4.5	0.5	6.1	4.6	1200	0.59	1.20	-68.1, 44.9	This study
USA-BF1	3.9	31.6	0.6	0.3	60.4	2.5	0.6	7.8	4.1	1000	0.64	1.47	-80.1, 41.6	This study
USA-CA2	29.7	50.1	5.3	0.2	11.5	2.7	0.4	10.3	8.0	400	0.15	0.88	-111.7, 36.1	This study
USA-CF1	4.9	31.8	1.1	0.6	56.2	4.3	1.1	5.3	3.9	1300	0.62	1.21	-74.3, 42.2	This study
USA-CF2	2.4	27.1	0.6	0.4	66.5	1.8	1.1	5.3	3.6	1300	0.69	1.58	-74.4, 41.9	This study
USA-CF3	1.1	18.8	0.5	0.4	76.1	1.8	1.2	5.3	3.6	1300	0.79	1.60	-74.1, 42.1	This study
USA-CM1	9.2	24.5	17.6	0.9	19.1	24.2	4.6	18.5	7.9	850	0.48	0.02	-96.2, 33.3	This study
USA-GB2	42.6	32.0	14.3	0.4	7.0	3.4	0.3	2.0	7.6	400	0.11	0.34	-111.5, 39.3	This study
USA-GB4	14.8	56.2	5.5	0.9	18.9	3.1	0.5	2.0	6.9	400	0.23	0.94	-111.5, 39.3	This study
USA-GB6	28.9	44.2	9.7	0.8	12.1	3.7	0.5	2.0	7.2	400	0.16	0.62	-111.5, 39.3	This study
USA-HF2	2.4	29.1	0.4	0.2	66.7	0.9	0.4	7.0	4.0	1100	0.68	1.86	-72.2, 42.5	This study
USA-HI3	2.6	28.4	9.6	0.5	37.9	19.1	2.0	22.8	6.5	1000	0.59	0.36	-155.7, 20.1	This study
USA-IE2	5.2	34.4	2.3	0.1	51.1	5.6	1.3	8.6	5.5	1200	0.58	1.03	-73.47, 41.8	This study
USA-IE3	7.8	39.3	5.1	0.2	36.2	9.3	2.1	8.6	5.7	1200	0.48	0.72	-73.47, 41.8	This study
USA-IE4	3.8	31.4	14.2	1.1	28.0	19.0	2.6	8.6	6.3	1200	0.50	0.25	-73.47, 41.8	This study
USA-IE5	5.3	33.4	2.8	0.1	49.7	7.0	1.6	8.6	5.6	1200	0.58	0.93	-73.47, 41.8	This study
USA-IT1	7.7	41.9	3.8	0.3	40.1	5.8	0.5	3.0	5.8	750	0.46	0.93	-95.2, 47.2	This study
USA-IT2	7.2	41.7	1.9	0.1	45.1	3.8	0.2	3.0	5.4	750	0.49	1.18	-95.2, 47.2	This study
USA-KP1	5.1	30.7	6.0	0.2	42.1	13.0	2.8	12.5	6.4	835	0.58	0.58	-96.6, 39.1	This study
USA-MP1	19.6	44.8	1.4	0.2	32.9	1.0	0.1	8.8	4.6	2200	0.34	1.51	-123.5, 49.5	This study
USA-RT1	7.9	24.4	19.6	1.0	18.1	23.7	5.1	18.1	7.9	840	0.47	-0.01	-96.9, 31.5	This study
USA-RT2	8.3	24.3	19.7	1.1	18.6	23.3	4.7	18.1	8.1	840	0.47	0.00	-96.9, 31.5	This study
USA-SP2	14.7	46.9	0.9	0.4	35.1	1.6	0.4	3.6	5.1	750	0.37	1.51	-111.6, 36.6	This study
China-MG1645	10.5	28.7	20.2	1.4	19.8	16.6	2.8	11.5	7.5	-a	0.39	0.12	102.11, 29.61	Peterse et al., 2009c
China-MG1740	7.2	28.4	13.8	0.8	34.4	13.2	2.1	11.0	6.7	-	0.50	0.37	102.11, 29.62	Peterse et al., 2009c
China-MG1800	14.8	36.3	15.5	1.2	19.9	10.8	1.4	10.6	7.1	-	0.32	0.33	102.09, 29.61	Peterse et al., 2009c
China-MG1850	12.5	34.9	18.0	1.3	19.6	11.9	1.7	10.3	7.5	-	0.33	0.26	102.09, 29.61	Peterse et al., 2009c
China-MG1915	5.2	34.7	4.7	0.4	43.3	10.0	1.5	9.9	6.9	-	0.55	0.72	102.09, 29.61	Peterse et al., 2009c
China-MG1973	18.3	30.9	24.6	2.0	11.1	11.6	1.5	9.6	7.7	-	0.24	0.06	102.07, 29.60	Peterse et al., 2009c
China-MG2005	10.3	39.3	9.1	1.2	30.9	7.4	1.8	9.4	7.5	-	0.40	0.63	102.07, 29.60	Peterse et al., 2009c
China-MG2115	19.2	28.4	25.5	2.6	10.8	11.1	2.4	8.7	7.1	-	0.24	0.03	102.07, 29.60	Peterse et al., 2009c
China-MG2160	14.1	35.6	13.5	1.6	21.6	11.2	2.5	8.4	7.9	-	0.35	0.36	102.06, 29.60	Peterse et al., 2009c

China-MG2220	13.1	43.2	6.0	0.9	29.6	5.8	1.5	8.1	6.6	-	0.37	0.79	102.05, 29.60	Peterse et al., 2009c
China-MG2300	13.9	41.3	2.9	0.3	37.0	3.9	0.7	7.6	6.7	-	0.42	1.06	102.05, 29.60	Peterse et al., 2009c
China-MG2350	14.5	39.4	8.4	1.1	28.9	6.5	1.3	7.3	6.9	-	0.37	0.66	102.05, 29.60	Peterse et al., 2009c
China-MG2420	22.0	39.4	9.3	0.9	22.0	5.2	1.1	6.9	7.2	-	0.28	0.63	102.04, 29.59	Peterse et al., 2009c
China-MG2470	21.4	40.6	10.3	1.2	19.7	5.6	1.2	6.6	7.9	-	0.27	0.58	102.04, 29.59	Peterse et al., 2009c
China-MG2540	22.3	30.5	19.6	2.5	16.2	7.6	1.4	6.2	7.8	-	0.25	0.23	102.03, 29.59	Peterse et al., 2009c
China-MG2620	15.9	35.5	12.1	1.9	23.4	8.7	2.5	5.7	6.5	-	0.35	0.45	102.03, 29.59	Peterse et al., 2009c
China-MG2742	3.1	28.4	0.8	0.6	63.7	2.3	1.2	4.9	4.4	-	0.67	1.47	102.03, 29.59	Peterse et al., 2009c
China-MG2764	10.8	43.0	1.6	0.7	40.0	2.9	1.0	4.8	5.9	-	0.44	1.26	102.02, 29.58	Peterse et al., 2009c
China-MG2808	6.5	34.3	1.5	0.6	53.3	2.7	1.1	4.6	5.0	-	0.57	1.32	102.01, 29.58	Peterse et al., 2009c
China-MG2920	14.3	44.6	1.3	0.4	37.0	2.0	0.4	3.9	5.2	-	0.39	1.40	102.01, 29.58	Peterse et al., 2009c
China-MG2960	15.5	38.9	9.3	1.8	24.3	6.5	3.7	3.6	7.2	-	0.34	0.60	102.00, 29.58	Peterse et al., 2009c
China-MG3049	8.7	42.4	0.9	0.5	45.6	1.5	0.4	3.1	4.5	-	0.48	1.56	1012.0, 29.58	Peterse et al., 2009c
China-MG3065	18.0	46.3	4.2	0.5	29.0	1.8	0.2	3.0	6.4	-	0.31	1.10	101.99, 29.58	Peterse et al., 2009c
China-MG3119	12.8	46.0	1.6	0.5	37.0	1.8	0.3	2.7	5.6	-	0.39	1.38	101.99, 29.58	Peterse et al., 2009c
China-MG3145	27.4	40.0	10.0	1.2	18.4	2.6	0.5	2.5	7.3	-	0.21	0.67	101.99, 29.58	Peterse et al., 2009c
China-MG3188	13.0	42.5	1.1	0.3	41.0	2.0	0.3	2.3	5.3	-	0.43	1.44	101.99, 29.58	Peterse et al., 2009c
China-MG3518	9.7	44.7	0.9	0.4	42.1	1.8	0.3	0.3	4.4	-	0.44	1.50	101.97, 29.55	Peterse et al., 2009c
China-MG3819	17.3	43.2	0.9	0.3	36.3	1.7	0.3	-1.5	5.0	-	0.38	1.48	101.96, 29.55	Peterse et al., 2009c
France-TES01	12.1	44.3	1.3	0.2	38.3	2.4	1.5	4.0	4.9	1009	0.42	1.34	1.98, 42.56	Kim et al., 2010b
France-TES011	19.3	42.6	9.7	1.2	20.8	5.1	1.3	12.9	6.8	556	0.27	0.63	2.39, 42.56	Kim et al., 2010b
France-TES012	24.7	41.9	6.8	1.0	19.1	5.4	1.3	11.7	6.6	719	0.26	0.70	2.34, 42.53	Kim et al., 2010b
France-TES013	9.7	39.1	16.6	1.7	18.9	11.9	2.2	12.8	6.3	568	0.33	0.31	2.38, 42.57	Kim et al., 2010b
France-TES016	12.9	45.8	7.5	1.2	22.8	7.5	2.3	11.5	6.4	770	0.33	0.66	2.30, 42.64	Kim et al., 2010b
France-TES018	13.5	45.8	1.3	0.9	36.0	1.9	0.5	10.1	5.5	959	0.38	1.40	2.27, 42.68	Kim et al., 2010b
France-TES02	17.1	46.2	1.4	0.6	31.9	2.1	0.7	3.9	4.7	1053	0.35	1.35	1.98, 42.57	Kim et al., 2010b
France-TES020	11.2	45.3	11.4	1.4	20.6	8.4	1.7	13.6	7.3	618	0.31	0.52	2.56, 42.66	Kim et al., 2010b
France-TES022	18.4	42.3	11.4	1.1	17.8	7.6	1.4	14.3	7.5	637	0.27	0.50	2.61, 42.67	Kim et al., 2010b
France-TES023	16.4	46.4	10.1	0.9	20.0	5.4	0.9	14.3	7.3	637	0.26	0.63	2.61, 42.67	Kim et al., 2010b
France-TES03	10.5	45.8	1.7	0.7	37.9	2.7	0.7	3.6	4.7	1052	0.41	1.28	1.97, 42.57	Kim et al., 2010b
France-TES031	19.6	31.9	17.3	0.6	16.6	13.5	0.6	15.3	7.5	634	0.31	0.20	2.79, 42.69	Kim et al., 2010b
France-TES032	8.0	49.0	1.3	0.9	36.9	3.1	0.8	15.3	6.8	634	0.41	1.29	2.79, 42.69	Kim et al., 2010b

Sample name	IIIa	IIa	IIb	IIc	Ia	Ib	Ic	MAT (°C)	soil pH	MAP(mm)	MBT'	CBT	Coordinates (X,Y)	Study
France-TESO33	4.0	35.6	2.5	0.7	51.3	4.1	1.8	15.3	7.8	638	0.57	1.11	2.79 , 42.69	Kim et al., 2010b
France-TESO34	14.1	32.6	24.1	2.8	11.3	12.0	3.1	15.3	8.1	617	0.26	0.09	2.82, 42.69	Kim et al., 2010b
France-TESO36	5.7	30.2	18.0	2.0	26.4	14.8	2.9	15.4	7.5	577	0.44	0.24	3.04, 42.71	Kim et al., 2010b
France-TESO4	17.2	47.5	0.7	0.2	33.4	0.8	0.1	3.6	4.1	1052	0.34	1.71	1.97, 42.57	Kim et al., 2010b
France-TESO43	7.4	49.9	12.0	0.8	21.9	7.1	0.9	15.2	6.9	605	0.30	0.57	2.98, 42.71	Kim et al., 2010b
France-TESO43B	13.0	43.7	12.8	1.2	21.5	6.6	1.1	15.2	7.5	605	0.29	0.53	2.98, 42.71	Kim et al., 2010b
France-TESO44	32.7	32.7	17.4	1.3	9.6	5.6	0.7	8.6	8.1	587	0.16	0.26	2.24, 42.53	Kim et al., 2010b
France-TESO45	21.2	44.2	8.0	1.0	18.3	6.0	1.3	8.5	7.0	613	0.26	0.65	2.22, 42.52	Kim et al., 2010b
France-TESO47	16.0	37.0	16.9	1.3	16.3	10.8	1.7	10.5	7.0	549	0.29	0.28	2.31, 42.56	Kim et al., 2010b
France-TESO48	12.6	43.0	1.3	0.7	37.8	3.0	1.7	6.4	4.6	728	0.42	1.27	2.08, 42.53	Kim et al., 2010b
France-TESO49	10.2	46.8	1.6	0.8	37.4	2.4	0.8	7.7	4.8	790	0.41	1.32	2.11, 42.51	Kim et al., 2010b
France-TESO5	12.0	39.4	2.2	1.1	40.2	4.6	0.7	3.6	4.2	1098	0.45	1.07	1.97, 42.57	Kim et al., 2010b
France-TESO50	16.7	45.1	7.3	1.1	21.9	6.2	1.6	8.2	6.7	671	0.30	0.69	2.18, 42.51	Kim et al., 2010b
France-TESO6	14.1	49.3	1.5	0.3	32.4	1.7	0.7	4.6	4.9	1054	0.35	1.40	1.99, 42.57	Kim et al., 2010b
France-TESO7	11.5	28.6	25.4	2.5	14.7	14.2	3.2	12.6	7.5	553	0.32	0.04	2.32, 42.57	Kim et al., 2010b
Svalbard-MP1	13.2	53.3	3.8	0.4	27.2	2.0	0.2	-6.0	7.1	190	0.29	1.14	11.17, 79.18	Peterse et al., 2009a
Svalbard-MP2	32.4	39.4	12.5	0.6	11.0	3.7	0.4	-6.0	8.3	190	0.15	0.49	11.2, 79.18	Peterse et al., 2009a
Svalbard-MP3	12.8	55.6	2.0	0.5	27.7	0.9	0.4	-6.0	5.5	190	0.29	1.46	11.27, 79.2	Peterse et al., 2009a
Svalbard-MP4	25.9	41.2	17.9	1.2	9.5	3.8	0.5	-6.0	8.3	190	0.14	0.37	11.3, 79.2	Peterse et al., 2009a
Svalbard-MP5	29.9	37.2	16.7	1.2	10.0	4.4	0.6	-6.0	8.3	190	0.15	0.35	11.32, 79.2	Peterse et al., 2009a
Svalbard-MP6	34.5	36.3	12.9	1.6	10.3	3.9	0.6	-6.0	9.3	190	0.15	0.44	11.32, 79.2	Peterse et al., 2009a

other soils not included in the calibration set

Sample name	IIIa	IIa	IIb	IIc	Ia	Ib	Ic	MAT (°C)	soil pH	MAP(mm)	MBT'	CBT	Coordinates (X,Y)	Study
Brazil-3	0.2	3.7	0.2	0	93.1	1.6	1.2	22.8	5.1	1177	0.96	1.74	-42.8, -21.13	Weijers et al., 2007c
China-19	0.3	4.3	0.1	0	92.9	1.8	0.7	22.4	4.6	2006	0.95	1.71	109.5, 18.9	Weijers et al., 2007c
China-7	0.5	4.0	0.4	0	93.7	0.6	0.8	21.9	4.9	1679	0.95	1.99	113.47, 23.38	Weijers et al., 2007c
Finland-2	2.4	28.1	0.2	0	68.6	0.5	0.3	3.9	3.7	547	0.69	2.15	34.1, 61.24	Weijers et al., 2007c
Finland-4	2.0	25.2	0.7	0	70.2	1.2	0.6	3.9	4.3	547	0.72	1.69	23.0, 62.11	Weijers et al., 2007c
Finland-P	5.0	40.4	0.4	0	54.2	0	0	1.1	3.9	525	0.54	2.41	24.7, 66.7	Weijers et al., 2007c
Gabon-3	0.1	1.3	0	0	97.6	0.4	0.6	24.1	4.7	2007	0.99	2.44	13.58, -1.68	Weijers et al., 2007c
Gabon-4	0.2	4.1	0	0	91.7	3.0	1.0	25.8	5.3	2158	0.96	1.50	11.53, -2.22	Weijers et al., 2007c
Gabon-5	0	1.9	0	0	97.2	0.4	0.5	26.3	5.1	2158	0.98	2.45	11.52, -0.38	Weijers et al., 2007c

Sample														Reference
Ghana-2	0	2.4	0.3	0	93.2	2.7	1.4	27.0	6.0	810.0	0.97	1.50	0, 5	Weijers et al., 2007c
Nigeria-15	0	1.0	0	0	97.4	0.5	1.1	26.7	4.4	2811	0.99	2.29	6.63, 5.3	Weijers et al., 2007c
Seychelles	0.1	1.5	0.1	0	96.0	0.6	1.7	26.6	5.2	235	0.98	2.17	55.31, -4.67	Weijers et al., 2007c
South Africa-16	1.1	15.0	1.0	0	77.6	4.1	1.3	19.9	6.0	759	0.83	1.26	30.38, -29.67	Weijers et al., 2007c
South Africa-7	0.9	6.9	0	0	90.6	0.8	0.8	18.0	5.5	1015	0.92	2.09	30.68, -29.78	Weijers et al., 2007c
Spain-7	6.6	53.1	0	0	40.3	0	0	16.4	5.4	486	0.40	n.c.	-6.33, 38.98	Weijers et al., 2007c
Spitsbergen-S	33.0	47.9	0	0	19.2	0	0	-6.7	8.0	197	0.19	n.c.	15.83, 78.33	Weijers et al., 2007c
Turkey-8	55.2	24.4	0	0	20.4	0	0	10.5	4.1	340	0.20	n.c.	33.57, 37.73	Weijers et al., 2007c
Zaire-2	0.1	2.4	0	0.2	94.1	1.8	1.2	24.6	3.9	1871	0.97	1.72	24.43, 0.77	Weijers et al., 2007c
Brazil-13	0.2	4.1	0.1	0	92.5	1.7	1.4	24.9	4.0		0.96	1.72	-54.93, -2.9	This study
Brazil-14	0.5	8.8	0.3	0	90.0	0.3	0.2	21.2	4.4		0.90	2.24	-47.7, -15.6	This study
Chile-2	7.1	38.3	0.2	0	53.9	0.3	0.1	5.0	4.0	268	0.54	2.21	-72.8, -53.47	This study
Colombia-10	0	0.5	0.1	0	97.6	0.9	1.0	26.2	4.8	2900	1.00	1.97	-72.22, -0.45	This study
Colombia-12	0.9	13.4	0.5	0	81.7	2.9	0.6	13.8	4.9		0.85	1.45	-77.33, 1.33	This study
Ecuador-6	0.3	6.2	0.5	0	86.6	5.3	1.1	26.2	-	2900	0.93	1.21	-76.93, -0.52	This study
Egypt-2	38.6	31.8	7.9	0	14.4	5.7	1.6	25.0	4.5	30	0.22	0.53	33.97, 28.53	This study
Peru-1	0	0.4	0.1	0	94.5	1.0	4.0	26.2	4.9	2900	1.00	1.94	-73.32, -3.82	This study
Peru-12	0.3	5.1	0.9	0	80.7	11.2	1.8	26.2	-	2900	0.94	0.85	-73.27, -4.04	This study
Peru-13	0	0.3	0	0	91.7	2.8	5.1	26.2	-	2900	1.00	1.51	-73.37, -3.92	This study
Peru-14	0.2	1.3	0.2	0.1	94.2	2.4	1.5	26.2	-	2900	0.98	1.56	-73.37, -3.92	This study
Portugal-1	7.4	42.4	0	0	50.2	0	0	15.0	7.5	950	0.50	n.c.	-8.6, 40.2	This study
USA-BP1	21.8	42.2	11.8	0	16.9	6.7	0.6	6.6	5.2	450	0.24	0.50	-102.4, 43.8	This study
USA-BZ2	16.1	50.2	0.9	0.3	31.9	0.5	0	-2.9	5.4	260	0.32	1.76	-148.3, 64.8	This study
USA-BZ3	14.4	44.8	0.6	0.1	39.3	0.8	0	-2.9	7.3	260	0.40	1.78	-148.3, 64.8	This study
USA-CA1	16.7	58.0	6.8	0	14.3	3.6	0.6	10.3	6.1	400	0.19	0.84	-111.8, 36.1	This study
USA-CC1	3.6	29.0	2.3	0	57.7	7.0	0.4	5.8	5.7	720	0.65	0.97	-93.2, 45.4	This study
USA-CL1	2.9	21.5	2.3	0	66.6	6.2	0.6	15.9	5.6	1250	0.73	1.02	-87.7, 34.6	This study
USA-CL2	1.3	21.0	1.6	0	70.2	5.5	0.5	15.9	4.9	1250	0.76	1.11	-87.7, 34.6	This study
USA-CL3	2.2	18.5	0.9	0	75.7	2.2	0.5	15.9	6.1	1250	0.78	1.48	-87.7, 34.6	This study
USA-CO1	22.2	50.9	2.9	0	22.2	1.6	0.3	-3.0	5.7	600	0.24	1.21	-105.7, 40.4	This study
USA-CO2	15.6	48.2	5.2	0	29.3	1.6	0	6.1	6.0	350	0.31	1.05	-105.3, 40.6	This study
USA-CO3	10.7	47.7	2.5	0	35.7	3.4	0	9.3	6.0	322	0.39	1.16	-104.8, 40.8	This study

Sample													
USA-DF1	3.2	22.6	0	0	71.7	2.2	0.4	14.6	5.4	1100	0.74	1.64	-78.1, 36	This study
USA-DF3	2.2	22.0	0	0	73.8	1.7	0.3	14.6	5.1	1100	0.76	1.74	-78.1, 36	This study
USA-GB3	24.4	46.3	8.8	0	16.3	4.2	0	2.0	7.2	400	0.20	0.68	-111.5, 39.3	This study
USA-GB5	56.0	35.6	0	0	8.4	0	0	4.8	8.2	400	0.08	n.c.	-111.5, 39.3	This study
USA-HJ1	11.3	43.4	1.0	0	42.6	1.8	0	9.4	5.4	2000	0.44	1.49	-122.2, 44.2	This study
USA-KP2	2.4	29.7	3.5	0	51.9	10.4	2.1	12.5	6.5	835	0.64	0.77	-96.6, 39.1	This study
USA-LQ2	0.2	5.5	0	0	90.4	1.0	2.9	21.5	5.0	3500	0.94	1.97	-65.8, 18.3	This study
USA-MD3	20.3	47.0	4.3	0	24.9	3.0	0.6	21.0	7.9	150	0.28	1.00	-115.9, 35.2	This study
USA-MD4	21.4	62.7	0	0	15.2	0.6	0	21.0	8.9	150	0.16	2.11	-115.9, 35.2	This study
USA-MP2	20.5	43.3	0.8	0.1	34.5	0.8	0	8.8	4.4	2200	0.35	1.71	-123.5, 49.5	This study
USA-SA1	25.2	48.3	2.6	0	22.0	1.9	0	10.3	6.9	400	0.24	1.20	-111.6, 35.4	This study
USA-SB1	31.5	53.7	2.3	0	11.1	1.3	0	15.0	7.9	550	0.12	1.25	-119.8, 34.5	This study
USA-SN1	20.5	40.6	18.1	0	20.8	0	0	3.6	5.0	600	0.21	0.53	-118.2, 36.5	This study
USA-SN3	15.0	43.4	0	0	40.6	1.0	0	3.6	5.7	600	0.42	1.94	-118.2, 36.5	This study
USA-SP1	15.3	47.4	3.0	0	30.7	3.4	0.3	12.7	6.3	650	0.34	1.09	-118.7, 36.5	This study
USA-SR1	15.2	57.5	4.0	0	21.0	2.3	0	17.2	6.8	500	0.23	1.10	-120.1, 34.7	This study
Usa-SR2	42.1	40.4	6.2	0	8.7	2.6	0	17.2	8.0	500	0.11	0.75	-120.1, 34.7	This study
USA-SR3	30.8	51.4	2.4	0	13.7	1.7	0	17.2	7.0	500	0.15	1.21	-120.1, 34.7	This study
USA-SV1	32.3	54.1	2.0	0	10.7	0.9	0	13.5	8.3	210	0.12	1.36	-106.7, 34.3	This study
USA-SV2	26.6	54.2	2.6	0	15.2	1.4	0	13.5	8.4	210	0.17	1.24	-106.7, 34.3	This study
USA-SV3	35.3	40.1	8.5	0	12.6	3.5	0	13.5	8.3	210	0.16	0.64	-106.7, 34.3	This study
USA-SV4	24.5	49.8	1.8	0	22.5	1.4	0	13.5	8.3	210	0.24	1.35	-106.7, 34.3	This study
USA-VC1	8.5	50.9	2.0	0	36.7	1.9	0	2.5	5.6	500	0.39	1.35	-106.6, 35.9	This study
USA-VC2	11.6	49.1	2.1	0	35.4	1.7	0	2.5	6.0	500	0.37	1.34	-106.6, 35.9	This study
China-MG1180	9.7	40.2	7.1	0	35.7	7.4	0	14.3	7.9	-	0.43	0.72	102.17, 29.62	Peterse et al., 2009c
China-MG1220	3.3	24.6	6.3	0	52.0	12.4	1.4	14.1	7.3	-	0.66	0.61	102.17, 29.6	Peterse et al., 2009c
China-MG1515	1.7	15.1	0	0	83.2	0	0	12.3	6.4	-	0.83	n.c.	102.13, 29.63	Peterse et al., 2009c
China-MG1610	18.3	44.3	12.8	0	24.7	0	0	11.7	7.8	-	0.25	0.73	102.12, 29.65	Peterse et al., 2009c
China-MG3140	4.3	37.7	0.6	0	55.7	1.5	0.3	2.6	4.9	-	0.57	1.65	101.98, 29.57	Peterse et al., 2009c
China-MG3209	24.3	41.7	1.1	0	31.3	1.5	0	2.1	5.0	-	0.33	1.44	101.98, 29.57	Peterse et al., 2009c
China-MG3676	20.7	42.1	1.6	0	34.4	1.2	0	-0.7	6.6	-	0.36	1.43	101.97, 29.55	Peterse et al., 2009c
China-MG3769	17.1	45.3	0.8	0	35.5	1.3	0	-1.2	6.3	-	0.37	1.59	101.97, 29.55	Peterse et al., 2009c

Sample												Coordinates	Reference
France-TESO10	28.4	42.4	4.2	0	20.0	3.7	1.2	8.4	6.5	758	0.25	0.90	2.35, 42.49	Kim et al., 2010b
France-TESO14	26.8	43.6	7.8	0	16.9	4.9	0	12.8	7.7	552	0.22	0.68	2.37, 42.58	Kim et al., 2010b
France-TESO14B	24.7	42.5	15.7	0	16.4	0.8	0	12.8	7.8	552	0.17	0.55	2.37, 42.58	Kim et al., 2010b
France-TESO15	24.2	42.8	8.1	0	19.5	5.4	0	11.5	6.4	770	0.25	0.66	2.49, 42.65	Kim et al., 2010b
France-TESO17	28.8	51.1	0	0	20.1	0	0	13.8	8.4	599	0.20	n.c.	2.402, 42.61	Kim et al., 2010b
France-TESO19	20.3	39.9	16.4	0	15.2	8.2	0	14.2	7.9	633	0.23	0.35	2.61, 42.67	Kim et al., 2010b
France-TESO22B	16.6	39.2	15.8	0	17.9	10.4	0	14.3	8.5	637	0.28	0.34	2.609, 42.67	Kim et al., 2010b
France-TESO24	22.9	43.9	9.8	0	18.6	4.8	0	14.6	7.8	648	0.23	0.63	2.67, 42.70	Kim et al., 2010b
France-TESO25	18.1	40.7	14.5	0	19.1	7.5	0	14.5	7.9	646	0.27	0.43	2.68, 42.71	Kim et al., 2010b
France-TESO26	15.3	38.2	16.8	0	16.7	10.9	2.1	14.9	7.3	648	0.30	0.30	2.70, 42.69	Kim et al., 2010b
France-TESO27	5.0	49.5	0	0	45.6	0	0	14.1	6.8	636	0.46	n.c.	2.61, 42.69	Kim et al., 2010b
France-TESO28	18.0	38.4	15.2	0	18.5	10.0	0	13.5	8.4	633	0.28	0.35	2.61, 42.70	Kim et al., 2010b
France-TESO29	29.0	40.5	7.1	0	17.8	5.6	0	14.1	7.7	633	0.23	0.66	2.61, 42.68	Kim et al., 2010b
France-TESO30	11.4	46.8	4.7	0	30.2	6.9	0	14.3	7.4	637	0.37	0.82	2.61, 42.67	Kim et al., 2010b
France-TESO35	14.7	43.3	11.7	0	23.3	7.0	0	15.4	8.9	577	0.30	0.55	3.04, 42.71	Kim et al., 2010b
France-TESO36B	18.5	40.3	14.4	0	19.4	7.4	0	15.4	8.8	577	0.27	0.44	3.04, 42.71	Kim et al., 2010b
France-TESO37	4.7	53.2	2.1	0	37.8	2.1	0	15.3	6.4	590	0.40	1.33	2.80, 42.72	Kim et al., 2010b
France-TESO38	12.5	31.5	14.8	0	24.6	16.6	0	15.0	7.3	619	0.41	0.25	2.75, 42.72	Kim et al., 2010b
France-TESO39	16.2	40.6	15.3	0	20.9	7.1	0	15.2	7.5	619	0.28	0.44	2.77, 42.71	Kim et al., 2010b
France-TESO40	9.6	35.4	23.9	0	17.7	13.3	0	15.1	7.8	611	0.31	0.15	2.76, 42.72	Kim et al., 2010b
France-TESO41	18.1	44.5	10.5	0	21.1	5.8	0	15.3	7.6	555	0.27	0.61	2.89, 42.70	Kim et al., 2010b
France-TESO42	6.9	35.9	2.5	0	48.6	4.4	1.6	15.3	7.7	611	0.55	1.08	2.99, 42.71	Kim et al., 2010b
France-TESO46	18.9	42.8	16.8	0	14.5	7.0	0	11.3	8.1	543	0.21	0.38	2.32, 42.55	Kim et al., 2010b
France-TESO51	27.1	41.2	8.1	0	17.0	5.4	1.3	8.5	6.9	613	0.24	0.64	2.22, 42.52	Kim et al., 2010b
France-TESO8	8.2	47.4	0	0	42.3	2.1	0	9.2	5.4	574	0.44	1.63	2.27, 42.54	Kim et al., 2010b
France-TESO9	13.2	38.2	15.4	0	22.1	11.1	0	9.2	8.1	574	0.33	0.36	2.27, 42.53	Kim et al., 2010b
Svalbard-LB1	14.2	57.6	6.1	0	19.0	3.2	0.0	-6.0	4.4	190	0.22	0.92	15.6, 78.22	Peterse et al., 2009a
Svalbard-NA1	36.7	41.3	8.0	0	11.3	2.7	0	-6.0	7.4	190	0.14	0.69	11.93, 78.92	Peterse et al., 2009a
Svalbard-NA2	14.4	56.5	1.4	0.4	26.2	1.0	0	-6.0	6.3	190	0.27	1.54	11.92, 78.93	Peterse et al., 2009a

[a] Data not available.
n.c. Could not be calculated.

Chapter 9

Decoupled warming and monsoon precipitation in East Asia over the last deglaciation

Francien Peterse, Maarten A. Prins, Christiaan J. Beets, Simon R. Troelstra, Hongbo Zheng, Zhaoyan Gu, Stefan Schouten, Jaap S. Sinninghe Damsté, 2011. *Earth and Planetary Science Letters* 301, 256-264.

Abstract

Our understanding of the continental climate development in East Asia is mainly based on loess–paleosol sequences and summer monsoon precipitation reconstructions based on oxygen isotopes ($\delta^{18}O$) of stalagmites from several Chinese caves. Based on these records, it is thought that East Asian Summer Monsoon (EASM) precipitation generally follows Northern Hemisphere (NH) summer insolation. However, not much is known about the magnitude and timing of deglacial warming on the East Asian continent. In this study we reconstruct continental air temperatures for central China covering the last 34,000 yr, based on the distribution of fossil branched tetraether membrane lipids of soil bacteria in a loess–paleosol sequence from the Mangshan loess plateau. The results indicate that air temperature varied in phase with NH summer insolation, and that the onset of deglacial warming at ~19 kyr BP is parallel in timing with other continental records from e.g. Antarctica, southern Africa and South-America. The air temperature increased from ~15 °C at the onset of the warming to a maximum of ~27 °C in the early Holocene (~12 kyr BP), in agreement with the temperature increase inferred from e.g. pollen and phytolith data, and permafrost limits in central China. Comparison of the tetraether membrane lipid-derived temperature record with loess–paleosol proxy records and stalagmite $\delta^{18}O$ records shows that the strengthening of EASM precipitation lagged that of deglacial warming by ca. 3 kyr. Moreover, intense soil formation in the loess deposits, caused by substantial increases in summer monsoon precipitation, only started around 12 kyr BP (ca. 7 kyr lag). Our results thus show that the intensification of EASM precipitation unambiguously lagged deglacial warming and NH summer insolation, and may contribute to a better understanding of the mechanisms controlling ice age terminations.

9.1. Introduction

Oxygen isotope (δ^{18}O) records of stalagmites from several caves in China have yieldedwell dated, high-resolution records of the timing and amplitude of changes in East Asian Summer Monsoon (EASM) precipitation during the last four glacial–interglacial cycles (e.g. Cheng et al., 2009; Dykoski et al., 2005; Wang et al., 2001, 2008; Yuan et al., 2004). Generally, these records revealed that the EASM follows Northern Hemisphere (NH) insolation patterns. Similarly, various climate-proxy records derived from loess–paleosol sequences from the Chinese Loess Plateau have also documented changes in EASM precipitation (e.g. An, 2000; Heslop et al., 1999; Porter and An, 1995; Sun and Huang, 2006; Wu et al., 2002). The build-up of the loess plateau relates to changes in monsoon intensity, varying temperature and moisture conditions; loess is mainly deposited during cool and dry periods, as a result of an intensified winter monsoon, whereas soil formation takes place predominantly during the warmer and wetter periods with strengthened summer monsoon (Porter and An, 1995). The loess–paleosol records, as well as the stalagmite proxy records match the climatic changes in the North Atlantic that are recorded in Greenland ice-core records (Chen et al., 1997; Porter and An, 1995).

Although a large number of speleothem and loess records documenting EASM intensity have been generated, only little is known on the development of atmospheric temperature over the East Asian conti-nent in relation to changes in monsoon precipitation intensity. Soil formation in loess sequences, caused by a substantial increase in summer monsoon precipitation, has been found to lag NH insolation (Heslop et al., 1999; Porter, 2001; Stevens et al., 2007). However, soil formation is not only stimulated by intensified sum-mer monsoon precipitation, but by higher temperatures as well (Jenny, 1941).

To gain more insight into the exact timing and amplitude of eastern Asian continental temperature changes over the last glacial termination, we used the recently developed MBT-CBT (methylation of branched tetraethers/cyclisation of branched tetraethers) paleothermometer, based on branched glycerol dialkyl glycerol tetraethers (GDGTs) (Weijers et al., 2007c), in a loess–paleosol sequence of the Mangshan loess plateau (*Fig. 9.1*) to reconstruct a continuous temperature record for this area. Branched GDGTs are membrane lipids from bacteria that occur ubiquitously in soils and peat (Weijers et al., 2006b, 2007c), and air temperatures can be reconstructed based on their distribution using the Methylation index of Branched Tetraethers (MBT) and the Cyclisation ratio of Branched Tetraethers (CBT) (Weijers et al., 2007c). The MBT-CBT proxy works well in geothermally heated soils (Peterse et al., 2009b) and branched GDGT distributions have been shown to reflect the adiabatic cooling of air along altitude gradients (Hren et al., 2010; Peterse et al., 2009c; Sinninghe Damsté et al., 2008). Also,when applied to marine surface sediments, branched GDGT-derived temperatures show good agreement with the annual mean air temperature of the adjacent river drainage basins (Rueda et al., 2009;Weijers et al., 2007a).

The paleosol–loess sequence from the Mangshan loess plateau investigated here mainly receives its sediment from the nearby Huang He floodplain (Yellow River), which has a relatively humid climate compared to the Central Loess Plateau. The availablemoisture enhances soil formation, and values of the branched and isoprenoid tetraether (BIT) index, that quantifies the content of soil-derived organicmat-ter in a system, are therefore high for these soils (typically > 0.8; Hopmans et al., 2004). This makes the sequence suitable for the application of the MBT-CBT proxy. This area is also ideal for a high-resolution reconstruction, as sedimentation rates are generally high (17 to 29 cm/kyr during the last 34 kyr; Prins et al., 2009; Zheng et al., 2007).
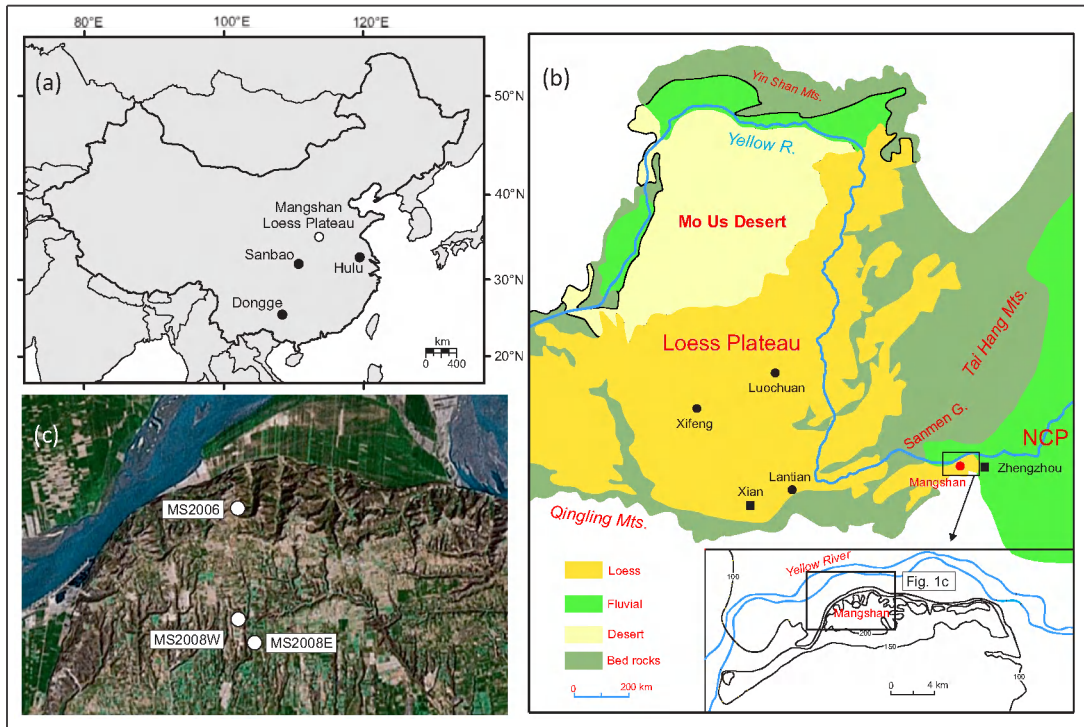
Fig. 9.1. Overview map showing a) China with the locations of the Mangshan Loess Plateau (white dot) and the Hulu, Sanbao, and Dongge caves (black dots), b) the Chinese Loess Plateau, the Mo Us Desert and the North China Plain (NCP), and c) the studied Mangshan loess sections. A blow up of the insert in b) is shown in c), and modified from Prins et al. (*2009*).

9.2. Material and methods

9.2.1. Sites and sampling

The Mangshan loess plateau lies 25 km west of Zhengzhou on the south bank of the Huang He (*Fig. 9.1*). The loess plateau is about 18 km in length (W–E) and 5 km in width (N–S), with its highest point reaching approximately 150 m above the Huang He floodplain. The Mangshan plateau receives ~645 mm precipitation per year, about 70% of which falls during the summer monsoon season (May–September). The air temperature is ~2 °C during the winter (December–February) and varies between 20 °C (May) and 27 °C (July) during the summer monsoon season. The mean annual air temperature is 15 °C (WMO, 2007). For this study, the upper part of the loess-pedogenic complex, covering the S0 (Holocene paleosol), L1 (last glacial loess deposit), and S1 (last interglacial paleosol) layers, has been sampled at two locations. The northern loess section, MS2006 (34°57.5'N, 113°22.2'E; *Fig. 9.1c*), is exposed on the northern slope of the Mangshan plateau, where the Huang He river and local gullies have cut through the loess, forming a valley with steep cliffs. The section is ~59 m thick and was continuously sampled in 36 partly-overlapping, freshly-dug, vertical trenches at a 5-cm resolution (Prins et al., 2009). At a southern location, two sections have been sampled, MS2008W (34°56.4'N, 113°22.2'E) and MS2008E (34°56.1'N, 113°22.4'E; *Fig. 9.1c*). Sections MS2008W and MS2008E are ~34 and ~14 m thick, respectively, and were sampled in total in 26 partly-overlapping vertical trenches at a 10-cm resolution. From field observations it is clear that the top part of the MS2008W section (0 to 45 cm) is disturbed by ploughing, as also evidenced by grain size data.

9.2.2. Magnetic susceptibility, organic matter and carbonate analysis

Samples were oven dried at 50 °C, lightly ground and aliquots of ~8 g were analyzed using a Bartington MS2 magnetic susceptibility meter at the School of Ocean and Earth Sciences, Tongji University. The organic matter and carbonate content of the samples were analyzed using a Leco TGA 601 at the VU University Amsterdam. Aliquots of ~2 g of the samples prepared for magnetic susceptibility analysis were used for thermo-gravimetric analysis (TGA).

9.2.3. Grain size analysis

Prior to the grain size measurement the samples were prepared according to the methods described by Konert and Vandenberghe (1997). Briefly, about 1–2 g of bulk sediment was pre-treated with solutions of 30% H_2O_2 and 1 N HCl in deinonized water to remove organicmatter and carbonates, respectively. In case of a violent reaction, additional aliquots of H_2O_2 and/or HCl solution were added to ensure complete removal of organic matter and/or carbonates. Consequently, the results reflect the grain size distribution of the siliciclastic loess fraction. All measurements were performed on a Fritsch Analysette 22 laser particle sizer at the VU University Amsterdam. The variation in mean grain size for this particular instrument has been shown to be < 0.5% (Jonkers et al., 2009). Grain size distributions were reported with 56 size classes between 0.15 and 2000 µm.

9.2.4. MBT-CBT analysis

Branched GDGTs were analyzed in the upper 5.9 m of section MS2008E and the upper 4.8 m of section MS2008W, using high performance liquid chromatography/atmospheric pressure chemical ionization-mass spectrometry (HPLC/APCI-MS) as described by Schouten et al. (2007a), with minor modifications in the instrument settings, as mentioned below. The loess samples from the MS2008W sequence were freeze-dried. All loess samples from MS2008W and MS2008E were then homogenized with a mortar and pestle, and extracted (3×5 min) with a dichloromethane (DCM):methanol (9:1, v/v) mixture using an accelerated solvent extractor (ASE 200, Dionex) at 100 °C and 7.6×10^6 Pa. The total extracts were dried using a rotary evaporator under near vacuum, then dissolved in DCM and passed over a $NaSO_4$ column to remove any remaining water. Known amounts of an internal C_{46} GDGT standard were added according to Huguet et al. (2006). Separation of the extracts in apolar and polar fractions was done by passing them over an activated Al_2O_3 column using hexane:DCM (9:1, v/v) and DCM:MeOH (1:1, v/v), respectively. The polar fraction (containing the branched GDGTs and the internal standard) was dried under N_2, ultrasonically dissolved in hexane:isopropanol (99:1, v/v) and filtered over a 0.45 µm PTFE filter. The polar fractions were concentrated to about 3 mg/ml prior to analysis by HPLC/APCI-MS on an Agilent 1100 series LC/MSD SL. Separation of the branched GDGTs was achieved on an Alltech Prevail Cyano column (150 mm×2.1 mm; 3 µm). The compounds were eluted isocratically with 90% A and 10% B for 5 min (flow rate 0.2 ml/min), and then with a linear gradient to 16% B for 34 min, where A=hexane and B=hexane:isopropanol (9:1, v/v). The injection volume was 10 µl for each sample. Selective ion monitoring of the [M+H]+ of the different GDGTs was used to detect and quantify them. Absolute quantification was achieved by calculating the area of the corresponding peaks in the chromatograms, comparing them with the peak area of the internal standard, and correcting themfor the different response factors (cf. Huguet et al., 2006).

Air temperatures were calculated based on the MBT and CBT indices and the following transfer func-

tion as defined by Weijers et al. (2007c):

$$MBT = 0.122 + 0.187 \times CBT + 0.020 \times MAT \qquad (r^2 = 0.77) \qquad (9.1)$$

The average analytical reproducibility of the MBT and CBT indices, based on duplicate injections of a selected set of loess samples on the HPLC/APCI-MS, is 0.003 for the MBT index and 0.004 for the CBT index, resulting in an analytical error in temperature estimates of ca. 0.2 °C. The error introduced due to scatter in the calibration of Eq. 9.1 is much larger, ca. 5 °C (Weijers et al., 2007b), however, this uncertainty can be considered mainly systematic, and is caused by the global spread of the soils in the calibration set and the accompanying variation in environmental parameters. When the proxy is applied on a relatively small scale, like here on the Mangshan plateau, this systematic error is likely to be much smaller. However, an exact estimate of the error is difficult to constrain, given that a local calibration of the MBT-CBT proxy is not available. Nevertheless, absolute temperature estimates should be interpreted with caution.

9.3. Results and discussion

9.3.1. Age model

The age model of the Mangshan loess–paleosol sequences is based on the correlation of loess proxy records, i.e. magnetic susceptibility, carbonate content and grain size characteristics, with the U–^{230}Th dated oxygen isotope records from Dongge, Sanbao and Hulu caves in central China (*Fig. 9.1a*). The EASM δ^{18}O record is dominated by 23,000-year long cycles that are synchronous (within dating errors) with summer insolation at 65°N (Berger, 1978), and the cycles are punctuated by millennial-scale strong summer monsoon events (Chinese interstadials; Cheng et al., 2006) and weak summer monsoon events (correlative with North Atlantic cold events, i.e. the Heinrich events; Wang et al., 2001). The ages of these events are exceptionally well constrained and may thus, as suggested by Wang et al. (2008), serve as benchmarks for correlating and calibrating climate records. The assumed match between the East Asian monsoon proxy records from the Mangshan loess–paleosol sequences and the Chinese speleothem records is independently supported by radiocarbon dating of fossil carbonate shells of land snails from a loess sequence close to site MS2006 for the time interval ~15–41 kyr BP (*Fig. 9.2*; Gu et al., 2009).

To match the proxy records of the Mangshan loess–paleosol sequence with the EASM δ^{18}O record, the carbonate and magnetic susceptibility records are used as tracers of soil development during humid interstadial and interglacial periods (cf. Maher and Thompson, 1992; *Fig. 9.2*). Consequently, carbonate minima and magnetic susceptibility maxima are correlated in time with the Chinese interstadials (speleothem δ^{18}O minima). The grain size profile is a tracer of eolian dust input,where clay content minima reflect periods of enhanced dust input and intensified winter monsoon, and is assumed to covary with the Chinese stadials (speleothem δ^{18}O maxima).Hence, matching of the loess proxy records of section MS2006 with the Sanbao/Hulu speleothem δ^{18}O record results in the age model shown in *Fig. 9.2*. The age models of sections MS2008W and MS2008E, that correlate very well to section MS2006 (*Supplementary Figure S9.1*), have been constructed in a similar way.

9.3.2. Continental air temperature record

The upper 5.9 m of loess–paleosol sequence MS2008E (*Fig. 9.1c*) corresponds to the last 34 kyr according to our age model. Branched GDGTs were detected throughout the whole loess–paleosol profile.

Their concentrations vary between 1 and 13 ng GDGTs/g dry weight loess (*Table 9.1*), and are higher in the paleosol layer than in the loess layer. Although atmospheric dust from the loess plateau has not been analyzed, branched GDGTs were below detection limit in a dust sample from near the West coast of Central Africa, suggesting that these components are unlikely to be transported through the atmosphere in large amounts (Hopmans et al., 2004). Thus, the branched GDGTs are likely produced in situ in the loess–paleosol sequence, and the MBT-CBT record, therefore, reflects local conditions of the Mangshan plateau area.

Calculation of the MBT and CBT indices and application of Eq. 9.1 for the whole sequence, resulted in a continuous air temperature record for the period covered by the MS2008E sequence (*Fig. 9.3b*; *Table 9.1*). The MBT-CBT-derived temperature for the upper layer of MS2008E compares well with the average present-day air temperature (~24 °C) of the summer season (May–September) on the Mangshan plateau area (*Fig. 9.3b*), indicating that our record is most likely representing mean summer air temperatures.
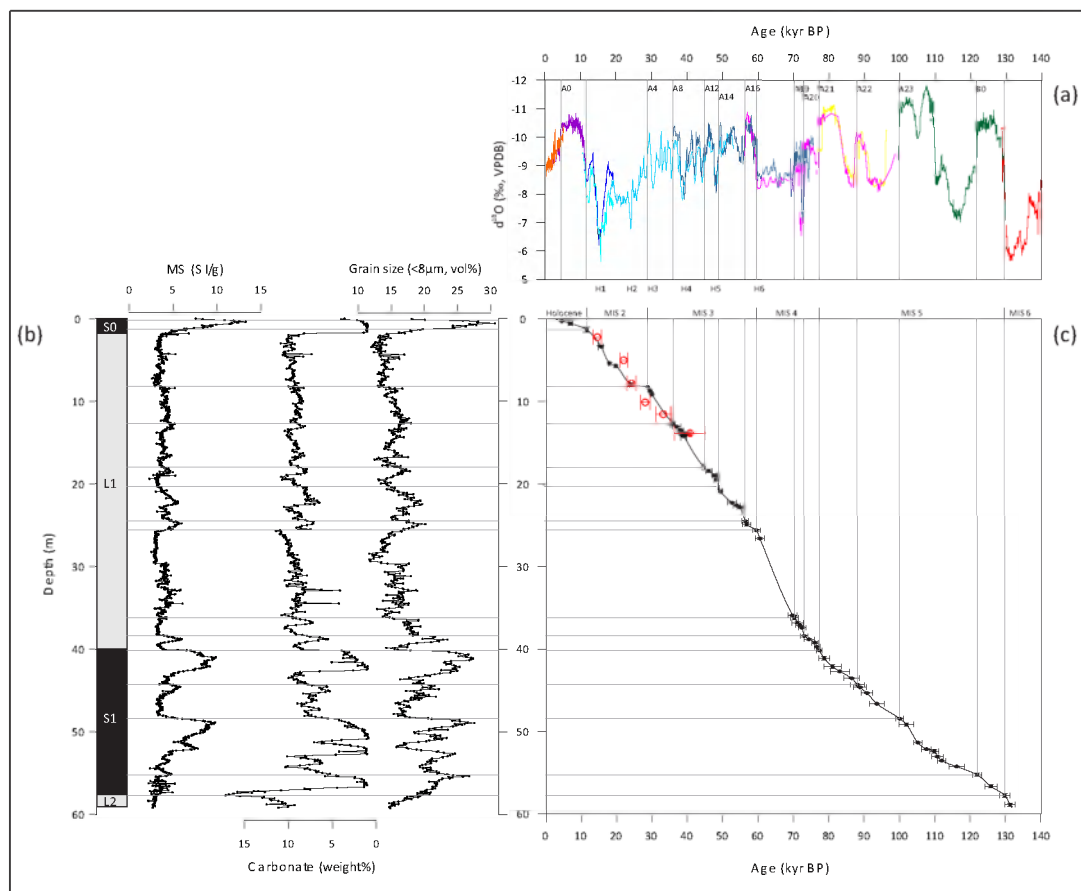
Fig. 9.2. Age model of the Mangshanloess record MS2006 based on correlation with the U-^{230}Th-dated Sanbao/Hulu speleothem δ^{18}O record of Wang et al. (*2008*) over the past ~131 kyr BP. a) Age versus δ^{18}O in the Sanbao (red, stalagmite SB11; green, SB23; yellow, SB25-1; pink, SB22; dark blue, SB3; purple, SB10; orange, SB26) and Hulu cave (three different hues of lighter blue, PD, D, and L) records. For comparison, the Hulu δ^{18}O record is plotted 1.6‰ more negative to account for the higher δ^{18}O values in the Hulu record compared to the Sanbao record (cf. *Wang et al., 2008*). Marine-siotope stages (Holocene/MIS1-MIS6), Heinrich events (H1-H6; *Wang et al., 2001*) and Chinese interstadials (cf. *Cheng et al., 2006*) are indicated. b) Magnetic susceptibility, carbonate content (weight%) and grain size (expressed as clay content) compared to paleosol (S0 and S1) and loess (L1 and L2) stratigraphy in sections MS2006 (*Prins et al., 2009*). c) Age-depth profile for loess record MS2006. Grey lines indicate the location of the 'age-control points' used to tie the loess to the spaleothem record. Red open circles indicate the radiocarbon dates of land snails (*Gu et al., 2009*; *Table 9.3*).

Although it is still unknown what group of bacteria is responsible for the production of branched GDGTs, and what their season of optimum growth is, microorganisms in general require moisture to live and grow. Since the Mangshan plateau receives over 70% of the annual amount of precipitation during the summer season (WMO, 2007), it is likely that this season is most suitable for bacterial productivity and thus the production of the branched GDGTs.

The MBT-CBT record reveals that summer air temperatures in the Mangshan plateau area were on average ~17 °C during the last glacial period, with a minimum of about 14 °C during the Last Glacial Maximum (LGM; ~21 kyr BP). The onset of deglacial warming around 19 kyr BP shown by our record matches with Antarctic warming (*Fig. 9.4e*), and is similar in timing with mid-latitude glacier retreat at the end of the LGM, as indicated by ^{10}Be exposure dates of boulders in moraines on both northern and southern hemispheres (Schaeffer et al., 2006). Also, TEX$_{86}$-inferred lake surface temperature reconstructions for lakes Malawi and Tanganyika suggest a similar timing of deglacial warming in southern Africa (Powers et al., 2005; Tierney et al., 2008), while atmospheric warming in tropical central Africa, reconstructed with the MBT-CBT proxy, may have started slightly later (Weijers et al., 2007a; *Fig. 9.4e*).

The reconstructed summer air temperatures in the Mangshan plateau area show an increase from ~15 °C at the onset of deglacial warming to ~27 °C at the beginning of the Holocene (~12 kyr BP), with an average rate of almost 2 °C/kyr. The difference between the present-day mean summer temperature (~24 °C) and the reconstructed air temperature during the LGM (~17 °C) is in agreement with other studies from this region: estimates based on pollen studies and permafrost limits in central China suggest 7–10 °C cooler air temperatures during the LGM (Zhou et al., 1998), whereas other pollen assemblage (Sun et al., 1997) or phytolith-based (Lu et al., 2007) temperature reconstructions suggest that the air temperature at that time was 4.5–9 °C cooler than present.

Maximum air temperatures on the Mangshan plateau occurred at the loess (L1) to paleosol (S0) transition that marks the beginning of the Holocene (*Fig. 9.3*). During the Holocene climatic optimum, which was around 6–7 kyr BP for this part of China (An, 2000), air temperatures were ca. 3 °C higher compared to present. This temperature difference is slightly larger than the ca. 1 °C suggested by the modelling study of Tao et al. (2010), although the proxy data that they use to compare their model with, suggest 2–3 °C higher temperatures (Tao et al., 2010 and reference therein), which is again in agreement with the MBT-CBT-derived record. Similar temperature estimates are reported based on pollen records (Zhou et al., 1998; 1–6 °C warmer than present, depending on the geographical location), and phytoliths (Lu et al., 2007; 1–2 °C warmer than present).

Evidence for the robustness of our temperature record, next to the generally good fit with previously published temperature estimates and trends, is provided by the analysis of the upper 4.8 m of the nearby loess–paleosol sequence MS2008W (*Fig. 9.1c*). According to our age model, this sequence covers the last 16 kyr. Since the top 45 cm is disturbed because of ploughing, the upper 3 samples are excluded from the discussion. The branched GDGT concentrations varied between 2 and 27 ng/g dwt loess (*Table 9.2*), showing the same variations with depth as seen in the MS2008E sequence. Comparison of the two resulting temperature records shows a similar timing and magnitude of deglacial warming, as well as absolute temperature estimates (*Fig. 9.4b,c*; *Table 9.2*).

Table 9.1. Depth, age, grain size (clay content), magnetic susceptibility (MS), organic matter (OM), branched GDGT abundance, and MBT-CBT-derived temperatures of paleosol–loess sequence MS2008E.

Depth (m)	Age (kyr BP)	<8 mm (%)	MS	OM (%)	branched GDGTs (ng/g dry wt loess)	MBT-CBT-derived MAT (˚C)
3.75	0.4	13.3	7.4	0.9	1.5	23.4
3.85	1.3	12.5	7.6	0.8	1.6	22.9
3.95	2.2	13.3	7.7	0.9	1.8	22.7
4.05	3.2	14.0	8.4	0.9	3.1	23.7
4.15	4.2	19.7	10.3	1.3	6.3	26.0
4.25	5.7	24.0	12.3	1.5	13.1	26.3
4.35	8.7	25.9	11.9	1.6	11.9	26.5
4.45	9.7	23.5	9.2	1.3	10.8	25.8
4.55	10.4	22.0	8.3	1.2	9.6	26.0
4.65	11.0	21.2	7.6	1.1	10.6	25.3
4.75	11.5	21.4	8.2	1.1	8.2	26.5
4.85	12.0	19.2	7.2	1.1	11.0	26.7
4.95	12.4	17.9	5.8	0.9	6.0	27.2
5.05	12.8	19.5	7.1	1.0	3.9	26.1
5.15	13.2	18.7	6.7	1.0	3.2	25.8
5.25	13.6	16.1	5.3	0.9	2.5	25.1
5.35	14.0	17.8	6.1	1.0	3.0	24.4
5.45	14.3	15.2	4.5	0.9	1.7	24.6
5.55	14.6	19.1	6.7	1.0	1.9	24.3
5.65	14.8	16.0	4.3	0.8	2.5	23.8
5.75	15.0	16.4	4.7	0.8	2.8	24.5
5.85	15.1	14.9	3.7	0.7	1.2	22.3
5.95	15.2	14.2	4.8	0.8	1.8	20.8
6.05	15.3	14.9	4.2	0.8	2.7	21.6
6.15	15.3	15.3	4.2	0.8	2.5	22.6
6.25	15.4	13.7	4.0	0.8	2.0	21.5
6.35	15.5	12.9	3.6	0.8	2.0	20.9
6.45	15.5	13.5	3.8	0.8	2.0	21.1
6.55	15.7	12.5	3.9	0.8	2.1	19.4
6.65	15.8	11.8	4.2	0.7	2.1	20.4
6.75	16.0	12.8	3.9	0.7	1.6	20.0
7.85	16.3	13.8	4.1	0.7	1.6	19.1
6.95	16.7	13.7	4.0	0.7	1.7	18.7
7.05	17.2	14.1	4.1	0.7	1.7	19.3
7.15	17.6	13.8	4.3	0.7	3.1	15.3
7.25	17.2	14.4	4.3	0.8	2.6	19.5
7.35	17.6	14.1	4.6	0.7	2.7	17.5
7.45	18.0	14.0	4.7	0.8	4.0	14.7

Depth (m)	Age (kyr BP)	<8 mm (%)	MS	OM (%)	branched GDGTs (ng/g dry wt loess)	MBT-CBT-derived MAT (˚C)
7.55	18.3	13.2	4.5	0.8	2.4	15.3
7.65	18.5	13.6	4.3	0.8	2.0	15.6
7.75	18.8	13.3	4.2	0.7	1.7	14.9
7.85	19.1	13.1	3.9	0.7	1.3	17.3
7.95	19.4	13.4	3.9	0.7	1.4	15.9
8.05	19.7	13.5	4.1	0.7	2.5	15.1
8.15	20.1	13.3	4.2	0.7	2.4	15.0
8.25	20.5	12.9	4.6	0.7	2.0	13.5
8.35	20.9	12.9	4.2	0.7	1.9	16.3
8.45	21.3	13.5	4.5	0.7	1.0	16.8
8.55	21.8	13.2	4.2	0.8	0.8	15.6
8.65	22.4	13.0	4.1	0.6	1.6	16.2
8.75	22.9	13.1	4.2	0.6	0.9	17.1
8.85	23.5	13.7	4.1	0.7	2.1	15.3
8.95	24.2	14.1	4.2	0.7	1.8	18.1
9.05	25.0	14.6	4.0	0.7	1.5	18.1
9.15	25.9	15.8	4.6	0.7	2.4	19.0
9.25	28.0	15.4	4.7	0.8	2.7	17.9
9.35	30.5	15.7	4.6	0.8	1.8	18.9
9.45	31.5	15.9	-[a]	0.8	2.2	18.1
9.55	32.6	16.5	4.8	0.8	2.3	18.4
9.65	33.6	16.2	5.0	0.8	2.9	16.9

[a] Not determined.

9.3.3. Comparison with NH summer insolation, loess–paleosol proxy records and stalagmite δ¹⁸O records

Our MBT-CBT record shows that summer air temperatures at the Mangshan plateau area have developed in phase with NH summer insolation throughout the whole record (*Fig. 9.3*), and that the onset of atmospheric warming is parallel in timing with that on Antarctica. Interestingly, the clay fraction, magnetic susceptibility, and organic carbon content that were measured for the MS2008E sequence, lag the onset of atmospheric warming, and start to only slowly increase from ~16 kyr BP onwards (Monsoon Intensification 1, *Fig. 9.3*; *Table 9.1*). This implies that during the first period of significant warming, the climate at the Mangshan plateau was still relatively dry, and limited soil formation was taking place, like previously suggested by Wu et al. (2002) based on mollusc studies. Pedogenic processes intensified at the start of the Holocene (~12 kyr BP), resulting in the formation of the S0 paleosol. This signifies that only then summer monsoon precipitation intensified to such an extent that conditions became substantially wetter (Monsoon Intensification 2, *Fig 9.3*), as is also shown in other Chinese loess records (Stevens et al., 2007). Similar lags have been reported for Africa, where deglacial warming after the LGM seems to coincide with the temperature increase in Antarctica, but where the onset of increased precipitation, in contrast, matches with northern hemisphere climatic changes (Gasse, 2000; Tierney et al., 2008).
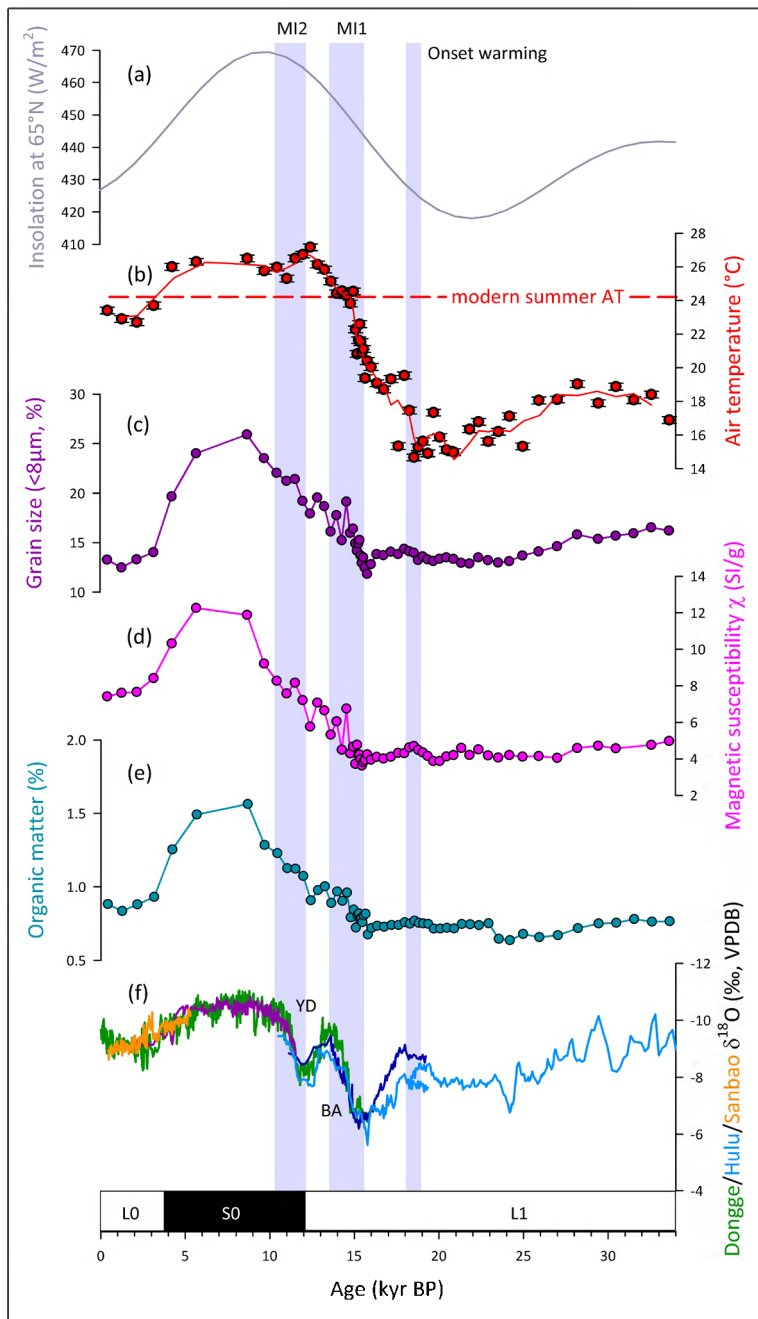
Fig. 9.3. Air temperature over the past 34 kyr for the Mangshan Loess Plateau area compared with Northern Hemisphere insolation and summer monsoon intensity. Records represent a) Northern Hemisphere July insolation at 65°N (*Berger, 1978*), b) 3 point moving average MBT-CBT-derived summer air temperatures for the MS2008E loess-paleosol sequence with bars indicating the analytical error, c) grain size (expressed as clay content), d) magnetic susceptibility, and e) organic matter content for the MS2008E sequence, and f) $\delta^{18}O$ records from Dongge (green; *Dykoski et al., 2005*), Sanbao (orange, SB26; purple, SB10; dark blue, SB3; *Wang et al., 2008*), and Hulu Caves (light blue; *Wang et al., 2001*). For comparison, the Hulu and Dongge $\delta^{18}O$ records are plotted 1.6‰ more negative to account for the higher $\delta18O$ values in the Hulu and Dongge records compared to the Sanbao record (cf. Wang et al., 2008). Grey bars indicate the onset of warming (~19 kyr BP) during the last glacial termination, and phases of increased summer monson precipitation at ~15 kyr BP (MI1) and at the start of the Holocene (~12 kyr BP; I2) reflected by changes in the loess-paleosol proxy records. L0 , S0 and L1 represent the Holocene loess, Holocene paleosol and last glacial loess layer, respectively, of the loess-paleosol sequence on the Mangshan Plateau.

128

The considerable continental warming during the last glacial termination (up to 13 °C), may potentially have had an imprint on the $\delta^{18}O$ values recorded by the Chinese cave stalagmites, as this signal is not only influenced by precipitation, but also by temperature. Although care has to be taken in extrapolating our air temperatures to those of caves, the 5–6 °C increase in temperature from ~17 kyr BP onwards to the peak of the Bølling–Allerød interstadial at ~14 kyr BP in the composite speleothem record could potentially have shifted the corresponding part of the $\delta^{18}O$ records by ~1.3‰ towards more negative values (-0.24‰/°C, according to Friedman and O'Neil, 1977). This would imply that the intensification of EASM precipitation during the initial stages of deglacial warming (*Fig. 9.3*; MI 1) would have been less intense than suggested by the $\delta^{18}O$ records. The substantial decrease in speleothem $\delta^{18}O$ values at the Younger Dryas to Holocene transition is only accompanied by minor air temperature changes, suggesting a large increase in EASM precipitation (*Fig. 9.3*; MI 2). This agrees well with the observed formation of the S0 paleosol, starting at ~12 kyr BP in our loess–paleosol record, as well as in other loess–paleosol records (Porter, 2001; Stevens et al., 2007). Thus, it seems that temperature has indeed affected the stalagmite $\delta^{18}O$ record, especially during times of rapid and large changes, i.e. during MI1.

Our records indicate that there is a considerable delay (up to ~7 kyr) in the intensification of EASM precipitation compared to continental warming and NH insolation. Several complex mechanisms have been put forward to explain the delayed response of EASM precipitation during glacial terminations. For example, latent heat export from the Southern Hemisphere Indian Ocean as well as glacial boundary conditions could have delayed the EASM onset (Clemens and Prell, 2007; Liu et al., 2006). It has also been hypothesized that the lag may have been caused by cold anomalies generated bydisintegrating ice sheets and sea-ice formation in the North Atlantic region (Cheng et al., 2009). This would have generated a colder North Atlantic that, through atmospheric teleconnections, has led to a weakening of the East Asian summer monsoon intensity. The records from the Mangshan plateau indicate that over the last deglaciation, intensification of the East Asian summer monsoon was mainly influenced by northern hemisphere climatic changes, whereas atmospheric warming coincides with the temperature increase on Antarctica. Our results thus support the statistical evaluation of the controls of East Asian monsoon variability by Rohling et al. (2009), who suggested a southern hemisphere 'push' during glacial times when the monsoon is weak, i.e. between ~28 and ~16 kyr BP.

Regardless of the exact mechanisms, our data suggest that the factors controlling the onset of deglacial atmospheric warming and the intensification of EASM precipitation may have been different. Generation of MBT-CBT records in high sedimentation rate loess–paleosol sequences, such as those from the Mangshan Plateau, now offers the opportunity to constrain the timing and magnitude of continental temperature changes in eastern Asia. They can be used to obtain a more accurate assessment of hydrological and thermal changes in this climatologically important area.

9.4. Conclusions

The application of the MBT-CBT proxy on paleosol–loess sequences from the Mangshan loess plateau has resulted in a continuous, high resolution air temperature record that provides an insight in the climate development of eastern Asia during the last 34,000 yr. The record shows that the onset of deglacial atmospheric warming is similar in timing with previous continental temperature records from e.g. Antarctica and Africa, and that air temperature varied in phase with Northern Hemisphere summer insolation. However, deglacial intensification of the East Asian Summer Monsoon, based on loess proxy
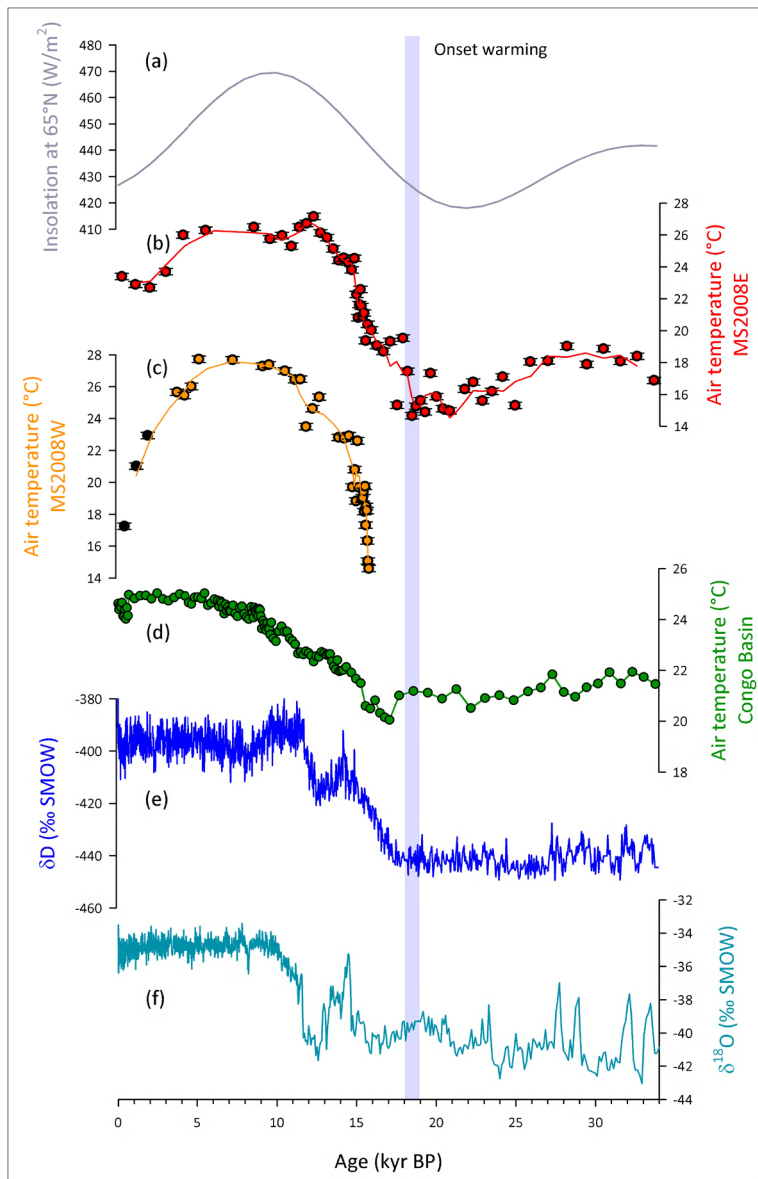
Fig. 9.4. Air temperature changes over the past 34 kyr for two loess–paleosol sequences from the Mangshan loess plateau area compared with Northern Hemisphere insolation, air temperatures from tropical Africa, and Antarctic and Arctic climate signals. Records represent a) Northern Hemisphere July insolation at 65°N (*Berger, 1978*), b) 3 point moving average MBT-CBT-derived air temperatures for the MS2008E and c) the MS2008W loess–paleosol sequence, with bars indicating the analytical error. Disturbed samples from the MS2008W section are coloured black. d) Air temperatures for the Congo Basin (*Weijers et al., 2007a*), e) the EPICA Dome C δD record indicative of Antarctic air temperature changes (*Jouzel et al., 2007*) and f) the Greenland Ice Sheet Project 2 (GISP2) δ^{18}O record indicative of Greenland air temperature fluctuations (*Stuiver and Grootes, 2000*).

records obtained from the same paleosol–loess sequence and δ^{18}O speleothem records, clearly lagged that of warming by > 3 kyr. Intense soil formation (i.e. development of the Holocene paleosol SO), depending on both higher temperatures and available moisture, even lagged deglacial warming by ~7 kyr. Our data and new MBT-CBT-derived temperature records may give us the opportunity to better understand the driving forces of deglacial warming and the monsoon system in eastern Asia.

Table 9.2. Depth, age, branched GDGT abundance, and MBT-CBT-derived temperatures of loess-paleosol sequence MS2008W.

Depth (m)	Age (kyr BP)	Branched GDGTs (ng/g dwt loess)	MBT-CBT-derived MAT (˚C)
0.05[a]	0.4	13.3	17.2
0.15[a]	1.1	12.8	21.0
0.25[a]	1.9	9.9	22.9
0.55	3.7	14.2	25.7
0.65	4.2	13.7	25.4
0.75	4.6	15.4	26.0
0.85	5.1	21.9	27.7
1.15	7.2	26.8	27.7
1.45	9.1	17.5	27.3
1.55	.5	9.1	27.4
1.85	10.5	7.0	27.0
2.05	11.2	7.6	26.4
2.15	11.5	6.9	26.5
2.25	11.9	3.5	23.5
2.35	12.3	3.0	24.6
2.45	12.7	4.0	25.3
2.75	13.9	3.0	22.8
2.85	14.3	2.6	22.8
2.95	14.6	5.8	22.9
3.05	14.8	2.2	19.7
3.15	15.0	3.1	20.8
3.25	15.0	2.7	18.8
3.35	15.1	3.3	22.6
3.45	15.2	2.7	19.7
3.75	15.4	2.1	18.9
3.85	15.5	3.0	19.0
3.95	15.5	5.2	19.4
4.05	15.6	3.8	18.2
4.15	15.6	1.6	19.7
4.25	15.6	3.0	17.3
4.35	15.7	2.4	18.5
4.45	15.7	3.6	18.2
4.55	15.7	2.1	16.3
4.65	15.8	3.8	15.1
4.75	15.8	1.8	14.6

[a] Disturbed sample.

131

Table 9.3. Calibrated radiocarbon dates of fossil aragonitic land snail shells in the MS2006 loess-paleosol sequence, inferred from Gu et al. (*2009*).

Depth (m)	Snail shells, calibrated age (kyr)	Error
2.175	14.6	1.1
4.975	22.1	1.1
7.775	24.3	1.3
10.075	28.2	1.3
11.525	33.3	2.1
13.825	40.9	4.4

Supplementary Figure S9.1. Magnetic susceptibility, carbonate content and grain size (expressed as clay content) compared to paleosol (S0, S1) and loess (L1, L2) stratigraphy in sections MS2006 (Prins et al., 2009), MS2008W and MS2008E from the Mangshan loess plateau. Dashed correlation lines coincide with lithological (and approximately with marine-isotope stage) boundaries. Note that section MS2006 and the two MS2008 sections are separated by ~2 km. Profiles MS2006 and MS2008W are lined up with respect to the top of their S0 units (ground level) to highlight the N-S thinning of the S0-L1-S1 sequence; profile MS2008E is lined up with respect to the S1 unit in profile MS2008E showing a local (paleo-)relief of ~3.7 meter.

References

Aerts R., Wallén B., Malmer N., 1992. Growth-limiting nutrients in *Sphagnum*-dominated bogs subject to low and high atmospheric nitrogen supply. *Journal of Ecology* 80, 131-140.

An Z., 2000. The history and variability of the East Asian paleomonsoon climate. *Quaternary Science Reviews* 19, 171–187.

Andrews J. N. and Lee D. J., 1979. Inert gases in groundwater from the Bunter Sandstone of England as indicators of age and palaeoclimatic trends. *Journal of Hydrology* 41, 233–252.

Bailey I.W. and Sinnott E.W., 1915. A botanical index of Cretaceous and Tertiary climates. *Science* 41, 831–834.

Ballantyne A.P., Greenwood D.R., Sinninghe Damsté J. S., Csank A.Z., Eberle J.J., Rybczynski N., 2010. Significantly warmer Arctic surface temperatures during the Pliocene indicated by multiple independent proxies. *Geology* 38, 603–606.

Barns S.M., Cain E.C., Sommerville L., Kuske C.R., 2007. *Acidobacteria* phylum sequences in uranium-contaminated subsurface sediments greatly expand the known diversity within the phylum. *Applied and Environmental Microbiology* 73, 3113–3116.

Barns S.M., Takala S.L., Kuske C.R., 1999. Wide distribution and diversity of members of the bacterial kingdom *Acidobacterium* in the environment. *Applied and Environmental Microbiology* 65, 1731–1737.

Bauersachs T., Speelman E.N., Hopmans E.C., Reichart G.J., Schouten S., Sinninghe Damsté, J.S., 2010. Fossilized glycolipids reveal past oceanic N_2 fixation by heterocystous cyanobacteria. *Proceedings of the National Academy of Sciences of the USA* 107, 19190-19194.

Beales N., 2004. Adaptation of microorganisms to cold temperatures, weak acid preservatives, low pH, and osmotic stress: a review. *Comprehensive Reviews in Food Science and Food Safety* 3, 1–20.

Bekku Y., Kume A., Nakatsubo T., Masuzawa T., Kanda H., Koizumi H., 1999. Microbial biomass in relation to primary succession on arctic deglaciated moraines. *Polar Bioscience* 12, 47–53.

Bendle J.A., Weijers J.W.H., Maslin M.A., Sinninghe Damsté J.S., Schouten S., Hopmans E.C., Boot C.S., Pancost R.D., 2010. Major changes in glacial and Holocene terrestrial temperatures and sources of organic carbon recorded in the Amazon fan by tetraether lipids. *Geochemistry Geophysics Geosystems* 11, 1–13, Q12007.

Berger A.L., 1978. Long-term variations of caloric insolation resulting from the Earth's orbital elements. *Quaternary Research* 9, 139–167.

Birks H.J.B., Jones V.J., Rose N.L., 2004. Recent environmental change and atmospheric contamination on Svalbard as recorded in lake sediments – an introduction. *Journal of Paleolimnology* 31, 403–410.

Blaga C.I., Reichart G.-J., Heiri O., Sinninghe Damsté J.S., 2009. Tetraether membrane lipid distributions in water-column particulate matter and sediments: a study of 47 European lakes along a north-south transect. *Journal of Paleolimnology* 41, 523-540.

Blaga C.I., Reichart G.-J., Schouten S., Lotter A.F., Werne J.P., Kosten S., Mazzeo N., Lacerot G., Sinninghe Damsté J. S., 2010. Branched glycerol dialkyl glycerol tetraethers in lake sediments: Can they be used as temperature and pH proxies? *Organic Geochemistry* 41, 1225-1234.

Blaga C.I., Reichart G.-J., Vissers E.W., Lotter A.F., Anselmetti F.S., Sinninghe Damsté J.S., 2011. Seasonal changes in glycerol dialkyl glycerol tetraether concentrations and fluxes in an alpine lake: Implications for the use of the TEX_{86} and BIT proxies. *Geochimica et Cosmochimica Acta*, in review.

Bligh E.G. and Dyer W.J., 1959. A rapid method of total lipid extraction and purification. *Canadian Journal of Biochemistry and Physiology* 37, 911–917.

Bowen G.J. and Revenaugh J., 2003. Interpolating the isotopic composition of modern meteoric precipitation, *Water Resources Research* 39, SWC9-1–SWC9-13.

Bowen G.J., 2009. The Online Isotopes in Precipitation Calculator, version 2.2, online available at: http://www.waterisotopes.org, last access: August 2009.

Brassel S.C., Eglinton G., Marlowe I.T., Pflaumann U., Sarnthein M., 1986. Molecular stratigraphy – A new tool for climatic assessment. *Nature* 320, 129-133.

Burns S.J., Matter A., Frank N., Mangini A., 1998. Speleothem-based paleoclimate record from northern Oman. *Geology* 26, 499-502.

Chappe B., Michaelis W., Albrecht P., 1980. Molecular fossils of Archaebacteria as selective degradation products of kerogen. *Physics and Chemistry of the Earth* 12, 265–274.

Chen F.H., Bloemendal J., Wang J.M., Oldfield F., 1997. High-resolution multi-proxy climate records from Chinese loess: evidence for rapid climatic changes over the last 75 kyr. *Palaeogeography Palaeoclimatology Palaeoecology* 130, 323–335.

Cheng H., Edwards L., Wang Y., Kong X., Ming Y., Kelly M.J., Wang X., Gallup C.D., Liu W., 2006. A penultimate glacial monsoon record from Hulu Cave and two phase glacial terminations. *Geology* 34, 217–220.

Cheng H., Edwards R.L., Broecker W.S., Denton G.H., Kong X., Wang Y., Zhang R., Wang X., 2009. Ice age terminations. *Science* 326, 248–252.

Clemens S.C. and Prell W.L., 2007. The timing of orbital-scale Indian monsoon changes. *Quaternary Science Reviews* 26, 275–278.

Colinvaux P.A., DeOliviera P.E., Moreno J.E., Miller M.C., Bush M.B., 1996. A long pollen record from lowland Amazonia: Forest and cooling in glacial times. *Science* 274, 85- 88.

Dansgaard W., 1964. Stable isotopes in precipitation. *Tellus* XVI, 436–468.

Davis K.E.R., Sangwan P., Janssen P. H., 2011. *Acidobacteria*, *Rubrobacteridae* and *Chloroflexi* are abundant among very slow-growing and mini-colony-forming soil bacteria. *Environmental Microbiology* 13, 798–805.

Dembitsky V.M., 1996. Betaine ether-linked glycerolipids: Chemistry and biology. *Progress in Lipid Research* 35, 1-51.

Dettman D.L. and Lohmann K.C., 2000. Oxygen isotope evidence for high-altitude snow in the Laramide Rocky Mountains of North America during the Late Cretaceous and Paleogene. *Geology* 28, 243–246.

Donders T.H., Weijers J.W.H., Munsterman D.K., Hoeve M.L. K. V., Buckles L.K., Pancost R.D., Schouten S., Sinninghe Damsté J.S., Brinkhuis H., 2009. Strong climate coupling of terrestrial and marine environments in the Miocene of northwest Europe. *Earth and Planetary Science Letters* 281, 215–225.

Drotz S.H., Sparrman T., Nilsson M.B., Schleucher J., Oquist M.G., 2010. Both catabolic and anabolic heterotrophic microbial activity proceed in frozen soils. *Proceedings of the National Academy of Sciences of the USA* 107, 21046–21051.

Dykoski C.A., Edwards R.L., Cheng H., Yuan D., Cai Y., Zhang M., Lin Y., Qing J., An Z., Revenaugh J., 2005. A high-resolution, absolute-dated Holocene and deglacial Asian monsoon record from Dongge Cave, China. *Earth and Planetary Science Letters* 233, 71–86.

Eberle J.J., Fricke H.C., Humphrey J.D., Hackett L., Newbrey M. G., Hutchison J.H., 2010. Seasonal variability in Arctic temperatures during early Eocene time. *Earth and Planetary Science Letters* 296, 481–486.

Eichorst S.A., Breznak J.A., Schmidt T.M., 2007. Isolation and characterization of soil bacteria that define *Terriglobus* gen. nov., in the phylum *Acidobacteria*. *Applied and Environmental Microbiology* 73, 2708–2717.

Elderfield H. and Ganssen G., 2000. Past temperature and $\delta^{18}O$ of surface ocean waters inferred from foraminiferal Mg/Ca ratios. *Nature* 405, 442-445.

Eldrett J.S., Greenwood D.R., Harding I.C., Huber M., 2009. Increased seasonality through the Eocene to Oligocene transition in northern high latitudes. *Nature* 459, 969-974.

Epstein S.E., Buchsbaum R., Lowenstam H.A., Urey H.C., 1953. Revised carbonate-water isotopic temperature scale. *Geological Society of America Bulletin* 64, 1315-1325.

Fang J.S., Barcelona M.J., Semrau J.D., 2000. Characterization of methanotrophic bacteria on the basis of intact phospholipid profiles. *FEMS Microbiology Letters* 189, 67-72.

Fawcett P., Werne J.P., Anderson R., Heikoop J., Brown E., Berke M., Smith S., Goff F., Hurley L., Cisneros-Dozal M., Schouten S., Sinninghe Damsté J.S., Huang Y., Toney J., Fessenden J., WoldeGabriel G., Atudorei V., Geissman J., Allen C., 2011. Extended megadroughts in the southwestern United States during Pleistocene interglacials. *Nature* 470, 518–521.

Feng X.J. and Simpson M.J., 2009. Temperature and substrate controls on microbial phospholipid fatty acid composition during incubation of grassland soils contrasting in organic matter quality. *Soil Biology and Biochemistry* 41, 804–812.

Frey S.D., Drijber R., Smith H., Melillo J., 2008. Microbial biomass, functional capacity, and community structure after 12 years of soil warming. *Soil Biology and Biochemistry* 40, 2904–2907.

Fricke H.C., Clyde W.C., O'Neil J.R., Gingerich P.D., 1998. Evidence for rapid climate change in North America during the latest Paleocene thermal maximum: oxygen isotope compositions of biogenic phosphate from the Bighorn Basin (Wyoming). *Earth and Planetary Science Letters* 160, 193-208.

Friedman I. and O'Neil J.R., 1977. Data of geochemistry, I. In: Friedman, O'Neil, J.R. (Eds.), U.S. Geological Survey (USGS) Professional Paper 440-KK, KK1-12, USGS, Washington, DC.

Garzione C.N., Dettman D.L., Horton B.K., 2004. Carbonate oxygen isotope paleoaltimetry: evaluating the effect of diagenesis on paleoelevation estimates for the Tibetan Plateau. *Palaeogeography Palaeoclimatology Palaeoecology* 212, 119–140.

Gasse F., 2000. Hydrological changes in the African tropics since the Last Glacial Maximum. *Quaternary Science Reviews* 19, 189–211.

Greenwood D.R., Wilf P., Wing S.L., Christophell D.C., 2004. Paleotemperature estimation using Leaf-Margin Analysis: is Australia different? *Palaios* 19, 129-142.

GRIP, 1993. Greenland Ice-core Project Members. Climate instability during the last interglacial period recorded in the GRIP ice core. *Nature* 364, 203-207.

Gu Z., Liu Z., Xu B., Wu N., 2009. Stable carbon and oxygen isotopes in land snail carbonate shells from a last glacial loess sequence and their implications of environmental changes. *Quaternary Sciences* 29, 13–22 (in Chinese with English abstract).

Harrod T.R. and Hogan D.V., 2008. The soils of North Wyke and Rowden. Available from: http://www.northwyke.bbsrc.ac.uk/assets/pdf_files/Soils%20of%20NW%20%20Rowden%202.pdf.

Hartman W.H., Richardson C.J., Vilgalys R., Bruland G.L., 2008. Environmental and anthropogenic controls over bacterial communities in wetland soils. *Proceedings of the National Academy of Sciences of the USA* 105, 17842–17847.

Harvey H.R., Fallon R.D., Patton J.S., 1986. The effect of organic matter and oxygen on the degradation of bacterial membrane lipids in marine sediments. *Geochimica et Cosmochimica Acta* 50, 795–804.

Hatte C., Roussen D.-D., Guiot J., 2009. Climate reconstruction from pollen and $\delta^{13}C$ records using inverse vegetation modeling – Implication for past and future climates. *Climate of the Past* 5, 147-156.

Hemp A., 2006a. Continuum or zonation? Altitudinal gradients in the forest vegetation of Mt. Kilimanjaro. *Plant Ecology* 184, 27–42.

Hemp A., 2006b. Vegetation of Kilimanjaro: hidden endemics and missing bamboo. *African Journal of Ecology* 44, 305–328.

Heslop D., Shaw J., Bloemendal J., Chen F., Wang J., Parker E., 1999. Sub-millennial scale variations in East Asian monsoon systems recorded by dust deposits from the north-western Chinese Loess Plateau. *Physics and Chemistry of the Earth* 24, 785–792.

Hobbie S.E., 1996. Temperature and plant species control over litter decomposition in Alaskan tundra. *Ecological Monographs* 66, 503–522.

Hobbie S.E., Schimel J.P., Trumbore S.E., Randerson J.R., 2000. Controls over carbon storage and turnover in high-latitude soils. *Global Change Biology* 6, 196–210.

Hodkinson I.D., Coulson S.J., Webb N.R., 2003. Community assembly along proglacial chronosequences in the high Arctic: vegetation and soil development in north-west Svalbard. *Journal of Ecology* 91, 651–663.

Hopmans E.C., Schouten S., Pancost R.D., van der Meer M.T.J., Sinninghe Damsté J.S., 2000. Analysis of intact tetraether lipids in archaeal cell material and sediments by high performance liquid chromatography/atmospheric pressure chemical ionization mass spectrometry. *Rapid Communications in Mass Spectrometry* 14, 585–589.

Hopmans E.C., Weijers J.W.H., Schefuß E., Herford L., Sinninghe Damsté J.S., Schouten S., 2004. A novel proxy for terrestrial organic matter in sediments based on branched and isoprenoid tetraether lipids. *Earth and Planetary Science Letters* 224, 107-116.

Hren M.T., Pagani M., Erwin D.M., Brandon M., 2010. Biomarker reconstruction of the early Eocene paleotopography and paleoclimate of the northern Sierra Nevada. *Geology* 38, 7–10.

Huber R., Wilharm T., Huber D., Trincone A., Burggraf S., Köning H., Rachel R., Rockinger, I., Fricke H., Stetter K.O., 1992. *Aquifex pyrophilus* gen nov. sp. nov., represents a novel group of marine hyperthermophilic hydrogen-oxidizing bacteria. *Systematic and Applied Microbiology* 15, 340–351.

Huguet A., Fosse C., Laggoun-Défarge F., Toussaint M.-L., Derenne S., 2010a. Occurrence and distribution of glycerol dialkyl glycerol tetraethers in a French peat bog. *Organic Geochemistry* 41, 559–572.

Huguet A., Fosse C., Metzger P., Fritsch E. and Derenne S., 2010b. Occurrence and distribution of extractable glycerol dialkyl glycerol tetraethers in podzols. *Organic Geochemistry* 41, 291–301.

Huguet C., Hopmans E.C., Febo-Ayala W., Thompson D.H., Sinninghe Damsté J.S., Schouten S., 2006. An improved method to determine the absolute abundance of glycerol dibiphytanyl glycerol tetraether lipids. *Organic Geochemistry* 37, 1036–1041.

IPCC, 2007. Climate Change 2007: Synthesis report. Contribution of working groups I, II and III to the fourth Assessment Report of the Intergovernmental Panel on Climate Change.

Janssen P.H., 2006. Identifying the dominant soil bacterial taxa in libraries of 16S rRNA and 16S rRNA genes. *Applied and Environmental Microbiology* 72, 1719–1728.

Jenny H., 1941. Factors of Soil Formation. McGraw-Hill, New York.

Jia G., Wei K., Chen F., Peng P., 2008. Soil *n*-alkane δD vs. altitude gradients along Mount Gongga, China. *Geochimica et Cosmochimica Acta* 72, 5165–5174.

Jones R.T., Robeson M.S., Lauber C.L., Hamady M., Knight R., Fierer N., 2009. A comprehensive survey of soil acidobacterial diversity using pyrosequencing and clone library analyses. *The ISME journal* 3, 442–453.

Jonkers L., Prins M.A., Brummer G.-J., Konert M., Lougheed B.C., 2009. Experimental insights into laser diffraction particle sizing of fine-grained sediments for use in palaeoceanography. *Sedimentology* 56, 2192–2206.

Jordan G.J., 1997. Uncertainty in paleoclimatic reconstructions based on leaf physiognomy. *Australian Journal of Botany* 45, 527-547.

Jouzel J., Lorius C., Petit J.R., Genthon C., Barkov N.I., Kotlyakov V.M., Petrov V.M., 1987. Vostok ice core: a continuous isotope temperature record over the last climatic cycle (160,000 years). *Nature* 329, 403-408.

Jouzel J., Alley R.B., Cuffey K.M., Dansgaard W., Grootes P., Hoffmann G., Johnsen S.J., Koster R.D., Peel D., Shuman C.A., Stievenard M., Stuiver M., White J., 1997. Validity of temperature reconstruction from water isotopes in ice cores. *Journal of Geophysical Research – Oceans* 102, 26471-26487.

Jouzel J., Masson-Delmotte V., Cattani O., Dreyfus G., Falourd S., Hoffmann G., Minster B., Nouet J., Barnola J.M., Chappellaz J., Fischer H., Gallet J.C., Johnsen S., Leuenberger M., Loulergue L., Luethi D., Oerter H., Parrenin F., Raisbeck G., Raynaud D., Schilt A., Schwander J., Selmo E., Souchez R., Spahni R., Stauffer B., Steffensen J.P, Stenni B., Stocker T.F., Tison J.L., Werner M., Wolff E.W., 2007. Orbital and millennial Antarctic climate variability over the past 800,000 years. *Science* 317, 793–796.

Kemp J.S., Paterson E., Gammack S.M., Cresser M.S., Killham K., 1992. Leaching of genetically modified *Pseudomonas fluorescens* through organic soils: influence of temperature, soil pH, and roots. *Biology and Fertility of Soils* 13, 218–224.

Kim J.-H., Schouten S., Buscail R., Ludwig W., Bonnin J., Sinninghe Damsté J.S., Bourrin F., 2006. Origin and distribution of terrestrial organic matter in the NW Mediterranean (Gulf of Lion): Exploring the newly developed BIT index. *Geochemistry Geophysics Geosystems* 7, Q11017.

Kim J.-H., Schouten S., Hopmans E.C., Donner B., Sinninghe Damsté J.S., 2008. Global sediment core-top calibration of the TEX$_{86}$ paleothermometer in the ocean. *Geochimica et Cosmochimica Acta* 72, 1154-1173.

Kim J.-H., van der Meer J., Schouten S., Helmke P., Willmott V., Sangiorgi F., Koç N., Hopmans E.C., Sinninghe Damsté J.S., 2010a. New indices and calibrations derived from the distribution of crenarchaeal isoprenoid tetraether lipids: Implications for past sea surface temperature reconstructions. *Geochimica et Cosmochimica Acta* 74, 4639-4654.

Kim J.-H., Zarzycka B., Buscail R., Peterse F., Bonnin J., Ludwig W., Schouten S., Sinninghe Damsté J.S., 2010b. Contribution of river-borne soil organic carbon to the Gulf of Lions (NW Mediterranean). *Limnology and Oceanography* 55, 507-518.

KNMI, 1997. World Climate Information (WKI) 2.0. Koninklijk Nederlands Meteorologisch Instituut (KNMI), De Bilt, The Netherlands. Available from: http://www.knmi.nl/klimatologie/normalen1971-2000/wki.html.

Kohn M.J. and Law M., 2006. Stable isotope chemistry of fossil bone as a new paleoclimate indicator. *Geochimica et Cosmochimica Acta* 70, 931-946.

Konert M. and Vandenberghe J., 1997. Comparison of laser grain size analysis with pipette and sieve analysis: a solution for the underestimation of the clay fraction. *Sedimentology* 44, 523–535.

Kurek J. and Cwynar L.C., Ager T.A., Abbott M.B., Edwards ME., 2009. Late Quaternary paleoclimate of western Alaska inferred from fossil chironomids and its relation to vegetation histories. *Quaternary Science Reviews* 28, 799-811.

Langworthy T.A., Holzer G., Zeikus J.G., Tornabene T.G., 1983. Iso- and anteisobranched glycerol diethers of the thermophilic anaerobe *Thermodesulfotobacterium* commune. *Systematic and Applied Microbiology* 4, 1–17.

Lauber C.L., Hamady M., Knight R., Fierer N., 2009. Pyrosequencing-based assessment of soil pH as a predictor of soil bacterial community structure at the continental scale. *Applied and Environmental Microbiology* 75, 5111–5120.

Leininger S., Urich T., Schloter M., Schwark L., Qi J., Nicol G.W., Prosser J.I., Schuster S.C., Schleper C., 2006. Archaea predominate among ammonia-oxidizing prokaryotes in soils. *Nature* 442, 806–809.

Li H.-C., Ku T.-L., You C.-F., Cheng H., Edwards L., Ma Z.-B., Tsai W.-S., Li M.-D., 2005. [87]Sr/[86]Sr and Sr/Ca in spelothems for paleoclimate reconstruction in Central China between 70 and 280 kyr ago. *Geochimica et Cosmochimica Acta* 69, 3933-3947.

Little S.A., Kembel S.W., Wilf P., 2010. Paleotemperature proxies from leaf fossils reinterpreted in light of evolutionary history. *PLoS ONE* 5, e15161.

Liu X., Liu Z., Kutzbach J.E., Clemens S.C., Prell W.L., 2006. Hemispheric insolation forcing of the Indian Ocean and Asian Monsoon: local versus remote impacts. *Journal of Climate* 19, 6195–6208.

Liu X.-L., Leider A., Gillespie A., Gröger J., Versteegh G.J.M., Hinrichs K.-U., 2010. Identification of polar lipid precursors of the ubiquitous branched GDGT orphan lipids in a peat bog in Northern Germany. *Organic Geochemistry* 41, 653–660.

Lotter A.F., Birks H.J.B., Hofmann W., Marchetto A., 1997. Modern diatom, cladocera, chironomids, and chrysophyte cyst assemblages as quantitative indicators for the reconstruction of past environmental conditions in the Alps. I. Climate. *Journal of Paleolimnology* 18, 395-420.

Longinelli A., 1984. Oxygen isotopes in mammal bone phosphate: A new tool for paleohydrological and paleoclimatological research? *Geochimica et Cosmochimica Acta* 48, 385-290.

Lu H.-Y.,Wu N.-Q., Liu K.-B., Jiang H., Liu T.-S., 2007. Phytoliths as quantitative indicators for the reconstruction of past environmental conditions in China II: palaeoenvironmental reconstruction in the Loess Plateau. *Quaternary Science Reviews* 26, 759–772.

Luthi D., Le Floch M, Bereiter B., Bluntier T., Barnola J.M., Siegenthaler U., Raynaud D., Jouzel J., Fischer H., Kawamura K., Sticker T.F., 2008. High-resolution carbon dioxide concentration record 650,000-800,000 years before present. *Nature* 453, 379-382.

Maher B.A. and Thompson R., 1992. Paleoclimatic significance of the mineral magnetic record of the Chinese loess and paleosols. *Quaternary Research* 37, 155–170.

Männistö M.K., Tiirola M., Häggblom M.M., 2007. Bacterial communities in Arctic fjelds of Finnish Lapland are stable but highly pH-dependent. *FEMS Microbiology Ecology* 59, 452–465.

Mazor E., 1972. Paleotemperatures and other hydrological parameters deduced from noble-gases dissolved in groundwaters – Jordan rift valley, Israel. *Geochimica et Cosmochimica Acta* 36, 1321-1336.

Meharg A.A., Killham K., 1990. The effect of soil pH on rhizosphere carbon flow of *Lolium perenne*. *Plant and Soil* 123, 1–7.

Morrill C. and Koch P.L., 2002. Elevation or alteration? Evaluation of isotopic constraints on paleoaltitudes surrounding the Eocene Green River Basin. *Geology* 30, 151–154.

Müller P.J., Kirst G., Ruhland G., von Storch I., Rosell-Melé A., 1998. Calibration of the alkenone paleotemperature index U$^k_{37}$ based on core-tops from the eastern South Atlantic and the global ocean (60°N-60°S). *Geochimica et Cosmochimica Acta* 62, 1757-1772.

Müller P.J. and Fischer G., 2004. Global core-top calibration of UK$_{37}$ (update). doi:10.1594/PANGAEA.126662

Nedwell D.B., 1999. Effect of low temperature on microbial growth: lowered affinity for substrates limits growth at low temperature. *FEMS Microbiology Ecology* 30, 101–111.

Nicol G.W., Leininger S., Schleper C., Prosser J.I., 2008.

The influence of soil pH on the diversity, abundance and transcriptional activity of ammonia oxidizing archaea and bacteria. *Environmental Microbiology* 10, 2966–2978.

Nurnberg D., Bijma J., Hemleben C., 1996. Assessing the reliability of magnesium in foraminiferal calcite as a proxy for water mass temperatures. *Geochimica et Cosmochimica Acta* 60, 803-814.

Oba M., Sakata S., Tsunogai U., 2006. Polar and neutral isopranyl glycerol ether lipids as biomarkers of archaea in near-surface sediments from the Nankai Trough. *Organic Geochemistry* 37, 1643–1654.

Oliver S.A., Oliver H.R., Wallace J.S., Roberts A.M., 1987. Soil heat-flux and temperature-variation with vegetation, soil type and climate. *Agricultural and Forest Meteorology* 39, 257–269.

Oppermann B.I., Michaelis W., Blumenberg M., Frerichs J., Schulz H.M., Schippers A., Beaubien S.E., Krüger M., 2010. Soil microbial community changes as a result of long-term exposure to a natural CO_2 vent. *Geochimica et Cosmochimica Acta* 74, 2697–2716.

Pancost R.D. and Sinninghe Damsté J.S., 2003. Carbon isotopic compositions of prokaryotic lipids as tracers of carbon cycling in diverse settings. *Chemical Geology* 195, 29-58.

Peel M.C., Finlayson B.L., McMahon T.A., 2007. Updated world map of the Köppen-Geiger climate classification. *Hydrology and Earth System Sciences* 11, 1633–1644.

Peterse F., Kim J.-H., Schouten S., Klitgaard Kristensen D., Koç N., Sinninghe Damsté J.S., 2009a. Constraints on the application of the MBT/CBT palaeothermometer at high latitude environments (Svalbard, Norway). *Organic Geochemistry* 40, 692–699.

Peterse F., Schouten S., van der Meer J., van der Meer M.T.J., Sinninghe Damsté J.S., 2009b. Distribution of branched tetraether lipids in geothermally heated soils: implications for the MBT/CBT temperature proxy. *Organic Geochemistry* 40, 201–205.

Peterse F., van der Meer M.T.J., Schouten S., Jia G., Ossebaar J., Blokker J., Sinninghe Damsté J.S., 2009c. Assessment of soil *n*-alkane δD and branched tetraether membrane lipid distributions as tools for paleoelevation reconstruction. *Biogeosciences* 6, 2799–2807.

Peterse F., Nicol G.W., Schouten S., Sinninghe Damsté J.S., 2010. Influence of soil pH on the abundance and distribution of core and intact polar lipid-derived branched GDGTs in soil. *Organic Geochemistry* 41, 1171–1175.

Peterse F., Prins M.A., Beets C.J., Troelstra S.R., Zheng H., Gu Z., Schouten S., Sinninghe Damsté J.S., 2011. Decoupled warming and monsoon precipitation in East Asia over the last deglaciation. *Earth and Planetary Science Letters* 301, 256–264.

Peterson T.C. and Vose R.S., 1997. An overview of the global historical climatology network temperature database. *Bulletin of the American Meteorological Society* 78, 2837-2849.

Pienitz R., Smol J.P., Birks H.J.B., 1995. Assessment of freshwater diatoms as quantitative indicators of past climate change in the Yukon and Northwest Territories, Canada. *Journal of Paleolimnology* 13, 21-49.

Pitcher A., Hopmans E.C., Schouten S., Sinninghe Damsté J.S., 2009. Separation of core and intact polar archaeal tetraether lipids using silica columns: insights into living and fossil biomass contributions. *Organic Geochemistry* 40, 12–19.

Poage M.A. and Chamberlain C.P., 2001. Empirical relationships between elevation and the stable isotope composition of precipitation and surface waters: Considerations for studies of paleoelevation change. *American Journal of Science* 301, 1–15.

Polissar P.J., Freeman K.H., Rowley D.B., McInerney F.A., Curry B.S., 2009. Paleoaltimetry of the Tibetan Plateau from *D/H* ratios of lipid biomarkers. *Earth and Planetary Science Letters* 287, 64–76.

Porter S.C., 2001. Chinese loess record of monsoon climate during the last glacial–interglacial cycle. *Earth Science Reviews* 54, 115–128.

Porter S.C. and An Z., 1995. Correlation between climate events in the North Atlantic and China during the last glaciations. *Nature* 375, 305–308.

Powers L.A., Werne J.P., Johnson T.C., Hopmans E.C., Sinninghe Damsté J.S., Schouten S., 2004. Crenarchaeotal membrane lipids in lake sediments: A new paleotemperature proxy for continental paleoclimate reconstruction? *Geology* 32, 613-616.

Powers L.A., Johnson T.C., Werne J.P., Castañeda I.S., Hopmans E.C., Sinninghe Damsté J.S., Schouten S., 2005. Large temperature variability in the southern African tropics since the Last Glacial Maximum. *Geophysical Research Letters* 32, L08706.

Powers L., Werne L.P., Vanderwoude A.J., Sinninghe Damsté J.S., Hopmans E.C., Schouten S., 2010. Applicability and calibration of the TEX_{86} paleothermometer in lakes. *Organic Geochemistry* 41, 404-413.

Prins M.A., Zheng H., Beets K., Troelstra S., Bacon P., Kamerling I., Wester W., Konert M., Huang X., Ke W., Vandenberghe J., 2009. Dust supply from river floodplains: the case of the lower Huang He (Yellow River) recorded in a loess–palaeosol sequence from the Mangshan Plateau. *Journal of Quaternary Science* 24, 75–84.

Rao Z., Zhu Z., Jia G., Henderson A.C.G., Xue Q., Wang S., 2009. Compound specific δD values of long chain *n*-alkanes derived from terrestrial higher plants are indicative of the δD of meteoric waters: Evidence from surface soils in eastern China. *Organic Geochemistry* 40, 922–930.

Rietti-Shati M., Yam R., Karlen W., Shemesh A., 2000. Stable isotope composition of tropical high-altitude fresh-waters on Mt. Kenya, Equatorial East Arfica. *Chemical Geology* 166, 341–350.

Rohling E.J., Liu Q.S., Roberts A.P., Stanford J.D., Rasmussen S.O., Langen P.L., Siddall M., 2009. Controls on the East Asian monsoon during the last glacial cycle, based on comparison between Hulu Cave and polar ice-core records. *Quaternary Science Reviews* 28, 3291–3302.

Rommerskirchen F., Plader A., Eglinton G., Chikaraishi Y., Rullkötter J., 2006. Chemotaxonomic significance of distribution and stable carbon isotopic composition of long-chain alkanes and alkan-1-ols in C_4 grass waxes. *Organic Geochemistry* 37, 1303–1332.

Rowley D.B. and Garzione C.N., 2007. Stable isotope-based paleoaltimetry. *Annual Reviews of Earth and Planetary Sciences* 35, 463–508.

Rozanski K. and Araguás Araguás L., 1995. Spatial and temporal variability of stable isotope composition of precipitation over the south american continent. *Bulletin de l'Institut Français d'Études Andines* 24, 379–390.

Rozanski K., Araguás-Araguás L., Gonfiantini R., 1992. Relation between long-term trends of O-18 isotope composition of precipitation and climate. *Science*, 258, 981–985.

Rueda G., Rosell-Melé A., Escala M., Gyllencreutz R., Backman J., 2009. Comparison of instrumental and GDGT-based estimates of sea surface and air temperatures from the Skagerrak. *Organic Geochemistry* 40, 287–291.

Sachse D., Radke J., Gleixner G., 2004. Hydrogen isotope ratios of recent lacustrine sedimentary *n*-alkanes record modern climate variability. *Geochimica et Cosmochimica Acta* 68, 4877–4889.

Sait M., Davis K.E.R., Janssen P.H., 2006. Effect of pH on isolation and distribution of members of subdivision 1 of the phylum *Acidobacteria* occurring in soil. *Applied and Environmental Microbiology* 72, 1852–1857.

Sauer P.E., Eglinton T.I., Hayes J.M., Schimmelmann A., Sessions A.L., 2001. Compound-specific *D/H* ratios of lipid biomarkers from sediments as a proxy for environmental and

climatic conditions. *Geochimica et Cosmochimica Acta* 65, 213–222.

Schaeffer J.M., Denton G.H., Barrell D.J.A., Ivy-Ochs S., Kubik P.W., Andersen B.G., Philips F.M., Lowell T.V., Schluchter C., 2006. Near-synchronous interhemispheric termination of the last glacial maximum in mid-lattitudes. *Science* 312, 1510–1513.

Schouten S., Hopmans E.C., Pancost R.D., Sinninghe Damsté J.S., 2000. Widespread occurrence of structurally diverse tetraether membrane lipids: evidence for the ubiquitous presence of low-temperature relatives of hyperthermophiles. *Proceedings of the National Academy of Sciences of the USA* 97, 14421–14426.

Schouten S., Hopmans E.C., Schefuß E., Sinninghe Damsté J.S., 2002. Distributional variations in marine crenarchaeotal membrane lipids: a new tool for reconstructing ancient sea water temperatures? *Earth and Planetary Science Letters* 204, 265-274.

Schouten S., Hopmans E.C., Sinninghe Damsté J.S., 2004. The effect of maturity and depositional redox conditions on archaeal tetraether lipid palaeothermometry. *Organic Geochemistry* 35, 567–571.

Schouten S., Huguet C., Hopmans E.C., Kienhuis M.V.M., Sinninghe Damsté J.S., 2007a. Analytical methodology for TEX$_{86}$ paleothermometry by highperformance liquid chromatography/atmospheric pressure chemical ionization-mass spectrometry. *Analytical Chemistry* 79, 2940–2944.

Schouten S., Ossebaar J., Brummer G.-J., Elderfield H., Sinninghe Damsté J.S., 2007b. Transport of terrestrial organic matter to the deep North Atlantic Ocean by ice rafting. *Organic Geochemistry* 38, 1161–1168.

Schouten S., Eldrett J., Greenwood D.R., Harding I., Baas M., Sinninghe Damsté J.S., 2008a. Onset of long-term cooling of Greenland near the Eocene–Oligocene boundary as revealed by branched tetraether lipids. *Geology* 36, 147–150.

Schouten S., Hopmans E.C., Baas M., Boumann H., Standfest S., Könneke M., Stahl D.A., Sinninghe Damsté J.S., 2008b. Intact membrane lipids of *"Candidatus Nitrosopumilus maritimus"*, a cultivated representative of the cosmopolitan mesophilic group I Crenarchaeota. *Applied and Environmental Microbiology* 74, 2433–2440.

Schouten S., Middelburg J.J., Hopmans E.C., Sinninghe Damsté J.S., 2010. Fossilization and degradation of intact polar lipids in deep subsurface sediments: a theoretical approach. *Geochimica et Cosmochimica Acta* 74, 3806–3814.

Sessions A.L., Burgoyne T.W., Schimmelmann A., Hayes J.M., 1999. Fractionation of hydrogen isotopes in lipid biosynthesis. *Organic Geochemistry* 30, 1193–1200.

Shakun J.D., Burns S., Fleitmann D., Kramers J., Matter A., Al-Subary A., 2007. A highresolution, absolute-dated deglacial speleothem record of Indian Ocean climate from Socotra Island, Yemen. *Earth and Planetary Science Letters* 259, 442-456.

Shimada H., Nemoto N., Shida Y., Oshima T., Yamagishi A., 2008. Effects of pH and temperature on the composition of polar lipids in *Thermoplasma acidophilum* HO-62. *Journal of Bacteriology* 190, 5404–5411.

Sinninghe Damsté J.S., Hopmans E.C., Pancost R.D., Schouten S., Geenevasen J.A.J., 2000. Newly discovered non-isoprenoid glycerol dialkyl glycerol tetraether lipids in sediments *Chemical Communications* 17, 1683–1684.

Sinninghe Damsté J.S., Hopmans E.C., Schouten S., van Duin A.C.T., Geenevasen J.A.J., 2002. Crenarchaeol: the characteristic core glycerol dibiphytanyl glycerol tetraether membrane lipid of cosmopolitan pelagic crenachaeota. *Journal of Lipid Research* 43, 1641–1651.

Sinninghe Damsté J.S., Rijpstra W.I.C., Hopmans E.C., Schouten S., Balk M., Stams A.J.M., 2007. Structural characterization of diabolic acid-based tetraester, tetraether and mixed ether/ester, membrane-spanning lipids of bacteria

from the order *Thermotogales*. *Archives of Microbiology* 188, 629–641.

Sinninghe Damsté J.S., Ossebaar J., Schouten S., Verschuren D., 2008. Altitudinal shifts in the branched tetraether lipid distribution in soil from Mt. Kilimanjaro (Tanzania): Implications for the MBT/CBT continental palaeothermometer. *Organic Geochemistry* 39, 1072–1076.

Sinninghe Damsté J.S., Ossebaar J., Abbas B., Schouten S., and Verschuren D., 2009. Fluxes and distribution of tetraether lipids in an equatorial African lake: Constraints on the application of the TEX$_{86}$ palaeothermometer and BIT index in lacustrine settings. *Geochimica et Cosmochimica Acta* 73, 4232-4249.

Smith F.A. and Freeman K.H., 2006. Influence of physiology and climate on δD of leaf wax *n*-alkanes from C_3 and C_4 grasses. *Geochimica et Cosmochimica Acta* 70, 1172–1187.

Stevens T., Thomas D.S.G., Armitage S.J., Lunn H.R., Lu H., 2007. Reinterpreting climate proxy records from late Quaternary Chinese loess: a detailed OSL investigation. *Earth Science Reviews* 80, 111–136.

Street-Perrott F.A., Huang Y.S., Perrott R.A., Eglinton G., BenKhelifa L., Harkness D.D., Olago D.O., 1997. Impact of atmospheric carbon dioxide on tropical mountain ecosystems. *Science* 278, 1422-1426.

Strous M., Heijnen J.J., Kuenen J.G., Jetten M.S.M., 1998. The sequencing batch reactor as a powerful tool for the study of slowly growing anaerobic ammonium-oxidizing microorganisms. *Applied Microbiology and Biotechnology* 50, 589–596.

Stuiver M. and Grootes P.M., 2000. GISP2 oxygen isotope ratios. *Quaternary Research* 53, 277–283.

Sturt H.F., Summons R.E., Smith K., Elvert M., Hinrichs K.-U., 2004. Intact polar membrane lipids in prokaryotes and sediments deciphered by high-performance liquid chromatography/electrospray ionization multistage mass spectrometry – new biomarkers for biogeochemistry and microbial ecology. *Rapid Communications in Mass Spectrometry* 18, 617-628.

Sun J. and Huang X., 2006. Half-precessional cycles recorded in Chinese loess: response to low-latitude insolation forcing during the last glaciation. *Quaternary Science Reviews* 25, 1065–1072.

Sun X., Song C., Wang F., Sun M., 1997. Vegetation history of the loess plateau of China during the last 100,000 years based on pollen data. *Quaternary International* 37, 25–36.

Tao W., Huijun W., Dabang J., 2010. Mid-Holocene East Asian summer climate as simulated by the PMIP2 models. *Palaeogeography Palaeoclimatology Palaeoecology* 288, 93–102.

Thomas, A., 1997. The climate of the Gongga Shan range, Sichuan Province, PR China. *Arctic and Alpine Research* 29, 226–232.

Thomas, A., 1999. Overview of the geoecology of the Gongga Shan range, Sichuan province, China. *Mountain Research and Development* 19, 17–30.

Tierney J.E., Russell J.M., Huang Y.S., Sinninghe Damsté J.S., Hopmans E.C., Cohen A.S., 2008. Northern hemisphere controls on tropical southeast African climate during the past 60,000 years. *Science* 322, 252-255.

Tierney J.E. and Russell J.M., 2009. Distributions of branched GDGTs in a tropical lake system: implications for lacustrine application of the MBT/CBT paleoproxy. *Organic Geochemistry* 40, 1032–1036.

Tierney J.E., Mayes M.T., Meyer N., Johnson C., Swarenski P.W., Cohen A.S., Russell J.M., 2010a. Late-twentieth-century warming in Lake Tanganyika unprecedented since AD 500. *Nature Geoscience* 3, 422-425.

Tierney J.E., Russell J.M., Eggermont H., Hopmans E.C., Verschuren D., Sinninghe Damsté J.S., 2010b. Environmental controls on branched tetraether lipid distributions in tropical East African lake sediments. *Geochimica et Cosmochimica Acta* 74, 4902-4918.

Tyler J.J., Nederbragt A.J., Jones V.J., Thurow J.W., 2010.

Assessing past temperature and soil pH estimated from bacterial tetraether membrane lipids: evidence from the recent lake sediments of Lochnar, Scotland. *Journal of Geophysical Research* 115, G01015.

Urey H.C., 1947. The thermodynamic properties of isotopic substances. *Journal of the Chemical Society*, 562-581.

van de Graaf A.A., de Bruijn P., Robertson L.A., Jetten M.S.M., Kuenen J.G., 1996. Autotrophic growth of anaerobic ammonium-oxidizing micro-organisms in a fluidized bed reactor. *Microbiology-UK* 142, 2187–2196.

Velle G., Brooks S.J., Birks H.J.B., Willassen E., 2005. Chironomids as a tool for inferring Holocene climate: an assessment based on six sites in southern Scandinavia. *Quaternary Science Reviews* 24, 1429-1462.

Walsh E.M., Ingalls A.E., Keil R.G., 2008. Sources and transport of terrestrial organic matter in Vancouver Island fjords and the Vancouver-Washington Margin: a multiproxy approach using $\delta^{13}C_{org}$, lignin phenols, and the ether lipid BIT index. *Limnology and Oceanography* 53, 1054–1063.

Wang Y.J., Cheng H., Edwards R.L., An Z.S., Wu J.Y., Shen C.-C., Dorale J.A., 2001. A high-resolution absolute-dated late Pleistocene monsoon record from Hulu Cave, China. *Science* 294, 2345–2348.

Wang Y., Cheng H., Edwards R.L., Kong X., Shao X., Chen S., Wu J., Jiang X., Wang X., An Z., 2008. Millennial- and orbital-scale changes in the East Asian monsoon over the past 224,000 years. *Nature* 451, 1090–1093.

Wang C., Xie S.-P., Carton J.A., 2004. A global survey of ocean-atmosphere interaction and climate variability. In: Earth Climate: The Ocean-Atmosphere Interaction, C. Wang, S-P. Xie, J.A. Carton (eds.), Geophysical Monographs 147, AGU, Washington D.C., 1-19.

Ward N.L., Challacome J.F., Janssen P.H., Henrissat B., Coutinho P.M., Wu M., Xie G., Haft D.H., Sait M., Badger J., Barabote R.D., Bradley B., Brettin T.S., Brinkac L.M., Bruce D., Creasy T., Daugherty S.C., Davidsen T.M., DeBoy R.T., Detter C., Dodson R.J., Durkin A.S., Ganapathy A., Gwinn-Giglio M., Han C.S., Khouri H., Kiss H., Kothari S.P., Madupu R., Nelson K.E., Nelson W.C., Paulsen I., Penn K., Ren Q., Rosovitz M.J., Selengut J.D., Shrivastava S., Sullivan S.A., Tapia R., Thompson L.S., Watkins K.L., Yang Q., Yu C., Zafar N., Zhou L., Kuske C.R., 2009. Three genomes from the phylum *Acidobacteria* provide insight into the lifestyles of these microorganisms in soils. *Applied and Environmental Microbiology* 75, 2046–2056.

Weijers J.W.H., Schouten S., van den Linden M., van Geel B., Sinninghe Damsté J.S., 2004. Water table related variations in the abundance of intact archaeal membrane lipids in a Swedish peat bog. *FEMS Microbiology Letters* 239, 51-56.

Weijers J.W.H., Schouten S., Hopmans E.C. Geenevasen J.A.J., David O.R.P., Coleman J.M., Pancost R.D., Sinninghe Damsté J.S., 2006a. Membrane lipids of mesophilic anaerobic bacteria thriving in peats have typical archaeal traits. *Environmental Microbiology* 8, 648-657.

Weijers J.W.H., Schouten S., Spaargaren O.C., Sinninghe Damsté J.S., 2006b. Occurrence and distribution of tetraether membrane lipids in soils: Implications for the use of the TEX$_{86}$ proxy and the BIT index. *Organic Geochemistry* 37, 1680–1693.

Weijers J.W.H., Schefuß E., Schouten S., Sinninghe Damsté J.S., 2007a. Coupled thermal and hydrological evolution of tropical Africa over the last deglaciation. *Science* 315, 1701-1704.

Weijers J.W.H., Schouten S., Sluijs A., Brinkhuis H., Sinninghe Damsté J.S., 2007b. Warm arctic continents during the Palaeocene-Eocene thermal maximum. *Earth and Planetary Science Letters* 261, 230-238.

Weijers J. W. H., Schouten S., van den Donker J. C., Hopmans E. C., Sinninghe Damsté J. S., 2007c. Environmental controls on bacterial tetraether membrane lipid distribution in soils. *Geochimica et Cosmochimica Acta* 71, 703-713.

Weijers J. W. H., Panoto E., van Bleiswijk J., Schouten S., Rijpstra W. I. C., Balk M., Stams A. J. M., Sinninghe Damsté J. S., 2009. Constraints on the biological source(s) of the orphan branched tetraether membrane lipids. *Geomicrobiology Journal* 26, 402-414.

Weijers J.W.H., Wiesenberg G L.B., Bol R., Hopmans E.C., Pancost R.D., 2010. Carbon isotopic composition of branched tetraether membrane lipids in soils suggest a rapid turnover and a heterotrophic life style of their source organism(s). *Biogeosciences* 7, 2959–2973.

Weijers J.W.H., Bernhardt B., Peterse F., Werne J.P., Dungait J.A.J., Schouten S., Sinninghe Damsté J.S., 2011. Absence of seasonal patterns in MBT-CBT indices in mid-latitude soils. *Geochimica et Cosmochimica Acta* 75, 3179-3190.

White D.C., Davis W.M., Nickels J.S., King J.D., Bobbie R.J., 1979. Determination of the sedimentary microbial biomass by extractable lipid phosphate. *Oecologia* 40, 51-62.

Winkelmann D. and Knies J., 2005. Recent distribution and accumulation of organic carbon on the continental margin west off Spitsbergen. *Geochemistry Geophysics Geosystems* 6, Q09012.

WMO, 2007. World Meteorological Organization. http://world-weather.wmo.int. On-line available.

Wolfe J.A., 1971. Tertiary climatic fluctuations and methods of analysis of Tertiary floras. *Palaeogeography Palaeoclimatology Palaeoecology* 9, 27–57.

Wu N., Liu T., Liu X., Gu Z., 2002. Mollusk record of millennial climate variability in the Loess Plateau during the Last Glacial Maximum. *Boreas* 31, 20–27.

Wuchter C., Schouten S., Coolen M.J.L, Sinninghe Damsté J.S., 2004. Temperature dependent variation in the distribution of tetraether membrane lipids of marine Crenarchaeota: Implications for TEX$_{86}$ paleothermometry. *Paleoceanography* 19, PA4028.

Yuan D., Cheng H., Edwards R.L., Dykoski C.A., Kelly M.J., Zhang M., Qing J., Lin Y., Wang Y., Wu J., Dorale J.A., An Z., Cai Y., 2004. Timing, duration and transitions of the last interglacial Asian monsoon. *Science* 304, 575–578.

Yuk H.-G. and Marshall D.L., 2004. Adaptation of *Escherichia coli* O157: H7 to pH alters membrane lipid composition, verotoxin secretion, and resistance to simulated gastric fluid acid. *Applied and Environmental Microbiology* 70, 3500–3505.

Zheng H., Huang X., Ji J., Liu R., Zeng Q., Jiang F., 2007. Ultra-high rates of loess sedimentation at Zhengzhou since Stage 7: implication for the Yellow River erosion of the Sanmen Gorge. *Geomorphology* 85, 131–142.

Zhong X., Zhang W., Luo J., 1999. The characteristics of the mountain ecosystem and environment in the Gongga Mountain region. *AMBIO* 28, 648–654.

Zhou Z., Baoyin Y., Petit-Maire N., 1998. Paleoenvironments in China during the Last Glacial Maximum and the Holocene Optimum. *Episodes* 21, 152–158.

Zink K.-G., Wilkes H., Disko U., Elvert M., Horsfield B., 2003. Intact phospholipids – microbial "life markers" in marine deep subsurface sediments. *Organic Geochemistry* 34, 755-769.

Zink K.-G., Vandergoes, M.J., Mangelsdorf K., Dieffenbacher-Krall A.C., Schwark L., 2010. Application of bacterial glycerol dialkyl glycerol tetraethers (GDGTs) to develop modern and past temperature estimates from New Zealand lakes. *Organic Geochemistry* 41, 1060-1066.

Dankwoord/Acknowledgements

Natuurlijk is het ook mij niet gelukt dit proefschrift zonder hulp en steun van anderen vol te kletsen, daarom hier het bekende stukje om iedereen te bedanken die me de afgelopen jaren heeft geholpen, op wat voor manier dan ook. Voor de afwisseling doe ik dat maar eens op alfabetische volgorde:

De eer om als eerste bedankt te worden valt dan aan **A**llert, maar wel gedeeld met Roos, Matthijs en Tamar. Dank voor jullie gastvrijheid, kopjes koffie en andere versnaperingen, en natuurlijk de avonden met spelletjes. Dat hadden we vaker mogen doen! Daarnaast verdient Allert een extra vermelding voor statistische bijstand. Als ik **C**ees, Furu en Lukas elk afzonderlijk zou bedanken voor de alternatieve koffieclub, gezelschap in de 12 Balcken, etentjes, de goede slechte grappen, gegarandeerde presentie bij Texel Wildlife excursies en andere ongein zou mijn proefschrift een stuk dikker zijn. Ik doe het met een hele dikke dankjewel voor jullie drieën! En Furu nog een keer apart voor het zijn van mijn de Ruyterstraatvriendinnetje, ookal woonde je het grootste deel van de tijd in Bremen. Two other people that have been very important to me during my time on Texel are my **D**epartment best friends Isla and Angela. Thank you so much for the many adventures, from serious scientific discussions to going to concerts, festivals, sharing hotel rooms and tents, holidays and (practical) jokes. You are great! Gedurende mijn laatste jaar op het NIOZ zorgde de 8 uur **K**offieclub ervoor dat mijn dag goed (?) begon met niet alleen koffie, maar ook een sudoku'tje om even op gang te komen, de laatste smartfoon updates en ander (vaak random) commentaar. Uit de serie **K**antoorgenoten heb ik het meeste tijd doorgebracht met Petra, but I would also like to thank Andrea, Jérôme, Adam, Kim and Arjan for office fun, as well as the other people of the MBT-~~CBT~~BGC department that I haven't mentioned separately.

I would also like to thank the following **P**eople from in- and outside the NIOZ that have provided me with samples, given me the opportunity to go on fieldwork, or helped me in another (significant) way and have co-authored one or even more chapters in this thesis: Jung-Hyun Kim, Marcel van der Meer, Jaap van der Meer, Johan Weijers, Guodong Jia, Graeme Nicol, Maarten Prins, Kay Beets, Simon Troelstra, Zhaoyan Gu, Hongbo Zheng, Anchélique Mets, Irene Rijpstra, Noah Fierer, Rob Jackson, Nalân Koç, Dorthe Klitgaard Kristensen, Jort Ossebaar, Jord Blokker, Beth Bernhardt, Joe Werne, Jennifer Dungait.

En hier zijn ze dan: **S**tefan en Jaap, heel erg bedankt voor alle uitleg, aanmoediging en begeleiding de afgelopen jaren, en dat alles met een verbluffende efficiëntie. Dankzij jullie heb ik als bodemkundige op het NIOZ behoorlijk veel nieuwe dingen geleerd (naast tafelvoetballen en wat voor een steen je precies nodig hebt om een autoruit in te tikken). Wat nieuwe dingen betreft ben ik ook veel dank verschuldigd aan Ellen voor kennis over IPLs, HPLCs, en gewoon omdat je deur altijd open staat (en anders kwam je wel bij mij binnenlopen, en daarna nog een keer om je theekop op te halen, en daarna nog een keer om te kijken of je theekop hier toevallig staat?). Ook van Jort en Michiel (ik hoor heus wel waar jullie het over hebben), Marianne en Irene heb ik de nodige assistentie en tips mogen ontvangen, dank jullie wel.

Texel, dinners, coffees and beers would not have been the same without the company of John, Jenny, Cecile, Rik, Maarten, Pieter, Babette, Lorendz, T, Jasperius, Marian, Andrea and many more. I also like to thank Craig and Julie, Jort and Sharyn, Raquel, Pedro, and Angela for providing a bed in Den Helder once in a while. Pieter en Babette (en een klein stukje Cees) wil ik hier nog een keer apart bedanken voor het regelen van een snelle overtocht op die ene donderdagavond in juli 2007. Daarnaast de mensen van buiten het NIOZ, maar des te meer van Texel en goed voor de integratie bovendien: de

rennerts van AV Texel en de maandagavond yogaclub.

Van de **U**trechtenaren noem ik het eerst Johan, natuurlijk, want zonder de MBT-CBT proxy was dit nogal een dun boekje geworden, maar ik wil ook Eveline, Cornelia en Appy bendanken voor conferentie-plezier en kopjes koffie. Wait, did I mention conferences? There is one that I remember very well, or rather the after conference fun trip in the White Mountains with T, Isla and Luke. Just one word: bears. Thanks for sharing that experience!

Dan nog mijn **V**rienden van voor het Texel tijdperk, onder wie mijn paranimfen Marg en Mart, zelf-benoemd (maar verdiend) biernimf Aal, andere (oud-)49ers, Ben, Cathelijne, Marieke, Joris, Kees-Jan, Elien, en en en. Het is (voor de meesten) iets verder weg, maar ook in Zürich zijn jullie te allen tijde van harte welkom.

Als laatste toch nog wat uitzonderingen op de volgorde: mijn vader, die me nog wel naar Texel heeft helpen verhuizen, maar dit eindresultaat helaas nooit zal zien, en natuurlijk mijn moeder en broeder. Lot en Tom, we kunnen het, ook met zn drieën.

En de allerlaatste woorden zijn speciaal voor Lukas(ius) ("je maakt toch wel even een foto als je echt je computer uit het raam gooit?"), zonder jou was ik nooit zo lekker bezig geweest, dankjewel! Echt.

About the author

Francien Peterse was born on the 6th of June 1980 in Amsterdam, the Netherlands. After finishing secondary school at the Montessori Lyceum Amsterdam in 1998, she spent one year in Iceland to experience glaciers, earthquakes and a volcanic eruption from close by. In 1999 she started the Soil, Water, Atmosphere program at Wageningen University, and later specialized in soil science. In 2001 Francien attended a 4-month interdisciplinary course on geology, hydrology and ecology at the Sogn og Fjordane Høgskole in Sogndal (Norway). In 2003 she worked for 3 months as an intern at the Nordic Volcanological Center in Reykjavik (Iceland), after which she took a year off to take seat in the Student Council of Wageningen Univeristy. Francien only properly dedicated herself to her studies during the field and lab work for her first thesis, on organic matter chemistry in Costa Rican volcanic ash soils. Once in the flow, she went to the Universidad de La Laguna on Tenerife (Spain) to work on her second thesis, which focused on the influence of irrigation with dairy effluent on chemical soil properties of volcanic ash soils. After her graduation in August 2006, Francien shortly worked as a research assistant at Wageningen University before starting as a PhD student at the Royal Netherlands Institute for Sea Research in January 2007. Here she worked on the environmental controls on the distribution of membrane lipids of soil bacteria and their suitability to reconstruct paleoclimatic changes under supervision of Stefan Schouten and Jaap Sinninghe Damsté. Francien received an ETH Fellowship to continue her scientific career as a postdoctoral researcher in the Biogeosciences group at the ETH in Zürich (Switzerland), where she started working in July 2011.